

SONGS U2C17 Steam Generator Operational Assessment for Tube-to-Tube Wear

**APPENDIX A: ESTIMATES OF FEI-INDUCED TTW RATES**

**A.1 Simple Estimates of the Maximum TTW Rate**

The maximum volume loss as a result of TTW in Unit 3 is 0.123 inches<sup>3</sup>. This was obtained by integration of the measured wear depth versus length profile with appropriate consideration of the cylindrical tube geometry. A site specific TTW eddy current standard was used to optimize wear depth measurement accuracy. The time to develop a volume loss of 0.123 inches<sup>3</sup> can be estimated using Archard’s rule. From Archard’s rule the wear volume is given by the wear coefficient, k, times the work rate times the wear time. Following standard practice the work rate for wear is taken as the product of normal force and sliding distance per unit time.



MHI Proprietary

- Pre-instability formation of the wear scar followed by loss of contact with the tube.
- Post-instability formation or elongation of the wear scar but with a limited AVB width in contact with the tube such as is produced by AVB twist.

Figure A-1 demonstrates that wear elongation at one AVB location can be used to calculate tangential displacements at other locations on the same tube. This calculation provides the sliding distance of interest.

The deepest TTW is observed in Unit 3, SG E-088, tubes R102 C78, R104 C78 and R106 C78. There are no elongated wear scars on tube R102, C78 and R106 C78. These are likely unstable driving tubes. There are elongated wear scars on tubes R100 C78, R104 C78 and R108 C78. These are likely tubes that were initially stable but driven to instability by repeated impacts from neighbor tubes. Tube R108 C78 has elongated wear scars at multiple locations. At AVB 8 the wear length is 1.28 inches, which is the longest wear scar on this tube. Assuming the tube is in contact with the AVB over its full width of 0.6 inches leads to an elongation of 0.68 inches at this location. This is caused by tangential displacements resulting from impacts with tube R106 C78. Half of the elongation of wear at AVB 8 is produced as the tube is forced toward the cold leg with the other half

SONGS U2C17 Steam Generator Operational Assessment for Tube-to-Tube Wear
 

---

generated as the tube is forced toward the hot leg. The tangential displacement of a U-bend at AVB 8 is 0.34 inches for a single impact event. The two centers of impact as a tube swings to and fro in Mode 1 are 48° up the semicircular portion of the U-bend from either the hot leg or cold leg. From the mode shape a tangential displacement of 0.34 inches at AVB 8 translates to a tangential displacement of 0.21 inches at the impact location. The sliding distance in TTW is twice the tangential displacement of the driving tube relative to the initial impact point with the neighbor tube to the maximum extent of tangential movement during the impact event. It is twice the value since the driving tube slides to the maximum extent and then back to the point of initial contact. During sliding the normal contact force increases from zero to a maximum and then back to zero. Elongation of wear scars sets the scale for the level of displacements involved. In actuality the driving tube impacts a neighbor with some degree of restriction to movement other than inertia. Both U-bends are deforming and moving. Determination of the actual sliding distance requires a dynamic rather than a static analysis. It is nonetheless useful to consider a static approximation. A sliding distance 0.21 inches is estimated in terms of a tangential displacement relative to a stationary point.

With a sliding distance estimated from eddy current measurements of elongated wear scars all that is needed to calculate a work rate is an estimate of the normal force required to produce the observed displacements. Figure A-2 shows the displacements generated by a radial load applied at the impact location as determined via an FEA model of the U-bend. For convenience in modeling, the U-bend is fixed at the top support plate. Modeling the entire tube with gap elements at the support plates is more appropriate. However, the resulting increase in displacements is not a significant consideration. An applied load of 14.14 lbs. leads to a radial displacement of 0.47 inches. With a Mode 1 displacement pattern and a sliding distance of 0.21 inches the matching radial displacement is 0.39 inches. The estimated radial load in a static analysis that is consistent with a radial displacement of 0.39 inches is then 11.7 lbs. This is an under estimate because at a radial displacement of about 0.2 inches the U-bend comes into contact with a neighbor tube. Thus as an impacted tube is displaced the load increases linearly up to a radial displacement of 0.2 inches then the slope of the radial load versus radial displacement increases since the radial load must then displace two tubes. The final load at a total radial displacement of 0.39 inches is 17.4 lbs. This load does not significantly distort either the driving or impacted tubes since it is actually distributed over a contact length of about 30 inches along the U-bend. From the area under the normal force versus sliding distance curve, the work done in the context of a wear calculation is 3.65 in.lbs. per impact event. The work rate is this value times the frequency or 21.1 in.lbs./sec.

Figure A-3 shows plots of work rate versus time leading to a wear volume of 0.123 inches<sup>3</sup>. The solid curve uses a wear coefficient of 35 times the wear coefficient of an Alloy 690 to Type 405 stainless steel wear couple while the dotted line is for a wear coefficient of 20 times that of an Alloy 690 to Type 405 stainless steel wear couple. The horizontal line is the work rate from a static analysis of the normal force and an essentially measured sliding distance. It leads to a wear time of about 5 months for the larger wear coefficient and 8 months for the smaller wear coefficient. However, the real impact event is dynamic not static. A common approximation of dynamic effects is to multiply the static force by a factor of 2. The upper horizontal line is an estimate of the work rate incorporating a dynamic effect. It leads to estimated wear times from 2.5 to 4.5 months.

In summary, simple estimates of the wear time which led to the deepest TTW in Unit 3 range from about 2.5 to 8 months. The lower wear coefficient from actual Alloy 690 to Alloy 690 wear couple tests is a reasonable choice. This leads to estimated wear times between 4.5 and 8 months. However, variations in wear coefficients dictates conservatism. The minimum estimate for the time interval for the development of worst case wear is 2.5 months.

[

] This is  
about a factor of 4 smaller than the radial displacement that is indicated from measurements of elongation of AVB





SONGS U2C17 Steam Generator Operational Assessment for Tube-to-Tube Wear

---

wear scars. In order to develop a better understanding of U-bend to U-bend impact events a parametric study of dynamic contact of one U-bend with another was undertaken. These results are described in the next section.



SONGS U2C17 Steam Generator Operational Assessment for Tube-to-Tube Wear

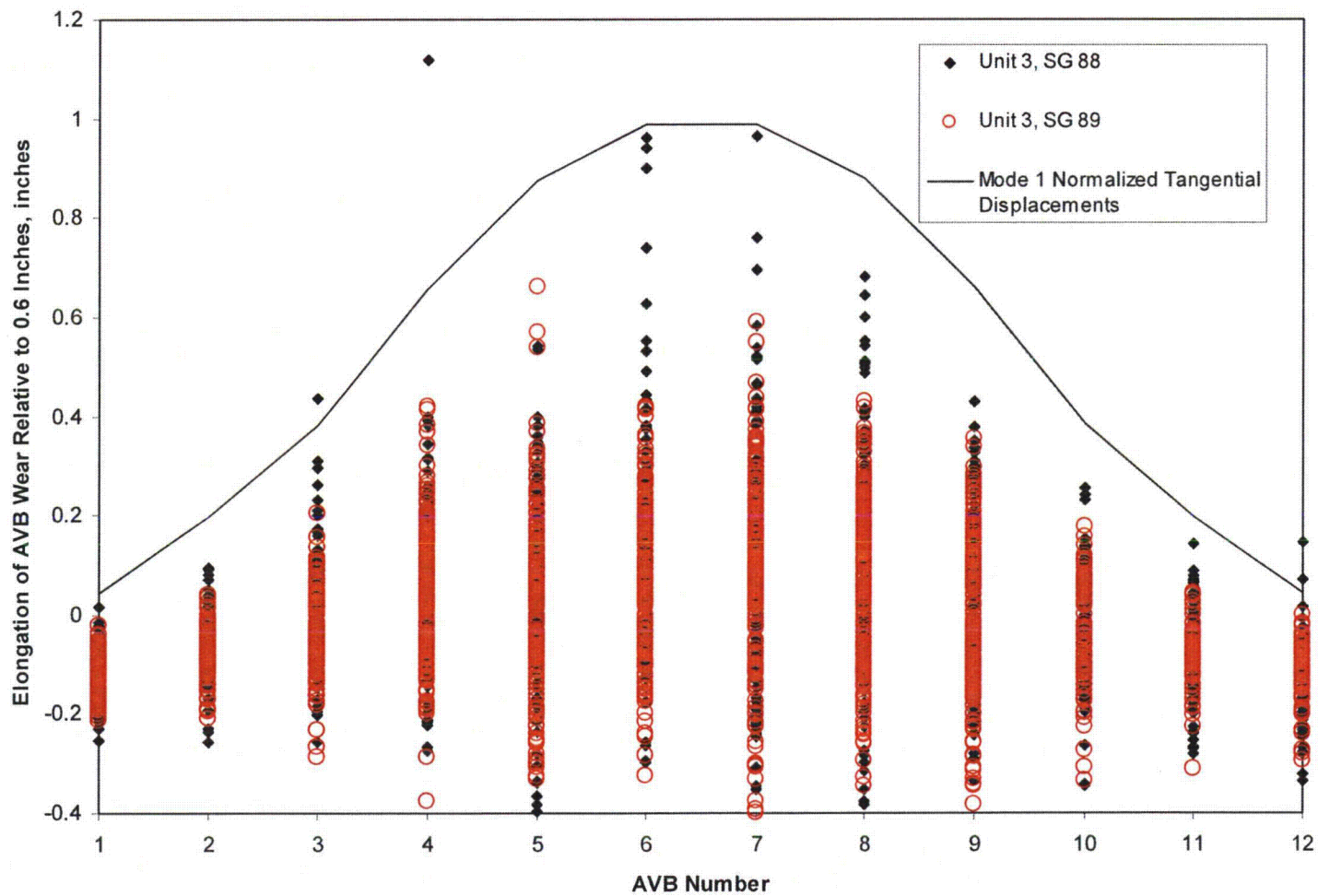
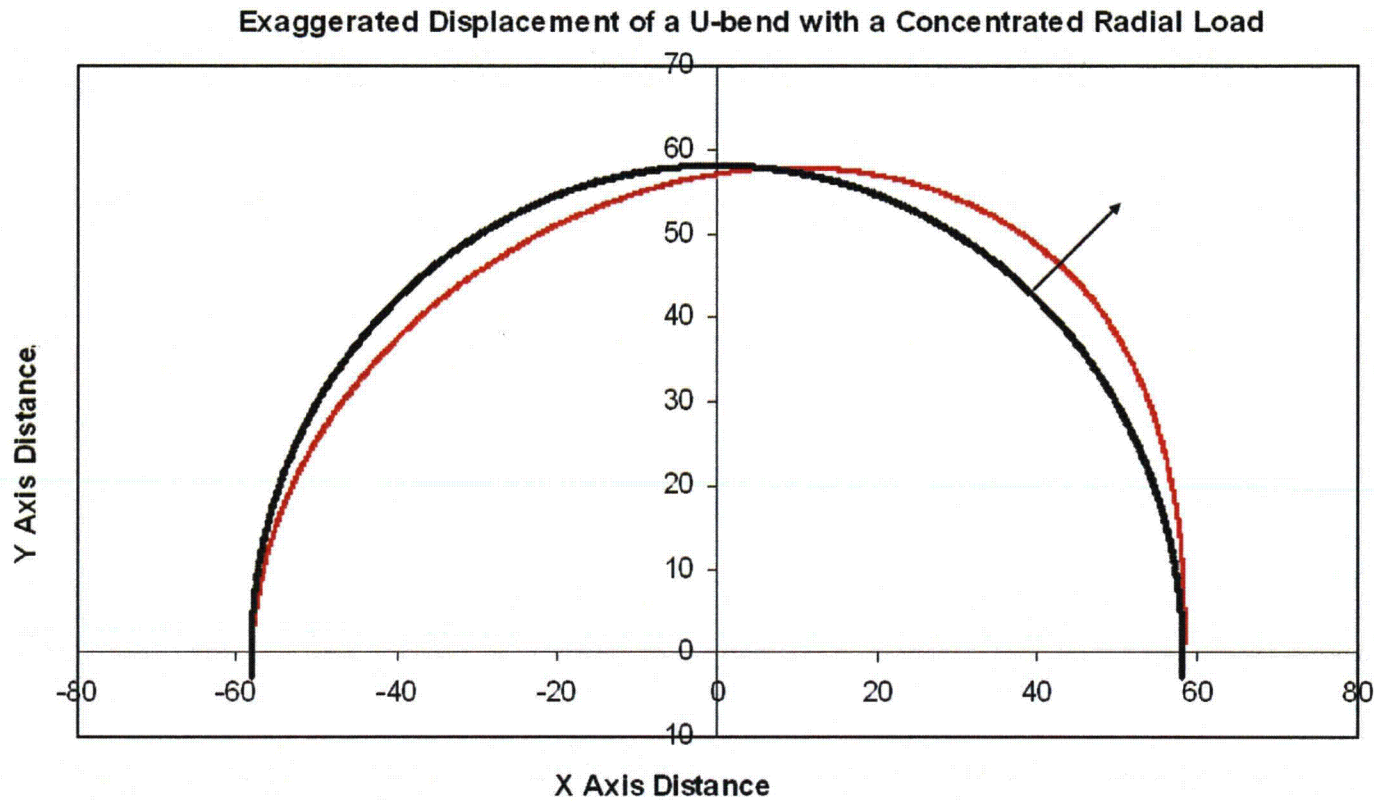


Figure A-1: Elongated Wear at AVBs, Only Observed on Tubes with TTW





SONGS U2C17 Steam Generator Operational Assessment for Tube-to-Tube Wear



**Figure A-2: Radial Load Applied to a U-bend at the Mode I Impact Location, Deformed Shape Greatly Exaggerated**



SONGS U2C17 Steam Generator Operational Assessment for Tube-to-Tube Wear

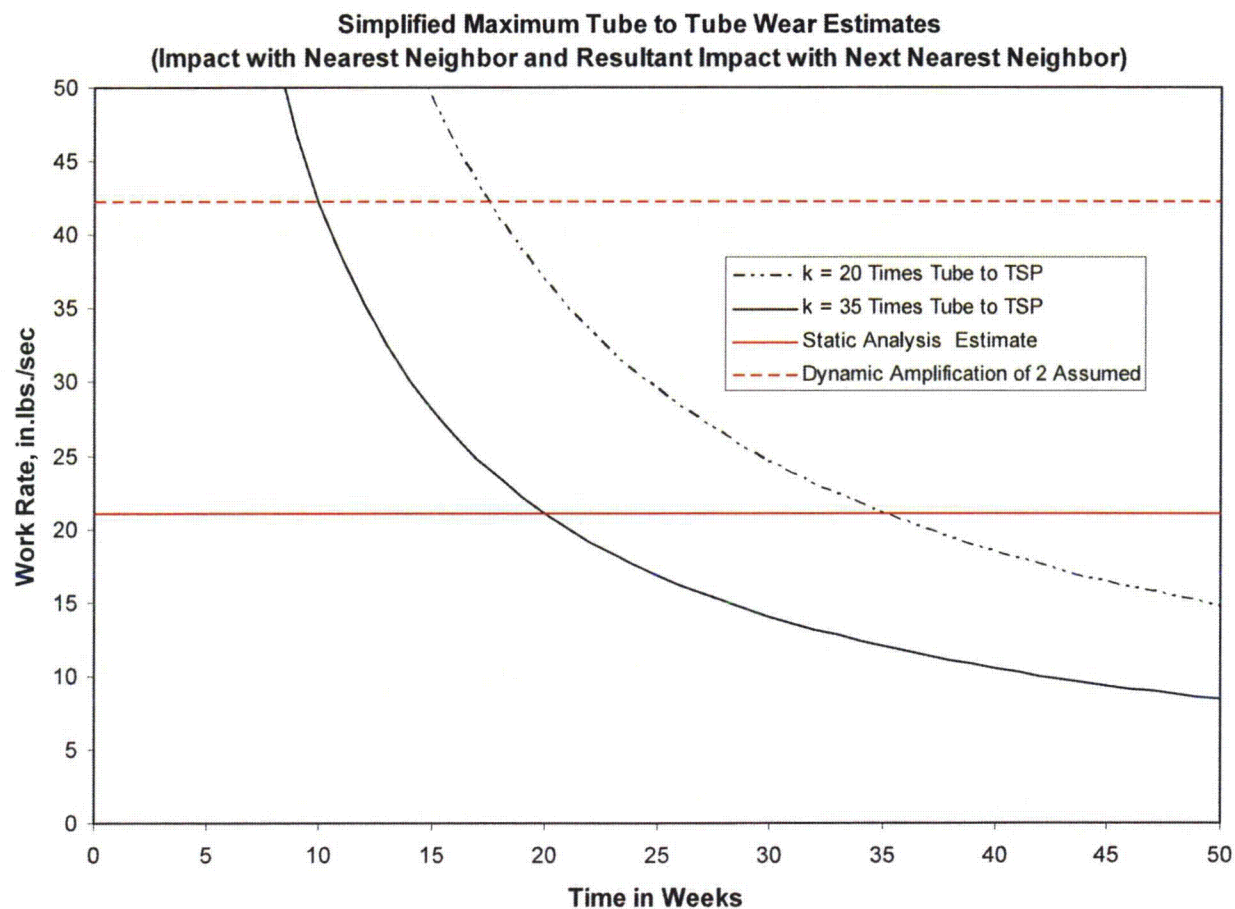


Figure A-3: Estimates of Time Needed to Develop Maximum TTW Volume Loss



SONGS U2C17 Steam Generator Operational Assessment for Tube-to-Tube Wear
 

---

## A.2 Parametric Time Domain Dynamic Analyses of U-Bend to U-Bend Impact

Dynamic simulations of U-bend to U-bend impact were performed using the ABAQUS Standard finite element program. Computation details can be found in Reference A.3.1. More than 150 simulations were conducted over a broad range of excitation force amplitudes, excitation frequencies, structural damping levels and tube-to-tube friction coefficients. This produced a wide range of contact forces and sliding distances. Only the driving tube and the nearest neighbor tube are modeled. The full length of the tube is included to capture the influence of tube support plates in the straight leg sections. Friction forces at AVB support locations are not included. Instead the overall role of structural damping was established. Friction forces during U-bend to U-bend contact were explicitly treated. It should be noted that the results described in Reference A.3.1 deal with a broad study of U-bend to U-bend impact. Evaluations of the implications of these results to TTW rates are only those of the authors of this report. They are presented in the following paragraphs.

Results are available for one U-bend impacting its outboard nearest neighbor. Possible interaction with the inboard neighbor is ignored. This consideration is mentioned in later paragraphs. The driving U-bend is excited by a cyclic distributed force on the extrados portion on one side of the U-bend above the contact region. The nearest neighbor U-bend is only supported at tube support plate intersections. No AVBs are included. For any given simulation the cyclic excitation force has a constant amplitude. However, a variety of excitation force amplitudes were considered. Several different excitation frequencies were used, bounding the natural frequency. Relative to estimation of TTW rates there are four outstanding features of the results of the Reference A.3.1 studies. These are:

- The normal contact force is highly variable from one impact event to another.
- The length of contact is highly variable from one impact event to another.
- During a single impact event the impact force and length of contact varies with time.
- For a given sliding distance, the maximum contact force is a very strong function of the value of structural damping.

Selected examples of these phenomena are presented below. A much better understanding of the process of U-bend to U-bend impact is obtained by repeated viewing of videos of tube motion.

As the excitation force is applied it takes a few cycles to accelerate to the maximum tube motion. Depending on the damping level the excitation force may result in a final amplitude that is too small to result in tube-to-tube contact. It is a simple matter to increase the excitation force amplitude to overcome damping and develop tube-to-tube contact. When tube-to-tube contact occurs, friction forces develop and are explicitly considered. Figure A-4 plots line contact stress for repeated impact events versus time. The line contact stress is expressed in terms of force per unit length. The total contact force is the product of line stress multiplied by the contact length. Note the variability in the line contact stress for repeated impact events. Also note the variability in the width of the contact spikes. Within a single impact event the contact line stress varies over very short time periods, i.e. it chatters.

Figure A-5 illustrates the variation in maximum contact arc length. This figure does not correspond with Figure A-4. Again notice the substantial variation in contact arc length from one impact event to another. Also, after the first impact event the nearest neighbor tube begins cyclic motion from the impact force. After this point both tubes are in motion and not necessarily in phase. Impact can occur with tubes moving toward each other. The



---

**SONGS U2C17 Steam Generator Operational Assessment for Tube-to-Tube Wear**

---

substantial temporal variation in line contact stress and contact arc length makes estimation//calculation of work rates a non-trivial exercise. Several additional factors add to the complexity of the problem.

Figure A-6 illustrates the fourth feature of U-bend to U-Bend impact noted above, for a given maximum sliding distance maximum contact force is a very strong function of the value of structural damping. Maximum contact force is plotted versus sliding distance. This force is taken as the product of maximum line contact stress and the maximum contact arc length. For a structural damping value of 2.5 % the impact force at a sliding distance of 0.21 inches is about 16 lbs. Recall that the simple estimates for contact force at this same sliding distance from the preceding section ranged between 11.7 lbs. static and 23.4 lbs. dynamic. The common factor of 2 amplification from a static to a dynamic event is reasonable, even if highly approximate. As damping increases the rate of movement of the impacted tube away from the impact event decreases and the contact force increases at a given sliding distance. At 5% damping the contact force is about 30.5 lbs. and at 10% damping it is about 84 lbs. In broad terms increased damping can be viewed as generally distributed Coulomb friction on the flanks of the U-bend. The flanks of the U-bend are the sides of the tube other than the intrados and the extrados. Hence for a given sliding distance the contact force depends on how tightly the impacted nearest neighbor tube is held in place by friction forces at AVB locations. If the neighbor tube is free to move after impact the contact force is light but if it is held tightly in place the contact force is very much larger.

Motion of tube R106 C78 leads to a measured tangential displacement of 0.21 inches on tube R108 C78 which in turn has an inferred normal displacement of 0.39 inches. Assuming a nominal tube-to-tube gap of 0.20 inches this leads to impact with the next nearest neighbor tube R110 C78. Given the Mode I displacements when contact with an outboard tube (higher row) occurs it must be accompanied by contact with an inboard tube on the opposite side of the U-bend at the same moment in time. Thus when tube R106 C78 impacts tube R108 C78 on the hot leg it impacts tube R104 C78 on the cold leg and drives it into tube R102 C78 on the cold leg. Hence motion of tube R106 C78 involves impact events during one half cycle and 4 impact events on the opposite legs on the other half cycle. The present dynamic analysis only considers impact interactions of two tubes. For the maximum displacement of interest the impact interactions of 5 tubes must be considered. This is another illustration of TTW as a sequence of dependent events and not a sequence of random independent events.

Another observation of interest is the fact that very strong local interactions with one or more AVBs can occur. Substantial stick/slip events can develop and thereby excite other modes of vibrations at other frequencies. This was not included in the analysis. In fact, impact locations consistent with Mode 2 and Mode 3 excitations have been observed. See Section 4.0 and Figure 4-17.

One of the implications of the dynamic parametric study is that the TTW rates should correlate with elongated wear at AVB locations. Elongated wear is indicative of supports with substantial friction hindering the motion of U-bends while being driven to instability by impacts from neighbor tubes. Strongly held tubes will suffer high wear rates from impacting neighbors. Hence a correlation of TTW depths with a tube wear index (summation of AVB wear depths) based only on elongated wear scars is expected. However elongated wear and TTW depths are dependent variables not independent variables. Both are post instability occurrences. While they should be correlated this correlation offers little predictive potential.

A parametric study of the dynamic aspects of U-bend to U-bend impact has led to an improved understanding of the factors involved in these impacts and an appreciation of the complexity of the problem. It underscores the uncertainties involved in estimates of TTW rates and re-enforces the basic premise of this operational assessment. Specifically TTW from in-plane fluid-elastic instability is not a tube degradation mechanism that can be managed in the conventional sense of accepting the fact of ongoing degradation and ensuring tube integrity by limiting the operating time to control the severity of degradation that is likely to develop. Rather actions must be taken to prevent the occurrence of in-plane fluid-elastic instability understood in an engineering sense as an acceptably



SONGS U2C17 Steam Generator Operational Assessment for Tube-to-Tube Wear

low probability of occurrence. This will be accomplished by a decrease to 70% power and an initial inspection interval of 5 months.

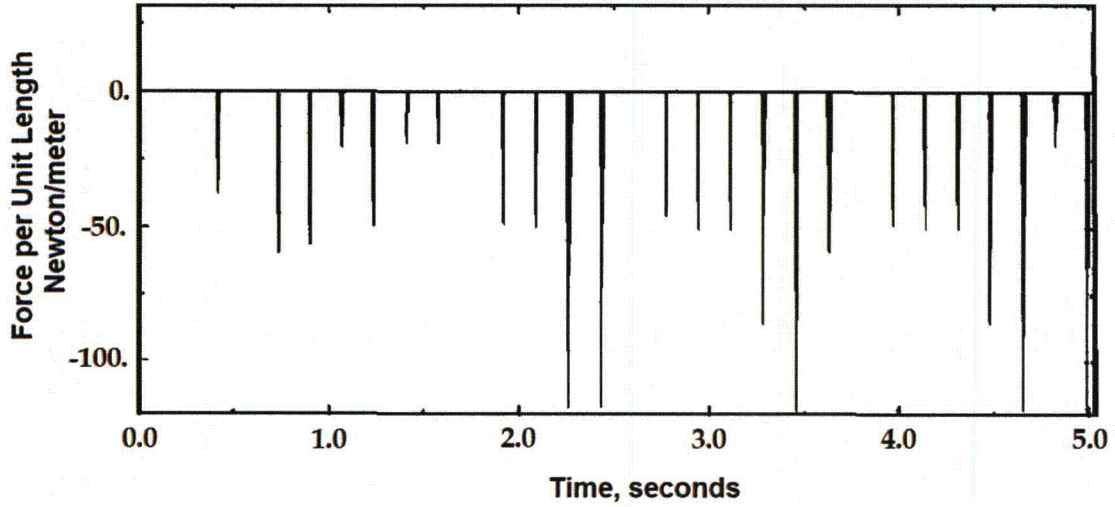


Figure A-4: Line Contact Stress versus Time

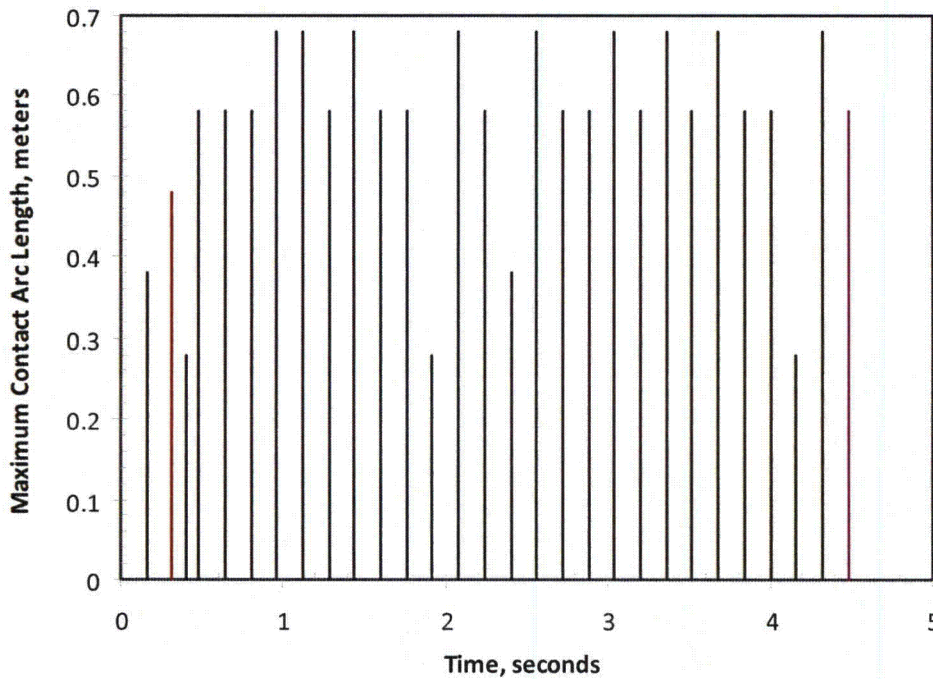


Figure A-5: Maximum Contact Arc Length versus Time

SONGS U2C17 Steam Generator Operational Assessment for Tube-to-Tube Wear

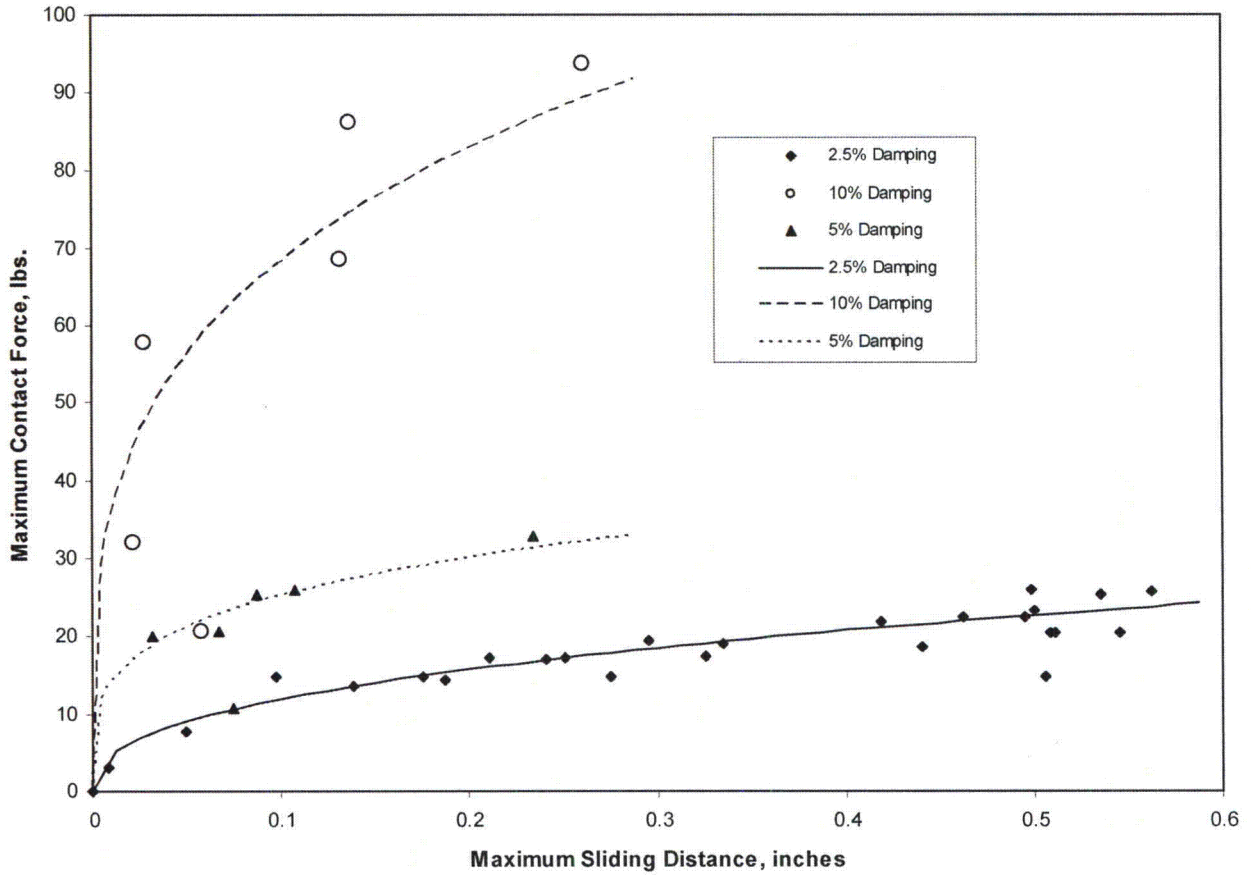


Figure A-6: Maximum Contact Force versus Sliding Distance

**A.3 References**

A.3.1 [ ], "Simulation of Tube-to-Tube Impact, Phase 2 Report," June 2012 (AREVA NP Document 38-9191195-000).



## **ATTACHMENT 6 – Appendix C**

### **Operational Assessment for SONGS Unit 2 SG for Upper Bundle Tube-to-Tube Wear Degradation at End of Cycle 16**



AES 12068150-2Q-1  
Revision 0  
September 2012

# Operational Assessment for SONGS Unit 2 Steam Generators for Upper Bundle Tube-to-Tube Wear Degradation at End of Cycle 16

Prepared By

Intertek APTECH  
601 West California Avenue  
Sunnyvale, California 94086-4831

Prepared For

AREVA, Inc.  
3315 Old Forest Road  
Lynchburg, VA 24501

Attention: Mr. Jeffrey Fleck

601 West California Avenue ■ Sunnyvale ■ California 94086-4831 ■ 408.745.7000 ■ FAX 408.734.0445  
16100 Cairnway Drive, Suite 310 ■ Houston ■ Texas 77084-3597 ■ 832.593.0550 ■ FAX 832.593.0551  
139,11215 Jasper Avenue ■ Edmonton ■ Alberta T5K 0L5 ■ 780.669.2869 ■ FAX 780.669.2509

Website: [www.aptecheng.com](http://www.aptecheng.com)



# Controlled Document

## Supplier Status Stamp

VPL No: 1814-AU651-M0145	Rev No: 1	QC: N/A
<input type="checkbox"/> DESIGN DOCUMENT    ORDER NO. <u>800918458</u>		
<input checked="" type="checkbox"/> REFERENCE DOCUMENT - INFORMATION ONLY <input type="checkbox"/> VIRP IOM MANUAL		
MFG MAY PROCEED: <input type="checkbox"/> YES <input type="checkbox"/> NO <input checked="" type="checkbox"/> N/A		
<small>STATUS - A status is required for design documents and is optional for reference documents. Drawings are reviewed and approved for arrangements and conformance to specification only. Approval does not relieve the submitter from the responsibility of adequacy and suitability of design, materials, and/or equipment represented.</small>		
<input checked="" type="checkbox"/> 1. APPROVED		
<input type="checkbox"/> 2. APPROVED EXCEPT AS NOTED - Make changes and resubmit.		
<input type="checkbox"/> 3. NOT APPROVED - Correct and resubmit for review. NOT for field use.		
<small>APPROVAL: (PRINT / SIGN / DATE)</small>		
RE: <u>E. GRIBBLE</u> <u>10/01/12</u>		
FLS: <u>A. MATHENY</u> <u>10/01/12</u>		
<small>Other:</small>		

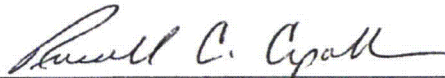
SCE DE(123) 5 REV. 3 07/11

REFERENCE: SO123-XXIV-37.8.26

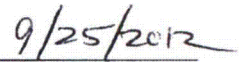
*This report was prepared by Intertek APTECH as an account of work sponsored by the organization named herein. Neither Intertek APTECH nor any person acting on behalf of Intertek APTECH: (a) makes any warranty, express or implied, with respect to the use of any information, apparatus, method, or process disclosed in this report or that such use may not infringe privately owned rights; or (b) assumes any liabilities with respect to the use of, or for damages resulting from the use of, any information, apparatus, method, or process disclosed in this report.*

**CERTIFICATE OF COMPLIANCE/CONFORMANCE**

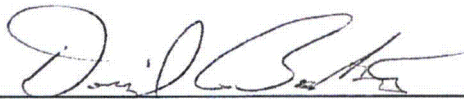
We, the undersigned, certify that the Intertek-APTECH Report AES 12068150-2Q-1, Revision 0, titled "Operational Assessment for SONGS Unit 2 Steam Generators for Tube-to-Tube Wear at End of Cycle 16," which was procured under AREVA NP, Inc. Purchase Order No. 1012045078 dated June 15, 2012, meets the requirements specified in AREVA's purchasing documents, and the quality requirements of the Intertek APTECH Quality Assurance Manual, Revision 7.4.




Russell C. Cipolla  
Project Manager



Date



David Bosko  
Acting Quality Assurance Manager



Date



**VERIFICATION RECORD SHEET**

Report No.: AES 12068150-2Q-1      Rev.: 0      Date: September 2012  
Report Title: "Operational Assessment for SONGS Unit 2 Steam Generators for Upper  
Bundle Tube-to-Tube Wear Degradation at End of Cycle 16."

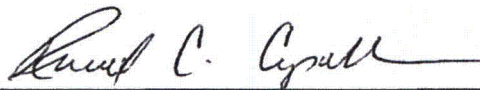
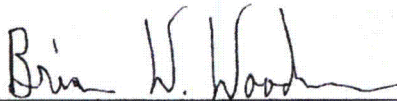
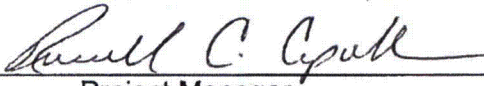
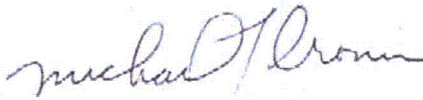
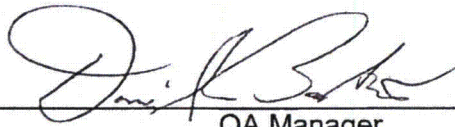
Originated By:	 _____ Project Engineer	<u>9-25-2012</u> Date
Reviewed By:	 _____ Project Engineer	<u>9-25-2012</u> Date
Approved By:	 _____ Project Manager	<u>9-25-2012</u> Date
Verified By:	 _____ Verifier	<u>9-25-2012</u> Date
QA Approved By:	 _____ QA Manager	<u>9-25-2012</u> Date

TABLE OF CONTENTS

<u>Section</u>	<u>Page</u>
Executive Summary .....	iv
<b>1 Introduction</b> .....	<b>1-1</b>
<b>2 Structural Requirements</b> .....	<b>2-1</b>
2.1 Background .....	2-1
2.2 Structural and Leakage Integrity .....	2-1
2.3 Tube Burst Model .....	2-3
2.4 Leak Rate Calculation .....	2-3
<b>3 Probabilistic Analysis</b> .....	<b>3-1</b>
3.1 Assessment Overview .....	3-1
3.2 Analysis Assumptions .....	3-2
3.3 State of Degradation – Wear Index .....	3-3
3.4 Probabilistic Model .....	3-5
3.5 Verification and Validation .....	3-6
<b>4 Analysis Input Parameters</b> .....	<b>4-1</b>
4.1 Tubing Properties .....	4-1
4.2 Operating Parameters .....	4-2
4.3 Degradation Characterization .....	4-2
4.4 Probability of Detection .....	4-4
4.4.1 Inspected Population .....	4-4
4.4.2 Undetected Population .....	4-5
4.5 Tube-to-Tube Wear Initiation .....	4-6
4.6 Degradation Growth Rates .....	4-10
4.6.1 AVB and TSP Growth Models .....	4-10
4.6.2 TTW Growth Model .....	4-11
4.7 Effect of Power Reduction .....	4-12
4.8 Measurement Uncertainty .....	4-13
<b>5 Operational Assessment</b> .....	<b>5-1</b>
5.1 Analysis Cases .....	5-1
5.2 Simulation Results .....	5-1
5.3 Structural Margin Evaluation .....	5-2
5.4 Leakage Evaluation .....	5-3
<b>6 Summary of Results</b> .....	<b>6-1</b>
<b>References</b> .....	<b>R-1</b>
<b>Appendix A – Report Acronyms</b> .....	<b>A-1</b>

## EXECUTIVE SUMMARY

The San Onofre Unit 2 (U2) plant has two new steam generators that replaced the original CE-70 design. The replacement steam generators are MHI Model 116TT1 and began operation in Year 2010. The generators have completed one cycle of operation (Cycle 16) with duration of 1.718 years at power (20.6 months). In the first cycle of operation, the U2 tubing has experienced substantial wear degradation at points of contact with anti-vibration bar (AVB) U-bend supports. There were 4348 indications detected at AVB contact points with a maximum NDE depth of 35%TW during the end-of-cycle (EOC) 16 tube examinations. To a much lesser extent, wear at tube support plates (TSP) was also detected (364 indications) with a maximum NDE depth of 20%TW.

While U2 was in refueling, San Onofre Unit 3 (U3) had a forced outage due to a leak in one of the steam generators after 338 days (0.926 years at power or 11.1 months). The leak was due to tube-to-tube wear (TTW) at freespan locations within the U-bend region. Tube-to-tube wear in U3 was caused by in-plane motion of tubes within a defined region of the bundle. The in-plane motion was due to conditions that created fluid-elastic instability (FEI) of one or more tubes. Subsequent examination of U2 steam generators specifically looking for TTW revealed two indications in 2SG89. Because of the generic designs of both units, and the nature of the FEI, the possibility of having further initiation and progression of TTW in U2 must be addressed in this OA.

This report describes the OA performed for the limiting steam generator (2SG89) in U2 for a simulated population of TTW degradation indications. The OA is a forward-looking process and provides an estimate of the operational period for which the steam generators will maintain tube integrity for both burst strength and through-wall leakage to meet industry margin requirements (Ref. 1). The U2 OA for TTW degradation was performed in a "traditional" manner following established industry assessment guidelines. It is traditional in that the general assessment process follows industry practices for applying current and past NDE inspection data to predict tube integrity at the next inspection. This is performed through empirical models for degradation growth and in combination with engineering models for determining burst pressure and through-



wall leak rates (Ref. 2). The non-traditional aspect of the OA model is the use of pattern recognition based models to characterize the presence and severity of TTW indications based on wear indices defined by the state of AVB and TSP wear for a specific tube. The U3 inspection data from the critical wear area were used to develop predictive models for TTW initiation and growth. The "wear index" defining the state of wear at tube supports in both U2 and U3 steam generators is the method by which initiation and growth of TTW observed at U3 are correlated to U2.

A fully probabilistic model representing the high-wear region of the tube bundle was used to evaluate TTW for Cycle 17. Calculated tube burst and leakage probabilities were obtained by Monte Carlo simulation for initiation and growth of TTW. The results for burst and leakage were compared with the structural and leakage performance margin requirements of NEI 97-06 (Ref. 1). The performance standards for assessing tube integrity to the required margins are delineated in the EPRI Integrity Assessment Guidelines (Ref. 2). This assessment established the probability of burst for the worst-case tube due to TTW predicted for the defined high-wear region.

The U3 wear behavior was used to establish the initiation and growth of TTW indications in U2 steam generators. An empirical correlation based on a wear index parameter (measure of the state of wear degradation in each tube) provided the method for scaling the U3 wear behavior to U2. Two OA analysis cases were evaluated based on the sizing techniques used to define the U3 TTW depths. Case 1 evaluated the situation where voltage based sizing for Eddy Current Testing Examination Sheet ETSS 27902.2 was used to establish the TTW depth distributions and the correlated wear rate with wear index. The results for Case 1 indicate that the SIPC margin requirements are satisfied for a Cycle 17 length of 1.33 years at 70% power level. For Case 2, where the TTW depths were resized by AREVA using a more realistic calibration standard, the SIPC margins will be met for a cycle length of 1.48 years at 70% power level. The plan for U2 is to operate for a short run (about 5 months) at a 70% reduced power level to provide additional margins to the industry requirements for tube integrity.

Tube burst at 3xNOPD is the limiting requirement for cycle length. Therefore, the accident-induced leakage requirements will be satisfied provided that burst margins at 3xNOPD are maintained during the operating cycle.

## Section 1 INTRODUCTION

The San Onofre Unit 2 (U2) plant has two new steam generators that replaced the original CE-70 design. The replacement steam generators are MHI Model 116TT1 and began operation in 2010. The generators have completed one cycle of operation (Cycle 16) with duration of 1.718 years at power. In the first cycle of operation, the U2 tubing has experienced substantial wear degradation at anti-vibration bar (AVB) U-bend supports. To a much lesser extent, wear at tube support plates (TSP) was also detected during the end-of-cycle (EOC) 16 tube examinations. A schematic illustration of the tube supports, AVBs labeled B01 through B12 and TSPs labeled 01C through 07C on the cold-leg side and labeled 01H through 07H on the hot-leg side, is shown in Figure 1-1 (Ref. 3).

While U2 was in refueling, U3 had a forced outage due to a leak in one of the steam generators after 338 days (0.926 years at power or 11.1 months). The leak was subsequently determined to be from tube-to-tube wear (TTW) at freespan locations within the U-bend region. Tube-to-tube wear had affected 161 tubes in 3SG88 and 165 tubes in 3SG89. Wear at AVBs and TSPs was also detected which was far more substantial than that observed in the U2 steam generators. Subsequent examination of U2 steam generators specifically looking for TTW revealed two indications involving contact between these tubes in 2SG89.

Tube-to-tube wear in U3 was caused by in-plane motion of tubes within a defined region of the bundle. The in-plane motion was due to conditions that created fluid-elastic instability (FEI). Because of the same design for both units and the nature of the FEI, the possibility of having further initiation and progression of TTW in U2 must be addressed in the OA. The OA is a forward-looking process and provides an estimate of the operational period by which the steam generators will maintain tube integrity for both burst strength and through-wall leakage.

This report describes the OA performed for the limiting steam generator (2SG89) in U2 for TTW degradation. Probabilistic methods have been employed and a Monte Carlo simulation model has been used for establishing the structural and leakage margins for the tubing for this wear

# Controlled Document

mechanism in a "traditional" manner following industry guidelines. These margins are compared with the structural integrity and leakage performance criteria requirements of Nuclear Energy Institute (NEI) 97-06 (Ref. 1). The performance standards for assessing tube integrity to the required margins are provided in the EPRI Integrity Assessment Guidelines (Ref. 2). This approach established the probability of burst (POB) for the worst-case tube due to TTW predicted for the defined high-wear region as observed in U3.

The scope of this OA is limited to TTW degradation mechanism. The other degradation mechanisms detected during EOC 16 tube examination are addressed in a separate OA performed by AREVA.

The OA was performed by computer analysis using the program TTWEAR\_U2. This program is a special-purpose code and has been verified for project use (Ref. 5). A summary of the verification and validation is described in Section 3.5.

A list of acronyms used in this report is given in Appendix A.



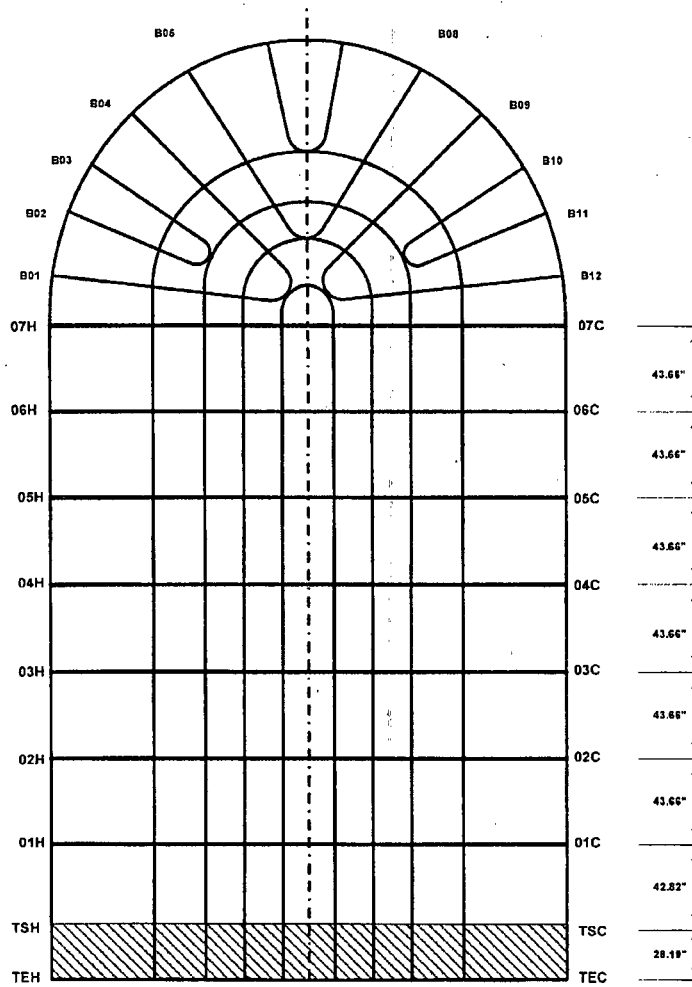


Figure 1-1 SONGS Steam Generator Tube Support Structure Schematic (Ref. 3)

## Section 2 STRUCTURAL REQUIREMENTS

### 2.1 BACKGROUND

In 2006, SONGS adopted the NEI 97-06 "Steam Generator Program Guidelines" (Ref. 1), through a change to the plant Technical Specification, Section 5.5.2.11 Steam Generator Program. The program guidelines specify both condition monitoring (CM) and operational assessment (OA) as a means to manage tube degradation. The preparation of a CM evaluation is a vital element of the NEI guidance and requirements. Condition monitoring provides a comparison between the as-found condition of the steam generators and performance criteria established in Ref. 2. The evaluation of NDE results determines the state of the steam generator tubing for the most recent period of operation relative to structural and leakage integrity performance criteria.

The CM results for U2 at EOC 16 were acceptable for all detected degradation mechanisms including TTW (Ref. 3).

Operational Assessment involves projecting the condition of the steam generator tubes to the time of the next scheduled inspection outage and determining their acceptability relative to the tube integrity performance criteria. All detected degradation mechanisms shall be evaluated, including secondary side inspection results. This OA addresses the TTW degradation mechanism. The required margins for an acceptable OA are discussed in Section 2.2.

### 2.2 STRUCTURAL AND LEAKAGE INTEGRITY

The structural integrity performance criteria (SIPC) and accident-induced leakage performance criteria (AILPC) applicable to any degradation mechanism including TTW are as follows (Ref. 1):

**Structural Integrity** — “All in-service steam generator tubes shall retain structural integrity over the full range of normal operating conditions (including startup, operation in the power range, hot standby, and cool down and all anticipated transients included in the design specification) and design basis accidents. This includes retaining a safety factor of 3.0 against burst under normal steady state full power operation primary-to-secondary pressure differential and a safety factor of 1.4 against burst applied to the design basis accident primary-to-secondary pressure differentials. Apart from the above requirements, additional loading conditions associated with the design basis accidents, or combination of accidents in accordance with the design and licensing basis, shall also be evaluated to determine if the associated loads contribute significantly to burst or collapse. In the assessment of tube integrity, those loads that do significantly affect burst or collapse shall be determined and assessed in combination with the loads due to pressure with a safety factor of 1.2 on the combined primary loads and 1.0 on axial secondary loads.”

**Accident-Induced Leakage** — “The primary to secondary accident leakage rate for the limiting design basis accident shall not exceed the leakage rate assumed in the accident analysis in terms of total leakage rate for all steam generators and leakage rates for an individual steam generator.”

For SONGS, the accident-induced leak rate is 0.5 gallons per minute (gpm) per generator cumulative for all degradation mechanisms.

The acceptance performance standard for structural integrity is (Ref. 2):

The worst-case degraded tube shall meet the SIPC margin requirements with at least a probability of 0.95 at 50% confidence.

The worst-case degraded tube is established from the estimation of lower extreme values of structural performance parameters (e.g., burst pressure) representative of all degraded tubes in the bundle for a specific degradation mechanism.



The acceptance performance standard for accident leakage integrity is (Ref. 2):

The probability for satisfying the limit requirements of the AILPC shall be at least 0.95 at 50% confidence.

The analysis technique for assessing the above conditions for TTW is a fully probabilistic assessment of all tubes in the at-risk region of the U2 steam generators.

### 2.3 TUBE BURST MODEL

Tube-to-tube wear indications involve axial volumetric degradation with limited circumferential extent as shown in Figure 2-1. Given the structurally significant length and depth dimensions, the burst pressure for TTW is computed from the burst relationship for axial wear given in Ref. 4:

$$P_b = 0.58(S_y + S_u)(t/R_i) \left[ 1 - \frac{L(d/t)}{L + 2t} \right] + 291 \text{ psi} + Z\sigma_B \quad (2-1)$$

where  $P_b$  is the estimated burst pressure,  $S_y$  is the yield strength,  $S_u$  is the tensile strength,  $t$  is the wall thickness,  $R_i$  is the tube inner radius,  $L$  is the characteristic degradation length,  $d$  is the characteristic wear depth, and  $d/t$  is the fractional normalized depth. Relational uncertainty in Eq. 2-1 is represented by the standard normal deviate,  $Z$ , ( $-\infty \leq Z \leq \infty$ ), and  $\sigma_B$ , the standard error of regression ( $\sigma_B = 282$  psi). The burst equation, when used with the structural significant dimensions ( $L_{ST}$  and  $d_{ST}$ ), produces consistently conservative burst pressure estimates compared with tube burst data.

### 2.4 LEAK RATE CALCULATION

Leakage predictions for wear-related degradation are subject to large uncertainties. Wear profiles at incipient leakage can vary significantly from simple slits to large holes caused by the blowout of thin membranes. For these situations, absolute leakage rates are not generally

# Controlled Document

computed. Rather, the probability of through-wall penetration is established from projected maximum depths and ligament rupture calculations. A ligament rupture is where the indication pops-through the remaining wall without causing tube burst. For TTW, leakage at limiting accident conditions (i.e., main steam line break) will not be controlling on cycle length. The requirements for burst at SIPC will be set by the distribution of maximum depths being significantly smaller than those necessary to produce ligament rupture (pop-through) events under accident pressures.

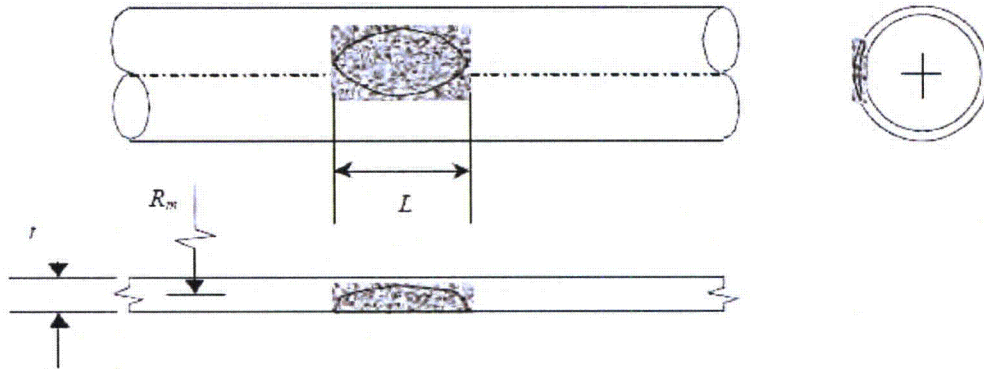


**Figure 2-1 — Idealized Wear Profile for Volumetric Degradation with Limited Circumferential Extent (Ref. 4)**



## Section 3 PROBABILISTIC ANALYSIS

### 3.1 ASSESSMENT OVERVIEW

A "traditional" operational assessment involves the formal analytical evaluation of inspection data in conjunction with a structural (burst) model for comparing the likelihood of tube burst with the SIPC margin requirements. In the same manner, through-wall leakage probabilities must satisfy the accident-induced leak rate limits. An allowable inspection interval is established by demonstrating the SIPC and AILPC margins will be satisfied for the operating period.

For fully probabilistic OAs for TTW degradation, the probability of detection (POD), the wear rate, and initiation function for creating new wear indications are explicitly treated by statistical distributions for direct input to the structural model. In addition, distributions for tubing strength and relational uncertainties on the tube burst model are addressed in accordance with industry guidelines.

The OA for TTW is performed with a simple single-cycle model applied to a defined region where TTW is assumed active. The models for TTW initiation and the determination and assignment of TTW rates will be the critical input variable to the OA. The overall logic for the OA is shown in Figure 3-1.

### 3.2 ANALYSIS ASSUMPTIONS

The following are the major assumptions used in OA model development for TTW and input parameters

- 1) Tube-to-tube wear is analyzed as a random process of independent events based on the state of tube support wear degradation of each individual tube in the high wear region at any point in time during the cycle. This philosophy is a consistent approach used in traditional OAs.

# Controlled Document

- 2) The critical region for evaluation is assumed as a box area defined by Rows 70 to 140 and Columns 60 to 120. This region bounds the high-wear region in the U-bends.
- 3) The state of wear degradation at tube supports for a given tube is assumed to be characterized by the summation of NDE depths at AVBs and TSPs wear locations. This is defined as the "wear index" for a degraded tube. This measure was chosen to capture both the total amount of wear as well as the spatial extent (loss of support from tube-end to tube end), both of which are assumed to be precursors of in-plane tube instability and the on-set of TTW for a given tube. It tracks both the vibratory activity of the tube (indicator of amount of support effectiveness) and the loss of wall thickness which will directly impact the local gaps between tube and supporting structure. Both the existence of TTW and distribution of TTW depths are strongly correlated to the wear index as shown later in Sections 4.5 and 4.6. This TTW behavior observed in U3 supports this modeling assumption.
- 4) The U3 data for TTW is used to define the likelihood of initiating TTW and what will be the TTW growth rate. These data are used to establish the probability of initiation and growth of TTW in U2 through the wear index parameter. Because the TTW degradation is much more extensive in U3 than in U2, use of this approach is conservative.
- 5) Tube-to-tube wear rate is conservatively based on the maximum depths of observed in U3. It is assumed that the TTW in U3 started very early in the cycle so that the growth of TTW occurred over the full cycle. Use of maximum NDE depths to establish TTW rates support this assumption.
- 6) The wear rates for AVB, TSP, and TTW indications are all based on 100% power operation data. This assumption is conservative since operation of U2 for Cycle 17 will be at a reduced power level of 70%.
- 7) The wear rate is based on constant growth on depth rather than constant wear volume basis. This assumption is conservative since wear generally evolves on a constant volume rate basis where the rate of change in depth will decrease as wear progresses.
- 8) It is assumed at the start of Cycle 17, that any tube within the high wear region can initiate TTW including tubes with no detected support wear at the beginning of the cycle. This is a conservative assumption.

- 9) The initiation model of TTW for U2 for operation at 70% power uses the ratio of maximum dynamic pressure to scale the U3 model data. This is supported by vendor analyses on stability ratio and the effect of power reduction on this parameter. This assumption is conservative since it is likely that the potential for tube instability will be significantly reduced to a level where the mechanism will not be active for the planned partial-cycle operation of 5 months.

### 3.3 STATE OF DEGRADATION – WEAR INDEX

The development of TTW is a complex process. In principle, TTW will initiate when the tube becomes unstable in the in-plane direction under local fluid-elastic conditions. In this assessment for U2, TTW is analyzed as a random process of independent events based on the state of degradation of each individual tube in the high wear region at any point in time during the cycle. It is proposed that the proper measure of the state of wear degradation is the observed wear associated with tube supports (AVBs and TSPs). This measure is taken as a direct indicator of both the likelihood of occurrence and severity of TTW during the operating cycle. This is a key assumption in the probabilistic model and relies on the premise that some significant amount of AVB and TSP wear precedes tube instability and subsequent tube-to-tube contact.

The indication of the state of degradation in the model is called the wear index (WI). The wear index parameter relates the observed AVB and TSP wear states of each tube in the high-wear region to both the initiation and rate of growth of TTW. The wear index captures both the total amount of wear as well as the spatial extent (loss of support), both of which are a precursor to potential in-plane tube instability and the on-set of TTW, as well as the severity (rate) of TTW. Wear depth was selected because it physically represents a change (increase) in the gap between tube and supports and would provide a better physical measure of the onset of tube instability than wear volume. In this capacity, the wear index is used as a means to determine the likelihood of having TTW as well as the rate of growth of TTW.

A model for correlating the observed TTW from the AVB and TSP wear states based on a wear index parameter was developed. The individual contributions from AVB and TSP wear to estimating the existence of TTW was also investigated with the single (combined) model as defined by Eq. 3-1 being used as the correlating parameter. It is clear that a strong correlation

# Controlled Document

exists for initiation and growth of TTW with the wear index (see Sections 4.5 and 4.6). The wear index model is based the summation of AVB and TSP wear depths in a given tube.

$$\begin{aligned} \text{Wear Index (WI)} &= \text{AVB Wear} + \text{TSP Wear} \\ \text{WI} &= \sum_{i=1}^{12} [\text{AVB depth}]_i + \sum_{j=1}^{14} [\text{TSP depth}]_j \end{aligned} \quad (3-1)$$

where WI is defined in %TW. This measure was chosen to capture both the total amount of wear as well as the spatial extent (loss of support), both of which is assumed to be a precursor to in-plane tube instability and the on-set of TTW for a given tube. It is physically appealing because it tracks both the vibratory activity of the tube (indicator of amount of support effectiveness) and the loss of wall thickness which will directly impact the local gaps between tube and supporting structure.

The observation of significant AVB wear in U2 with only two TTW initiations in 2SG89 and none in 2SG88 suggests that the wear index can be a viable method for comparison of the future performance of U2 for this mechanism compared with U3 past behavior. The TTW indications were small and were sized at 14% TW by ETSS 27902.2. Resizing by AREVA with a different calibration standard suggests these indications could be on the order of 7% TW.

From the magnitude and pattern of tubes having TTW, both initiation and growth of TTW in U2 will be established from the TTW observations in U3 through the wear index parameter. The end of cycle wear degradation states of U2 and U3 is shown in Figure 3-2. There are many more wear indications especially at higher wear index values for U3 compared with U2. The wear index for U3 was as high as 625 (not shown in the graph). The distribution of wear index for U2 was achieved after completion of full cycle of operation (21 months) whereas the U3 wear indices are from about half that operation time. The tubes with TTW in U2 had a maximum wear index value of approximately 82.

The number of affected supports is reflected in the wear index on a tube-by-tube basis. The extent of wear among the tubes supports is shown in Figures 3-3 and 3-4 (Ref. 6). Figure 3-3 shows a comparison of affected AVB supports between U2 and U3. The average number of AVBs that have contacted the tubes is about three per tube in either steam generator of each unit (see Figure 3-3). However, there was a significantly larger number of AVBs associated with tube contact in U3 compared with U2. For U2, there was only one tube having 9 out of the 12



AVB locations with wear contact. For U3, there were about 15 tubes where all 12 AVB locations exhibited tube contact.

Figure 3-4 shows a similar unit comparison for TSP locations with wear. The average number of affected TSPs is one for U2 and six for U3. Many more TSP locations experienced wear for U3 as illustrated in Figure 3-4.

The U2 data shown in Figure 3-3 and 3-4 for the number of affected wear locations was used to define the likelihood for having potential wear locations in those tubes with no detected wear (NDD). All tubes that are NDD within the high wear region are conservatively assumed to have both AVB and TSP wear present at BOC 17. The number of tube intersections with wear is determined by sampling from the cumulative distributions derived from the histograms for U2. The assumed wear depths at these postulated wear locations are based on the POD for the bobbin probe as discussed later in Section 4.4.

### 3.4 PROBABILISTIC MODEL

A Monte Carlo simulation process was used to solve the probabilistic model for TTW. The simulation process is shown in Figure 3-1, which illustrates one Monte Carlo trial. The probabilistic model includes the processes of initiation, growth, and integrity calculations for the degraded tubes projected to EOC 17. The population contains tubes that are located in the high-wear region. Tubes that have been preventatively plugged based on wear patterns observed in U3 have been removed from the population. This includes Tubes 113-81 and 111-81 in 2SG89 with detected TTW. Therefore, the degraded tubes at BOC 16 include inservice tubes that have detected AVB and TSP wear and tubes that are NDD for any wear within the high-wear region.

The state of degradation of the steam generator tubing is simulated in the model for the total indication population defined in the high wear region of 2SG89. The attributes assigned to each degraded tube are the depth and length of the indications, material properties, and the degradation growth rate. These parameters are treated in a randomized manner and the estimates of burst pressure and leakage are made for each indication of the in the population.

The major steps in the process are:

- 1) Initiation of TTW indications based on the wear degradation state in 2SG89. This is accomplished with the wear index parameter from existing AVB and TSP wear. The initiation of TTW is based on the change in wear index during Cycle 17 as a result of further growth of AVB and TSP wear.
- 2) Define the attributes for each degraded tube for a single trial representing one operating cycle. This includes tube strength properties, the degraded length, and the indication shape factor. This information and the information for the undetected population of wear define the BOC 17 population.
- 3) Growth of the TTW degradation indications for the cycle by sampling from the wear rate distribution dependent on the wear index at the time of initiation. At the end of this step, the EOC 17 degradation indication distribution is defined.
- 4) The set of TTW degradation indications are evaluated for burst pressure and leakage. The degraded tube with the lowest burst pressure is retained for each trial to establish the distribution of worst case values for comparing with the SIPC margin requirements and acceptance standards. Likewise, the leakage probabilities for each trial are retained to determine the 95% probability with 50% confidence (95-50) leak rate for comparison with AILPC.
- 5) In a post-analysis assessment, the POD function can be applied to the degraded tube population at EOC 17 to estimate the number of TTW indications that would be detected at EOC 17.

The simulation process generates a record of the results of all trials performed from which overall burst and leakage probabilities may be inferred and appropriate distributional information obtained.

Discussion and development of the input distributions for the probabilistic model are given in Section 4.

### 3.5 VERIFICATION AND VALIDATION

A special-purpose computer program called TTWEAR\_U2 was developed to perform the Monte Carlo simulation and required calculations as shown in Figure 3-1. The confirmation process of

# Controlled Document

TTWEAR\_U2 followed Intertek APTECH Quality Assurance Procedures for verification and validation of computer software and hardware systems. The main steps followed in the verification process are:

- 1) Line-by-line checking of the coding and logic against the calculation procedure as described in the report.
- 2) Compilation of the program on a different computer using a different compiler by an independent checker. This process verifies hardware compatibility and uncovers code errors and warnings that could be missed in the original code development.
- 3) Checking the program output through statistical methods and selected simulations to establish the output distributions from the analysis subroutines are expected outcomes from the underlying engineering model and statistical input distributions. This is a robust way to verify probabilistic algorithms using the Monte Carlo simulation method.
- 4) Use of a test case for validation the program results against a known outcome. The test case used to validate TTWEAR\_U2 was the Cycle 16 operation for U2 and compare program predictions to the actual EOC 17 NDE results regarding wear index distribution and the number of initiated TTW indications.

The documentation of the verification and validation of TTWEAR\_U2 is given in Ref. 5.

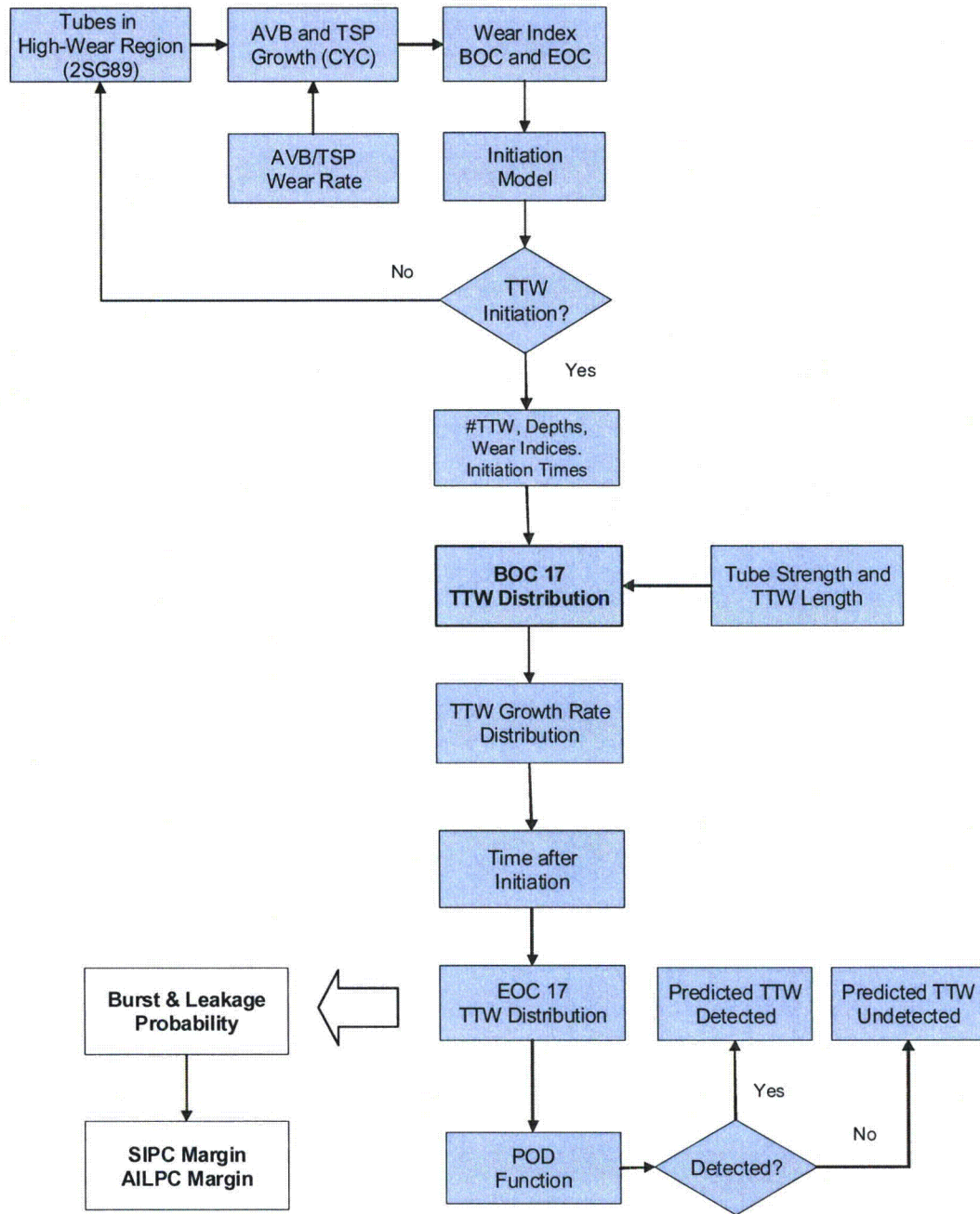


Figure 3-1 — Operational Assessment Logic Flowchart



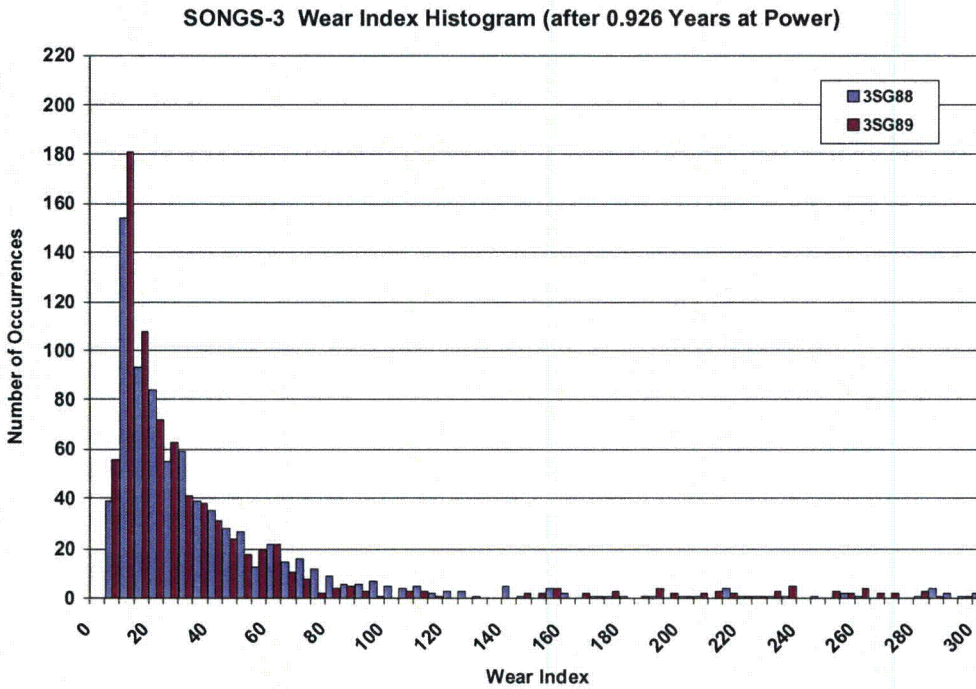
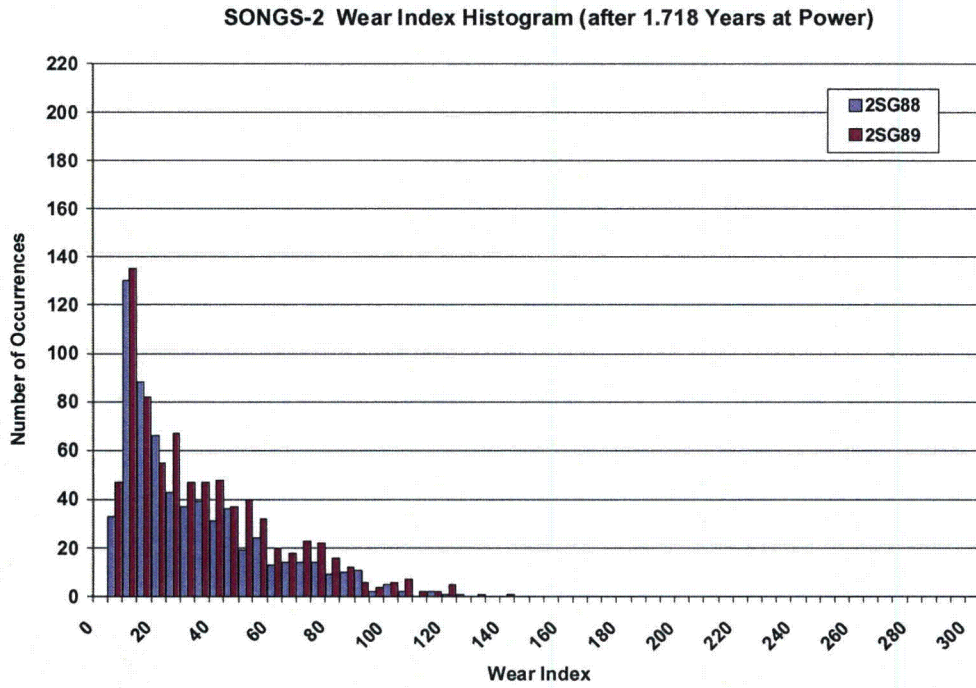
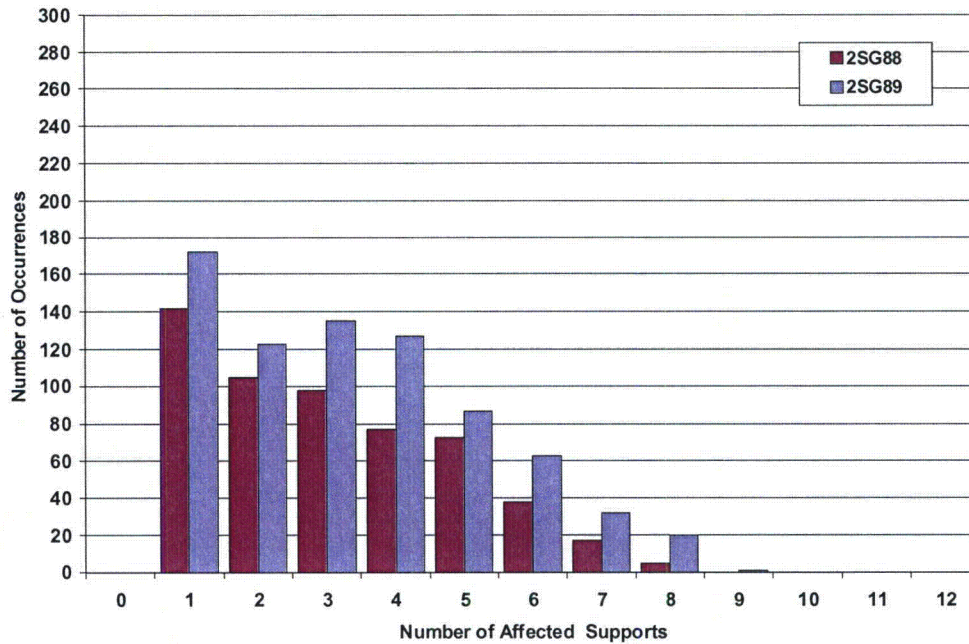


Figure 3-2 — Comparison of Tube Support Wear State for SONGS Units 2 and 3

SONGS-2 Distribution of Wear at AVB Supports



SONGS-3 Distribution of Wear at AVB Supports

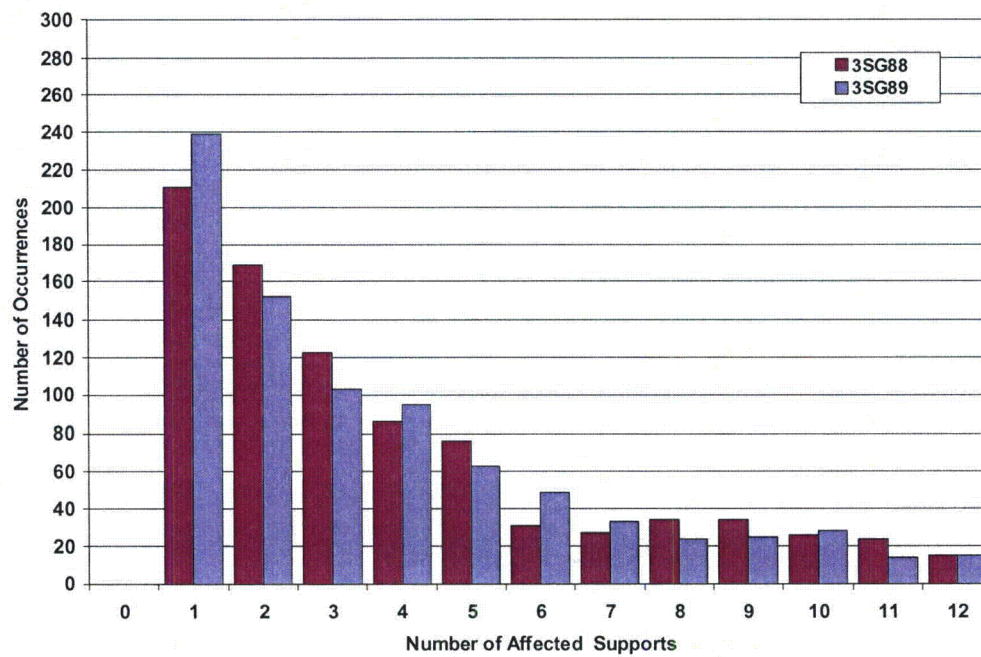
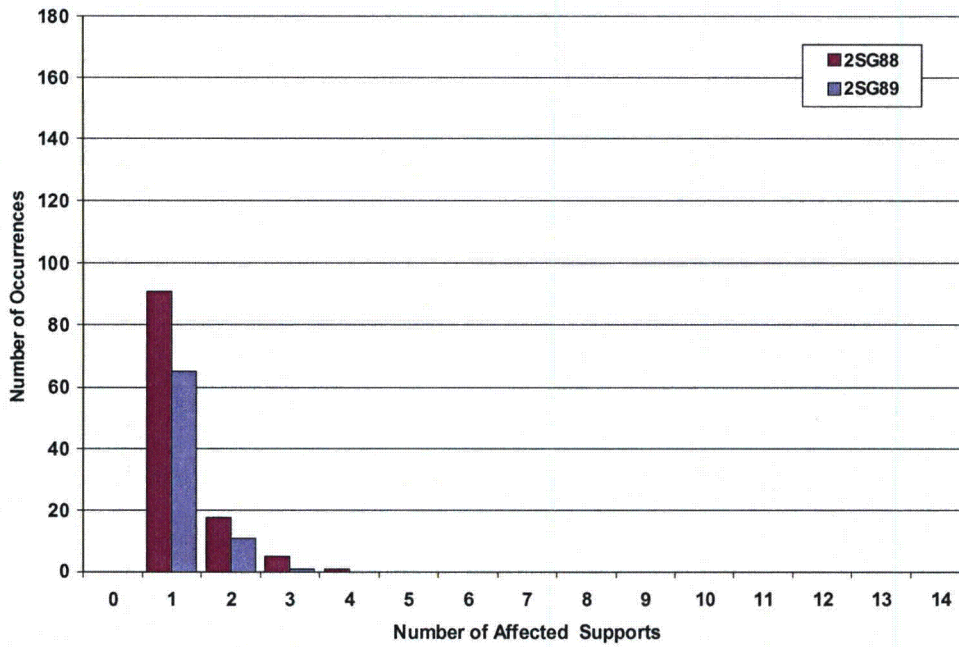


Figure 3-3 — Number of Support Locations per Tube Exhibiting AVB Wear

SONGS-2 Distribution of Wear at TSP Supports



SONGS-3 Distribution of Wear at TSP Supports

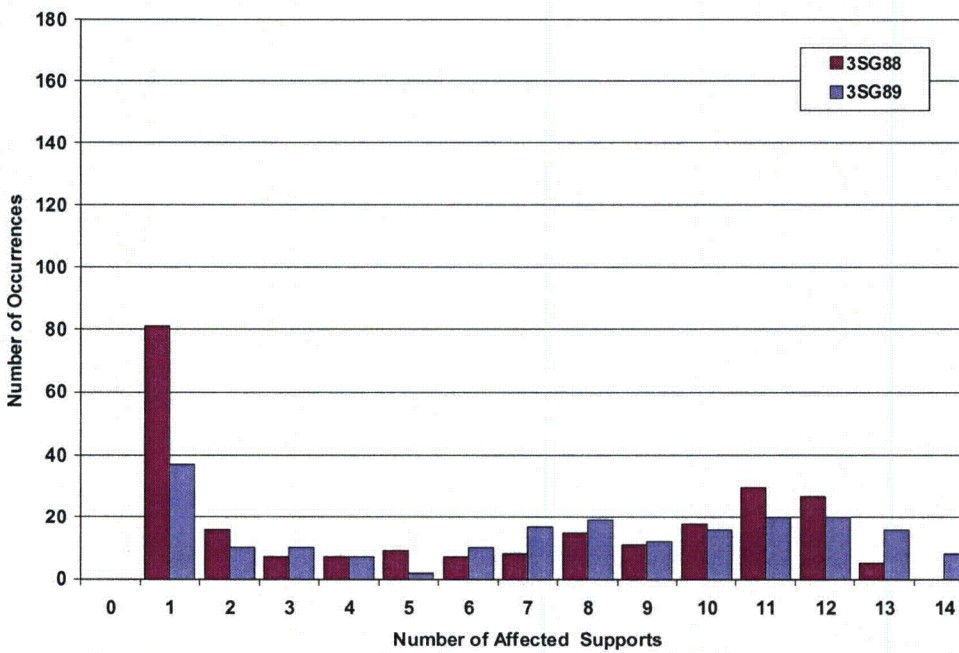


Figure 3-4 — Number of Support Locations per Tube Exhibiting TSP Wear

**Section 4**  
**ANALYSIS INPUT PARAMETERS**

The input parameters for the OA for TTW by fully probabilistic methods are discussed in this section. These include the mechanical strength, degradation characterization (indication sizes and shapes), the probability of detection function (POD) and most importantly, the initiation and growth rate models for TTW indications projected during Cycle 17.

**4.1 TUBING PROPERTIES**

The U2 steam generators have 9727 tubes. The steam generator tubing has an outside diameter of 0.75 inch and a nominal wall thickness of 0.043 inch (Ref. 3). The tube material is Alloy 690 thermally treated (A690 TT). The mechanical properties corrected to a temperature of 650°F were provided by AREVA (Ref. 6b) with the following parameters for  $S_y + S_u$ :

**Tubing Yield plus Ultimate Strength Values (psi)**

Parameter	S/G 88	S/G 89
$S_y + S_u$ (mean)	115,361	116,633
$S_y + S_u$ (St. Dev)	2,023	2,504
$S_y + S_u$ (min)	108,700	109,900
$S_y + S_u$ (max)	121,600	123,900

These values were obtained from the certified material test report (CMTR) data sheets for the supplied tubing. The value for  $S_y + S_u$  for any tube is assumed to be normally distributed with the above parameters for the mean and standard deviation. A plot of the distribution is shown in Figure 4-1.



**4.2 OPERATING PARAMETERS**

Tube pressure differential under normal operating conditions during Cycle 16 was 1430 psi. Three times normal operating pressure (3xNOPD) is therefore 4290 psi. The operating conditions assumed for Cycle 17 are listed below (Ref. 7 through 9).

Cycle Conditions	Operating Length, (Years at Power)	Steam Pressure, (psi)	NOPD, (psi)
Cycle 16 (actual steam pressures at 100%)	1.718	820	1430
Cycle 17 (w/T <sub>COLD</sub> implemented at 100% w/3% plugging)	1.578	925	1325
Cycle 17 (w/T <sub>COLD</sub> implemented with reduced power to 70% w/3% plugging)	1.578	945	1305

For accident conditions, maximum steam line break pressure is assumed at 2560 psi (Ref. 3).

**4.3 DEGRADATION CHARACTERIZATION**

It is beneficial for the OA to focus on the tubes most at-risk to TTW. The numbers of tubes that will be directly affected by TTW are those tubes in the high AVB and TSP wear regions. Wear patterns for AVB and TSP wear encompass the region where TTW was observed and serves as a first cut in defining the size of the at-risk population. A reasonable bound of the TTW region are all tubes within rows 70 to 140, and columns 60 to 120. This at-risk wear region was based on EOC 16 wear patterns for both TTW and AVB wear observed in U3. The table below shows the nature of degradation within the defined high-wear region.

**Summary of Degraded Tubes in the U2 Steam Generators High Wear Region**

Description	2SG88	2SG89
Total Number of Tubes (High Wear Region)	2121	2121
Tubes Plugged	111	211
Number of TTW Indications	0	2
Number of AVB Indications	1706	2537
Number of TSP Indications	146	90
TSP Indications with No AVB wear	72	11
BOC Tubes with Wear Degradation	516	560
BOC NDD Tubes	1494	1350

# Controlled Document

It should be noted that five additional tubes in the high-wear region are being preventably plugged: two in 2SG88 and three in 2SG89. This would mean there are actually 113 and 214 tubes removed from service in 2SG88 and 2SG89. The OA contains the three tubes in 2SG89 in the evaluation.

Given the more adverse numbers in 2SG89 and the fact that two TTW indications were detected, 2SG89 is selected as the limiting steam generator for the OA. It will therefore be reasonable to use the NDE data from 2SG89 to establish input distributions for number of degraded tubes and estimated future wear behavior. The number of tubes included in the OA is (Ref. 6 and 10a):

Tubes with existing support wear	560
Tubes with no detected wear	1350
Tubes removed from service	211

Wear at AVB and TSP supports will be randomly assigned to the NDD tubes using the cumulative distributions developed from past observed active wear for 2SG89 shown in Figures 3-3 and 3-4 (Ref. 6). Depths for these wear indications are defined by the POD performance for the bobbin probe (see Section 4.4).

The shapes of the indications were determined by line-by-line +Point™ sizing for U3 tubes exhibiting TTW. The shape factor parameter ( $F$ ) is defined as the ratio of maximum depth of the indication to the structural average depth of the indication,  $d_{MAX}/d_{ST}$ . The shapes were relatively flat ( $F=1.0$ ) with long structural lengths.

The structural lengths ( $L_{ST}$ ) as determined by the structural-minimum method using the profile data from U3 is shown in Figure 4-2 (Ref. 11). The structural lengths represent the burst-effective lengths from each TTW indication and range between 1 to 8 inches. The cumulative distribution (CDF) of these data is fitted to a lognormal model. This CDF will be sampled in the simulation analysis to define the length of each TTW indication that is calculated to initiate during Cycle 17.

**4.4 PROBABILITY OF DETECTION**

**4.4.1 Inspected Population**

The probability of detection performance of the bobbin probe shows that it is capable of reliably detecting AVB wear, TSP wear, and TTW indications in the U-bends. The probability of detection for eddy current test techniques has been established from industry data and made available through published ETSS data. For ETSS 96004.1, Rev. 13 (Ref. 12), the expected POD performance is shown as a log-logistic function in Figure 4-3. For comparison, the expected performance for +Point™ inspection (ETSS 27902.2) is also plotted in Figure 4-3 (Ref. 13). The log-logistic model for POD (Ref. 2) and the parameters for the examination techniques used for support and TTW, are given below:

$$POD(h) = \left[ \frac{1}{1 + \exp[A + B \text{Log}(h)]} \right]$$

Probe	ETSS	Intercept (A)	Slope (B)
Bobbin	96004.1	10.61	-11.20
+Point™	27902.2	14.24	-17.22

where  $h = d/t$  and is the degradation depth in % TW. The parameters for ETSS 96004.1 were derived from hit-miss ECT data used to establish the ETSS data statistics. The parameters for ETSS 27902.2 were estimated from the tabular data set in ETSS 27902.2. These data show one missed call at 5% TW depth (0 out of 1 fractional detected) and 100% hit rate (47 out of 47 fractional detected) for depths from 8% to 86% TW. To estimate the POD, a 0.1 fractional detection rate was given to the one missed call at 5% TW and a 0.8 fraction detection rate assigned to 8% TW depth. The log-logistic equation was fit to these two detection levels giving the curve shown in Figure 4-3.

Tubes within the high-wear region that had significant AVB and TSP wear in U2 had received bobbin probe examination. Subsequent to the U3 inspection findings, supplemental +Point™ inspections were performed in U2 to specifically look for TTW with an improved POD. Two TTW indications were found in 2SG89 and none were detected in 2SG88. Therefore, the most

# Controlled Document

susceptible group of tubes within the high-wear region has been thoroughly examined with a more sensitive inspection with an improved POD.

## 4.4.2 Undetected Population

It is appropriate to use the POD model to define the undetected indications for the BOC population. A reasonable assumption is to use POD performance for some reasonably conservative level to assign the depth of any undetected indications. This can be used for AVB, TSP, and TTW indications as required for the OA model.

The model addresses three possible scenarios for including additional wear for tubes in the high wear region:

- 1) Tubes with no detected wear (NDD) that may have low level of wear at tube supports (AVB and TSP)
- 2) Tubes that may have support wear but may develop additional wear locations in the during Cycle 17
- 3) Tubes that may have undetected TTW

For the NDD tubes within the high-wear region, degradation sites are assigned by the expected number of AVB and TSP locations that may develop wear during Cycle 17. The depth of degradation is defined by the bobbin probe POD performance for an assumed low POD level.

$$\text{Log}_{10}(h) = \frac{\text{Ln}\left[\frac{1}{\text{RN}(\text{POD})} - 1\right] - A}{B} \quad (4-1)$$

where

$h$  = wear depth equal to  $(d/t)$ , (% TW)

POD is the assumed performance level for NDD ( $\text{POD} \leq 0.05$ )

RN is a randomly selected number between 0 and 1.

A and B are constants (intercept and slope) in the log-logistic function for the bobbin probe POD

The depths are determined by a random process with this equation used for each active wear location (AVB and TSP) in the 1350 NDD tubes. The bobbin probe POD is used in this process.

# Controlled Document

For the 560 tubes where TTW may have initiated during the prior cycle (Cycle 16), Eq. 4-1 is applied with the +Point™ parameters.

Past operating experience for a similar replacement steam generator provided data on the evolution of tube support wear after two cycles of operation. It has been observed that the number of AVB supports that develop wear in the second cycle of operation can increase dependent on the number of worn AVB locations at the beginning of the second cycle. These data were used in the OA to add AVB locations at the start of Cycle 17 from a statistical representation of these data. It is also observed that number of TSP locations in a given tube do not increase so only AVB wear locations are modeled with increasing affected numbers. When new AVB wear locations are added to a given tube, wear is assumed to start at BOC 17 from an initial zero depth. Wear from all AVB and TSP supports (including the newly added AVB support locations) are used in computing the wear index for the tube.

For undetected TTW, the initiation model for TTW is used to define the situations where there may have been TTW that went undetected at the EOC 16 inspection. When pre-existing TTW is determined, depths are randomly assigned using Eq. 4-1 with the +Point™ POD performance parameters at the lower 5% detection level. Additional discussion on the model prediction of undetected TTW is provided in Section 4.5.

## 4.5 TUBE-TO-TUBE WEAR INITIATION

This section describes the development of a fundamental empirical model necessary to describe the presence and expected growth rate for TTW on a specific tube, based on the presence and magnitude of existing AVB and TSP support wear on that tube. It relies on the observed TTW at U3 in order to construct the appropriate Cycle 16/17 model for U2.

In principle, TTW will initiate when the tube becomes unstable in the in-plane direction under local fluid-elastic conditions. It is assumed that the existence of TTW in U3 after operating 0.926 years at power can be used to form the basic fundamental model for predicting TTW in U2. This prediction model for TTW will be constructed as a time-to-initiate function based on the likelihood of having TTW for a given wear degradation state. The correlating factor between the two units is the wear index (see Section 3.2). Since the state of wear degradation in U2 is significantly less than that for U3, an adjustment to the distribution describing the existence of TTW in U3 will be required. This is accomplished by benchmarking the model from the U3 data



# Controlled Document

set of many existing TTW indications, to give approximately the same number of detected TTW indications at EOC 16 for U2, specifically two indications in 2SG89. Because we want the initiation model to account for both detected and undetected indications, the benchmarking process will include the POD model behavior at the appropriate detected depths.

The initiation of TTW was established through an empirical model that relates the probability of initiation (POI) and subsequent growth for TTW based on the wear index parameter. The wear index parameter relates the observed AVB and TSP wear states of each tube in the high-wear region to the POI and rate of growth. The wear index parameter is the calculated sum of all AVB and TSP wear depths in a given tube. Wear depth was selected because it physically represents a change in the gap between tube and supports and would provide a better physical measure to the onset of tube instability than wear volume.

The initiation model was developed using a U3 data base consisting of tubes within a high-wear region of steam generators 3-88 and 3-89 (Ref. 10a). The data base consisted of all records where wear was detected at any of the 26 supports (12 AVB and 14 TSP), and where TTW had occurred or had not occurred. Tube-to-tube wear depths were included where the phenomenon was present. For the correlation work, an AVB index was determined, which was simply a summation of NDE AVB wear depths for a given tube. A TSP index was also computed which was the sum of NDE TSP wear depths. The tube wear index was defined as the sum of the AVB and TSP indices.

The resulting database was partitioned into two groups, one containing TTW indications (initiated) and the other which had no TTW indications (non-initiated). From a data regression point-of-view, this problem is analogous to that of probability of detection. In both situations, the dependent variable is dichotomous (hit/miss). Although a logistic regression is the preferred tool for this particular type of correlation work, a Beta distribution was found to be a better model for representing the U3 data. The Beta distribution has additional fitting parameters that provide more flexibility (degrees of freedom) in fitting both the lower and upper tails of the data distribution.

Two models for correlating TTW presence with wear index are shown in Figure 4-4. The first model distribution, which lies to the left, was developed from the complete data set (both generators) for U3. This model represents the likelihood of having TTW for a given wear index value. The second model is the one developed for U2 based on U3 data set but is

# Controlled Document

benchmarked to replicate the two detected indications at EOC 16. This benchmarking was necessary because simulations with the more conservative U3 model combined with U2 wear indices resulted in many more initiations of TTW at EOC 16 than were observed in 2SG89 and 2SG88. This alone, provided evidence enough to reject the more conservative model.

This adjusted model was obtained under the following constraints:

- 1) All 2SG89 tubes with wear in the high-wear region at EOC 16 were used as the defined benchmarking population (total of 771 tubes).
- 2) Number of tubes with TTW for benchmarking will be based on POD considerations where only two indications (~7% TW) were detected in the 771 tubes. The lower limit for detection for ETSS 27902.2 is around 5%TW as illustrated in Figure 4-5. For this depth size, the POD is about 0.12.
- 3) Both the base (U3) and adjusted (U2) models should give approximately the same number of existing TTW indications observed in U3 when the U3 wear state is used in the model. This is to ensure that the frequency of TTW for U2 will approach that of U3 in the extreme case of high wear indices.

The two indications found in 2SG89 were sized at 7% TW following review of the NDE results. For the +Point™ POD, the probability of detecting a 7% TW indication is on the order of 50-50 as shown in Figure 4-5. However, the data set for ETSS 27902.2 had limited data in this size range with one flaw at 5% TW being NDD and the next larger flaw at 8% TW being detected. To provide for a conservative model benchmark, the POD for a 5%TW flaw is used which corresponds to a one chance in eight for discovery. Therefore, the model was calibrated to predict about 16 indications on average so that approximately two of them would be detected as was the case for 2SG89.

The benchmarking was done iteratively by progressively changing the U3 model parameters to shift the POI curve to the right while having the two models converging together at the higher wear index values. This was accomplished by filtering some of the initiated (hit) data at the low wear index values. These data points were not removed arbitrarily. A careful examination of the data base revealed a common element among the low index value hits. They were almost all at endpoints of a string of TTW instances. The indices for the remainder (interior) of these

# Controlled Document

strings were much higher, strongly suggesting that these endpoint tubes were not where the instability initiated but were victims of other initiation events. The simulation results of the benchmarking process are shown in Figure 4-6.

As a final benchmark, the adjusted model was applied to the wear indices for U3. The number of tubes having TTW in both 3SG88 and 3SG89 is 326. The adjusted POI model predicted 290 initiations, which is close to the number of tubes with TTW in U3. When the U3 POI model is used with U3 wear data, 315 tubes with TTW is computed. This serves as confirmation that the U2 initiation model converges to U3 behavior as the state of wear approaches that seen in U3. The final results are shown below:

**Average Number of Initiated TTW Model Indications**

First Cycle Degradation State	U2 POI Model	U3 POI Model
U2 Wear Index (2SG89)	16	34
U3 Wear Index (Both SGs)	290	315

The U2 initiation model is implemented in a way that both the POI and the time when initiation occurs can be established. Since there is a possibility that TTW may exist undetected in the BOC 17 tube population, the initiation model was adapted to determine under what conditions TTW is pre-existing. Figure 4-7 is an illustrative example on the estimation of the time of initiation for TTW and identifying cases where TTW initiated in Cycle 16 and was undetected. The POI curve is the adjusted model for U2 at 100% Power. For illustrative purposes, the wear index for BOC and EOC for a tube is shown. The condition for initiation of TTW is determined by a random process with the outcome of three different trials shown. The situation for no initiation occurs when the EOC wear index is insufficient to produce TTW for that trial (random sample produces number greater than POI curve).

For cases where initiations are predicted sometime during the cycle but not at or before BOC, the point of initiation is computed from the intersection between the random trial parameter with the POI value for the model function as shown by the middle dashed line. In this situation, initiation is calculated to occur at a wear index between BOC and EOC values. The point in time is determined from the interpolation on the wear index with operating time. The TTW indication is assumed to start growing at the point of initiation with an initial depth of zero and at a wear rate determined from the wear index value at the time of initiation.

The bottom horizontal dashed line shows the situation when initiation occurred during the prior cycle (Cycle 16). For this sample trial, the point in time in Cycle 16 when TTW began can be determined. However, because the tube was NDD at EOC 16, the TTW indication is assumed to begin growing at BOC, with a starting depth determined by a random selection process from the lower 5% tail of the POD curve, and with a wear rate determined from the BOC wear index value. The time of growth is the full cycle length.

When the U2 POI model is applied to a full cycle of operation at 100% power, the model predicts about 50 to 70 TTW initiations by EOC 17. The initiation events are roughly uniformly distributed over the cycle. It is assumed that all tubes in the high-wear region (1910 tubes) have the potential to initiate TTW indications and the indications are subject to growth immediately following initiation.

## **4.6 DEGRADATION GROWTH RATES**

Wear rates for three mechanisms are required for the OA of TTW. The required wear rate distributions are for AVB wear, TSP wear, and TTW. The wear rate is conservatively based on a constant growth in depth.

### **4.6.1 AVB and TSP Growth Models**

The AVB and TSP wear rates are necessary to track the increase in wear index for each tube in the BOC population. The wear rates for AVB degradation were developed from EOC 16 NDE data (Ref. 6). The extent of wear as observed at each of the 12 AVB and 14 TSP tube intersections for U2 is shown in Figure 4-8. It can be seen that there are three distinct groups among the AVB locations where wear rates are substantially different. For Group 1 (B01, B02, B11, and B12), the detected wear depths are less than 15% TW. For Group 2 (B03 and B10), wear depths are elevated and numbers have increased. For Group 3 (B04 through B09), AVBs wear depths are larger and in greater numbers at the middle supports. This suggests the main interactions between tubes and AVBs are in the upper support structure. Wear rates for the three groups are plotted in Figure 4-9 for the two steam generators. As expected, the apparent wear rates for Group 3 are higher on average and in the extremes than Groups 1 and 2. A

# Controlled Document

similar wear rate determination was performed for TSP wear and a combined generator model for TSP wear rate was developed.

The final wear rate distributions for AVB and TSP wear are shown in Figure 4-10. The AVB wear rate distribution was developed using Group 3 data from both steam generators to provide a conservative growth model for this mechanism. The fitted function uses a lognormal statistical model for sampling in the simulation.

## 4.6.2 TTW Growth Model

The wear rates for TTW are defined from U3 data. Such rates can be scaled to U2 based on the state of wear using the wear index. Specifically, the extent of both AVB and TSP wear is much less in U2 after 22 months of operation compared with U3 after 11 months of service.

The growth rate model developed from the U3 data base utilized +Point™ data from tubes with freespan wear indications. Such rates are correlated to U2 based on the tube wear index. When all data were examined including tubes which had multiple TTW, large scatter was observed. To address this situation, only the maximum wear depths observed in the tubes were used to define a conservative measure for growth. Since only one TTW indication in a tube is assumed in the assessment, use of the maximum wear depth is appropriate.

The maximum TTW depth has a direct relationship with the observed wear at tube supports over the domain of wear index values. This is shown in Figure 4-11 for depth sizing using ETSS 27902.2 (Ref. 13). A second sizing method was used to explain better the measured sizes with ISPT results. The sizing technique was developed by AREVA using a different calibration standard built by AREVA (Ref. 14). The final sizing technique uses the lower portion of the AREVA sizing curve but fixes the upper part of the curve adjusted to match the 7.54 volt, 100% TW indication in 3SG88. The depth distribution versus wear index for the "AREVA" resizing is also shown in Figure 4-11. The regression fits for both data sets are given below:

$$\text{Depth} = 17.257 + 0.0703 \text{ Wear Index} \quad (\text{ETSS 27902.2 Sizing})$$

$$\text{Depth} = 12.747 + 0.0701 \text{ Wear Index} \quad (\text{AREVA Resized})$$



The scatter in the data at any given wear index shows central tendency so that linear regression error can be statistically defined. The residuals from the regression analysis are well modeled by a normal distribution over the range of interest for wear index. The relational error for both regression models is normally distributed with a mean of zero and a standard deviation of 10.99% TW. The distribution plots of the residuals from the regression analysis are shown Figure 4-12.

The effective TTW growth rates are ultimately computed by dividing the sampled depth from the above relations by the actual cycle length for the first U3 operating period after replacement (0.926 years at power). The TTW growth rates as a function of wear index are shown in Figure 4-13.

#### 4.7 EFFECT OF POWER REDUCTION

It is intended that U2 will begin Cycle 17 operation with power level reduced to 70%. It is expected that the effect of power reduction on dynamic pressure ( $\rho v^2$ ) will have a net beneficial effect on TTW initiation and tube burst probabilities. The maximum dynamic pressure acting on the U-bends decreases significantly with power level. At 100% power,  $\rho v^2$  is 4,140 N/m<sup>2</sup> (Ref. 15). At 70% power, the dynamic pressure reduces to 2,430 N/m<sup>2</sup>. This is a reduction factor (RF) of 0.586. This reduction factor on dynamic pressure is employed in the initiation model for TTW as a direct multiplier on POI where,

$$POI_{70\%} = \frac{\rho v^2|_{70\%}}{\rho v^2|_{100\%}} POI_{100\%} = 0.586 POI_{100\%}$$

The above equation is the assumed behavior for POI model based the uniform population risk reduction using combined probability for 70% power operation. The effect of power reduction will be conservatively assumed to have no lowering effect on AVB, TSP, and TTW wear rates. Consequently, the wear rate distributions for the active wear mechanisms will be based on observed wear at 100% power. The above assumption can be relaxed for future cycle assessments when sufficient data become available to justify attenuation in wear rates at reduced power operation.

As technical basis for using maximum dynamic pressure as a means for reducing the initiation behavior for TTW, the reduction in  $\rho v^2$  at 70% power was compared with the in-plane stability ratios computed by MHI (Ref. 7). The evaluation of stability ratio (SR) to mitigate FEI was studied for different power levels (50% to 100%) and for various support configurations (i.e., number of consecutive AVB supports that are no longer effective due to loss of contact force).

For comparing SR with the reduction in  $\rho v^2$ , the ratio of stability parameter at reduced power to the same parameter at 100% was used as another measure of improvement on POI. A plot of the evaluated tubes in the MHI assessment is shown in Figure 4-14. As can be seen, the normalized stability ratio decreases monotonically from 100% to 50% power levels for the range of support effectiveness. At 70% power, the normalized SR for the various cases when supports are modeled as inactive falls between 0.528 and 0.652 with an average value of 0.608. The ratio on  $\rho v^2$  falls within the scatter for normalized SR and represents a reasonable estimate of the effect of power reduction on initiation. Equation 4-2 is therefore used in the OA to account for the benefit of reduced power operation during Cycle 17.

## 4.8 MEASUREMENT UNCERTAINTY

Measurement uncertainty for sizing of indications is defined in the ETSSs for estimating actual (true) structural parameters (depth and length) from NDE size data. The OA procedure was constructed so that adjusting for measurement error will not be required. Wear index and any correlations between SONGS units is consistently based on NDE data. Initial depths assigned at BOC are actual values. Growth applied to BOC depths during the cycle are derived from +Point™ depth sizing (ETSS 27902.2) where the systematic error from linear regression is very small. Therefore, sizing uncertainty is not significant for estimating TTW rates.

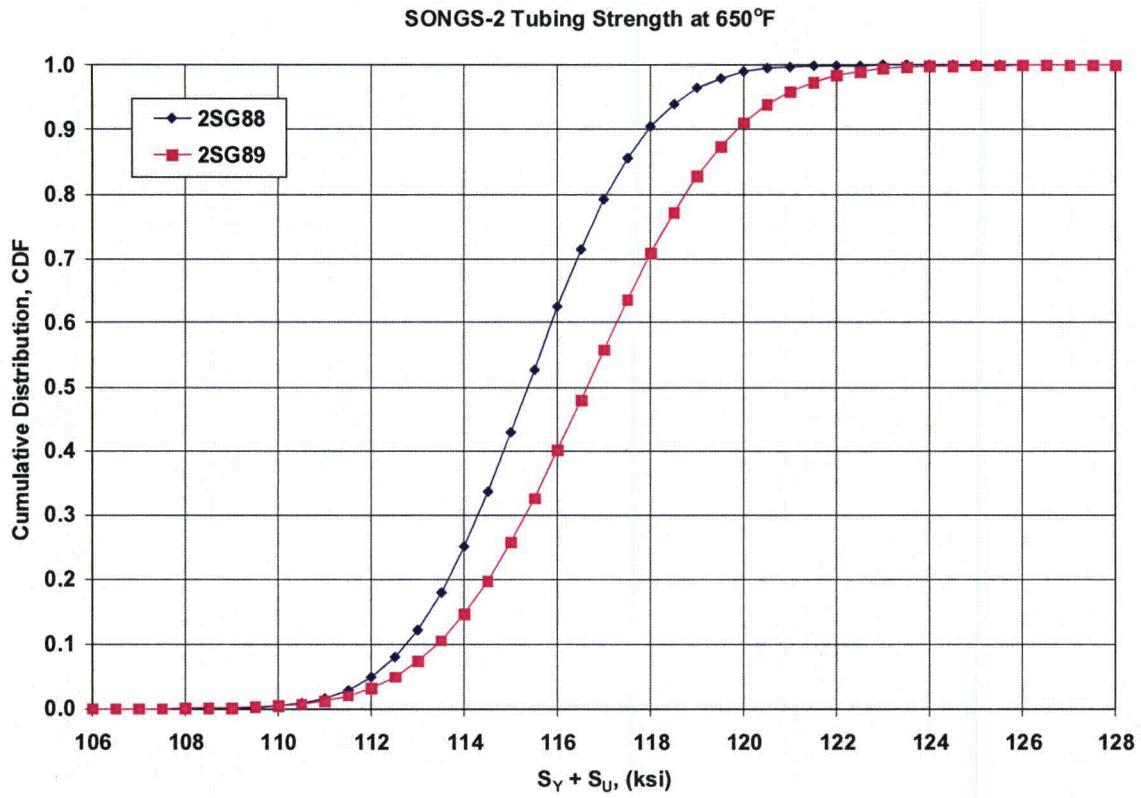


**Figure 4-1 — Distribution of Tubing Strength Properties at 650°F**

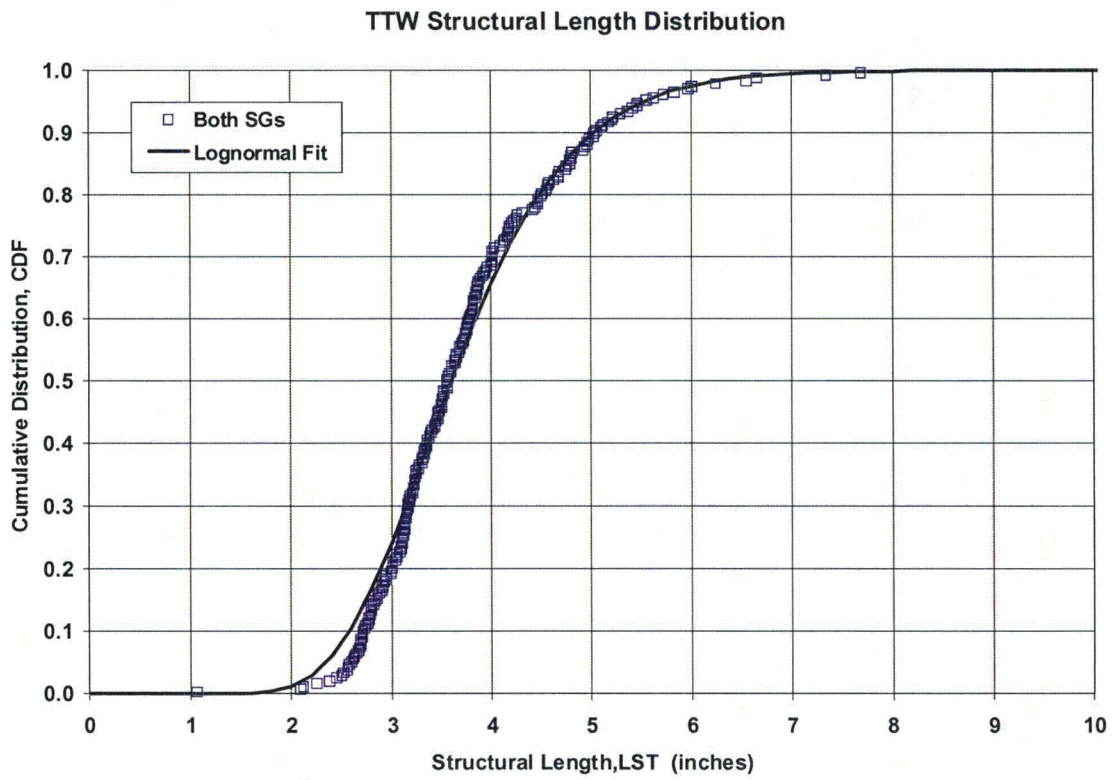


Figure 4-2 — Structural Length Distribution for TTW in U3

SONGS ECT Techniques

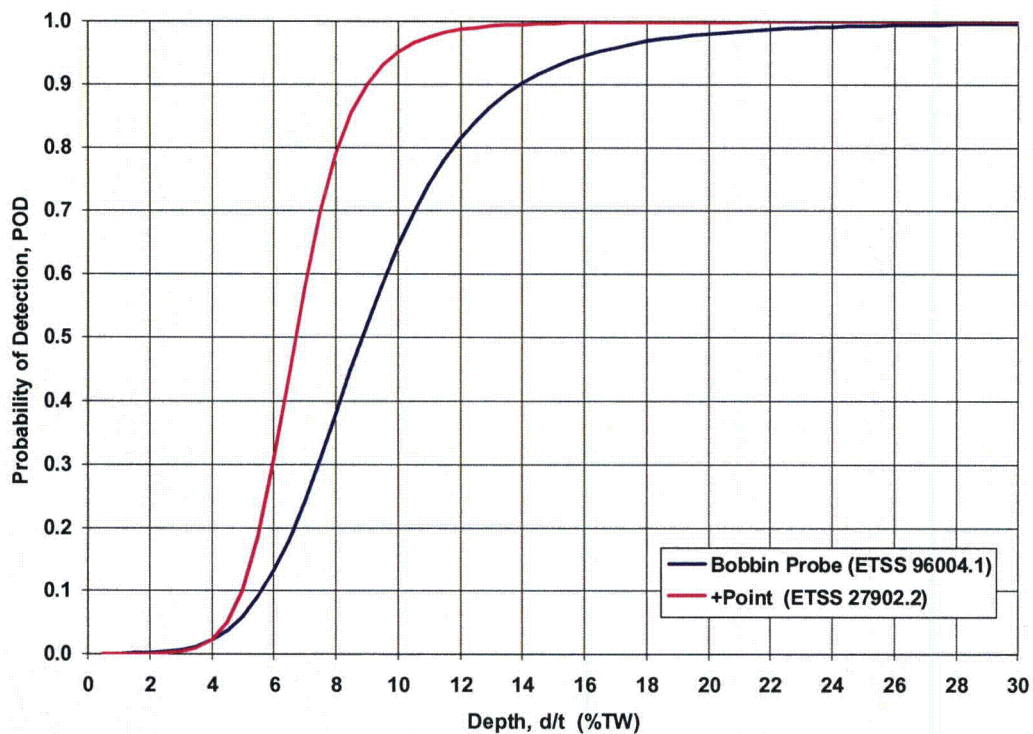


Figure 4-3— Probability of Detection for Tube Wear



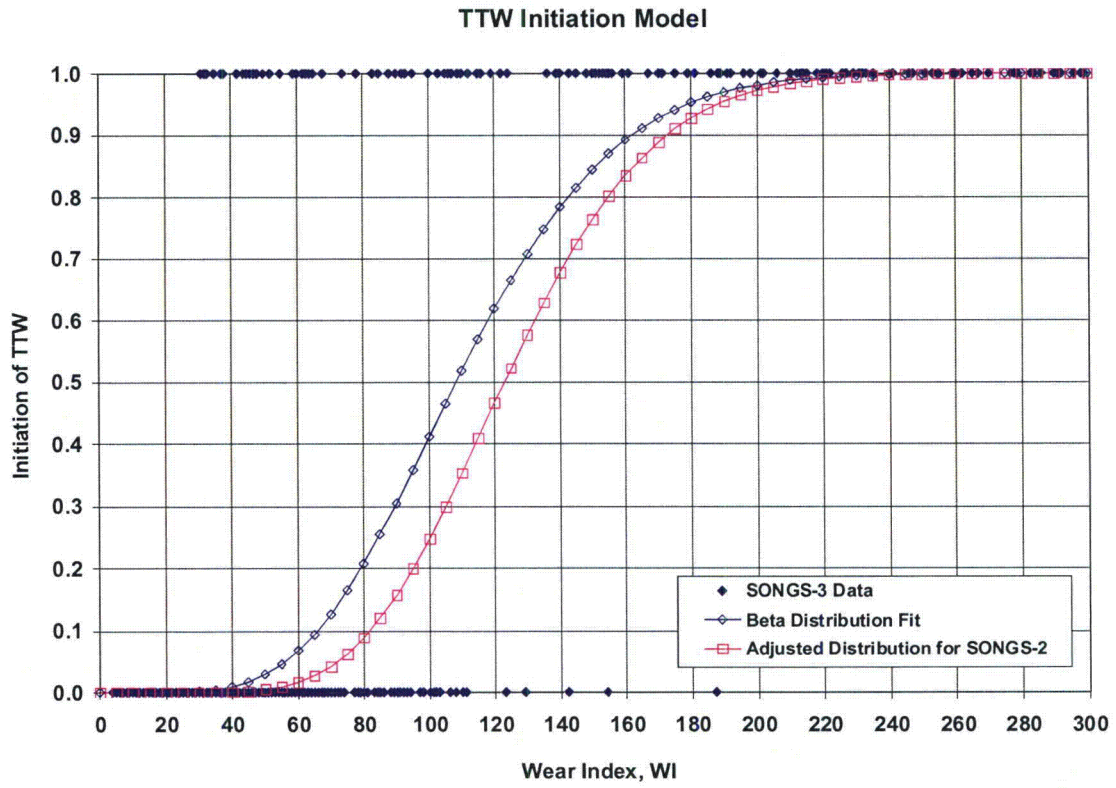


Figure 4-4— Tube-to-Tube Wear Initiation Model Based on Wear Index

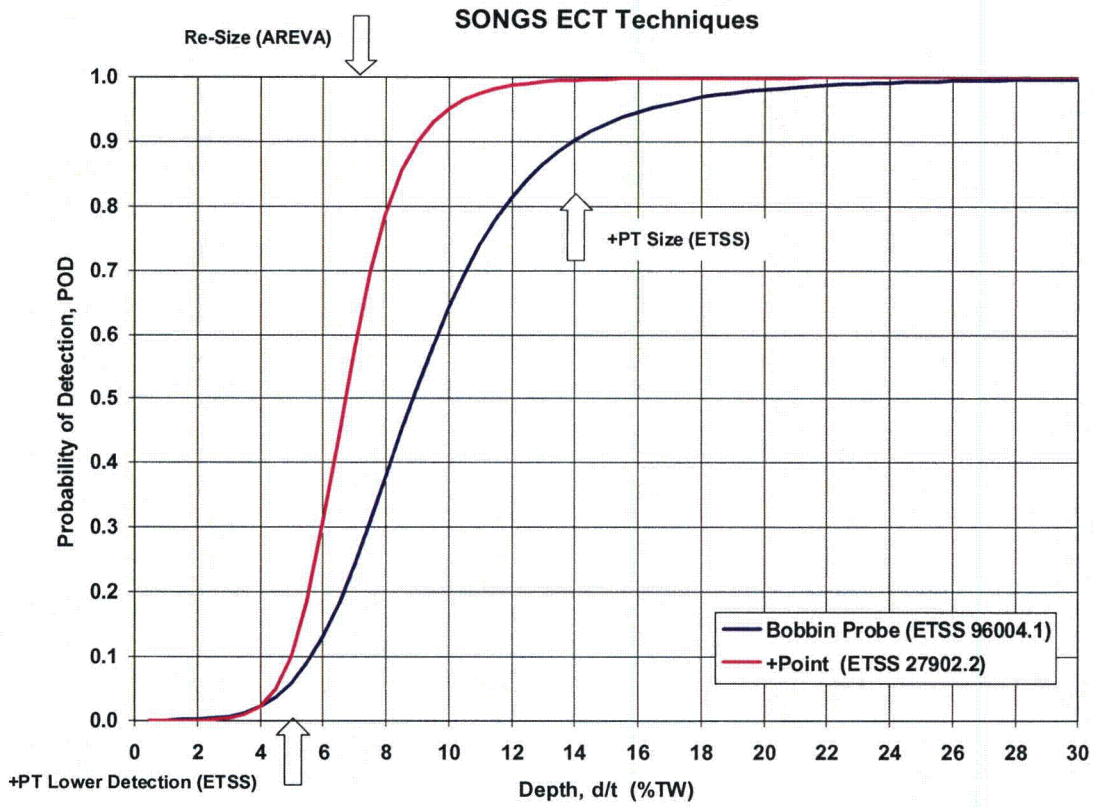
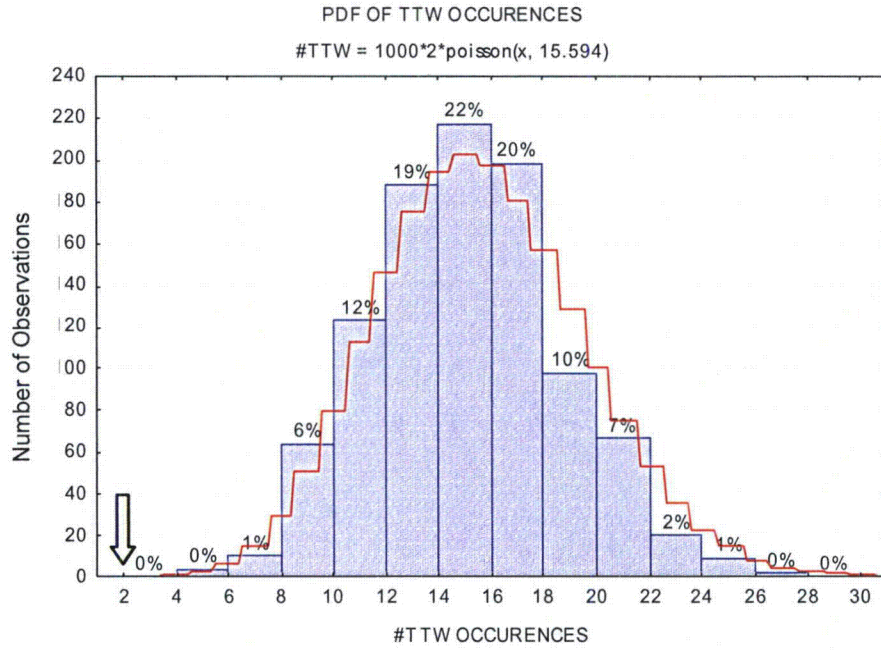
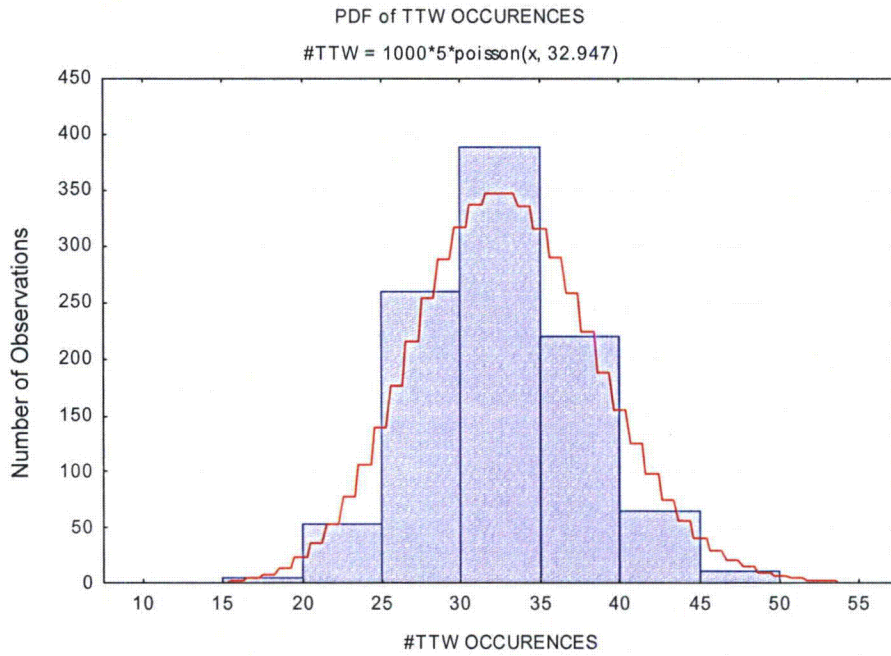


Figure 4-5 — Tube-to-Tube Wear Initiation Model Based on Wear Index



a) U2 Model TTW Occurrences Benchmark Results



b) U3 TTW Occurrences Model Prediction

Figure 4-6 — Initiation Model Adjustment for U2

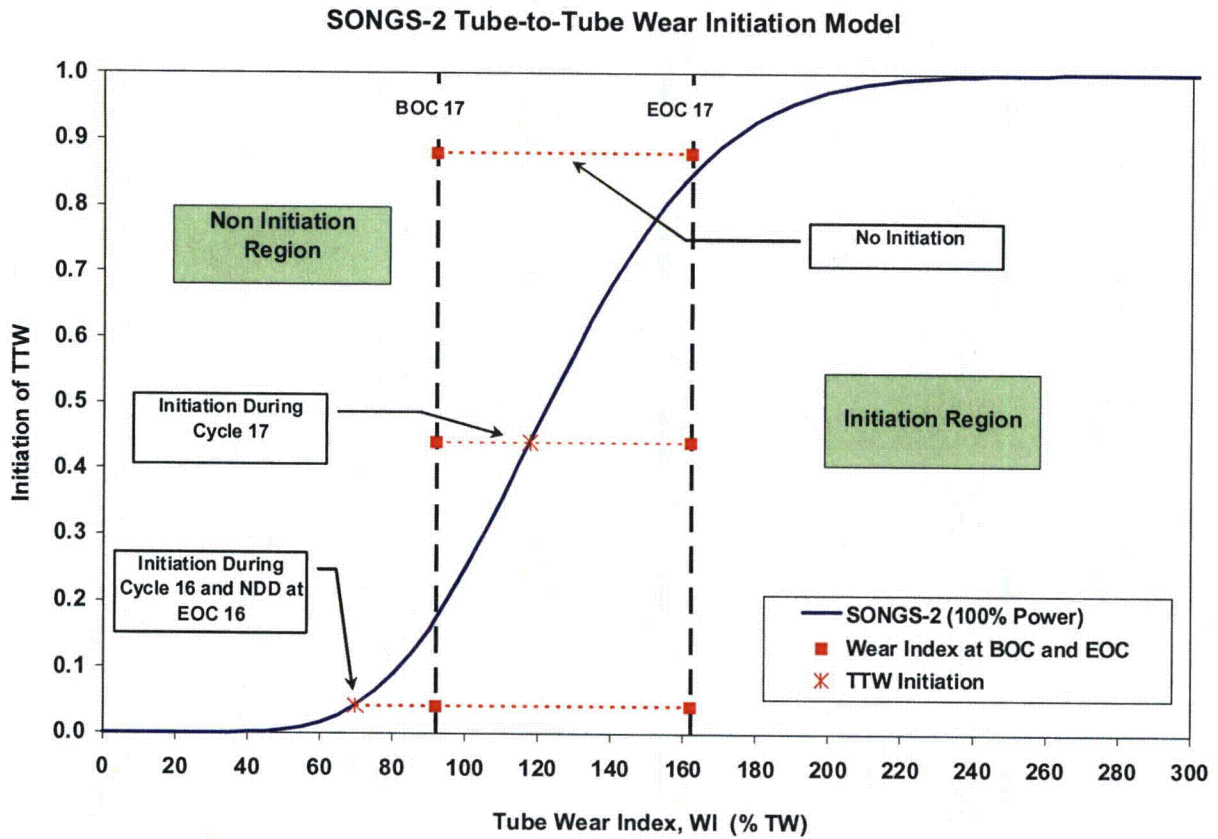
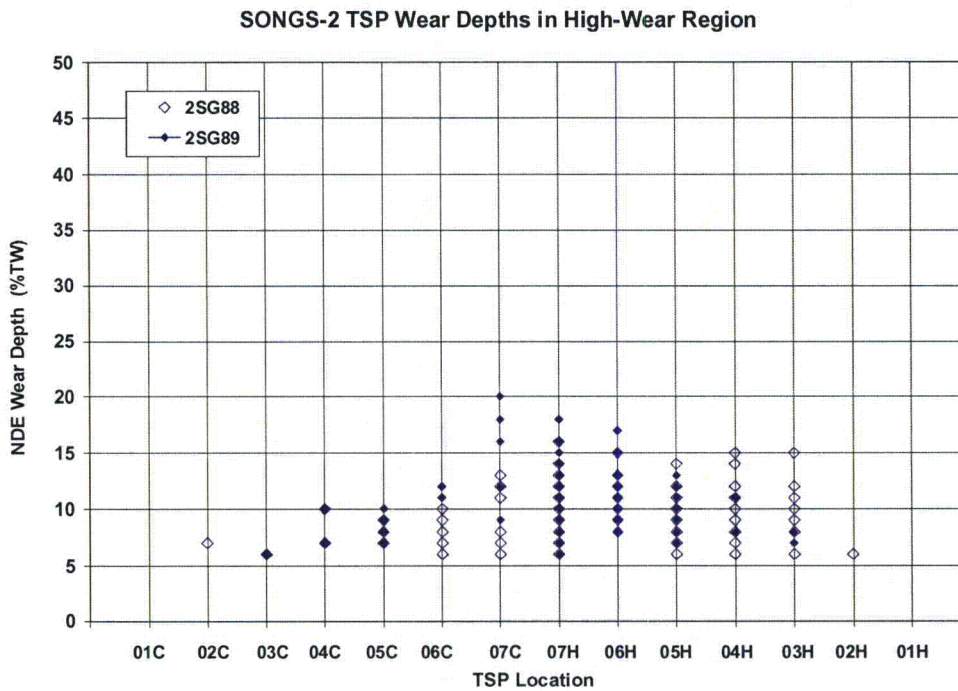
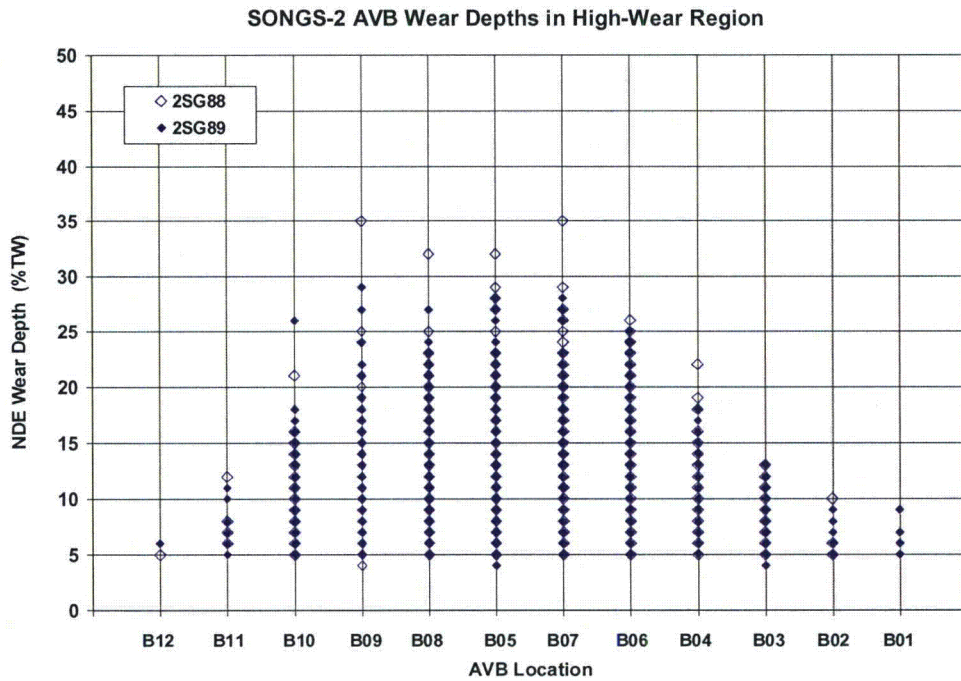


Figure 4-7 — Illustration of TTW Initiation Time Model Estimation





**Figure 4-8 — NDE Depth Distributions for AVB and TSP by Support Location**



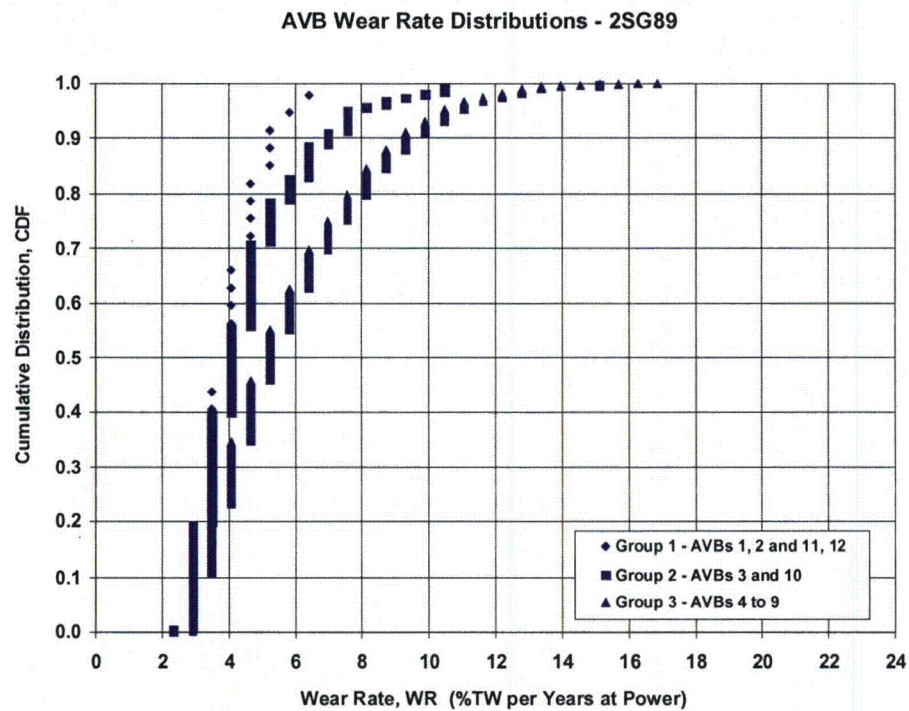
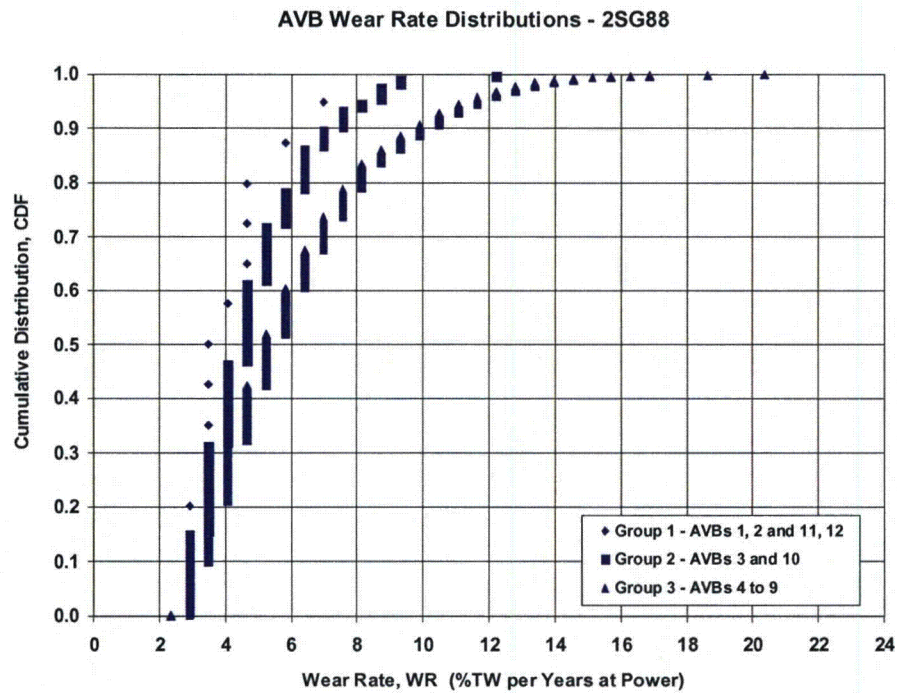


**Figure 4-9 — Apparent Wear Rates for AVB Supports**

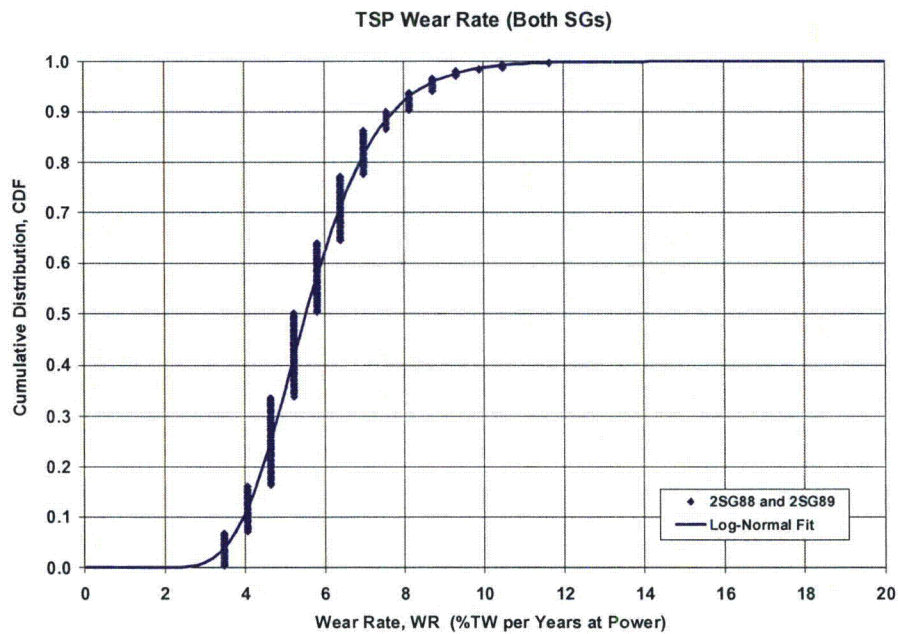
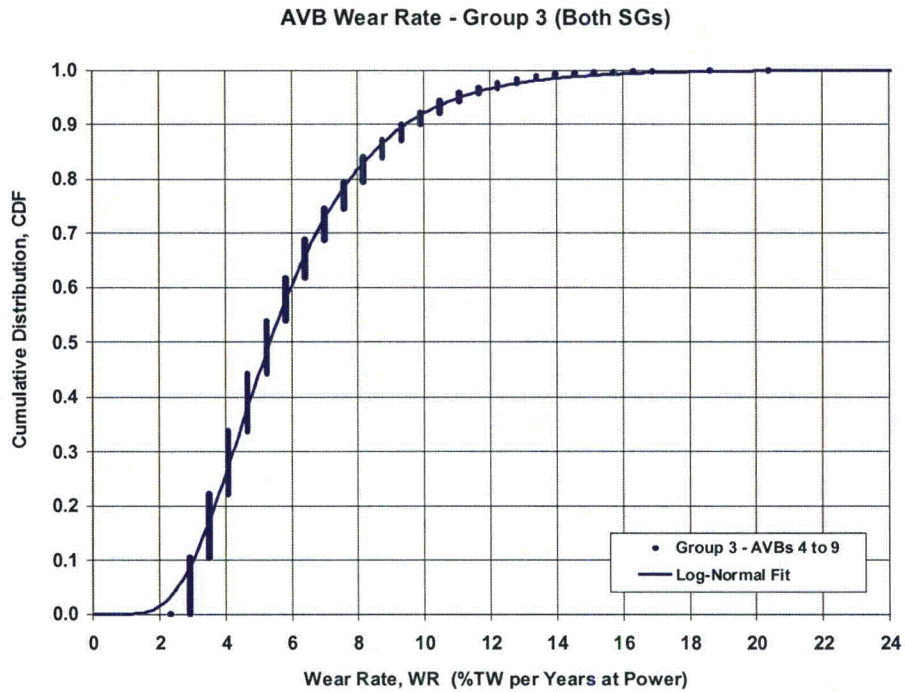


**Figure 4-10 — Wear Rate Distributions for AVB and TSP Wear Mechanisms**

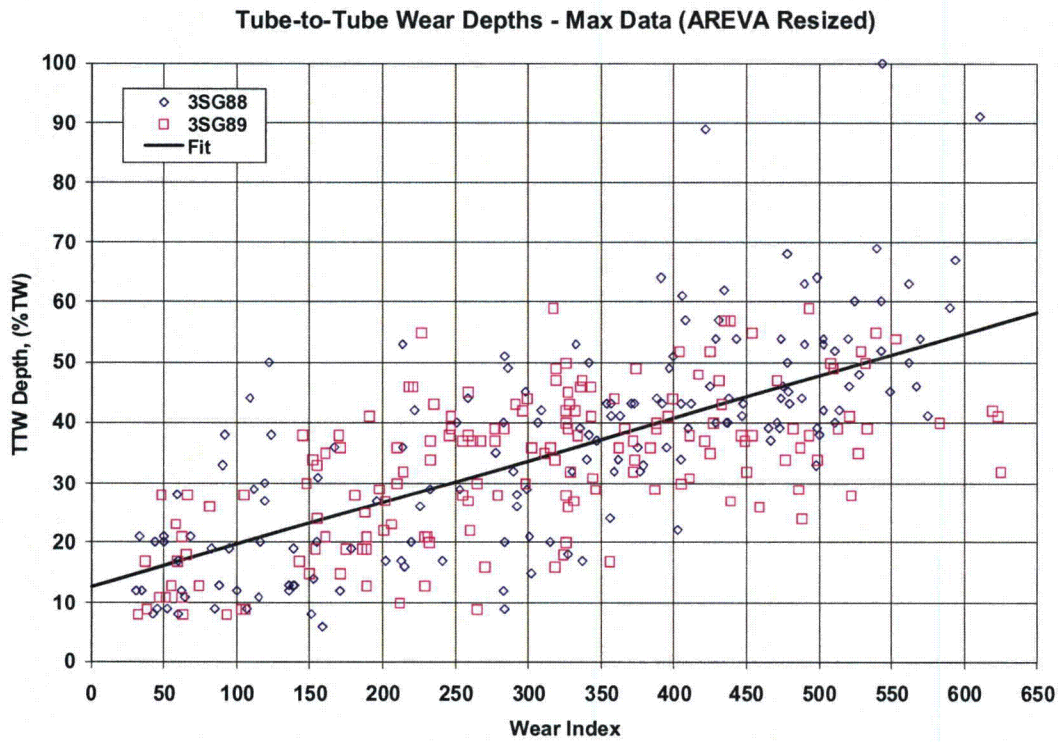
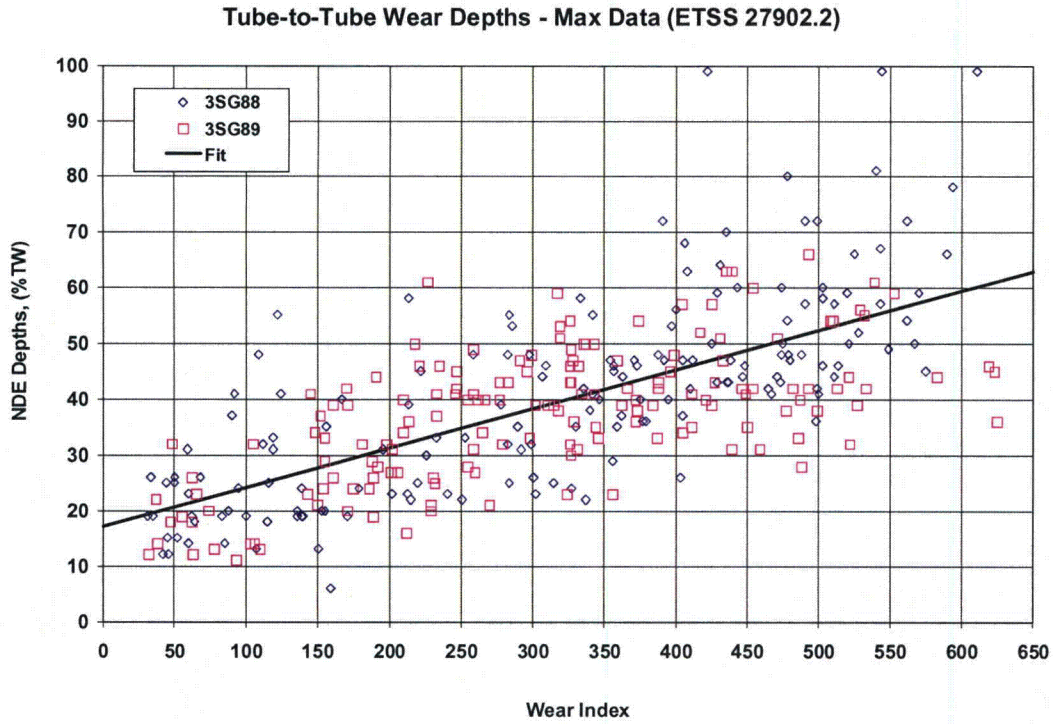


**Figure 4-11 — Maximum NDE Depths for TTW**



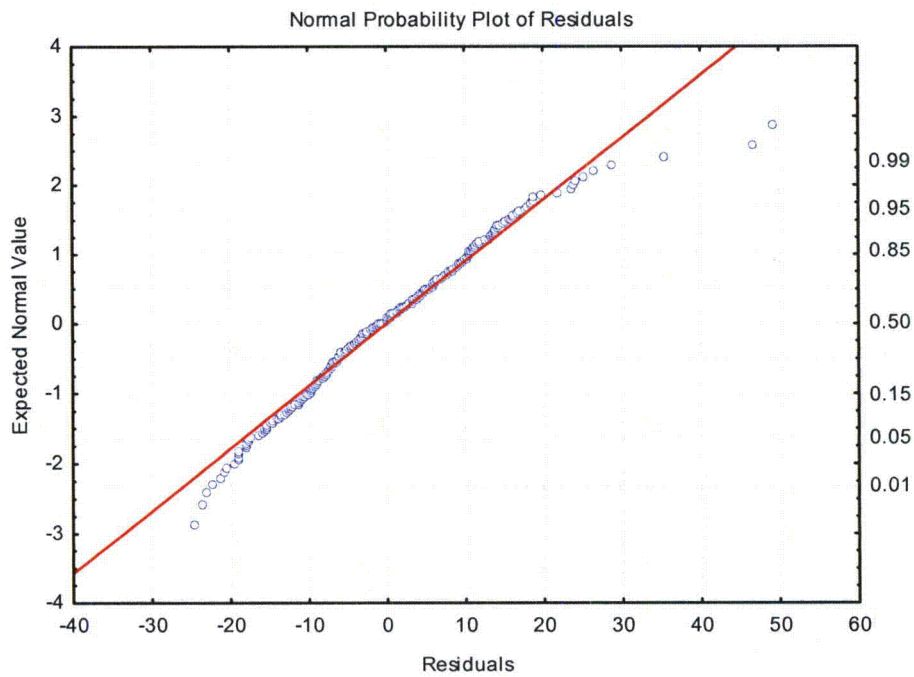
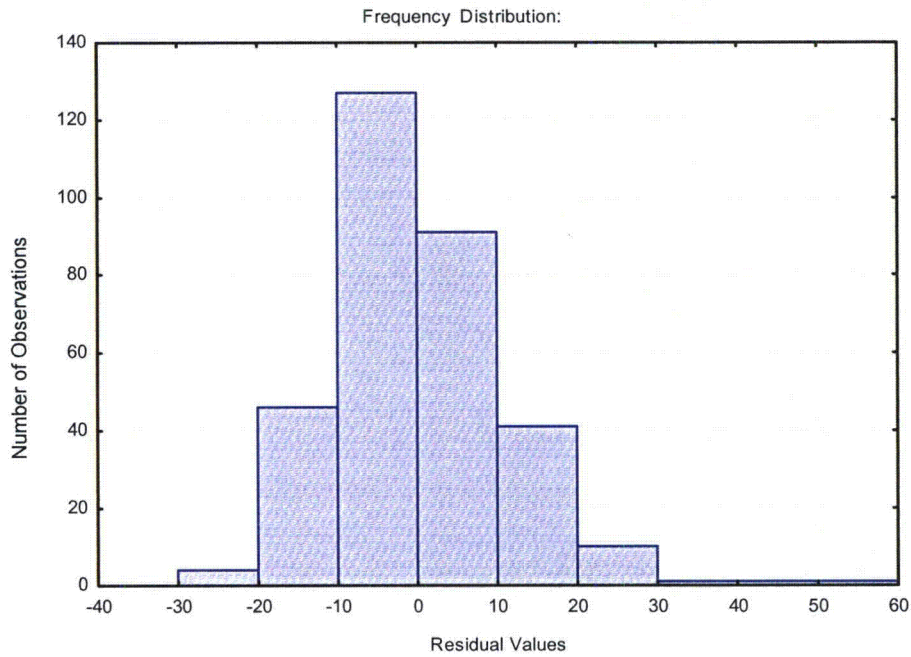
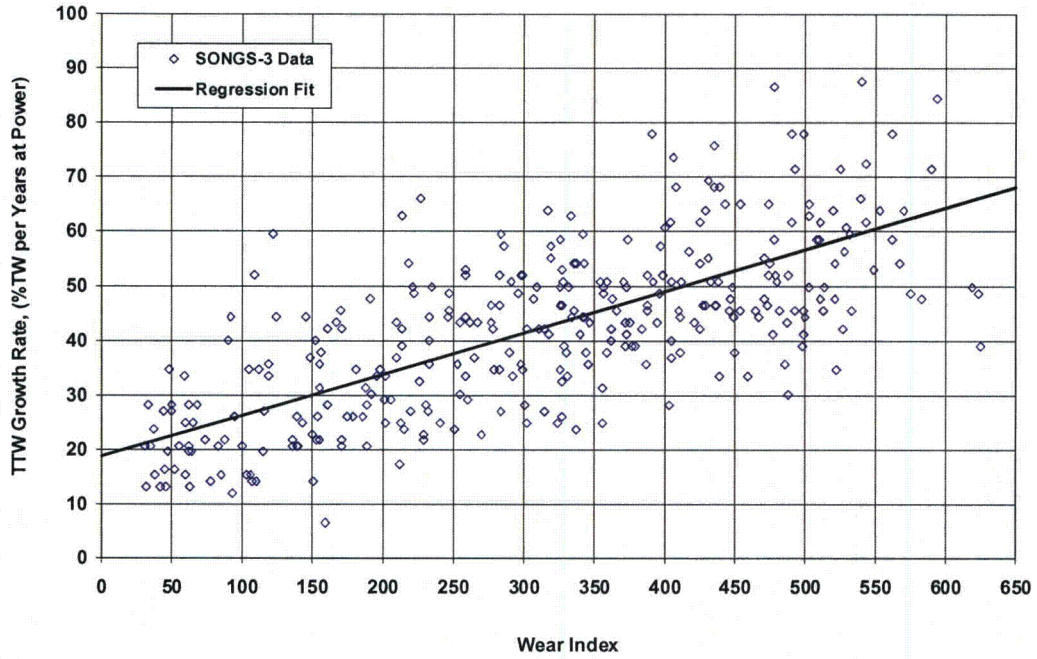


Figure 4-12 — Regression Analysis Results for TTW Depth Data

ETSS 27902.2 Sizing



AREVA Resized

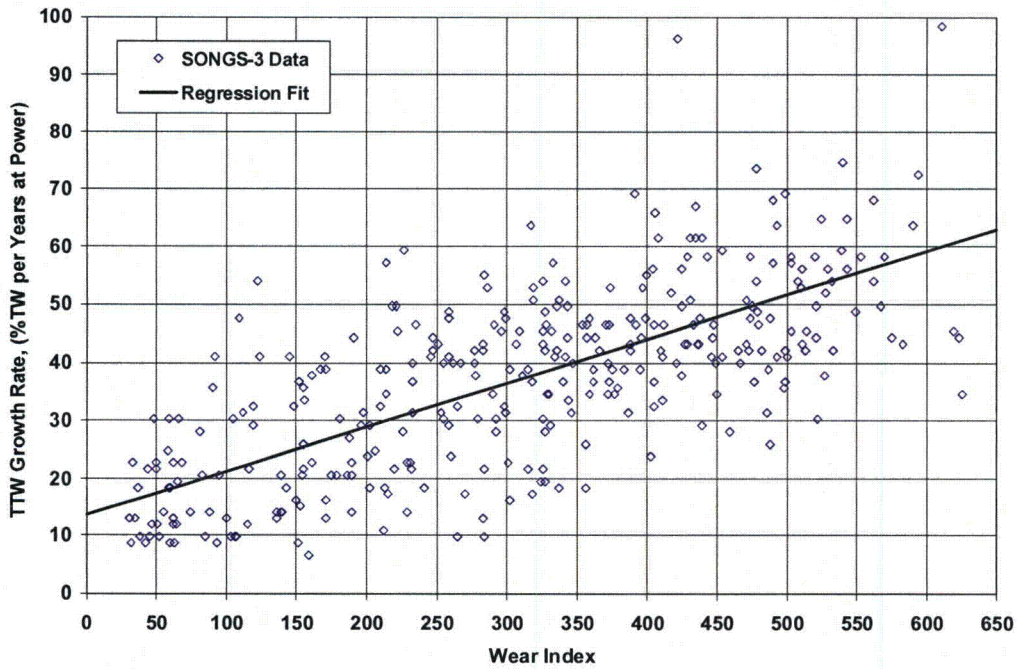


Figure 4-13 — Tube-to-Tube Wear Rate as a Function of Wear Index



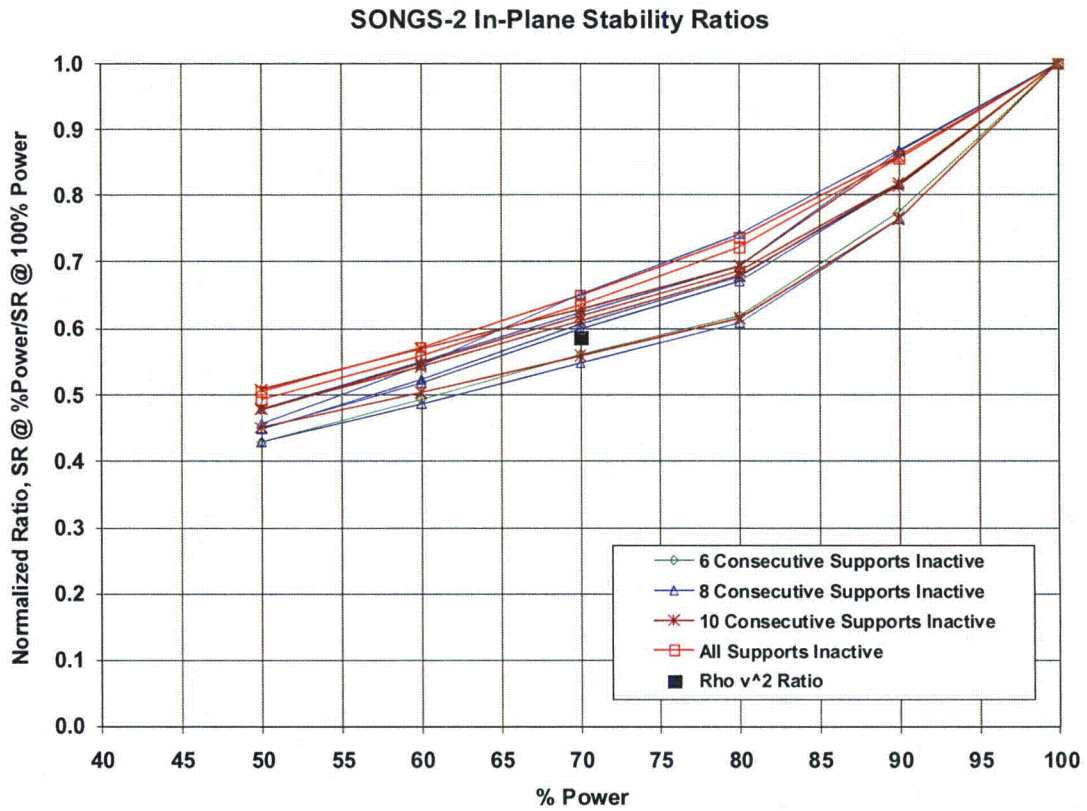


Figure 4-14— Effect of Reduced Power Conditions on Fluid Elastic Instability Ratio for Various Inactive Support Configurations (Ref. 7)

**Section 5**  
**OPERATIONAL ASSESSMENT**

**5.1 ANALYSIS CASES**

The OA for TTW degradation was performed by Monte Carlo simulation with 10,000 trials applied to produce the minimum burst pressure and maximum depth distributions at EOC 17. Two basic cases were evaluated that look at the effect of TTW rate models as described below:

Case 1 – Tube-to-tube wear rate based on the U3 wear depths after 0.926 years at power sized with ETSS 27902.2 (Ref. 13)

Case 2 – Tube-to-tube wear rate based on the U3 wear depths after 0.926 years at power sized with AREVA hybrid voltage model (Ref. 14)

Each case was evaluated for 70% reduced power operation. The original schedule length for Cycle 17 is 1.578 years at power and was used as a starting cycle length to evaluate in the OA. The effect of running a shorter cycle was parametrically analyzed. The actual schedule length for Cycle 17 may be as short as 5 months in order to have additional margins for U2 operation.

In the model development, a decrease in NOPD is due to reduced power operation. This effect is included in the assessment for 70% reduced power operation. The effect of the decrease in  $\rho v^2$  due to the reduced power is also included in the TTW initiation model as discussed in Section 4.7.

**5.2 SIMULATION RESULTS**

The structural analysis to establish the margins against tube burst was performed for the two analysis cases. The parameters for the input distributions are given in Table 5-1. Some simulation results are presented to show the evolution of the wear index for Cycle 17 and the effect of sizing assumptions (Cases 1 and 2). For one trial out of 10,000 total trials per simulation, the histogram of BOC and EOC wear index is shown in Figure 5-1. The BOC

distribution begins the cycle with relatively large number of low wear indices that grow over the cycle, 1.578 years at power in this case, to a broader spread of wear index values. For this trial, the largest wear index is about 170% TW projected at EOC 17. In general, the EOC wear index for the worst tube is less than 200% TW.

The EOC wear index is a key indicator on the likelihood that a TTW will initiate sometime during the cycle. The longer the cycle length assumed for Cycle 17, the greater the chance to initiate and grow a TTW flaw to a depth that challenges SIPC margin requirements. The number of initiated TTW flaws for a single trial is shown in Figure 5-2, where the number of initiations is plotted against the time at which initiation is calculated to occur. The total number of TTW initiations in this single trial is 64. Although not shown, the effect of power level has a significant impact on the number of initiations.

As illustrated in Figure 5-2, most TTW flaws are predicted to initiate after half-way through the cycle. A few initiations are calculated to occur early in the cycle. As expected, the increase in TTW flaws increases with operation time. Operating U2 for shorter cycle lengths significantly decreases the chance in having TTW. In most all simulations, the lowest burst pressure tube has initiated TTW at BOC or very early in the cycle. The POB results for the full simulation of TTW degradation mechanism are discussed in Section 5.3.

### 5.3 STRUCTURAL MARGIN EVALUATION

The structural analysis for tube burst and leakage was completed for a range of operating periods. The POB was determined from the distribution of worst case burst pressures which is compared to the SIPC margin of 3xNOPD. Figure 5-3 illustrates the burst pressure distributions at EOC 17 at 70% power for the two NDE sizing cases. The lower extreme values for the AREVA resized case crosses the  $POB \leq 0.05$  line at a burst pressure below the 3xNOPD margin limit. The case using ETSS 27902.2 or the AREVA technique for sizing TTW depths do not satisfy the SIPC margins for the scheduled cycle length of 1.578 years at power.

To determine the effect of cycle length on POB, several simulations were performed for different operating periods. The POB results from this parametric assessment are given in Figure 5-4. Again, it can be seen that full-cycle operation is not achieved at 70% power level for either analysis cases, but the margin requirements can be met at somewhat shorter operating times.

# Controlled Document

The following allowable cycle lengths have been computed:

## Cycle Lengths at POB = 5%

Analysis Case	Years at 70% Power
Case 1 – ETSS 27902.2 Sizing	1.33
Case 2 – AREVA Resized	1.48

The allowable operating cycle times are only 1 to 3 months shorter than the original scheduled operation for U2. The minimum length for Cycle 17 at 70% power is 16 months.

## 5.4 LEAKAGE EVALUATION

Regarding calculated accident-induced leakage, due to the long and flat nature of TTW degradation, the limiting condition for EOC 17 is tube burst at 3xNOPD as opposed to leakage. This will be the case for all inservice tubes.

Table 5-1

OPERATIONAL ASSESSMENT INPUT PARAMETERS  
TTW FOR U2 – EOC 16

Distribution	Type	Parameters	S/G 89 <sup>(1)</sup>	Basis <sup>(2)</sup>
Probability of Detection	Log-Logistic	Intercept, A Slope, B	10.61 -11.20	ETSS 96004.1 (Ref. 12)
Probability of Detection	Log-Logistic	Intercept, A Slope, B	14.24 -17.22	ETSS 27902.2 (Ref. 13)
AVB Wear Rate (% TW per Years at Power)	Log Normal	Mean Ln(WR) Std Dev Ln(WR) Max Rate	1.68 0.45 20	U2 (Ref. 6b)
TSP Wear Rate (% TW per Years at Power)	Log Normal	Mean Ln(WR) Std Dev Ln(WR) Max Rate	1.71 0.26 20	U2 (Ref. 6b)
TTW Rate (% TW) <sup>(3)</sup> ETSS 27902.2	Normal	Intercept Slope Std Dev	17.257 0.0703 10.99	U3 (Ref. 13)
TTW Rate (% TW) <sup>(3)</sup> AREVA Resized	Normal	Intercept Slope Std Dev	12.747 0.0701 10.99	U3 (Ref. 14)
TTW Initiation Model	Beta	Shape 1 Shape 2	9.839 39.138	U3 (Ref.10a & 16))
Structural Length L <sub>ST</sub> , (in.)	Log Normal	Mean Ln (L <sub>ST</sub> ) Std Dev Ln (L <sub>ST</sub> )	1.28 0.26	U3 (Ref. 11)
Shape Factor, F = d <sub>MAX</sub> /d <sub>ST</sub>	Normal	Mean (F) Std Dev (F)	1.00 0.0	U3
Strength, S <sub>y</sub> + S <sub>u</sub> (psi)	Normal	Mean (S <sub>y</sub> + S <sub>u</sub> ) Std Dev (S <sub>y</sub> + S <sub>u</sub> ) Min (S <sub>y</sub> + S <sub>u</sub> ) Max (S <sub>y</sub> + S <sub>u</sub> )	116,633 2,504 109,900 123,900	U2 CMTR Data 2SG89 (Ref. 10b)
Normal Operating Pressure Differential, (psi)	Constant	NOPD at 100% NOPD at 70%	1325 1305	U2 (Ref. 7 & 9)
Limiting Accident Pressure Differential, (psi)	Constant	LAPD	2560	U2 (Ref. 3)
Cycle 17 Length (Years at Power)	Constant	τ	1.578	Operating Schedule (Ref. 9)

Notes

- (1) 2SG89 is taken as the limiting steam generator
- (2) Databases for U2 and U3 data are from cited references
- (3) TTW rates computed by dividing depth distribution by 0.926 years at power



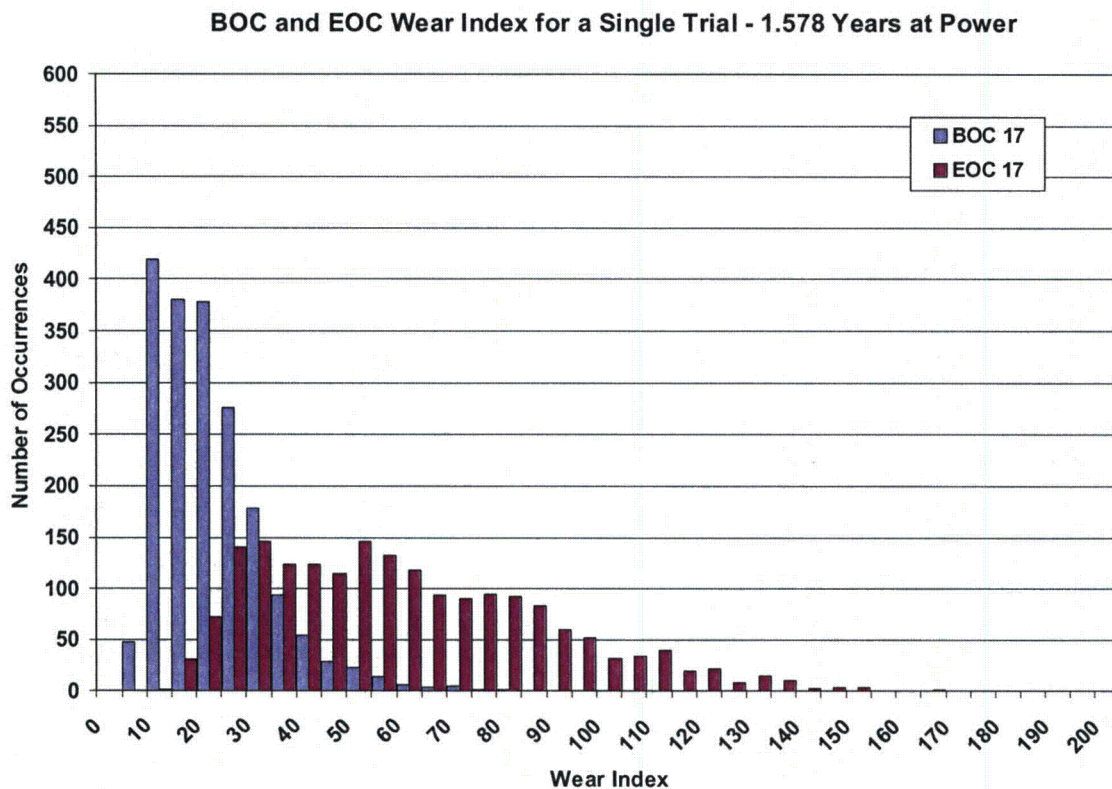


**Figure 5-1 — Histogram of BOC and EOC Wear Index for a Single Trial for Cycle 17 (1.578 Years at Power)**

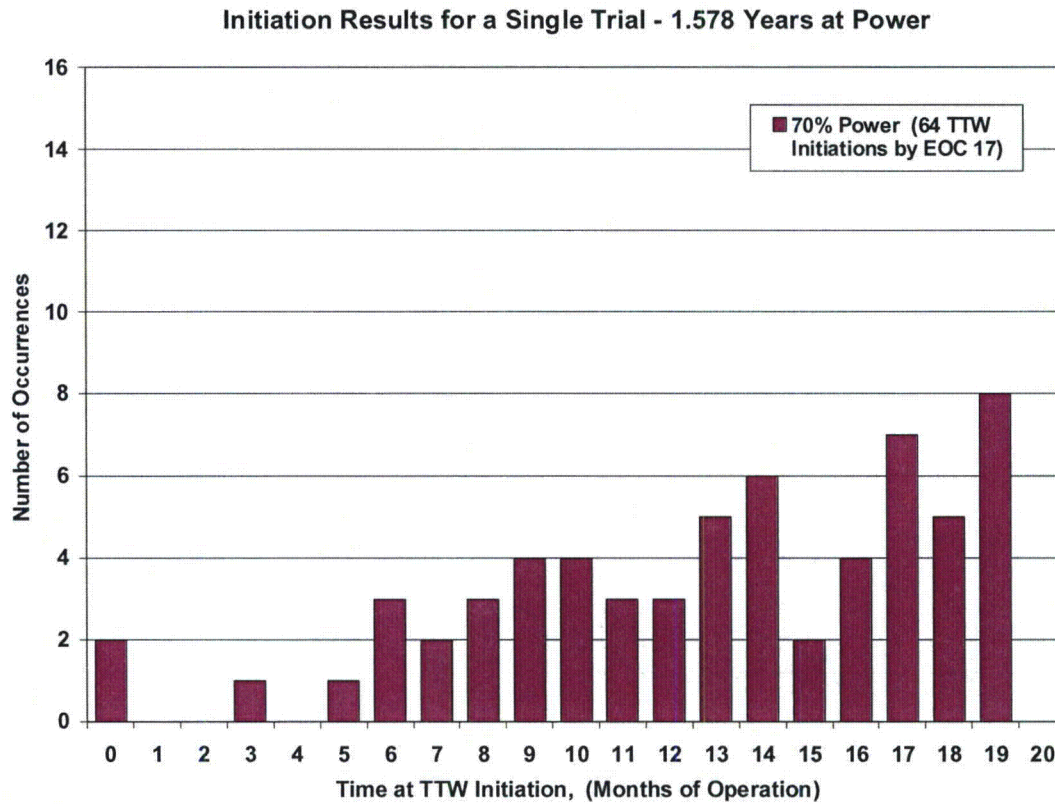


**Figure 5-2 — Histogram of TTW Initiations at 70% Power for a Single Trial for Cycle 17 (1.578 Years at Power)**

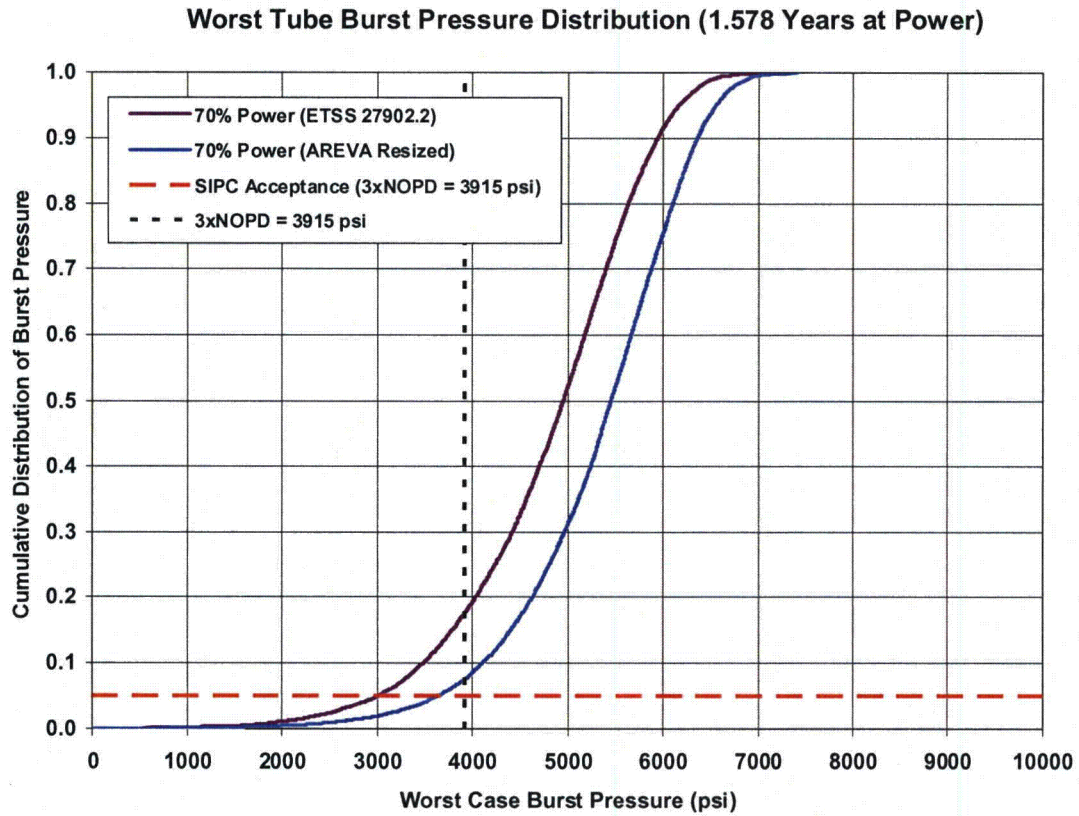


**Figure 5-3 — Burst Pressure Distribution for the Worst Tube in the High-Wear Region at EOC 17 after 1.578 Years at 70% Power**

Operational Assessment for TTW for Cycle 17

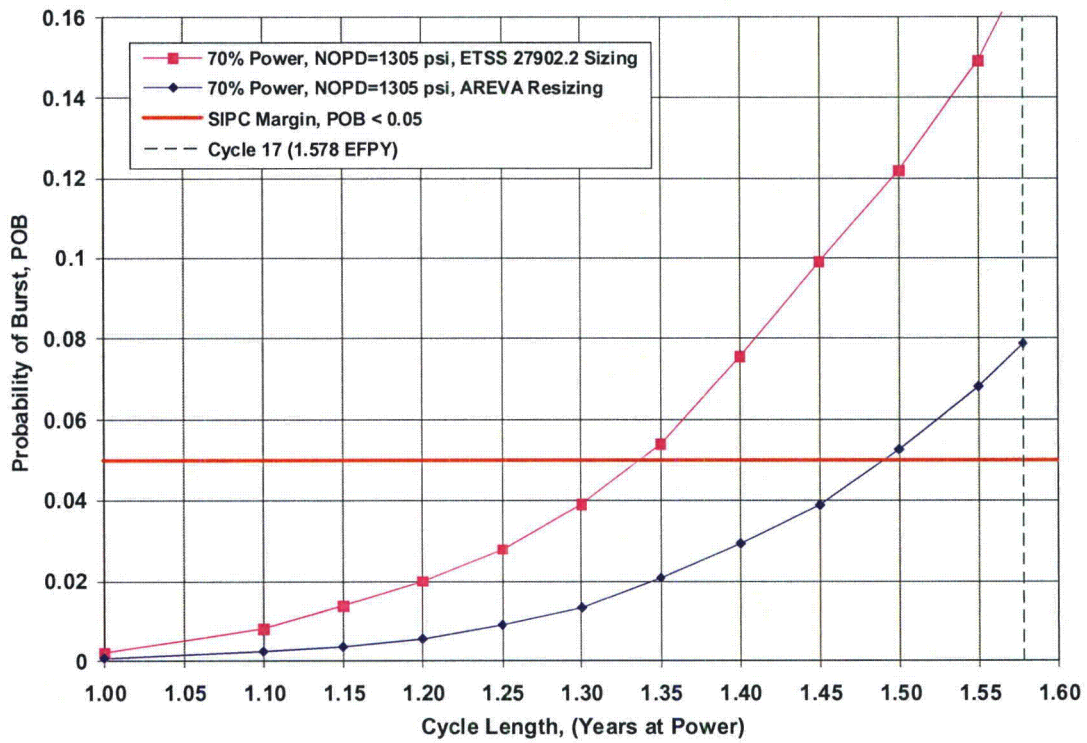


Figure 5-4 — Probability of Burst at 70% Power Level for TTW Growth Rate Models Based on Case 1 - ETSS 27902.2 Sizing (Ref. 13) and Case 2 - AREVA Resizing Models (Ref. 14)

## Section 6 SUMMARY OF RESULTS

The steam generator tube examinations for U2 and U3 identified significant wear degradation. The limiting wear mechanism for U3 is freespan TTW in the U-bends where through-wall leakage had occurred after only 0.926 years at power. The cause of this degradation is in-plane tube vibratory motion due to fluid elastic instability under full power operation. The observed wear degradation in U2 is far less than that detected U3. Only minor TTW was detected in U2 steam generator (2SG89), however, both units are basically the same design and Cycle 17 operation for U2 must address TTW degradation mechanism. The U3 wear behavior was used to establish the initiation and growth of TTW indications in U2 steam generators. An empirical correlation based on a wear index parameter (measure of the state of wear degradation in each tube) provided the method of scaling the U3 wear behavior to U2.

Two OA analysis cases were evaluated based on the sizing techniques used to define the U3 TTW depths. Case 1 used ETSS 27902.2 (Ref. 13) for the voltage based sizing and these data were used to establish the TTW growth rate distribution in Figure 4-13. The OA results for Case 1 indicate that the SIPC margin requirements are satisfied for a Cycle 17 length of 1.33 years at the 70% power level. For Case 2, where the wear rates were based on TTW depths as resized by AREVA using a different calibration standard, the SIPC margins will be met for a cycle length of 1.48 years at 70% power level. Therefore, the minimum length for Cycle 17 at 70% power is 16 months based on the more conservative Case 1 results.

Because of the character of TTW indications, being relatively flat and long in the axial direction, tube burst at 3xNOPD is the limiting requirement for cycle length. The projected accident-induced leak rates for TTW will not be limiting since ligament pop-through at limiting accident pressures will not precede burst condition at 3xNOPD. The predicted EOC 17 maximum depths for TTW will not create thin remaining ligaments subject to pop-through conditions. Therefore, the accident-induced leakage requirements will be satisfied provided that burst margins at 3xNOPD are maintained during the operating cycle..

# Controlled Document

## REFERENCES

1. "Steam Generator Program Guidelines," Nuclear Energy Institute NEI 97-06 Rev. 3, (January 2011)
2. "Steam Generator Integrity Assessment Guidelines, Revision 3," Electric Power Research Institute, Steam Generator Management Program, EPRI Report 1019038, (November 2009)
3. "SONGS 2C17 Steam Generator Condition Monitoring Report," Document No. 51-9182368-002, AREVA NP.
4. "Steam Generator Degradation Specific Management Flaw Handbook, Revision 1," 1019037, Electric Power Research Institute, Steam Generator Management Program (December 2009)
5. "Verification of Program TTWEAR\_U2 for the Operational Assessment for SONGS Unit 2," Draft Calculation No, AES-C-8150-1, Intertek APTECH, (September 2012)
6. Email from A. Brown (AREVA) to R. Cipolla (Intertek APTECH), "SONGS Tube to-Tube Wear Indications," dated June 09, 2012, Attachments:
  - a) SONGS3 AVB and TSP Wear Depth Distribution.xlsx
  - b) SONGS2 AVB and TSP Wear Depth Distribution.xlsx
7. "Evaluation of Stability Ratio for Return to Service," MHI, L5-04GA567, Rev. 6, (September 11, 2012)
8. Letter from A. Matheny (SCE) to A. Brown (AREVA), "Numerical Values for the Steam Generator Degradation Assessment San Onofre Nuclear Generating Station, Unit 2, Southern California Edison," (January 18, 2012)
9. Letter from A. Matheny (SCE) to A. Brown (AREVA), "Numerical Values for the Steam Generator Operational Assessment San Onofre Nuclear Generating Station, Units 2 and 3," (February 8, 2012)
10. Email from A. Brown (AREVA) to R. Cipolla (Intertek APTECH), "OA Data Request," dated June 14, 2012, Attachments:
  - a) SONGS Wear Table w All Tubes.xlsx
  - b) SONGS2 CMTR.xlsx
11. Email from A. Brown (AREVA) to R. Cipolla (Intertek APTECH), "AVB Wear Info," dated June 16, 2012, Attachments:
  - a) SONGS2 AVB Wear Structural Dimensions.xlsx
  - b) SONGS AVB Wear Length Review.xlsx



# Controlled Document

12. ETSS 96004.1, Revision 13 (April 2010), Test Application: Wear at tube supports, anti-vibration bars, vertical and diagonal straps," Source: Electric Power Research Institute, EPRIq.com Performance Database.
13. ETSS 27902.2, Revision 1 (May 2012), Test Application: Detection of Axial Groove Volumetric indications and depth sizing within the freespan area, loose part not present," Source: Electric Power Research Institute, EPRIq.com Performance Database.
14. Email from A. Brown (AREVA) to R. Cipolla (Intertek APTECH), "OA Data Request," dated June 14, 2012, Attachments:
  - a) SONGS Sizing Summary.xlsx
  - b) SONGS2 TTW Sizing Comparison.xlsx
15. Email from C. Waskey (AREVA) to R. Cipolla (Intertek APTECH), "Dynamic Pressure Data for Power Reduction," (June 27, 2012)
16. Emails from A. Brown (AREVA) to R. Cipolla (Intertek APTECH), "SONGS Tube-to-Tube Wear Indications," Attachment  
SONGS TTW Depth Distributions 2012.xlsx, (June 9, 2012)

# Controlled Document

## Appendix A REPORT ACRONYMS

Acronym	Description
2SG88	Unit 2 Steam Generator 88
2SG89	Unit 2 Steam Generator 89
3SG88	Unit 3 Steam Generator 88
3SG89	Unit 3 Steam Generator 89
3xNOPD	Three times normal operating pressure differential
95-50	95% probability at 50% confidence
AILPC	Accident Induced Leakage performance Criteria
AVB	Anti-vibration bar
BOC	Beginning of operating cycle
CM	Condition monitoring
CYC	Length of cycle
EOC	End of operating cycle
EPRI	Electric Power Research Institute
ETSS	Examination Technique Specification Sheets
GPM	Gallons per minute
NDD	No degradation detected
NDE	Non destructive examination
NEI	Nuclear Energy Institute
OA	Operational assessment
POB	Probability of burst
POD	Probability of detection
POI	Probability of initiation
QA	Quality assurance
RN	Random number
SG	Steam generator

# Controlled Document

## REPORT ACRONYMS (Cont'd)

Acronym	Description
SIPC	Structural Integrity Performance Criteria
SR	Stability ratio
TSP	Tube support plate
TTW	Tube-to-tube wear
TW	Through wall
U2	San Onofre Unit 2 (also SONGS-2)
U3	San Onofre Unit 3 (also SONGS-3)
WI	Wear index
WR	Wear rate

## **ATTACHMENT 6 – Appendix D**

### **Operational Assessment of Wear Indications In the U-bend Region of San Onofre Unit 2 Replacement Steam Generators**

**Operational Assessment of  
Wear Indications in the U-bend Region of  
San Onofre Nuclear Generating Station Unit 2  
Replacement Steam Generators**

**August 2012**

**(Revision 3: October 2012)**

Prepared by: Electronically Approved\*  
P. J. Prabhu, Fellow Engineer  
Steam Generator Management Programs

Reviewed by: Electronically Approved\*  
D. J. Ayres, Consultant  
Steam Generator Management Programs

Approved by: Electronically Approved\*  
W. J. Bedont, Manager  
Steam Generator Management Programs

*\* Electronically approved records are authenticated in the electronic document management system.*

©2012 Westinghouse Electric Company LLC  
All Rights Reserved

STATUS STAMP ON PAGE 2



**Table of Contents**

Executive Summary .....	4
1 Introduction .....	5
2 Overall Analytical Methodology .....	6
2.1 Outline of Methodology .....	6
2.2 Thermal-Hydraulic Analysis .....	7
2.2.1 Methods .....	7
2.2.2 Results Summary .....	9
2.3 Flow-Induced Vibration Analysis .....	10
2.3.1 Methods .....	10
2.3.2 FIV Results Summary .....	17
2.4 Determination of Tube Support Effectiveness from Eddy Current Data .....	17
2.4.1 Out-of-plane Vibration .....	17
2.4.2 In-plane Vibration .....	19
2.5 Tube Wear Progression .....	19
2.5.1 Methods .....	19
2.5.2 Application to SONGS Steam Generators .....	23
2.5.3 Results Summary .....	24
2.5.4 Wear Projection Uncertainty .....	26
2.6 Evaluation of the Potential for In-Plane Vibration .....	27
2.6.1 Methodology Benchmarking Using Unit 3 Findings .....	28
3 Operational Assessment .....	82
3.1 Tube Wear at AVBs .....	82
3.1.1 Structural Limits .....	82
3.1.2 Evaluation Method .....	83
3.1.3 Results for Active Tubes .....	84
3.1.4 Results for Plugged Tubes .....	84
3.1.5 Evaluation for 18 Months of Operation .....	85
3.2 Tube-to-Tube Wear in U-bend Free Span .....	85
3.2.1 Eddy Current Inspection Results .....	85
3.2.2 Flow-Induced Vibration Analysis Results .....	85
3.2.3 Assessment of Tube-to-Tube Wear Mechanism .....	87
3.3 Potential for In-Plane Vibration .....	88
3.4 Operational Assessment Conclusion .....	89
4 References .....	96
5 Nomenclature .....	98
Appendix A. Tube-to-Tube Wear in Unit 2 U-bend Free Span .....	100

**Supplier Status Stamp**

VPL No: 1814-AA086-M0190	Rev No: 4	QC: N/A
<input type="checkbox"/> DESIGN DOCUMENT    ORDER NO. 800918458 <input checked="" type="checkbox"/> REFERENCE DOCUMENT - INFORMATION ONLY <input type="checkbox"/> VIRP IOM MANUAL		
MFG MAY PROCEED: <input type="checkbox"/> YES <input type="checkbox"/> NO <input checked="" type="checkbox"/> N/A		
STATUS - A status is required for design documents and is optional for reference documents. Drawings are reviewed and approved for arrangements and conformance to specification only. Approval does not relieve the submitter from the responsibility of adequacy and suitability of design, materials, and/or equipment represented.		
<input checked="" type="checkbox"/> 1. APPROVED <input type="checkbox"/> 2. APPROVED EXCEPT AS NOTED - Make changes and resubmit. <input type="checkbox"/> 3. NOT APPROVED - Correct and resubmit for review. NOT for field use.		
APPROVAL: (PRINT / SIGN / DATE)		
RE:	E. GRIBBLE	10/02/12
FLS:		
Other:		

SCE DE(123) 5 REV. 3 07/11

REFERENCE: SO123-XXIV-37.8.26

**List of Tables & Figures**

Table 2-1. ATHOS Model R- $\theta$ Finite Difference Grid .....	31
Table 2-2. ATHOS Model Axial Direction (Z) Finite Difference Grid .....	32
Table 2-3. SONGS Unit 2 RSG 2E088 Tube Plugging List .....	33
Table 2-4. SONGS Unit 2 RSG 2E089 Tube Plugging List .....	34
Table 2-5. Cycle 17 Operating Parameters with 205 Plugged Tubes (SG 2E088).....	35
Table 2-6. Cycle 17 Operating Parameters with 305 Plugged Tubes (SG 2E089).....	36
Table 2-7. Summary of ATHOS Results .....	37
Table 2-8. Possible AVB Support Cases with Adjacent Ineffective AVBs (Page 1 of 15).....	38
Table 2-9. Wear Projection Results for Limiting Active Tubes and Plugged Tubes.....	53
Table 2-10. In-Plane Stability Ratios for Limiting Tubes .....	54
Table 2-11. Benchmarking Results for Boundary and Adjacent Tubes (Page 1 of 2) .....	55
Table 2-12. Benchmarking Results for Interior Tubes (Page 1 of 2).....	57
Table 3-1. Condition Monitoring Limit for Axial Thinning .....	90
Table 3-2. Wear Projection Results for Active Tubes with Limiting AVB Wear Indications.....	91
Table 3-3. Wear Projection Results for Plugged Tubes with Limiting AVB Wear Indications .....	92
Table 3-4. Wear Projection Results for Limiting AVB Wear Indications for 18 Months of Operation .....	93
Figure 2-1. ATHOS Finite Difference Grid in the Horizontal (R- $\theta$ ) Plane .....	59
Figure 2-2. ATHOS Finite Difference Grid in the Vertical (R- $\theta$ ) Plane .....	60
Figure 2-3. SG 2E089 Tube Row 141/Col. 89: Comparison of Gap Velocities at 50% Power .....	61
Figure 2-4. SG 2E089 Tube Row 141/Col. 89: Comparison of Gap Velocities at 60% Power .....	62
Figure 2-5. SG 2E088 Tube Row 141/Col. 89: Comparison of Gap Velocities at 70% Power .....	63
Figure 2-6. SG 2E089 Tube Row 141/Col. 89: Comparison of Gap Velocities at 70% Power .....	64
Figure 2-7. SG 2E089 Tube Row 141/Col. 89: Comparison of Gap Velocities at 80% Power .....	65
Figure 2-8. Representative FASTVIB / FLOVIB Tube Model.....	66
Figure 2-9. Straight Leg Tube Damping in Liquid .....	67
Figure 2-10. Out-of-Plane Excitation ratio Map – 100% Power – 7 AVBs Ineffective (Case 60) .....	68
Figure 2-11. In-Plane Stability Ratio Map – 100% Power – 7 AVBs Ineffective (Case 60).....	69
Figure 2-12. Out-of-Plane Excitation Ratio Map – 70% Power – 7 AVBs Ineffective (Case 60).....	70
Figure 2-13. In-Plane Stability Ratio Map – 70% Power – 7 AVBs Ineffective (Case 60).....	71
Figure 2-14. Schematic Illustrations of Triangular Pitch Tube Array Patterns .....	72
Figure 2-15. Comparison of Analytical Models of FIV Mechanisms.....	73
Figure 2-16. Typical Application of Semi-Empirical Wear Calculation Methodology.....	74
Figure 2-17. Fundamental Characteristic Trends Treated in Semi-Empirical Methodology.....	75
Figure 2-18. Wear Depth vs. Wear Volume (0.75 inch OD Tube, 0.59 inch AVB Width).....	76
Figure 2-19. U-bend OP Mode in Sample Evaluation Showing First Unstable FASTVIB Case and Postulated Initial Positions of AVBs 4 and 5 Relative to Mode Shape .....	77
Figure 2-20. Significant U-bend OP Modes in Sample Evaluation Showing Two FASTVIB Cases and Postulated Initial Positions of AVBs 3, 4, 5, and 6 Relative to Mode Shape .....	78
Figure 2-21. Example Illustration of AVB Wear Projection (Tube R121C91 in SG 2E089) .....	79
Figure 2-22. Logic Applied for Benchmarking the In-Plane Vibration Methodology Using Unit 3 .....	80
Figure 2-23. Location of SG 3E088 Tubes Evaluated for Benchmarking .....	81
Figure 3-1. Condition Monitoring Limit for Axial Thinning .....	94
Figure 3-2. Operational Assessment Methodology for the Potential for In-Plane Vibration.....	95

## Executive Summary

This report documents the operational assessment (OA) of the tube wear indications in the U-bend region of San Onofre Nuclear Generating Station (SONGS) Unit 2 steam generators (SG) based on inspection results from the 2012 outage (U2C17). This evaluation is a supplement to the OA which uses traditional/probabilistic methods. This evaluation is based on well-established methodology on flow-induced vibration of SG tubes. It utilizes the available test data on in-plane and out-of-plane instability and wear rate resulting from out-of-plane vibration of the tubes against anti-vibration bars (AVB).

Evaluation was performed for three degradation mechanisms: tube wear at AVBs, tube-to-tube wear in the U-bend free span as reported in two tubes in SG 2E089 during U2C17, and the potential for in-plane vibration of the tubes leading to tube-to-tube wear as has been reported in the Unit 3 SGs.

Evaluation of the AVB wear mechanism focused on projecting the flaw depths of AVB wear indications in active tubes (those remaining in service) and in plugged tubes until the next inspection. SCE is planning to perform a Unit 2 mid-cycle inspection after operating for 150 effective days of operation at 70% power. Since the next inspection is planned to be within five months of operation in Cycle 17, projections were carried out at 70% power for an operating duration of six months allowing additional margin. Projected wear depths in the active tubes are compared against allowable depths to satisfy the SG performance criteria. This comparison confirmed that SG performance criteria will be satisfied during the next operating period. The wear projections of plugged tubes confirmed that severance of such tubes will not occur during the next cycle.

An evaluation of the tube-to-tube wear reported in two tubes in SG 2E089 showed that, most likely, the wear did not result from in-plane vibration of the tubes since all available eddy current data clearly support the analytical results that in-plane vibration could not have occurred in these tubes. There is evidence of proximity in these tubes from pre-service inspection results. Hence, the tube-to-tube wear is most likely a result of out-of-plane vibration of the two tubes in close proximity to the level of contact during operation (see Appendix A). The evaluation shows that similar conditions are unlikely in other tubes. An evaluation was performed for an undetected flaw that may be left in service, comparable in size to the detected TTW flaws. This evaluation showed that the SG performance criteria will be satisfied during the next cycle.

Eddy current data (lack of wear scar extension beyond the width of the AVBs in any of the AVB wear indications) clearly suggests that in-plane vibration has not occurred in the Unit 2 SGs during the first operating cycle. The methodology was benchmarked using the Unit 3 results; this indicated that the U-bend free span tube wear in Unit 3 resulted from in-plane vibration of the given tube or in-plane vibration of the neighboring tube with matching wear indication. The active and plugged tubes in the Unit 2 RSGs were evaluated using the same methodology for the potential for in-plane instability. The results show that none of the tubes will be subject to in-plane instability. Therefore, tube-to-tube wear from in-plane vibration will not occur in the next operating cycle and SG performance criteria will be satisfied until the next inspection.

This evaluation concludes that, for the assessed degradations, the SG performance criteria will be satisfied during the planned operating period of five months at 70% power. The evaluations also support the satisfaction of the performance criteria for an operating duration of 18 calendar months at 70% power, for these degradation mechanisms.

## 1 Introduction

As per the Steam Generator Program Guidelines, NEI 97-06 (Reference 1), a condition monitoring assessment, which evaluates structural and leakage integrity characteristics of the steam generator (SG) at the end of the last operating period, is to be performed following each inspection. This evaluation is "backward looking" and compares the observed SG tube eddy current indication parameters against leakage and structural integrity. Additionally, an operational assessment, or "forward looking" evaluation is used to project the inspection results and trends to confirm that the SG performance criteria will be met during the operating period until the next inspection. This report documents the operational assessment of the indications in the U-bend region of the San Onofre Nuclear Generating Station (SONGS) Unit 2 SGs based on inspection results from the U2C17 refueling outage (2012). It is consistent with the guidelines described in Reference 2.

Southern California Edison (SCE) is preparing an operational assessment for all of the tube degradation mechanisms in the SGs using traditional and probabilistic methods (References 3 and 4). This report documents an evaluation using semi-empirical methodology applicable to tube wear resulting from flow-induced vibration.

The U2C17 inspection was conducted in 2012 which formed the first in-service inspection of these SGs when their accumulated operating life was 1.72 effective full power years (EFPY). SCE is planning to perform a Unit 2 mid-cycle inspection after operating for 150 effective days of operation at 70% power.

## 2 Overall Analytical Methodology

Most of the evaluation supporting this operational assessment is documented in a detailed technical report (Reference 5). This section provides a summary of the evaluations and results from that report that support the operational assessment.

### 2.1 Outline of Methodology

This subsection provides an outline of the evaluation methodology. This outline may be useful as a roadmap for the discussions in various sections of this report. The list of references is shown in Section 4 and a list of acronyms used in this report is compiled in Section 5.

A thermal-hydraulic computer code was used to evaluate the secondary side flow conditions in the tube bundle using a three-dimensional analytical model. This evaluation is discussed in Section 2.2. The results of the thermal-hydraulic analysis in the form of secondary side velocity, density and void fraction distributions along the length of individual tubes formed inputs to the flow induced vibration (FIV) analysis. The FIV analysis is discussed in Section 2.3. The results of the FIV analysis included out-of-plane excitation ratios and in-plane stability ratios for various tube support conditions in the U-bend. Various tube support conditions were identified by unique case numbers, each case number describing the specific combinations of AVB locations that are ineffective. The actual tube support conditions of the tube are derived from the eddy current test data collected during the U2C17 outage. The rationale for the use of the eddy current data for this purpose and why an effective support location will remain effective for several cycles are discussed in Section 2.4.

Projection of the depths of tube wear indications at AVB locations is discussed in Section 2.5. In brief, the methodology involves determining the values of several input variables that results in matching the reported wear depths of the indications at U2C17, and using these input values to project the wear depths at the next inspection. The FIV analysis results form an important input to the wear projection evaluation. The projected wear depths are compared to the allowable flaw depths to support the operational assessment discussed in Section 3.1.

The tube-to-tube wear in the U-bend free span reported in two tubes in Unit 2 is determined to be the result of a different mechanism than the tube-to-tube wear reported in the Unit 3 RSGs. One plausible explanation of how the alternate mechanism could manifest is discussed in Appendix A. The operational assessment for this mechanism is treated in Section 3.2.

In-plane vibration has resulted in tube-to-tube wear in the U-bend free span in dozens of tubes in the Unit 3 RSGs. Benchmarking of the Westinghouse evaluation methodology against the Unit 3 findings is discussed in Section 2.6.1. The potential for the occurrence of in-plane vibration in Unit 2 in the next operating cycle is evaluated in Section 2.6. The FIV analysis and the tube support conditions determined from eddy current data formed the inputs for this evaluation. The results of this evaluation are used in Section 3.3 to support the operational assessment for this potential degradation mechanism.

Computer codes used in the evaluations described in this report have been verified and validated as per Westinghouse quality procedures.

## 2.2 Thermal-Hydraulic Analysis

### 2.2.1 Methods

Thermal-hydraulic analysis of the SONGS Unit 2 RSGs was performed using the ATHOS (Analysis of the Thermal Hydraulics of Steam Generators) computer code. ATHOS is a three-dimensional computational fluid dynamics (CFD) code for analyzing steam generator (SG) thermal-hydraulic (TH) performance characteristics (Reference 6). ATHOS analysis of a SG involves the execution of a suite of codes consisting of the pre-processors ATHOGPP and PLATES, the ATHOS solver, and the post-processor VGUB. A brief overview of these codes follows.

#### ATHOGPP

The pre-processor, ATHOGPP, calculates the geometric parameters required for the ATHOS thermal-hydraulic analysis. For each node the code computes: the secondary fluid volume, the flow areas in the R,  $\theta$ , and Z directions (cylindrical coordinate system), the heat transfer and friction surface areas, the approach to device area ratios required to compute pressure drops through concentrated resistances (flow distribution plate, tube support plates, primary separator, etc.), and the primary fluid flow partitioning factor. The input parameters include: grid distribution in R,  $\theta$ , and Z directions, shell and shroud (wrapper) dimensions, tube layout and individual tube dimensions as well as the location (row and column numbers) of plugged tubes, inlet (feedwater) and primary separator locations and dimensions, as well as the location of all internal devices (tube support plates, stay-cylinders, etc.). Geometry data processed by ATHOGPP are then transferred via a binary file to the PLATES code for further refinement of the flow areas through the tube support plates. The EPRI version (named ATHOSGPP) of the ATHOGPP pre-processor has been modified by Westinghouse to simulate: anti-vibration bars (AVBs) in the U-bend region and at locations without tubes in the central bundle, and separator openings in the lower deck plate (Reference 7). AVBs are simulated in ATHOGPP by reducing the fluid volume and flow areas of flow cells where the bars are located.

#### PLATES

The pre-processor, PLATES, calculates the cut-out areas and/or flow holes in the tube lane region of the tube support plates in more detail than ATHOGPP. In ATHOGPP, a tube support plate (TSP) is treated as a homogeneous plate with uniform metal area density which removes all areas attributed to tube holes, flow holes (if any), gaps between the TSP and wrapper, and cut-out areas. In addition, the PLATES code can model the blockage areas associated with tube lane blocking devices if present in the steam generator. The PLATES code reads the binary output file generated by ATHOGPP. The code processes the TSP, tube lane, and central cavity related information and generates a new binary file to be read by the ATHOS thermal-hydraulic solver.

#### ATHOS

The ATHOS code module solves the governing conservation equations in conjunction with empirical correlations and boundary conditions. For the thermal-hydraulic analysis of a steam generator, boundary conditions include: mass flow rate of primary fluid, initial "guess" for the primary fluid inlet temperature, feedwater flow rate, feedwater temperature, steam pressure, and water level.



## VGUB

Post-processor, VGUB, calculates tube gap velocity, density, and void fraction distributions along the steam generator tubes. Local tube gap velocities are calculated from ATHOS cell velocities which are based on the porous media concept. In general, gap velocity components normal to the tube (cross flow) are used in flow-induced vibration and wear analyses since these components produce significantly greater tube vibration than components parallel to the tube (axial flow).

The gap velocities for the SONGS RSG tube bundle were calculated based on the "gap center" method which interpolates velocity components at each gap in the tube array. With this method, VGUB calculates the average and resultant gap velocity for each tube of interest. An alternate method of calculating tube velocities is the simpler "tube center" method which assumes that every tube is fully surrounded by neighboring tubes. The two methods produce similar results within the bundle interior. However, the "tube center" method significantly over-predicts fluid velocities for peripheral tubes. Since the "tube center" method does not accurately capture physical effects around the edge of the tube bundle it was not used in this analysis.

## Discussion of Significant Assumptions

1. For ATHOS simulations, each half of the steam generator, Columns 1 through 89 and 89 through 177 are modeled separately to capture the effects of asymmetric tube plugging. The primary and the secondary side operating conditions and properties for both halves are assumed to be the same.
2. Thermal-hydraulic evaluations are performed using the slip flow option. This option is customarily used by Westinghouse as it is more realistic and produces conservative results for two-phase quality, void fraction and velocities.
3. Steam carry under in the recirculating fluid is assumed to be 0.0.

## Analysis Inputs

The ATHOS model covers the secondary side flow field inside the steam generator shell from the top surface of the tubesheet to the lower deck plate and from the center of the wrapper to wrapper wall and the downcomer annulus between the wrapper and the shell walls. Design geometry and thermal-hydraulic symmetry is assumed with respect to the diametrical plane perpendicular to the tube lane. Because of this assumption, the analysis model consists of one-half of the steam generator, i.e., an 180°-sector encompassing one half of the hot leg and one half of the cold leg.

The ATHOS finite difference grid in the horizontal plane (radial (R) and circumferential ( $\theta$ ) directions) is listed in Table 2-1 and depicted in Figure 2-1. The grid is selected to optimize the modeling of the wrapper and the tube bundle design. The axial (ZW) locations are selected based on wrapper, shell, tube support, and tube bundle geometry obtained from RSG design documents. The axial grid is presented in Table 2-2 and Figure 2-2. The tube plugging locations in RSGs 2E088 and 2E089 for the evaluations of the next operating cycle are listed in Table 2-3 and Table 2-4; these were not used in the evaluation of the first operating cycle of the RSGs.

ATHOS inputs were prepared for the operating conditions specified in Reference 9. The operating conditions represent 205 out of 9727 plugged tubes in RSG 2E088 and 305 plugged tubes in RSG 2E089. The primary flow rates in RSG 2E088 and 2E089 for the next operating cycle are slightly different: 207,726 gpm in 2E088 versus 206,695 gpm in 2E089 due to different plugging levels. ATHOS analyses for RSG 2E089 were performed at 50%, 60%, 70%, and 80% power levels. For

RSG 2E088, ATHOS analyses were performed only at 70% power level, a likely power level at restart. Based on comparison of the results at 70% power level between two steam generators, it was concluded that flow-induced vibration evaluations are reasonably close and, therefore, do not require ATHOS evaluations for both RSGs at all power levels. As shown in Table 2-3 and Table 2-4, tube plugging locations are asymmetrical between Columns 1-89 and 89-177. The operating conditions for RSG 2E088 and 2E089 utilized for ATHOS analyses are presented in Table 2-5 and Table 2-6. Subsequent to the completion of this analysis, five additional tubes were preventively plugged in the Unit 2 RSGs, two tubes in SG 2E088 and three tubes in SG 2E089. The impact of the additional plugging on the results of the analysis is negligible (see the third paragraph of Section 2.2.2).

### 2.2.2 Results Summary

Table 2-7 provides an overall summary of the primary and secondary side conditions in the RSGs for ten cases at the part power conditions and the reference case at 100% power (1729 MWt Nuclear Steam Supply System power). Both the calculated and input parameters are included in the table. For the FIV and tube wear evaluations, the TH variables of interest are the gap velocities, densities, and void fraction along the tubes. Table 2-7 includes the maximum quality, void fraction, and velocity in the tube bundle at 50% through 80% power levels, and the reference case at 100% power. There is a significant reduction (improvement) in secondary fluid quality and velocity at the reduced power levels. The void fraction, a fraction of volume occupied by vapor phase in a control volume, shows less reduction than the secondary fluid quality and velocity. This is because of the density difference between the liquid and vapor phases. At the RSG operating conditions, the vapor phase occupies approximately 22 to 25 times more volume per pound of mass than the liquid phase. As a result, the additional liquid inventory at the lower power levels increases the liquid volume by a smaller margin than the decrease in steam volume due to reduced steam mass.

A number of tubes have been plugged in the two RSGs in Unit 2 during the U2C17 outage. As a result, when the RSGs return to service in the next operating cycle, the three-dimensional thermal-hydraulic conditions may be affected as a result of the tube plugging. In addition, since the number of plugged tubes in each half of the SG is different from the other half, the evaluation performed for one half may not be applicable to the other. In order to resolve this difference, separate evaluations were made for the 70% power condition for each half of each SG using four separate models (four different plugging levels corresponding to the actual plugging distribution in the four halves of the two SGs).

At 70% power level, there are no significant differences in thermal-hydraulic characteristics between RSG 2E088 with 205 out of 9727 or 2.1% plugged tubes and 2E089 with 305 or 3.1% plugged tubes. The ATHOS model of RSG 2E089, representing Columns 89 through 177, has slightly higher values for the secondary fluid quality, void fraction and velocities than the other three ATHOS models for the Unit 2 RSGs. Table 2-7 also includes the values for the gap velocity, density and relative dynamic pressure ( $\rho V^2$ ) in the U-bend region of Tube Row 141 / Column 89. These values are provided at the location in the U-bend where the dynamic pressure value is the highest. As expected, these values decrease as the power level decreases. Subsequent to the completion of this analysis, five additional tubes were preventively plugged in the Unit 2 RSGs, two

tubes in SG 2E088 and three tubes in SG 2E089. The impact of the additional plugging on the results of the analysis is negligible.

#### Local Flow Conditions along Tubes

VGUB (Reference 10) calculates the local flow conditions for all tubes in the bundle for input to the tube vibration and wear analysis to support the operational assessment of the Unit 2 RSGs. Local tube gap velocities are calculated from ATHOS cell velocities based on the cell porosity and the characteristic geometry of the tube array (pitch and diameter).

VGUB-calculated secondary tube gap fluid velocities along the tube Row 141 / Column 89 at part power conditions are compared with the reference case (100% power) in Figure 2-3 through Figure 2-7. This tube has the longest bend radius within the bundle and has relatively high gap velocities in the hot leg side of the U-bend region. Each figure compares the gap velocities at a partial power with 100% power for both ATHOS models representing Columns 1 through 89 (LC) and Columns 89 through 177 (HC) for a given steam generator. Results for RSG 2E089 for power levels of 50%, 60%, 70%, and 80% are shown in Figure 2-3, Figure 2-4, Figure 2-6, and Figure 2-7, respectively. ATHOS analyses were also performed for RSG 2E088 at 70% power for both LC and HC models. The gap velocities for this case are compared in Figure 2-5. For most of the straight leg section of the tube, the gap velocities at lower power levels and at 100% power are similar. As shown in Table 2-7, the recirculating fluid flow rate is relatively constant at all power levels. However, in the U-bend region, the gap velocities are a strong function of power level. The steam flow in the bundle is cumulative and increases as a function of the power level and the bundle height which causes high fluid quality, void fraction, and secondary fluid velocities in the upper bundle. As illustrated in these figures, an asymmetric plugging in the bundle has a small effect on velocities. In RSG 2E089, differences in gap velocities are higher than in RSG 2E088. There are 218 plugged tubes in Columns 1-89 (LC) and 101 plugged tubes in columns 89-177 (HC) in RSG 2E089 compared to 113 plugged tubes in LC model versus 106 plugged tubes in HC model in RSG 2E088. Also, the differences in gap velocities increase with power level. Subsequent to the completion of this analysis, five additional tubes were preventively plugged in the Unit 2 RSGs (R135C93 and R137C89 in SG 2E088 and R80C68, R104C72 and R132C94 in SG 2E089). The impact of the additional plugging on the results of the analysis is negligible.

## **2.3 Flow-Induced Vibration Analysis**

### **2.3.1 Methods**

The flow-induced vibration analysis methods described in this section are covered in References 11 through 22.

Flow-induced vibration (FIV) models of the SONGS replacement steam generators (RSGs) were developed to evaluate the effects of secondary side flow on the tubes. The FIV models included the 7 tube support plates along with the 12 anti-vibration bars (AVBs). Figure 2-8 contains a representative sketch of the model used in the analysis. Table 2-8 contains a listing of the various cases considered with respect to the boundary conditions at the AVB that were imposed on the model. The FIV analysis was performed with the FASTVIB and FLOVIB computer codes using thermal-hydraulic results discussed in Section 2.2. The post-processor that interpolates tube-specific gap velocities from the ATHOS volumetric output recognizes the actual boundary

conditions around the periphery of the bundle; therefore, gap velocities for tubes in Row 142 are not as large as for tubes in Row 141. This effect can be observed in the figures contained in Section 2.3.2 where the outermost tubes have slightly lower excitation ratios than the neighboring in-board tubes. FASTVIB calculates relevant FIV responses for all tubes in a given row, and as can be observed in Section 2.3.2, multiple rows are considered. The result is a 'tubesheet' map of responses that help to identify regions that are more susceptible to FIV for a given support condition.

There are several tasks in the FIV evaluation. The first task was to develop tube stability information for power levels of 100%, 80%, 70%, 60% and 50%. The next task was to provide the input necessary to complete the wear projection evaluations for the tubes of interest discussed in Section 2.5 of this report. In addition to these tasks, there was also a comparative study performed to determine the impact on the FIV response as a result of plugging a tube and whether or not the plugged tube contained a stabilizer. Another comparison was performed to determine the difference between the 2E088 and 2E089 steam generators as well as low column tubes and the high column tubes (symmetry concerns). Tubes that were plugged in the steam generators were not symmetrical about the center column of the tube bundle and the same tubes were not plugged in both steam generators. As a result, potentially different thermal-hydraulic conditions could exist. The purpose of this comparison was to determine the impact that non-uniform plugging has on the FIV evaluation results.

Initially, linear dynamic analyses to characterize the response of the entire tube bundle to flow-induced excitation were performed using FASTVIB. These analyses identify limiting locations for various support conditions and show how the tubes of interest relate to the total bundle response as described in Section 2.3.2. FASTVIB incorporates the analytical approaches that were largely defined by the work of H.J. Connors at the Westinghouse Research Laboratories. Verification and qualification of this methodology for steam generator applications includes not only the analytical comparisons in configuration control files, but also many comparisons with results from tests and operating steam generators. These include comparisons with a 49-tube test model of the inlet region in water flow, a quarter-scale model of the U-bend tested in air, a .01 power scale Model F steam generator (MB-2), cantilever tube air flow tests, and operating Model 51 and Model F steam generators.

FASTVIB uses an assembly of structural elements and lumped masses with up to six degrees of freedom per node in a formulation adapted from FLOVIB, one of the earliest finite element programs applied to FIV analysis. Natural frequencies and mode shapes of the elastic structure are determined by conventional eigenvalue/modal decomposition techniques. Tube response to both flow turbulence and fluidelastic excitation is calculated consistent with the framework and empirical constants originally determined by H.J. Connors that have been applied for decades with confirmatory field experience. Fluid density and gap velocity distributions obtained from VGUB post-processing of ATHOS results are used along with structural properties of the tube and support configuration in these solutions. FASTVIB automates multiple solutions and stores limiting parameters in a format that is very useful for screening and subsequent evaluation (such as inputs to the wear evaluation). Total tube responses to the external flow excitation are obtained during evaluation of the SONGS RSGs, but only the response in the U-bend region of interest has been retained to manage the size of output files.

Velocity components normal to the tube (cross flow) are much more effective in causing tube vibration than components parallel to the tube (axial flow). Therefore, this discussion and subsequent analyses address only the cross flow distribution that results in vibration response that is typically an order of magnitude greater than that for comparable axial flows.

The evaluation of tube wear in the U-bend region focuses on the fluidelastic instability thresholds for various postulated tube/AVB support condition assumptions, but displacements and stresses arising from flow turbulence and the specific excitation applied to each tube of interest are also retained. Separate computer runs are required to obtain out-of-plane (OP) and in-plane (IP) responses.

#### Fluidelastic Excitation

Fluidelastic tube vibration is potentially more severe than the always present background flow turbulence because it is a self-excited mechanism. That is, relatively large tube amplitudes can feed back proportionally large driving forces if an instability threshold is exceeded as a consequence of fluid-coupled damping or stiffness interaction with tube velocity or displacement. This mechanism is the primary focus of this evaluation because no other flow-induced vibration mechanism is capable of producing the kind of response observed in the highly turbulent, two-phase flow U-bend region of the SONGS steam generators. Tube support spacing incorporated into the design of the tube support system typically provides tube response frequencies such that the instability threshold is not exceeded for anticipated secondary fluid flow conditions. This approach provides margin against initiation of fluidelastic vibration for tubes that are effectively supported as designed for anticipated flow excitation levels.

However, clearances between the tubes and supporting structure introduce the potential that any given tube support location may not be totally effective in restraining tube motion. Initiation of fluidelastic tube response within available support clearances is possible if secondary flow conditions exceed the instability threshold when no support or frictional constraint is assumed at a location with a gap around the tube as a consequence of the longer span initially afforded by the gap. This kind of gap-limited fluidelastic vibration is not as severe as classical instability response between spans that are too long for the existing flow field. This is the result of the constraint of the gap after the tube moves across the available gap when modulation occurs as fluidelastically induced tube/support interaction momentarily increases damping and higher modal frequencies in response to initiation of fluidelastic vibration within the gap. The temporary increase in damping and energy dissipation from the interaction then momentarily reduces or eliminates the fluidelastic component of vibration, which in turn reduces tube/support interaction and some higher frequency response, thereby decreasing damping again.

While the consequential tube/support interaction with intermittent impact/sliding conditions is not as severe as that for classical fluidelastic instability, it is much more severe than interaction induced by flow turbulence alone. This type of motion involves the potential for significant tube wear and fatigue damage and is the mechanism resulting in tube wear at an AVB.

Fluidelastic instability initiates when the fluidelastic stability ratio (FSR) exceeds unity (1.0). FSR is the ratio between the effective velocity ( $U_e$ ) and the critical velocity ( $U_c$ ). A more conservative limit can be applied by using a smaller allowable (such as 0.75 in design rather than field evaluation), but the degree of conservatism inherent in the analysis is also directly dependent upon the conservatism of the empirical constants chosen to characterize the instability threshold and overall tube damping. The critical velocity,  $U_c$ , at which instability initiates, is calculated in FASTVIB using an equation of the form

$$\frac{U_c}{f_n D} = \beta \left( \frac{m_o \delta_n}{\rho D^2} \right)^{1/2}$$

where  $f_n$  is the natural frequency in the  $n^{\text{th}}$  normal mode,  $D$  is the tube diameter,  $\beta$  is the empirical threshold instability constant, and the term in brackets is a damping parameter.  $U_c$  is the critical gap velocity for the mode/frequency being considered based on a consistently derived threshold instability constant,  $\beta$ . The damping parameter is a function of the effective or virtual tube mass per unit length,  $m_o$ , the damping log decrement in the  $n^{\text{th}}$  normal mode,  $\delta_n = 2\pi\zeta_n$ , the outside or secondary fluid density,  $\rho$ , and the tube diameter,  $D$ . The virtual tube mass per unit length,  $m_o$ , includes contributions to effective mass from the fluid inside the tube, the tube itself, and the displaced fluid outside the tube and is calculated by

$$m_o = A_i \rho_i + A_t \rho_t + C_m A_o \rho_o$$

where  $C_m$  is an added mass multiplier that is applied to reflect added fluid/structure interaction in closely packed arrays. The added mass multiplier for a single tube in uniform flow is considered to be unity, but it can increase significantly depending upon the confinement effect of the array pattern and spacing and also upon the analytical objective.

There is extensive treatment of inertial coupling and the added mass multiplier in the literature with theoretical derivations, test data and correlations provided as a function of array pattern and pitch spacing. The appropriate value depends somewhat on the immediate objective with lower values recommended when simulating conditions where there is no significant tube coupling (e.g., at low turbulence levels) and higher values where there is significant coupling (e.g., near fluidelastic instability).

The most important input parameter for evaluation of potential for fluidelastic instability is the constant,  $\beta$  that characterizes the threshold of self-excited interaction between the tube motion and the external flow field. There is extensive treatment of this parameter that is a function of the array pattern, the external flow regime, and many other factors in the literature, but most is for straight tubing. Westinghouse uses two different discrete lower bound values for the straight leg and U-bend portions of tubing in recirculating steam generators.

#### Instability Constant for Straight Leg Region

H.J. Connors first obtained  $\beta$  for the straight leg region from simple tests in both water and air environments for both normal  $90^\circ$  and rotated  $45^\circ$  orientations that simulated Westinghouse steam generators with square arrays and a pitch/diameter ratio of 1.41. Later tests for triangular arrays with similar  $p/D$  ratios yielded higher values for the triangular pitch that reflects the reduced tendency for initiation of instability in triangular arrays compared to square arrays. Additional tests and open literature that reference different  $p/D$  ratios indicate the trend for significant reduction in instability threshold as  $p/D$  decreases, so the value used in FASTVIB for the SONGS evaluation has been reduced to account for the tighter arrangement characterized by  $p/D=1.33$ . However, focus on the U-bend response for this study means this parameter has no impact on the subsequent discussion.

#### Instability Constant for U-bend Region



Tests of a 0.214 scale model of a square-pitch U-bend region in the Westinghouse wind tunnel test facility provided lower bound values of 5.23 for tubes without AVBs, and 5.24 for the same tubes with AVBs having gaps so large that tube/AVB interaction did not occur. Later tests on full-size cantilevered straight tubes mounted in the same wind tunnel with different stiffnesses in the lift and drag directions (to simulate relative U-bend tube stiffnesses) resulted in an almost identical value of 5.25. These results are all consistent with instability constants that were derived from testing the MB-2 0.01 power scale model of a Model F steam generator operating in a prototypic steam/water environment without AVBs: individual values ranged from 5.0 to 7.1 with an average of 6.3. In-plane fluidelastic instability could not be induced in the Westinghouse tests with AVBs in place.

A similar range from 5.3 to 9.4 was derived from MB-3 steam/water testing when developing the  $\beta = 5.2$  value for U-bend that was used for evaluating a tube without AVB support that involved a tube rupture event. As more supports were added and higher frequencies resulted in the scale model tests, the threshold instability constant tended toward a lower bound of 4.2 for square-pitch arrays. These internally consistent tests with a characteristic downward trend with increasing frequency all indicated that a higher instability threshold existed in the U-bend relative to the straight leg region. These results all refer to initiation of OP instability. IP instability was never observed in any of these square-pitch U-bend tests despite early attempts to force its occurrence without any AVB support for flows up to three times the OP instability threshold.

Subsequent tests of triangular arrays in the same scaled wind tunnel configuration yielded a higher margin against fluidelastic instability in the U-bend region as expected based on prior tests that characterized straight leg response. The same trend of decreasing instability threshold with increasing frequency was observed for configurations with very little support, but continued increases in frequency with more supports being added resulted in a reversing of the downward trend to the point where instability could not be achieved up to the limits of the wind tunnel. The lower bound instability constant over the frequency range had the same relative factor increase over the lower bound for the square array in the U-bend as in the straight leg, but much higher factors for both the very low and very high frequency range. The lower bound value obtained from these tests is typically used for evaluation of the U-bend region of steam generators with triangular array configurations with recognition that actual margin against instability may be much higher depending upon the number of effective supports. This approach is also applied to the SONGS evaluation in this study with the same adjustment factor for p/D ratio that was used for the straight leg region. As was the case for square array patterns, no in-plane (IP) instability was observed in these tests even for U-bend tubes with no supports above the top tube support plate.

When computing the effective velocity that is the numerator of the FSR equation, FASTVIB uses normal mode theory considering span-wise variations in external flow velocity and density. This involves translation of the varying external flow conditions into an effective velocity that can be used to calculate a stability ratio for each normal mode, n, using

$$U_{en}^2 = \frac{\sum_{j=1}^N \frac{\rho_j}{\rho_o} U_j^2 \phi_{jn}^2 \Delta z_j}{\sum_{j=1}^N \frac{m_j}{m_o} \phi_{jn}^2 \Delta z_j}$$

This equation sums contributions from each element having incremental length  $\Delta z_j$ , where  $U_j$ ,  $\rho_j$ , and  $m_j$  are the gap velocity, fluid density, and incremental mass at span-wise locations along the tube, and  $\Phi_{jn}$  is the normalized displacement (mode shape factor) of the  $j^{\text{th}}$  lumped mass in the  $n^{\text{th}}$  mode of vibration.

A threshold fluidelastic instability constant ( $\beta$ ) of 5.0 was used when evaluating the U-bend region of the SONGS RSGs. This value was derived from tests of triangular-pitch U-bend configurations and scaled down to reflect the smaller pitch/diameter ratio for the SONGS configuration relative to the Westinghouse tested configurations that had a pitch/diameter ratio equal to 1.42. This value of  $\beta$  is applicable to OP instability. A value of  $\beta = 7.8$  was conservatively applied for IP instability based on the maximum velocity tested in the same U-bend configuration with all AVBs removed and still without encountering IP instability. For the straight leg sections, based on an evaluation of normalized trends from open literature and Westinghouse tests, a  $\beta$  value of 3.1 was used. This was derived by applying the same scale factor for the tighter pitch in the SONGS design.

#### Flow Turbulence

This background mechanism is not a primary focus for this evaluation. However, tube displacements from random flow turbulence are calculated in response to a specified spectrum of flow turbulence forces derived from Westinghouse tests using an equation of the form

$$\frac{y_n}{D} = C_1 \left( \frac{\rho_o D^2}{m_o} \right) \left( \frac{U}{f_n D} \right)^{3+S} \left( \frac{1}{\delta_n} \right)^{0.5} \left( \frac{D}{L} \right)^{0.5}$$

where  $y_n$  is the desired statistically defined root mean square displacement amplitude for mode  $n$ ,  $C_1$  and  $S$  are the empirical constants derived to envelope test data as shown on Figure 2-9, and  $\delta_n = 2\pi\xi_n$  is the damping log decrement. The appropriate damping for use in turbulence calculations is a key variable for this and all flow-induced excitation mechanisms of interest. Hence, it is discussed separately at the end of this section with separate explanations appropriate to the straight leg and U-bend regions.

Two different spectra of turbulent cross flow forces are typically used in vibration analyses to reflect different exposure deep inside the tube bundle relative to the inlet region. The higher spectrum, normally used only for evaluation of the straight leg response of tubes located on the bundle periphery and along the tube lane, is conservatively used for all calculations in this evaluation. The bilinear nature of each spectrum assures that calculated responses are either appropriate or conservative regardless of which portion of the curve is used. The statistically defined root mean square (RMS) displacement is a convenient measure for comparison with test or operating plant data. The calculated SRSS (square root of the sum of the squares) of the RMS modal displacements is typically consistent with measured tube response in operating steam generators.

#### Damping in the Straight Leg Region

Theoretical considerations and correlations from heat exchanger test data cited in open literature are used when evaluating tubes with pinned and open support conditions in the straight leg region of operating steam generators. Analyses typically reference a configured spreadsheet formulation that calculates the constants  $A$  and  $B$  as a function of specified parameters for the tube, array pattern, and internal and external fluid conditions of interest. This reference equation for the percent of critical damping,  $\zeta$ , is

$$\zeta = A \left( \frac{1}{f} \right)^{1/2} + \left( \frac{B}{f} \right)$$

where the constant A scales viscous contributions and B scales squeeze-film contributions. The constants A and B are calculated from pertinent properties of the tube and thermal-hydraulic flow field including the tube diameter, the equivalent hydraulic diameter that accounts for array confinement fluid coupling effects, the secondary fluid density, the virtual mass per unit length as defined previously, the kinematic viscosity, the number of spans with significant response, the density of the saturated liquid in the tube/support crevice, the support plate thickness, and a characteristic tube length for the number of spans considered.

#### Damping in the U-bend Region

A generic two-phase damping model has been developed for the U-bend region using multiple sets of steam-water data at steam generator operating conditions. This generic model has the form

$$\zeta = A + B\alpha + Cf^n$$

where  $\zeta$  is the percentage of critical damping,  $\alpha$  is the two-phase modal effective void fraction calculated using a slip model obtained from ATHOS analyses,  $f$  is the tube modal response frequency, and A, B, C,  $n$  are empirically derived constants. Multiple-model, multiple-linear-regression fits of all available data were considered to arrive at the final form of the damping equation with three independent terms to address baseline support conditions, void fraction, and frequency effects.

Derived empirical coefficients are consistent with the 10<sup>th</sup>-15<sup>th</sup> percentile such that 85-90 percent of the data are less than the resulting calculations. However, there is an added conservatism in that the lowest damping values measured at any response amplitude were chosen when establishing the empirical constant A for each type support condition. The data were insufficient to include response amplitude as an independent variable, so the most conservative data at the smallest amplitudes were used when establishing correlations for six different support configurations.

For any variation of or typical support conditions with the tube "pinned" at the top TSP

$$B = -7.853, C = 7.691, \text{ and } n = -0.5$$

with the constant "A" a function of the degree of interaction between tubes and AVB's such that "A" is

- 6.693 for tubes without any AVB support,
- 6.775 for tubes with preloaded contacts at AVB supports,
- 7.113 for tubes in contact with AVB's without preload, and
- 7.225 for tubes which have gaps at AVB supports.

When calculating damping for any combination of typical support conditions (pinned with preloads, pinned without preloads, pinned at some locations with gaps at others), a minimum value is imposed to reflect mechanical/frictional contributions. The mechanical damping floor is also a function of the tube support configuration and varies with selection of the overall constant A. While it is likely that higher minima actually apply in a steam generator, conservative lower bound values were derived by evaluating results of tests with rounded contacts that provided line contact in an air environment. The lower bound values vary from 0.10 to 0.25 percent for the four itemized support configuration

options. These minima have no practical significance except at locations that have extremely high modal effective void fractions, greater than about 95 percent, depending upon the frequency.

At the other extreme, a ceiling of 3.0 percent is imposed when direct calculations yield higher values. Empirical constants derived from this comprehensive evaluation of available two-phase damping data are considered valid for modal effective void fractions in the 0.8-1.0 range for frequencies between 10 and 100 Hz.

### 2.3.2 FIV Results Summary

Stability ratio (SR) is the ratio between effective velocity and critical velocity. This term is used in this report in the context of in-plane vibration. For out-of-plane vibration, the presence of the AVBs limits the vibration amplitude and instability in the classical sense cannot occur. Therefore, the term excitation ratio (ER) is used to denote the ratio between effective velocity and critical velocity.

Excitation ratio maps were generated for the various ineffective AVB cases. An excitation ratio map shows the excitation ratios calculated for a given case with specific ineffective AVB(s) for several tube locations displayed in the map. The map uses row and column numbers as abscissa and ordinate respectively, and is populated by excitation ratios for the tubes at corresponding row-column locations. Although all columns from 9 through 89 are displayed (Column 10 is not shown since there are no tubes in the displayed rows), only selected rows are shown in order to fit the map on a page and since the excitation ratios in adjacent rows are comparable in magnitude to those in displayed rows. Further, lower numbered rows have smaller U-bend radii and hence shorter span lengths between supports. Therefore, the excitation ratios for the lower rows tend to be smaller for any support condition and only a few lower rows are selected for display in the stability map.

A typical stability map is shown in Figure 2-10. This example map is for OP excitation ratios at full power (Cycle 16) for Case 60 with seven consecutive ineffective AVBs (specifically, AVB3 through AVB9). The map for IP stability for the same case (60) is shown in Figure 2-11. Note that the IP stability ratio is smaller than the OP excitation ratio for every tube. This is because, for a given support condition, a tube is more stable in the IP mode compared to the OP mode.

At 70% power (Cycle 17), the excitation ratios and stability ratios go down significantly for OP and IP modes, respectively. For Case 60, the excitation ratio and stability ratio plots at 70% power are displayed in Figure 2-12 and Figure 2-13, respectively.

## 2.4 **Determination of Tube Support Effectiveness from Eddy Current Data**

Application of the Westinghouse methodology for evaluating the tube wear in the SG U-bend involves the use of eddy current results to determine the tube support boundary condition at anti-vibration bars (AVB). Further, the support condition is expected to remain unchanged for several fuel cycles. Hence it is important to describe the rationale and implications associated with this. In the following discussion, out-of-plane (OP) motion due to vibration is treated first followed by in-plane (IP) vibration.

### 2.4.1 Out-of-plane Vibration

Support at an AVB is considered effective when the gap between the tube and the AVB is small such that the tube motion in the out-of-plane direction is severely limited. However, it does not require a contact force to be present, though a contact force is acceptable. The small gap limits the

amplitude of tube motion at this location. Test data shows that when the AVB gap is small, the limited amplitude of motion reduces the wear rate of the tube due to fretting at that location to be negligibly small. As a result, a tube will not display detectable wear at such a location for several cycles of operation.

If the AVB gap is large, appreciable tube motion becomes possible at the given location. However, the occurrence of tube motion and its amplitude will be determined by fluid forces. Below the onset of fluidelastic excitation, the amplitude of motion will be limited to that resulting from random turbulence. The typical turbulent forces in the U-bend of a SG are not sufficient to cause detectable AVB wear. Occurrence of appreciable AVB wear requires fluidelastic excitation. The discussion of fluidelastic vibration and stability ratio are provided in Section 2.3. Since the tube motion is constrained by the AVB, the stability ratio may be called amplitude-limited fluidelastic excitation ratio (ER).

When ER is below 1, the tube is stable and the amplitude of motion remains near the turbulence level. As the value of ER increases above 1, the increasing level of excitation sets in and the potential for tube wear occurs. The value of ER increases as the span length of tube between effective supports increases (due to adjacent inactive AVB locations in a tube). Under such conditions, the tube moves within the confines of the local geometry and the possible mode shapes that become active. This leads to tube wear at those AVBs with which the tube comes into contact within the unsupported span. For longer unsupported spans, the tube may not contact all AVBs within the span due to geometric constraints, especially at the beginning of operation. Such conditions may lead to an AVB wear pattern in a tube that is not continuous, i.e., one or two AVB location(s) without wear that is possibly nestled between AVB locations with wear. As wear progression occurs at the contacting AVBs, the tube may come into contact with the other AVBs in the unsupported span and wear will initiate at such locations thereby "filling in" the AVB wear pattern.

As described in Section 2.5.1, the rate of progression of wear (volume) at an AVB location is directly proportional to the fluidelastic excitation force. The fluidelastic excitation force, in turn, is directly proportional to the amplitude of vibration which is the gap between the tube and the AVB. When the AVB gap is small, the fluidelastic excitation force and hence, the wear rate will be small. Such locations are defined as effective support locations. Since the wear rate at such locations is small, effective support locations will display no significant tube wear and will remain effective for several fuel cycles of operation. On the other hand, the ineffective support locations have larger gaps and will be subject to higher wear rate (when ER exceeds 1) such that AVB wear will be reported at such sites within one or two fuel cycles of operation at full (100%) power. This is the basis for using the eddy current data to identify whether effective support is present at an AVB location.

An AVB wear indication suggests that the AVB gap at that location is large enough to allow tube wear and hence, is an ineffective support location. It is not the size (depth) of the wear indication, but the mere presence that identifies it as an ineffective AVB. This explains the rationale involved in the use of eddy current data to define U-bend support conditions in a tube.

Note that the amplitude of motion remains small at the AVBs that provide effective support located at both ends of the unsupported span. This is also true for effective AVBs located external to the unsupported span. Hence, no discernible tube wear occurs at such locations. This is a very important point. What this means is that continued wear at unsupported AVBs does not significantly impact effective AVB locations; and thus, the unsupported span remains unaffected. The small impact decreases with increasing unsupported span length. Therefore, the unsupported span length remains stable over time (several fuel cycles).

As described above, occasionally nestled AVB locations without reported wear indications may also be locations of ineffective support. In the case of the SONGS RSGs, since they have operated for only one fuel cycle (at most), wear depths at some of the AVB locations are small and hence, below bobbin probe detection threshold. Westinghouse has reviewed +Point inspection data to identify low level wear at AVBs that was not previously reported in order to identify ineffective support locations. This has resulted in identifying several ineffective support locations.

#### 2.4.2 In-plane Vibration

Test data shows that the onset of IP vibration requires much higher velocities than the onset of OP fluidelastic excitation. Hence, a tube that may vibrate IP would definitely be unstable OP. A small AVB gap that would be considered active in the OP mode would also be active in the IP mode because the small gap will prevent significant in-plane motion due to lack of clearance (gap) for the combined OP and IP motions. Thus, a contact force is not required to prevent significant IP motion.

The above conclusion was demonstrated by a series of tests described in Reference 24. The tests were conducted with U-bends under controlled conditions at different AVB gaps. It was found that "the effect of flat bar supports with small clearance is to act as apparent nodal points for flow-induced tube response. They not only prevented the out-of-plane modes as expected, but also the in-plane modes. No in-plane instabilities were observed, even when the flow velocity was increased to three times that expected to cause instability in the apparently unsupported first in-plane mode." These tests clearly demonstrated that a contact force is not required to prevent in-plane vibration. A small gap (e.g., 3 mils) is sufficient to prevent in-plane vibration.

Since the eddy current reported AVB wear indications can be used to define the support conditions for OP mode the same support conditions can also be used for the IP mode. This has been demonstrated by benchmarking of the Westinghouse methodology against the Unit 3 data where significant amount of IP motion and tube-tube wear has occurred.

As discussed above, an active AVB location will continue to remain active (at least for several cycles) even though tube wear may occur at other AVB locations in the tube. Hence, a tube that was stable IP during one cycle will remain stable in the next cycle unless the thermal-hydraulic conditions become more severe. The thermal-hydraulic impact can be evaluated analytically.

### 2.5 Tube Wear Progression

#### 2.5.1 Methods

Tube and support interaction leading to rapid wear in the U-bend region is a complex, highly nonlinear process involving impact dynamics, friction, boundary conditions and forcing functions that change with time during the process. Rather than attempt to calculate and benchmark the nonlinear calculations, Westinghouse performed baseline tests that incorporated the nonlinear interaction for a range of tube and AVB support conditions and measured enveloping workrates that could be scaled to other conditions using forcing functions that are obtained from results of linear vibration analyses. Workrate is the product of the tube/AVB impact force and the sliding distance per unit time during impact. Tube wear is then calculated as a function of time following Archard wear theory using the equation

$$V = K(WR)(t)$$

where V is the calculated wear volume, K is the appropriate tube wear coefficient, WR is the workrate, and t is time. The same equation is used to determine the corresponding AVB wear



volume using an appropriate wear coefficient for the AVB as relative tube and AVB wear volumes are apportioned for conformal interaction. These calculations require three inputs:

1. Specific wear coefficients for the tube and AVB,
2. The normal force/sliding motion workrate, and
3. The depth-volume relationship at the interface.

Each is discussed below in the context of testing, design bases, and application to SONGS operating experience.

The methodology that is applied in this evaluation treats the mechanism that was found to be the cause of moderate wear in the U-bend region of conventional Westinghouse Model 51 and Model F steam generators before the development of advanced tube/AVB support configurations in the mid 1980s. This mechanism has been variously referred to as "fluidelastic vibration in the support inactive mode," "double-span behavior," "fluidelastic rattling within loose supports," and "amplitude or gap limited fluidelastic vibration." Its characteristics are fundamentally different in many respects from those of random flow turbulence that is always present in steam generators. Given the evolving state of knowledge and analytical capabilities at the time, Westinghouse developed a semi-empirical methodology to use as a design tool in treating the fundamental characteristics observed in testing.

#### Westinghouse Test Programs

Extensive flow-induced vibration testing and evaluation to support steam generator design were performed using a broad array of consistent methods for much of four decades at the Westinghouse Research Laboratories (now Science and Technology Center). Only those tests pertinent to the methodology applied in evaluation of SONGS flow-induced vibration and wear potential are described in this report.

Figure 2-14 shows the idealized triangular arrangements that were tested first in the same water tunnel that had been used two decades earlier for square pitch configurations. Figure 2-15 provides a context and reference for discussion of tube vibration response characteristics and flow-induced vibration (FIV) mechanisms using sample results that were obtained from one of those tests. The tube response data on Figure 2-15 includes vortex shedding contributions in the idealized water test that may exist around the periphery of the steam generator inlet regions, but they are not a concern in the two-phase, highly turbulent flow in the U-bend region of interest to this evaluation. The narrow band tube response to random flow turbulence typically varies with velocity raised to about the second power<sup>1</sup> and is illustrated by the red line on Figure 2-15. However, there is a critical velocity above which fluidelastic instability initiates and tube response is so extreme that it must be avoided altogether in design. For illustration purposes, the black line on Figure 2-15 varies with velocity to the tenth power, and it envelopes the tube response in the sample shown.

Several overall conclusions from the test programs are important to subsequent discussion:

1. The tests for triangular array configurations are most applicable to the evaluation of the SONGS steam generators. However, the methodology and design bases were originally developed for square pitch configurations based on earlier tests. The amplitude limited fluidelastic vibration mechanism leading to tube/AVB wear affects a larger percentage of tubes in square pitch configurations.

---

<sup>1</sup> The specific exponent applicable to FIV analyses and to the trend line on this plot using the same correlation is 2.67.

2. Displacements, impact forces, and workrates derived for wear calculations from these laboratory tests are more modulated in steam generators with complex geometry and variations in two-phase flow. This implies they are conservative for the range of tested configurations for the design purposes for which they were intended, but in that sense may overpredict wear in steam generators.
3. Conversely, the range of tube/AVB support conditions tested for design purposes does not cover the apparent range of support conditions implied from the ECT wear indications in the SONGS steam generators. In this sense, the test and design bases may underpredict the extreme wear in the SONGS steam generators prior to benchmarking calculations. In order to overcome this hurdle, the AVB wear depth distribution for each tube was calculated to match the observed wear depths at U2C17 as explained in Section 2.5.2.

### Wear Coefficients

Determination of appropriate wear coefficients is based on both extensive testing within Westinghouse and correlation of results from licensees and external sources. Specific wear coefficients for the Alloy 690 tubes ( $K_t$ ) and 405 Stainless Steel (SS) TSP/AVBs ( $K_a$ ) were derived from all available impact/sliding wear test data. The median value of the wear coefficient for tubing when interacting with 405 SS from the raw test data was 98 ( $10^{-12}$  in<sup>2</sup>/lb).

The average ratio of AVB material wear coefficient to tubing wear coefficient in the original impact/sliding test data was 2.1. However, this data included much softer AVBs. Relatively harder AVBs that wear slower in the early stages are especially limiting if the AVB is not perfectly aligned with the tube. Therefore, the AVB specific wear coefficient is typically considered to be the same as the tubing for reference calculations, but is varied from 0.01 times (negligible AVB wear) up to two times (more AVB wear than tube wear) in normal design calculations.

### Workrates

Workrates are scaled from baseline mechanical shaker test trends using inputs from qualified thermal-hydraulic and FIV analyses such as ATHOS/VGUB and FASTVIB. Evaluating any other geometry, including tube row and AVB location, and any other flow field, requires adjustment of experimentally determined workrates using parameters appropriate to the configuration of interest. In this case, workrates for the SONGS steam generators were determined using scaling factors derived from analyses. This is done using an equation that is a function of tube frequency, secondary fluid density, effective velocity of the fluid for the limiting vibration mode, fluidelastic excitation ratio, effective tube span length, and tube/AVB clearance. The form of this semi-empirical equation for predicting workrates uses an analytical expression of the fluidelastic excitation force,

$$F_n = c_f \rho_o D U_{en}^2 \left( \frac{C_e}{D} \right) \left[ 1 - \frac{U_{cn}^2}{U_{en}^2} \right] L_{cn}$$

that is consistent with measured wind tunnel test results, taken together with experimental trends determined in the baseline U-bend shaker tests. Overall results of the test program were provided in the form of workrate coefficients,  $W_r$ , for use in an equation of the form

$$WR = W_r f_n D F_n$$

where  $F_n$  is the appropriate fluidelastic force calculated from the previous equation that is a function of cross flow excitation. Values for the parameters are obtained from linear vibration analyses using FASTVIB and the extracted ATHOS properties that have been interpolated using VGUB for the tube.

The semi-empirical formulation was developed to envelope workrates using interactions characterizing the tube/AVB interactions at up to three ineffective supports. Figure 2-16 illustrates the typical logic diagram followed during design analyses. Figure 2-17 shows the basic characteristics of the measured workrate trends from U-bend shaker tests as described more fully in Reference 23. The methodology uses the workrate trend ACDE on Figure 2-17 as the dominant characteristic of the limiting wear from amplitude limited fluidelastic excitation. It therefore captures the effects of increasing flow rates and increasing gaps due to wear on the excitation and impact forces, but it does not explicitly calculate what is happening at the effective support intersections on each end of a long span that would be unstable if the supports with large gaps were actually not present. For nominal tube/AVB gaps, the adjacent effective intersections may indeed have higher initial workrates that could lead to gaps and longer spans as shown on the left side of Figure 2-17. Thus, when performing normal design calculations, a range of potential support conditions must be evaluated separately. However, as wear progresses for any given support configuration, the workrate at the large gap becomes limiting after some point illustrated by D on Figure 2-17. This methodology, therefore, does not explicitly calculate details of modal interactions and detailed physics of the process for the entire tube, but it does follow the dominant trend for the mechanism that can lead to rapid wear in tubes with ineffective supports from large gaps that allow amplitude limited fluidelastic rattling within the clearances. The semi-empirical methodology takes workrates that include all nonlinear interactions present in the shaker tests, scales them to levels appropriate to the design being evaluated using results of thermal-hydraulic and linear FIV analyses, and preserves the mode shape for the unstable frequency as wear progresses.

For fundamental modes resulting from multiple consecutive gaps, wear progresses at the first support with tube/AVB interaction, depending upon the mode shape and the existing gaps, to interaction with successive supports as the tube amplitudes fill the gap as it grows from wear at both the tube and the support. If more ineffective locations with gaps are involved in a configuration being evaluated, the first three to interact depending upon the gaps and relative mode shapes can be evaluated. The total workrate that is available to wear the interacting sites (WR) is determined by scaling the characteristic workrate trend from shaker tests ( $W_r$ ) using the excitation force ( $F_n$ ) apportioned to the various intersections to preserve the fundamental mode shape. Sharing among the different intersections depends upon whether one, two, or three intersections are wearing at the same time as illustrated on the right side of Figure 2-17. This process is sensitive to the mode shape and the gaps at the three intersections such that wear begins, pauses or stops at any given location to preserve the dominant mode shape.

One additional factor has a significant effect on the depth of wear at an intersection. If the tube is off-centered more than about ten percent between AVBs, then displacements will be determined by the nearest AVB. While tube displacements are similar for single-sided interaction with one AVB and for double-sided interaction with opposing AVBs, the impact forces are greater for single-sided interaction. This was observed in the U-bend air flow tests, and relative workrates were confirmed during the shaker tests to be about twice as high for single-sided interaction on one side of a tube as for splitting the available energy to wear both sides of the tube at the same intersection. Current coding allows either choice for all sites, but all intersections in the configuration being evaluated must be either single- or double-sided.

#### Depth-Volume Relationship

Depth-volume relationships are calculated based on tube and matching support geometric relationships. Figure 2-18 illustrates those applicable to 0.750-inch diameter tubing and 0.59-inch wide AVBs for various degrees of twist. Note that there is almost an order of magnitude difference in the depth of the combined tube and AVB wear that results from the volume removed from wear required to reach the dashed line that represents 40% through-wall (TW) for the 0 to 4 degree range illustrated on Figure 2-18. The factor is even higher for smaller wear depths, e.g., about 25 at 10%

TW. The relative factor for the tube alone depends upon the size of the corner radius and the relative tube and AVB wear coefficients in addition to the unknown degree of actual twist.

### 2.5.2. Application to SONGS Steam Generators

The semi-empirical wear calculation methodology developed for design, and based on testing described, was adapted for characterizing the SONGS tube wear experience. It includes projecting expectations for future operation at different power levels. The only change to the structure of the coding was to allow continued operation from an existing conformal tube/AVB wear geometry developed during an earlier time period with a different excitation level for the new time period. Without this change, the highly nonlinear effects of beginning with a fresh tube and AVB depth-volume relationship as shown on Figure 2-18 would have prevented meaningful extrapolation of continued operation of the existing steam generators.

Normal design practice involves definition of ranges of potential parameter variables and tube/AVB geometry configurations and then demonstrating that the maximum tube wear consequences are less than a design margin. For the SONGS application, the resulting wear distribution after a cycle of operation is known, or can be inferred from existing ECT data, but for any given tube, there are many parameters that resulted in the wear distribution that are unknown. For example, neither the tube nor the AVB wear coefficient is known except over a range of possibilities for the two materials (Alloy 690 TT tubing and 405 SS AVBs). Whether the inferred tube wear distribution has less wear on the AVB, equal wear on the AVB, or more wear on the AVB markedly affects the combination of other parameters that would produce the same tube wear depth distribution. It can be assumed that the tube and AVB surfaces will not have significant run-in effects for the first cycle of operation, but even this assumption involves a potential error of several hundred percent. Most importantly, the tube/AVB geometry is expected to be different than the original design intent, but all that can be inferred with the available information is the minimum length of the dominant tube vibration span. In the largest sense, the answer (wear distribution) is known, but the inputs are unknown.

Calculation of tube/AVB wear for SONGS Unit 2 follows the semi-empirical methodology adapted as described earlier in this section to continue from the end of Cycle 16 interface conditions. The process can be illustrated by an example tube for which ECT indicates wear at intersections with AVB 4 and AVB 5. The first step is to adjust the raw ECT indication to wear depth using the correlation of metallurgical to non-destructive examination (NDE) reported depths for the NDE technique from Reference 25:

$$W_i = 0.98 ECT_i + 2.89$$

where  $W_i$  is the wear depth for eddy current indicated depth  $ECT_i$  at the tube intersection with AVB<sub>*i*</sub>. Then FASTVIB solutions for various cases of postulated ineffective AVB supports are reviewed to obtain the case with the lowest number of missing AVBs that is unstable in the OP direction. Values for the reference density,  $\rho_o$ , modal effective velocity,  $U_{en}$ , excitation ratio,  $ER=U_{en}/U_{cn}$ , and modal effective length,  $L_{en}$ , are then extracted for use in the fluidelastic force scaling equation. These values, along with the corresponding modal frequency for the unstable mode,  $f_n$ , are then used in the equation to scale the U-bend shaker test reference workrate,  $W_r$ , to obtain the workrate, WR, applicable to the SONGS flow excitation and support configuration being evaluated.

The semi-empirical wear calculation procedure apportions the overall workrate available for the limiting vibration amplitude determined by  $C_e$  among the interacting AVBs depending upon the relative clearances at each intersection. Figure 2-19 illustrates this example with a postulated set

of initial clearances that could have produced approximately equal wear at AVBs 4 and 5. Following the observed trends for displacements to fill the available clearance, amplitude limited vibration occurs with the overall workrate applied at the first intersection to interact with the dominant unstable mode. Wear progresses at that AVB until the clearance becomes big enough from combined wear at the tube and the AVB to allow the dominant mode to begin impacting at the second AVB. As shown on Figure 2-19, the workrates and wear volumes at AVBs 4 and 5 will be about equal to half the total amount that is possible for the configuration being evaluated.

If the observed ECT wear indications are not equal, the postulated initial gaps can be changed to make the site with the highest wear closer than the other and wear longer than the second site with all the energy on the first site until impacting at the second site begins. Wear volumes at each site are converted into depths (for both tubes and AVBs) following the selected correlation for different degrees of twist. A manual, iterative "tuning" process then apportions the available energy to produce the relative wear depths observed from ECT. These depths, which have been tuned to match the observations, could have been obtained with many different combinations of wear coefficients, amounts of AVB cross-sectional twist, workrate trends (nominal or maximum to cover individual tests), single- or double-sided interaction choices, and various factors of uncertainty on FIV parameters. After achieving wear at both sites consistent with ECT after Cycle 16, the combination that produced the result can be held constant while evaluating various excitation levels for subsequent operation using FIV scaling parameters from FASTVIB calculations based on appropriate part power ATHOS analyses. This is the approach that has been used to obtain results described in the following section.

When choosing a set of initial conditions for observed wear at AVBs 4 and 5, it is also possible that a different FASTVIB case corresponding to a different span length with more than two AVBs having ineffective supports could exist. Figure 2-20 shows one such possibility with similar clearances that could have existed at AVBs 3, 4, 5, and 6, but the wear during the first cycle did not progress deep enough to lead to interaction at AVBs 3 and 6. An entirely different set of geometric and material parameters could be used with this case to tune the computed wear at AVBs 4 and 5 to match the observed wear. Then, this new combination could also be used to project expectations for future operation at different levels of excitation.

There is no a priori way to know what the correct combination of geometric and material properties is for various tubes in the SONGS steam generators. However, this methodology follows dominant trends of the mechanism considered to be the source of the observed tube/AVB wear in the SONGS Unit 2 steam generators. It takes the available energy arising from constrained amplitude fluidelastic excitation for any support configuration, matches the starting levels of wear for subsequent operation, and allows evaluation of the relative effects of many variables. The methodology benchmarks the calculated wear distribution at each limiting tube to the actual ECT wear depths at U2C17. The overall "work" required to do this (workrate x time) is therefore matched to actual experience for the first operating cycle. Only the level of flow excitation is changed thereafter for projecting future wear. The methodology is therefore appropriate for the gap limited fluidelastic excitation mechanism.

### 2.5.3 Results Summary

Projection of AVB wear in the limiting active tubes and limiting plugged tubes was performed as described above. Some of the detailed results are explained below using an example.

Tube R121C91 in SG 2E089 is used as the example. This tube had four AVB wear indications with bobbin reported depths of 12%, 15%, 28%, and 23% at AVBs 4 through 7, respectively at U2C17. Wear projection was made for the three deepest indications at AVBs 5 through 7. Projection results

for this tube are shown in Figure 2-21. These values are shown in the small table appearing on the upper left hand corner of the figure as well as on the plots. The bobbin reported wear depths are converted to expected ("true") wear depths based on the correlation between metallurgical depth and NDE-reported wear depth for the eddy current technique (Reference 25). The resulting "true" wear depths for the three indications are shown in the row below the bobbin reported depths in the small table. The projection of the deepest indication (28%TW by bobbin) is shown plotted in red, the next deepest in green, and the third in blue. The abscissa shows operating duration in months and the ordinate is the maximum wear depth in %TW. It may be noted from the start of the curves that, as per these calculation results, the first location to initiate wear was AVB7. This is because the mode shape allowed contact only at this AVB initially. Once the wear at AVB7 reached approximately 11% after about one month of operation, tube contact with AVB6 was possible and the wear initiated at AVB6. Subsequently, tube wear continued at both of these AVB locations. After five months of operation, the tube started to make contact with AVB5 and wear progression continued at all three locations. After 22 months of operation, wear depths matched the "true" estimated depths at U2C17. The matching of U2C17 values were obtained by manually iterating on relative gaps and other parameters.

A software limitation does not allow calculation of wear progression in more than three AVB intersections in a tube. Hence, the shallowest wear indication was excluded from the calculation. For the deeper indications in a tube with more than three wear scars, for which the wear projection was carried out, the resulting process leads to more conservative results since the workrate is shared by three AVB intersections instead of a higher number of intersections. If the workrate is shared by a higher number of intersections, the projected wear rate at every intersection would be smaller. Therefore, the projected wear depths in such cases are likely to be higher than expected.

The projection in Cycle 17 was performed by maintaining the values of input variables from the iterative calculation. The Cycle 17 projection was performed for different power levels of operation including 100%, 80%, 70%, and 60% for up to 18 months. Taking the deepest indication at AVB6 as an example, its projected depth at the end of 18 additional months of operation at 100% power in Cycle 17 was calculated as 38.5%TW. For the lower power levels of 80%, 70% and 60%, the corresponding calculated wear depth values are 32.5%, 31.6%, and 30.4% respectively. The wear depths at 6 months into Cycle 17 are also listed in the figure for each of the four power levels. At 70% power, the wear depth of the indication at AVB6 is 30.8% after 6 months and 31.6%TW after 18 months.

Similarly, for the indication at AVB7, the projected wear depth at 70% power is 25.7%TW after 6 months and 26.2% after 18 months. For the indication at AVB5, the projected wear depth at 70% power is 18.3% after 6 months and 19.2% after 18 months. This example illustrates the detailed results for one tube.

The calculations were repeated for several limiting active tubes and for several limiting plugged tubes. The results are shown in Table 2-9. In this table, the first column shows the tube number, the second column shows the SG, and the third column shows the tube status. The fourth column lists the bobbin reported wear depth and the fifth column shows the expected or "true" depth based on the correlation between metallurgical and NDE wear depth for the inspection technique (25). Both of these values are in %TW. The next five columns show the baseline calculations. The sixth column shows the FASTVIB case number (see Table 2-8) and the seventh column shows the number of consecutive ineffective AVBs. The next three columns (8 through 10) show the wear depths after six months of operation in Cycle 17 at power levels of 100%, 80%, and 70%, respectively. The 100% power level is labeled as Cycle 1 to denote that the full power conditions corresponding to the Cycle 16 operation were used (T-hot = 598°F). The next five columns (11 through 15) are similar to the base line results, but are based on additional AVBs considered as ineffective and the corresponding FASTVIB case numbers as shown.



The results listed in rows are sorted in the order of active tubes and plugged tubes and within each group in the order of SGs 2E088 and 2E089. Rows showing no tube designation in the first column correspond to the last tube listed in the prior row(s). Reviewing the results for the baseline cases at 70% power, the deepest wear depth projected for active tubes for six months in the next cycle is 31.2%TW (R119C89 in SG 2E089 which had a bobbin reported wear depth of 28% at U2C17) and for plugged tubes is 38.5% (R112C88 in SG 2E088 which had a bobbin reported wear depth of 35% at U2C17). None of the results shown in this table includes accounting of the wear projection technique uncertainty. Impact of uncertainty on the projected wear depth is addressed in Sections 3.1.3 and 3.1.4 and its derivation is described in Section 2.5.4.

#### 2.5.4 Wear Projection Uncertainty

As described in the prior subsections, the wear projection methodology applied here is based on selecting the input variables related to the materials and geometry of the tube-AVB intersections to match the wear depth reported in the 2C17 inspection. The methodology then uses the same values of the input variables for projection of the wear depth in Cycle 17. Since values of several input variables are unknown, this approach involves selecting input values within an expected range based on test results, published data and experience, and using these values to obtain a match for the 2C17 inspection results by trial and error. There will be a number of possible "solutions" (combinations of different values of the given input variables) that satisfy the criteria.

The wear projection process applied here is very time consuming due to the trial and error involved in obtaining a match for the inspection results, often for three different AVB wear indications in a given tube. Therefore, the uncertainty evaluation is based on the following analysis applied to one tube. In this evaluation, the method uncertainty (standard deviation of growth) is determined as a fraction of the mean estimated growth of an AVB wear indication. This allows estimation of the growth uncertainty from the estimated growth by applying this ratio. Tube R121C91 in SG 2E089, which has four AVB indications reported in the 2C17 inspection, was selected since this is one of the tubes that will be returned to service with the deepest wear scar.

First, a solution for the input variables was obtained as described in Section 2.5.3. Then a given input variable was selected and an alternate input value was assigned to it, which is within the variable's expected range. Values close to the extremes of the range were selected in order to obtain very dissimilar solutions for the input variable combinations. The trial and error process was repeated to obtain another alternate solution that matched the wear depths reported for this tube at each of the three AVB locations with the deepest wear indications reported in 2C17. This process was repeated ten times and a total of eleven different solutions were obtained with different combinations of input values that allowed close match between calculated wear depths and the reported inspection results for this tube.

Using the calculated input values of the variables, the wear projection for Cycle 17 was made for each of the eleven solutions described above. This yielded a set of eleven wear depth projections. For each of the three AVB wear indications (at B5, B6, and B7), wear depths at two different time frames in Cycle 17 were obtained for full power, 80% power, and 70% power operation during the cycle. Thus each indication had six sets (three operating power levels at two time points in Cycle 17) of wear projections each set having eleven projections corresponding to the eleven "solutions." Hence, there were six sets of eleven separate growth values over the 2C17 inspection results for each of three AVB indications.

Each set consists of eleven separate possible solutions of wear projection for the same tube location, operating power, and Cycle 17 duration (operating length). For each set of growth values, the mean and standard deviation were calculated. The ratio of standard deviation to the mean,

referred to as the normalized standard deviation, was also calculated. The 22 values of the normalized standard deviation ranged from 0.04 to 2.12. The large values of the normalized standard deviations were for the 80% and 70% power cases where the growth values were very small. For the full power cases where the growth values ranged from 1.9% (in 6 months) to 12.4% (in 18 months), the normalized standard deviations ranged from 0.04 to 0.20. Conservatively, the maximum calculated value of 0.20 for the full power cases was selected as the normalized standard deviation for use in this evaluation.

Hence, the standard deviation of growth will be calculated as 0.20 times the estimated growth for an indication. Using this standard deviation, the growth at 95% probability and 50% confidence can be estimated using the normal distribution ( $z = 1.645$ ).

The growth uncertainty will be applied as follows:

- Estimated growth,  $g = \text{Projected wear depth in Cycle 17} - \text{Actual wear depth at 2C17}$
- Normalized standard deviation = 0.20
- Standard deviation,  $\sigma = 0.20 * g$
- Growth at 95% probability =  $g + 1.645 \sigma = g * (1 + 1.645 * 0.20)$

A common sense test of the derived normalized standard deviation was applied as follows. Using the first of the eleven solutions, the growth at 95% probability and 50% confidence was calculated and added to the reported wear depth at 2C17. This was done for each of the three AVB indications at each of the three power levels and two durations of Cycle 17. The number of times the estimated Cycle 17 wear depth in the eleven solutions exceeded the 95% probability 50% confidence values by more than  $0.5\%^2$  was counted. It was found that, of the 198 projected depths in the eleven solutions, only 4 exceeded the 95 percentile values. Hence, the uncertainty evaluation was validated.

A question may be raised regarding the uncertainties in the supporting evaluations such as thermal-hydraulic evaluation and flow-induced vibration evaluations that formed the inputs to the wear projection. Results of those evaluations were applied consistently for both the Cycle 16 assessments that benchmarked the solutions with the 2C17 inspection results and to the Cycle 17 assessments resulting in the wear projection. Hence the uncertainties in those results, present in both cases, balance out each other and are considered irrelevant.

## 2.6 Evaluation of the Potential for In-Plane Vibration

An evaluation was performed to assess the potential for in-plane vibration to occur when the Unit 2 SGs are returned to service. This evaluation is discussed in this section. The flow-induced vibration methodology was described in Section 2.3.

The potential for the occurrence of in-plane vibration during the upcoming cycle was performed for limiting tubes. The tubes with the highest potential for in-plane vibration are the tubes having the longest unsupported spans in the U-bend. The unsupported span length increases with the number of ineffective AVB locations, which do not provide adequate support for the tubes against vibration. Since the threshold for instability is much lower for the out-of-plane vibration mode compared to

---

<sup>2</sup> For four of the 22 cases, the calculated growth was 0. Hence the estimated uncertainty (standard deviation) was also 0, although the true uncertainty is not. Thus the small 0.5% grace value was used to account for such cases. It is possible to apply a small (0.5% or 1%) grace value as the minimum uncertainty allowance (1.645 times the standard deviation) for growth to overcome this drawback. However, it is judged to be so small and, hence, inconsequential. Thus, the simple approach without any adjustment in the uncertainty value to overcome the calculated growth value of 0 was applied in this evaluation.

the in-plane mode, the unsupported span length required for out-of-plane vibration is shorter than for in-plane vibration. Hence, a tube may exhibit out-of-plane vibration even when in-plane vibration may not be present. There are several such tubes in the Unit 2 SGs. Such tubes have experienced tube-to-AVB wear due to out-of-plane vibration. Therefore, the tubes that have the highest potential for in-plane vibration are those with several AVB wear indications. When a tube vibrates within the constrained geometry of the local AVBs, it is possible that the tube may not contact an AVB due to a large gap such that the tube is restrained by another ineffective AVB within the unsupported span. Therefore, when an AVB location without a wear indication is nestled between AVB wear indications in a tube, such nestled locations are conservatively assumed to be unsupported so as to yield the maximum unsupported span length.

Active tubes in the Unit 2 SGs having several AVB wear indications were identified. Flow-induced vibration results for these tubes for their potential for in-plane vibration were evaluated. This evaluation used a value of 7.8 for the instability constant,  $\beta$ . Westinghouse test data discussed in Section 2.3 suggest that the value of the instability constant may be higher for in-plane vibration. A higher value of instability constant would lead to a lower stability ratio. Hence, the IPSR evaluated using a value of 7.8 for the instability constant is conservative.

The results of the evaluation are shown in Table 2-10. All of the tubes in this table were plugged during U2C17, most of them plugged preventively. The U2C17 eddy current data from all of the tubes in this table were evaluated by Westinghouse for any evidence of in-plane vibration. The eddy current data review clearly showed that the wear indications at AVBs did not extend beyond the width of the AVBs in any of these tubes. This strongly suggests that none of these tubes were subjected to in-plane vibration during Cycle 16. Three of the tubes in the list show IPSR values slightly greater than 1 at full power. Since the tubes were not experiencing IP vibration, it adds support for the statement in the last paragraph that the value of 7.8 for the instability constant is indeed conservative. A value closer to 10 for the instability constant would have resulted in IPSR values of less than 1 at full power for all of these tubes, which is more realistic and supported by the eddy current test results.

It may be noted from Table 2-10 that all of the limiting tubes have predicted in-plane stability ratios of less than 1 at 70% power. Since these are the limiting tubes (tubes with largest number of ineffective AVB supports) in the Unit 2 RSGs, all of the other tubes will have even smaller stability ratios. Therefore, all tubes in the Unit 2 SGs will be stable against in-plane vibration in the next operating cycle.

The methodology used for the assessment of the potential for in-plane vibration in the Unit 2 RSGs was benchmarked against the tube-to-tube wear reported in dozens of tubes in the Unit 3 RSGs. This is discussed in more detail below.

### 2.6.1 Methodology Benchmarking Using Unit 3 Findings

In summary, a sample of 86 tubes from Unit 3, each having tube-to-tube wear in the U-bend free span, was evaluated. The logic used in the benchmarking evaluation is displayed in Figure 2-22. It was demonstrated in each case that the free span wear resulted either from in-plane vibration of the given tube or from in-plane vibration of the neighboring tube, which also had a matching wear scar at the same axial location as the given tube.

More severe tube/AVB wear occurred in Unit 3 than in Unit 2. Unit 3 also experienced significant tube-to-tube wear and more extensive tube/TSP wear than in Unit 2. Therefore, the Unit 3 tube wear experience was reviewed to correlate the Unit 3 results in order to apply the same methodology to Unit 2. A large (86) sample of tubes from SG 3E088 that had experienced tube-to-tube wear was selected for this evaluation. There was a focus on 16 tubes that had tube-to-tube

wear with only a few bobbin-reported indications of tube/AVB wear because these tubes would be the most difficult to explain the tube-to-tube wear using the methodology. It is not likely just a coincidence that these tubes happened to be around the boundary of the region with the most severe tube-to-tube wear as shown on Figure 2-23<sup>3</sup>. These "boundary tubes" reflect the transition from severe free span wear experienced by the "interior tubes" in Figure 2-23. While developing criteria to correlate these two extremes of tube-to-tube wear experience, 15 additional "adjacent tubes" were added to the evaluation.

The 86 tubes from SG 3E088, comprising 55 interior tubes, 16 boundary tubes, and 15 adjacent tubes, were subjected to an in-depth, independent evaluation of RPC results contained in the digital ECT files provided by SCE. Both the original reported wear indications from bobbin data and the new RPC results were used to define a range of potential ineffective AVB locations. This range of potential support conditions was evaluated using various FASTVIB cases using the methods described in Section 2.3. Then, all calculations and ECT observations were reviewed to establish the most likely physical explanation for the tube-to-tube wear that occurred in the Unit 3 RSGs. Table 2-11 and Table 2-12 provide a summary of the pertinent results.

Table 2-11 addresses the more difficult to explain boundary tubes along with the adjacent tubes that are required to explain the occurrence of free span (FS) tube-to-tube wear in some instances. Notes explaining legends used in the evaluation follow at the bottom of the second page. The first tube in the table, R114C74, is a boundary tube that has an indicated FS wear depth of 26 %TW on the hot leg side between AVBs B3 and B4, but the only indications of tube/AVB wear are at AVBs B3 and B4 from the bobbin data plus an indication of very small wear (too small for the bobbin detection threshold) at B2 from the RPC evaluation. The support conditions evaluated for the implied support configuration Cases 15 and 25 (see Table 2-8), that simulated ineffective supports at the AVBs with wear, show that OP gap limited fluidelastic excitation could produce wear at those AVBs. The same support configuration Cases 15 and 25 are also clearly insufficient to have the possibility of IP fluidelastic instability as the explanation for the FS wear because the calculated stability ratio is only about half the required threshold using a value of  $\beta_{IP} = 7.8$  for the instability constant. Furthermore, the wear scars that were present showed no extensions beyond the AVB intersections, so there had been no apparent significant in-plane motion of this tube.

The next tube in the Column R112C74 (nearest inside neighbor in the same column) was already in the list as a boundary tube because it had only one wear call at B5, so it was also reviewed to determine if it could be the source of the FS wear that had been found on R114C74. Table 2-11 shows how this is considered to be a possible explanation since it showed indications of in-plane motion as the wear scar extended outside the AVB at B8, and the IP stability ratio would have exceeded the threshold if the nestled AVBs B2, B6, and B7 had been ineffective in providing support in-plane in addition to the seven other locations with small wear observed only with detailed RPC inspection. Since the Unit 3 RSGs operated for only half of a fuel cycle, it is not surprising that the wear depth resulting from out-of-plane vibration at some of the ineffective AVB locations were too small to be detectable by the bobbin probe, and in some cases by the +Point RPC probe. The wear depths on these two boundary tubes were similar (26% and 25 %TW) to support this conclusion.

The inside neighbor adjacent Tube R110C74 had 4 bobbin indications and 4 more low level RPC indications, and it also required 3 additional nestled AVBs to be ineffective at preventing in-plane motion in order to have potential IP instability. It also had reasonably similar FS wear between B3

---

<sup>3</sup> Note that the tubes later called "boundary tubes" due to their location on the map were originally selected by sorting ECT data results and choosing ones that appeared not to have many tube wear indications at the AVBs. The adjacent tubes were added later. The original terminology was retained for the evaluation and the map labels.

and B4 (19%TW). These three tubes illustrate tubes that are most challenging to identify by observation of FS wear on the tube or an adjacent neighbor that interacts with it.

The next two tubes are similar in that one (R101C75) has FS wear on the cold leg between AVBs B9 and B10, but there is no analytical basis to explain it. However, the adjacent Tube R103C75 is potentially unstable in the IP direction using support conditions evident from both bobbin and RPC test results. The FS wear scars also match at 19% and 18%TW, and there is clear evidence of in-plane motion demonstrated by wear scar extensions.

The remaining tubes in Table 2-11 with FS wear that were selected as being the most difficult to explain all have adjacent neighbors that appear to be the sources of IP motions that cause wear at the interface of both tubes. Some are obvious after reviewing the additional RPC indications while others require reasonable, but not obvious, assumptions that are consistent with physical observations and analytical predictions of potential for IP instability. However, the main conclusion of the evaluation is that tubes with FS wear can all be explained as either having that potential, or by interacting with neighbors that have the potential to be unstable in-plane.

The results of the evaluation of the interior tubes in the 86-tube sample are shown in Table 2-12. Here, due to the large number of ineffective AVBs identified by the eddy current inspection results, it is easy to conclude that vibration resulting from in-plane instability led to the free span tube wear in the sample tubes. The long unsupported spans lead to higher SR values for these tubes compared to those in Table 2-11.

A second major conclusion relates to the observed levels of TSP wear that characterize the results shown for most of the interior tubes in Table 2-12 and for several of the adjacent tubes in Table 2-11. Tubes with significant TSP wear correspond to the calculated OP gap limited stability ratios from about 7 to 9 and IP stability ratios greater than about 1.5. As such, they correspond to tubes having very long unsupported spans with obvious potential for IP instability based on the FASTVIB cases considered most representative of the available observations.

The benchmarking evaluation showed that the methodology is capable of accurately predicting the potential for the occurrence of in-plane vibration. It was demonstrated in each case that the free span wear resulted either from in-plane vibration of the given tube or from in-plane vibration of the neighboring tube, which also had a matching wear scar at the same axial location as the given tube.

Table 2-1. ATHOS Model R-θ Finite Difference Grid

IX	Circumferential Grid (XU) (Degrees)	IY	Radial Grid (YV) at Tubesheet (inches)	Radial Grid (YV) at Lower Deck (inches)
1	6.00	1	7.023	9.371
2	12.00	2	12.077	16.113
3	18.00	3	17.130	22.855
4	24.00	4	21.070	28.112
5	30.00	5	26.123	34.854
6	36.00	6	31.177	41.596
7	42.00	7	36.230	48.338
8	48.00	8	40.170	53.595
9	54.00	9	45.223	60.337
10	60.00	10	50.277	67.079
11	66.00	11	55.330	73.821
12	72.00	12	59.270	79.078
13	78.00	13	64.323	85.820
14	84.00	14	69.377	92.563
15	90.00	15	74.430	99.305
16	96.00	16	77.400	103.267
17	102.00	17	79.980	106.710
18	108.00			
19	114.0			
20	120.0			
21	126.0			
22	132.0			
23	138.0			
24	144.0			
25	150.0			
26	156.0			
27	162.0			
28	168.0			
29	174.0			
30	180.0			



**Table 2-2. ATHOS Model Axial Direction (Z) Finite Difference Grid**

<b>IZ</b>	<b>ZW(in)</b>	<b>Comment</b>		
1	3.75			
2	7.50			
3	11.25			
<b>4</b>	<b>15.00</b>	<b>DC Opening</b>		
5	21.95			
6	28.91			
7	35.86			
<b>8</b>	<b>42.81</b>	<b>TSP #1</b>		
9	53.73			
10	64.65			
11	75.56			
<b>12</b>	<b>86.48</b>	<b>TSP #2</b>		
13	97.39			
14	108.31			
15	119.22			
<b>16</b>	<b>130.14</b>	<b>TSP #3</b>		
17	141.05			
18	151.97			
19	162.88			
<b>20</b>	<b>173.80</b>	<b>TSP #4</b>		
21	184.71			
22	195.63			
23	206.55			
<b>24</b>	<b>217.46</b>	<b>TSP #5</b>		
25	228.38			
26	239.29			
27	250.21			
<b>28</b>	<b>261.12</b>	<b>TSP #6</b>		
29	268.06			
30	274.99			
31	281.92			
32	288.86			
<b>33</b>	<b>295.79</b>	<b>Start of Shell Exp.</b>		
34	300.29			
<b>35</b>	<b>304.78</b>	<b>TSP #7</b>		
<b>36</b>	<b>317.41</b>	<b>Start of Wrapper Exp.</b>		
37	325.13			
38	332.84			
39	340.56			
40	348.28			
41	353.42			
42	358.57			
<b>43</b>	<b>363.71</b>	<b>End of Wrapper Exp.</b>		
<b>44</b>	<b>371.39</b>	<b>Top of Shell Cone</b>		
45	377.01			
46	382.63			
<b>47</b>	<b>388.25</b>	<b>Above the U-Bend Region</b>		
48	394.11			
49	399.98			
<b>50</b>	<b>405.84</b>	<b>Bottom of Moisture Sep. Barrel</b>		

Table 2-3. SONGS Unit 2 RSG 2E088 Tube Plugging List

Row	Column																				Col ≤ 89	Col ≥ 89
88	88																				1	0
94	90	94																			0	2
95	89	91																			1	2
97	85	89																			2	1
98	84	86	92																		2	1
99	85	93																			1	1
100	86	88	90	92																	2	2
101	87	89	91	93																	2	3
102	86	88	90	92																	2	2
103	85	87	89	91	93																3	3
104	84	86	88	90	92																3	2
105	83	85	87	89	91																4	2
106	84	86	88	90	92																3	2
107	83	85	89	91	93																3	3
108	34	84	86	90	92	144															3	3
109	35	91	143																		1	2
110	34	36	88	90	92	142	144														3	4
111	35	37	87	89	91	93	141	143													4	5
112	36	38	86	88	90	92	140	142													4	4
113	37	39	87	89	91	139	141														4	4
114	38	40	86	88	90	92	138	140													4	4
115	39	41	85	87	89	91	137	139													5	4
116	40	42	86	88	90	92	136	138													4	4
117	41	43	89	91	93	135	137														3	5
118	42	44	88	92	134	136															3	3
119	43	45	89	133	135																3	3
120	44	46	82	88	92	132	134														4	3
121	45	47	81	85	87	89	131	133													6	3
122	46	48	84	86	88	130	132														5	2
123	47	49	85	87	89	129	131														5	3
124	48	50	86	88	92	128	130														4	3
125	49	51	87	127	129																3	2
126	50	52	86	126	128																3	2
127	51	53	89	125	127																3	3
128	52	54	94	124	126																2	3
129	53	55	93	123	125																2	3
130	54	56	122	124																	2	2
131	55	57	121	123																	2	2
132	56	122																			1	1
133	85	91																			1	1
134	94																				0	1
136	92																				0	1
<b>Total:</b>																					<b>113</b>	<b>106</b>

Note: Tubes R135C93 and R137C89 in this SG were plugged subsequent to this analysis.



Table 2-4. SONGS Unit 2 RSG 2E089 Tube Plugging List

Row	Column																					Col ≤ 89	Col ≥ 89
87	79																					1	0
88	86																					1	0
89	83																					1	0
90	82	84																				2	0
91	81	83	85																			3	0
92	80	82	84	86																		4	0
93	81	83	85	87																		4	0
94	80	82	84	86	88																	5	0
95	81	83	85	87	89																	5	1
96	80	82	84	86	88																	5	0
97	79	81	83	85	87	89																6	1
98	76	80	82	84	86	88	92															6	1
99	79	81	83	85	87	89	91															6	2
100	78	80	82	84	86	88	90															6	1
101	79	81	83	85	87	89																6	1
102	78	80	82	84	86	88	90	94														6	2
103	77	81	83	85	87	89	93	95														6	3
104	78	82	84	86	88	90	92															5	2
105	81	83	85	87	89	91	95															5	3
106	82	84	86	88	90																	4	1
107	81	83	85	87	89	91	95															5	3
108	34	78	82	84	86	88	90	92	144													6	3
109	35	77	81	83	85	87	89	91	95	97	143											7	5
110	34	36	78	80	82	84	86	88	90	98	142	144										8	4
111	35	37	77	79	81	83	85	87	89	141	143											9	3
112	36	38	78	80	82	84	86	88	90	98	140	142										8	4
113	37	39	81	83	85	87	89	91	139	141												7	4
114	38	40	80	82	84	86	88	90	92	94	138	140										7	5
115	39	41	81	83	85	87	89	91	93	95	137	139										7	6
116	40	42	82	84	86	88	90	92	94	136	138											6	5
117	41	43	81	83	85	87	89	91	135	137												7	4
118	42	44	82	84	86	88	90	134	136													6	3
119	43	45	81	83	85	87	133	135														6	2
120	44	46	82	84	90	132	134															4	3
121	45	47	81	83	85	89	131	133														6	3
122	46	48	82	84	86	130	132															5	2
123	47	49	91	129	131																	2	3
124	48	50	128	130																		2	2
125	49	51	127	129																		2	2
126	50	52	84	126	128																	3	2
127	51	53	85	125	127																	3	2
128	52	54	84	124	126																	3	2
129	53	55	87	123	125																	3	2
130	54	56	86	90	122	124																3	3
131	55	57	89	121	123																	3	3
132	56	84	90	122																		2	2
134	90																					0	1
138	88																					1	0
<b>Total:</b>																						<b>218</b>	<b>101</b>

Note: Tubes R80C68, R104C72 and R132C94 in this SG were plugged subsequent to this analysis.

**Table 2-5. Cycle 17 Operating Parameters with 205 Plugged Tubes (SG 2E088)**

Case	50%	60%	70 %	80 %	90 %	100 %	100 % with no plugging
Plugging <sup>*6</sup>	205	205	205	205	205	205	0
Thermal power (MWt)	869.5 (50%)	1041.4 (60%)	1213.3 (70%)	1385.2 (80%)	1557.1 (90%)	1729 (100%)	1729
RCS flow rate (gpm) <sup>*1</sup>	207,726	207,726	207,726	207,726	207,726	207,726	209,880
T <sub>hot</sub> (Tsg-in) (°F)	576.9	583.0	589.1	595.0	600.7	606.3	597.7
T <sub>sg-out</sub> (°F) <sup>*2</sup>	547.2	547.7	548.3 <sup>*4</sup>	548.8 <sup>*4</sup>	549.3	549.7	541.0
T <sub>cold</sub> (°F) <sup>*2</sup>	547.5	548.0	548.6 <sup>*4</sup>	549.1 <sup>*4</sup>	549.6	550.0	541.3
Saturation Steam Pressure (psia)	956	951	946	940	935	928	864
Fouling Factor (ft <sup>2</sup> hr°F /Btu)	0	0	0	0	0	0	0
T <sub>feedwater</sub> (°F)	375.2	390.9	406.5 <sup>*5</sup>	419.6 <sup>*5</sup>	430.5	443	443
Circulation Ratio	7.5	6.2	5.2	4.4	3.8	3.3	3.3
Steam Mass Flow (lb/hr)	3,404,000	4,274,500	5,087,100	5,914,000	6,750,600	7,630,800	7,611,000
Feed Water Mass Flow (lb/hr) <sup>*3</sup>	3,598,000	4,378,800	5,191,600	6,018,800	6,855,600	7,736,000	7,716,900
Blowdown flow rate (gpm)	270	270	270	270	270	270	270

Note: Two additional tubes were plugged in this SG after the completion of this analysis.



**Table 2-6. Cycle 17 Operating Parameters with 305 Plugged Tubes (SG 2E089)**

Case	50%	60%	70 %	80 %	90 %	100 %	100 % with no plugging
Plugging <sup>6</sup>	305	305	305	305	305	305	0
Thermal power (MWT)	869.5 (50%)	1041.4 (60%)	1213.3 (70%)	1385.2 (80%)	1557.1 (90%)	1729 (100%)	1729
RCS flow rate (gpm) <sup>11</sup>	206,695	206,695	206,695	206,695	206,695	206,695	209,880
T <sub>hot</sub> (Tsg-in) (°F)	577.0	583.1	589.2	595.2	601.0	606.6	597.7
T <sub>sg-out</sub> (°F) <sup>12</sup>	547.2	547.7	548.3 <sup>4</sup>	548.8 <sup>4</sup>	549.3	549.7	541.0
T <sub>cold</sub> (°F) <sup>12</sup>	547.5	548.0	548.6 <sup>4</sup>	549.1 <sup>4</sup>	549.6	550.0	541.3
Saturation Steam Pressure (psia)	955	950	945	939	933	926	864
Fouling Factor (ft <sup>2</sup> hr <sup>2</sup> F /Btu)	0	0	0	0	0	0	0
T <sub>feedwater</sub> (°F)	375.2	390.9	406.5 <sup>5</sup>	419.6 <sup>5</sup>	430.5	443	443
Circulation Ratio	7.5	6.2	5.2	4.4	3.8	3.3	3.3
Steam Mass Flow (lb/hr)	3,493,900	4,274,300	5,086,800	5,913,700	6,750,200	7,630,300	7,611,000
Feed Water Mass Flow (lb/hr) <sup>3</sup>	3,597,900	4,378,600	5,191,400	6,018,500	6,855,200	7,735,500	7,716,900
Blowdown flow rate (gpm)	270	270	270	270	270	270	270

Note: Three additional tubes were plugged in this SG after the completion of this analysis.

Table 2-7. Summary of ATHOS Results

Parameter	ATHOS Analysis Case Number										
	Reference	1-a	1-b	2-a	2-b	3-a	3-b	3-c	3-d	4-a	4-b
Power Level (%)	100	50		60		70				80	
Steam Generator	Units 2 and 3	2E89		2E89		2E88		2E89		2E89	
Number of Plugged Tubes	0	306		306		206		306		306	
Tube Columns	All	1 - 86	89 - 177	1 - 89	86 - 177	1 - 89	89 - 177	1 - 89	89 - 177	1 - 89	89 - 177
Tube Bundle Mode	N/A	2E89LC	2E89HC	2E89LC	2E89HC	2E88LC	2E88HC	2E89LC	2E89HC	2E89LC	2E89HC
Number of Plugged Tubes <sup>(1)</sup>	0	216	101	216	101	113	106	218	101	218	101
<b>Operating Conditions and ATHOS Calculated Thermal-Hydraulic Characteristics</b>											
NSSB Power <sup>(2)</sup> , per SG MWt	1728	870.6	570.6	1042.6	1342.6	1214.6	1214.6	1214.6	1214.6	1336.6	1386.6
Primary Flow Rate, Mlbm/hr	79,779	77,926	77,926	77,873	77,873	78,198	78,198	77,810	77,810	77,757	77,757
Primary Pressure, psia	2250	2250	2250	2250	2250	2250	2250	2250	2250	2250	2250
Primary Inlet Temperature <sup>(2)</sup> , °F	598.02	576.48	579.13	586.76	586.35	591.60	601.67	532.06	591.61	595.06	597.55
Primary outlet Temperature <sup>(2)</sup> , °F	541.35	549.64	549.29	550.32	549.91	550.75	550.72	550.99	550.53	551.54	551.04
Feedwater/Steam Flow rate <sup>(2)</sup> , Mlbm/hr	7,603	3,614.7	3,514.7	4,293	4,293	5,104	5,104	5,104	5,104	5,929	5,929
Feedwater Temperature, °F	442.0	375.2	375.2	360.9	360.9	406.5	406.6	406.5	406.5	419.8	419.6
Steam Pressure in the Dome, psia	837.6	666.0	665.0	660.0	660.0	646.0	646.0	646.0	646.0	630.0	630.0
Circulation Ratio <sup>(2)</sup>	3.26	6.62	6.92	6.75	6.75	4.87	4.87	4.87	4.87	4.20	4.20
Downcomer Flow Hot Side <sup>(2)</sup> , Mlbm/hr	12,454	12,207	12,208	12,395	12,393	12,481	12,401	12,490	12,481	12,492	12,493
Downcomer Flow Cold Side <sup>(2)</sup> , Mlbm/hr	12,297	12,108	12,099	12,287	12,283	12,362	12,362	12,363	12,361	12,367	12,364
Maximum Quality <sup>(2)</sup>	0.8955	0.1636	0.1948	0.2636	0.2632	0.3686	0.3693	0.3697	0.3673	0.6113	0.6260
Maximum Void Fraction <sup>(2)</sup>	0.9955	0.8405	0.8413	0.8876	0.8874	0.9254	0.9256	0.9253	0.9251	0.9724	0.9739
Maximum Velocity <sup>(2)</sup> , ft/s	25.12	9.66	9.99	11.34	11.93	12.66	12.68	12.37	12.65	14.07	14.06
<b>Thermal-Hydraulic Parameters at the Maximum <math>\rho V^2</math> Location in the U-bend Section of Row 141 / Column 89</b>											
Gap Velocity, ft/sec	16.83	8.62	8.95	9.99	10.29	11.61	11.64	11.29	11.69	12.68	13.03
Secondary Fluid Density, lbm/ft <sup>3</sup>	7.04	16.11	16.22	13.92	14.33	12.08	12.05	11.98	12.03	10.22	10.24
Relative $\rho V^2$	1.00	0.60	0.65	0.70	0.74	0.80	0.80	0.77	0.81	0.82	0.87

**Notes:**

- (1) There are 14 plugged tubes in Column 89 in both steam generators. Column 89 is a common column for each half of ATHOS tube bundle mode.
- (2) ATHOS calculated values. These values may be different than SG parameters in Reference 3-1.



Table 2-8. Possible AVB Support Cases with Adjacent Ineffective AVBs (Page 1 of 15)

FASTVIB - FLOVIB Case Descriptions																
Case	0	All Supported	Group	Rows	AVB Number											
					1	2	3	4	5	6	7	8	9	10	11	12
Case 0	0	All Supported	Group 1	Rows 48 to 142	1	2	3	4	5	6	7	8	9	10	11	12
			Group 2	Rows 27 to 47	1	2	3	4	5	n.a	n.a.	8	9	10	11	12
			Group 3	Rows 15 to 26	1	n.a	n.a	4	5	n.a	n.a.	8	9	n.a	n.a.	12
			Group 4	Rows 1 to 14	1	n.a	n.a	4	n.a	n.a	n.a.	n.a	9	n.a	n.a.	12
Case 1	1	AVB 1 Missing	Group 1	Rows 48 to 142	X	2	3	4	5	6	7	8	9	10	11	12
			Group 2	Rows 27 to 47	X	2	3	4	5	n.a	n.a.	8	9	10	11	12
			Group 3	Rows 15 to 26	X	n.a	n.a	4	5	n.a	n.a.	8	9	n.a	n.a.	12
			Group 4	Rows 1 to 14	X	n.a	n.a	4	n.a	n.a	n.a.	n.a	9	n.a	n.a.	12
Case 2	1	AVB 2 Missing	Group 1	Rows 48 to 142	1	X	3	4	5	6	7	8	9	10	11	12
			Group 2	Rows 27 to 47	1	X	3	4	5	n.a	n.a.	8	9	10	11	12
			Group 3	Rows 15 to 26	1	n.a	n.a	4	5	n.a	n.a.	8	9	n.a	n.a.	12
			Group 4	Rows 1 to 14	1	n.a	n.a	4	n.a	n.a	n.a.	n.a	9	n.a	n.a.	12
Case 3	1	AVB 3 Missing	Group 1	Rows 48 to 142	1	2	X	4	5	6	7	8	9	10	11	12
			Group 2	Rows 27 to 47	1	2	X	4	5	n.a	n.a.	8	9	10	11	12
			Group 3	Rows 15 to 26	1	n.a	n.a	4	5	n.a	n.a.	8	9	n.a	n.a.	12
			Group 4	Rows 1 to 14	1	n.a	n.a	4	n.a	n.a	n.a.	n.a	9	n.a	n.a.	12
Case 4	1	AVB 4 Missing	Group 1	Rows 48 to 142	1	2	3	X	5	6	7	8	9	10	11	12
			Group 2	Rows 27 to 47	1	2	3	X	5	n.a	n.a.	8	9	10	11	12
			Group 3	Rows 15 to 26	1	n.a	n.a	X	5	n.a	n.a.	8	9	n.a	n.a.	12
			Group 4	Rows 1 to 14	1	n.a	n.a	X	n.a	n.a	n.a.	n.a	9	n.a	n.a.	12
Case 5	1	AVB 5 Missing	Group 1	Rows 48 to 142	1	2	3	4	X	6	7	8	9	10	11	12
			Group 2	Rows 27 to 47	1	2	3	4	X	n.a	n.a.	8	9	10	11	12
			Group 3	Rows 15 to 26	1	n.a	n.a	4	X	n.a	n.a.	8	9	n.a	n.a.	12
			Group 4	Rows 1 to 14	1	n.a	n.a	4	n.a	n.a	n.a.	n.a	9	n.a	n.a.	12

**Table 2-8. Possible AVB Support Cases with Adjacent Ineffective AVBs (Page 2 of 15)**

Case 6	1	AVB 6 Missing	Group 1	Rows 48 to 142	1	2	3	4	5	X	7	8	9	10	11	12
			Group 2	Rows 27 to 47	1	2	3	4	5	n.a.	n.a.	8	9	10	11	12
			Group 3	Rows 15 to 26	1	n.a.	n.a.	4	5	n.a.	n.a.	8	9	n.a.	n.a.	12
			Group 4	Rows 1 to 14	1	n.a.	n.a.	4	n.a.	n.a.	n.a.	n.a.	9	n.a.	n.a.	12
Case 7	1	AVB 7 Missing	Group 1	Rows 48 to 142	1	2	3	4	5	6	X	8	9	10	11	12
			Group 2	Rows 27 to 47	1	2	3	4	5	n.a.	n.a.	8	9	10	11	12
			Group 3	Rows 15 to 26	1	n.a.	n.a.	4	5	n.a.	n.a.	8	9	n.a.	n.a.	12
			Group 4	Rows 1 to 14	1	n.a.	n.a.	4	n.a.	n.a.	n.a.	n.a.	9	n.a.	n.a.	12
Case 8	1	AVB 8 Missing	Group 1	Rows 48 to 142	1	2	3	4	5	6	7	X	9	10	11	12
			Group 2	Rows 27 to 47	1	2	3	4	5	n.a.	n.a.	X	9	10	11	12
			Group 3	Rows 15 to 26	1	n.a.	n.a.	4	5	n.a.	n.a.	X	9	n.a.	n.a.	12
			Group 4	Rows 1 to 14	1	n.a.	n.a.	4	n.a.	n.a.	n.a.	n.a.	9	n.a.	n.a.	12
Case 9	1	AVB 9 Missing	Group 1	Rows 48 to 142	1	2	3	4	5	6	7	8	X	10	11	12
			Group 2	Rows 27 to 47	1	2	3	4	5	n.a.	n.a.	8	X	10	11	12
			Group 3	Rows 15 to 26	1	n.a.	n.a.	4	5	n.a.	n.a.	8	X	n.a.	n.a.	12
			Group 4	Rows 1 to 14	1	n.a.	n.a.	4	n.a.	n.a.	n.a.	n.a.	X	n.a.	n.a.	12
Case 10	1	AVB 10 Missing	Group 1	Rows 48 to 142	1	2	3	4	5	6	7	8	9	X	11	12
			Group 2	Rows 27 to 47	1	2	3	4	5	n.a.	n.a.	8	9	X	11	12
			Group 3	Rows 15 to 26	1	n.a.	n.a.	4	5	n.a.	n.a.	8	9	n.a.	n.a.	12
			Group 4	Rows 1 to 14	1	n.a.	n.a.	4	n.a.	n.a.	n.a.	n.a.	9	n.a.	n.a.	12
Case 11	1	AVB 11 Missing	Group 1	Rows 48 to 142	1	2	3	4	5	6	7	8	9	10	X	12
			Group 2	Rows 27 to 47	1	2	3	4	5	n.a.	n.a.	8	9	10	X	12
			Group 3	Rows 15 to 26	1	n.a.	n.a.	4	5	n.a.	n.a.	8	9	n.a.	n.a.	12
			Group 4	Rows 1 to 14	1	n.a.	n.a.	4	n.a.	n.a.	n.a.	n.a.	9	n.a.	n.a.	12



**Table 2-8. Possible AVB Support Cases with Adjacent Ineffective AVBs (Page 3 of 15)**

Case 12	1	AVB 12 Missing	Group 1	Rows 48 to 142	1	2	3	4	5	6	7	8	9	10	11	X
			Group 2	Rows 27 to 47	1	2	3	4	5	n.a	n.a.	8	9	10	11	X
			Group 3	Rows 15 to 26	1	n.a	n.a	4	5	n.a	n.a.	8	9	n.a	n.a.	X
			Group 4	Rows 1 to 14	1	n.a	n.a	4	n.a	n.a	n.a.	n.a	9	n.a	n.a.	X
Case 13	2	AVB 1, 2 Missing	Group 1	Rows 48 to 142	X	X	3	4	5	6	7	8	9	10	11	12
			Group 2	Rows 27 to 47	X	X	3	4	5	n.a	n.a.	8	9	10	11	12
			Group 3	Rows 15 to 26	X	n.a	n.a	4	5	n.a	n.a.	8	9	n.a	n.a.	12
			Group 4	Rows 1 to 14	X	n.a	n.a	4	n.a	n.a	n.a.	n.a	9	n.a	n.a.	12
Case 14	2	AVB 2, 3 Missing	Group 1	Rows 48 to 142	1	X	X	4	5	6	7	8	9	10	11	12
			Group 2	Rows 27 to 47	1	X	X	4	5	n.a	n.a.	8	9	10	11	12
			Group 3	Rows 15 to 26	1	n.a	n.a	4	5	n.a	n.a.	8	9	n.a	n.a.	12
			Group 4	Rows 1 to 14	1	n.a	n.a	4	n.a	n.a	n.a.	n.a	9	n.a	n.a.	12
Case 15	2	AVB 3, 4 Missing	Group 1	Rows 48 to 142	1	2	X	X	5	6	7	8	9	10	11	12
			Group 2	Rows 27 to 47	1	2	X	X	5	n.a	n.a.	8	9	10	11	12
			Group 3	Rows 15 to 26	1	n.a	n.a	X	5	n.a	n.a.	8	9	n.a	n.a.	12
			Group 4	Rows 1 to 14	1	n.a	n.a	X	n.a	n.a	n.a.	n.a	9	n.a	n.a.	12
Case 16	2	AVB 4,5 Missing	Group 1	Rows 48 to 142	1	2	3	X	X	6	7	8	9	10	11	12
			Group 2	Rows 27 to 47	1	2	3	X	X	n.a	n.a.	8	9	10	11	12
			Group 3	Rows 15 to 26	1	n.a	n.a	X	X	n.a	n.a.	8	9	n.a	n.a.	12
			Group 4	Rows 1 to 14	1	n.a	n.a	X	n.a	n.a	n.a.	n.a	9	n.a	n.a.	12
Case 17	2	AVB 5, 6 Missing	Group 1	Rows 48 to 142	1	2	3	4	X	X	7	8	9	10	11	12
			Group 2	Rows 27 to 47	1	2	3	4	X	n.a	n.a.	8	9	10	11	12
			Group 3	Rows 15 to 26	1	n.a	n.a	4	X	n.a	n.a.	8	9	n.a	n.a.	12
			Group 4	Rows 1 to 14	1	n.a	n.a	4	n.a	n.a	n.a.	n.a	9	n.a	n.a.	12

**Table 2-8. Possible AVB Support Cases with Adjacent Ineffective AVBs (Page 4 of 15)**

Case 18	2	AVB 6, 7 Missing	Group 1	Rows 48 to 142	1	2	3	4	5	X	X	8	9	10	11	12
			Group 2	Rows 27 to 47	1	2	3	4	5	n.a	n.a.	8	9	10	11	12
			Group 3	Rows 15 to 26	1	n.a	n.a	4	5	n.a	n.a.	8	9	n.a	n.a.	12
			Group 4	Rows 1 to 14	1	n.a	n.a	4	n.a	n.a	n.a.	n.a	9	n.a	n.a.	12
Case 19	2	AVB 7, 8 Missing	Group 1	Rows 48 to 142	1	2	3	4	5	6	X	X	9	10	11	12
			Group 2	Rows 27 to 47	1	2	3	4	5	n.a	n.a.	X	9	10	11	12
			Group 3	Rows 15 to 26	1	n.a	n.a	4	5	n.a	n.a.	X	9	n.a	n.a.	12
			Group 4	Rows 1 to 14	1	n.a	n.a	4	n.a	n.a	n.a.	n.a	9	n.a	n.a.	12
Case 20	2	AVB 8, 9 Missing	Group 1	Rows 48 to 142	1	2	3	4	5	6	7	X	X	10	11	12
			Group 2	Rows 27 to 47	1	2	3	4	5	n.a	n.a.	X	X	10	11	12
			Group 3	Rows 15 to 26	1	n.a	n.a	4	5	n.a	n.a.	X	X	n.a	n.a.	12
			Group 4	Rows 1 to 14	1	n.a	n.a	4	n.a	n.a	n.a.	n.a	X	n.a	n.a.	12
Case 21	2	AVB 9, 10 Missing	Group 1	Rows 48 to 142	1	2	3	4	5	6	7	8	X	X	11	12
			Group 2	Rows 27 to 47	1	2	3	4	5	n.a	n.a.	8	X	X	11	12
			Group 3	Rows 15 to 26	1	n.a	n.a	4	5	n.a	n.a.	8	X	n.a	n.a.	12
			Group 4	Rows 1 to 14	1	n.a	n.a	4	n.a	n.a	n.a.	n.a	X	n.a	n.a.	12
Case 22	2	AVB 10, 11 Missing	Group 1	Rows 48 to 142	1	2	3	4	5	6	7	8	9	X	X	12
			Group 2	Rows 27 to 47	1	2	3	4	5	n.a	n.a.	8	9	X	X	12
			Group 3	Rows 15 to 26	1	n.a	n.a	4	5	n.a	n.a.	8	9	n.a	n.a.	12
			Group 4	Rows 1 to 14	1	n.a	n.a	4	n.a	n.a	n.a.	n.a	9	n.a	n.a.	12
Case 23	2	AVB 11, 12 Missing	Group 1	Rows 48 to 142	1	2	3	4	5	6	7	8	9	10	X	X
			Group 2	Rows 27 to 47	1	2	3	4	5	n.a	n.a.	8	9	10	X	X
			Group 3	Rows 15 to 26	1	n.a	n.a	4	5	n.a	n.a.	8	9	n.a	n.a.	X
			Group 4	Rows 1 to 14	1	n.a	n.a	4	n.a	n.a	n.a.	n.a	9	n.a	n.a.	X



**Table 2-8. Possible AVB Support Cases with Adjacent Ineffective AVBs (Page 5 of 15)**

Case 24	3	AVB 1, 2, 3 Missing	Group 1	Rows 48 to 142	X	X	X	4	5	6	7	8	9	10	11	12
			Group 2	Rows 27 to 47	X	X	X	4	5	n.a	n.a.	8	9	10	11	12
			Group 3	Rows 15 to 26	X	n.a	n.a	4	5	n.a	n.a.	8	9	n.a	n.a.	12
			Group 4	Rows 1 to 14	X	n.a	n.a	4	n.a	n.a	n.a.	n.a	9	n.a	n.a.	12
Case 25	3	AVB 2, 3, 4 Missing	Group 1	Rows 48 to 142	1	X	X	X	5	6	7	8	9	10	11	12
			Group 2	Rows 27 to 47	1	X	X	X	5	n.a	n.a.	8	9	10	11	12
			Group 3	Rows 15 to 26	1	n.a	n.a	X	5	n.a	n.a.	8	9	n.a	n.a.	12
			Group 4	Rows 1 to 14	1	n.a	n.a	X	n.a	n.a	n.a.	n.a	9	n.a	n.a.	12
Case 26	3	AVB 3, 4, 5 Missing	Group 1	Rows 48 to 142	1	2	X	X	X	6	7	8	9	10	11	12
			Group 2	Rows 27 to 47	1	2	X	X	X	n.a	n.a.	8	9	10	11	12
			Group 3	Rows 15 to 26	1	n.a	n.a	X	X	n.a	n.a.	8	9	n.a	n.a.	12
			Group 4	Rows 1 to 14	1	n.a	n.a	X	n.a	n.a	n.a.	n.a	9	n.a	n.a.	12
Case 27	3	AVB 4, 5, 6 Missing	Group 1	Rows 48 to 142	1	2	3	X	X	X	7	8	9	10	11	12
			Group 2	Rows 27 to 47	1	2	3	X	X	n.a	n.a.	8	9	10	11	12
			Group 3	Rows 15 to 26	1	n.a	n.a	X	X	n.a	n.a.	8	9	n.a	n.a.	12
			Group 4	Rows 1 to 14	1	n.a	n.a	X	n.a	n.a	n.a.	n.a	9	n.a	n.a.	12
Case 28	3	AVB 5, 6, 7 Missing	Group 1	Rows 48 to 142	1	2	3	4	X	X	X	8	9	10	11	12
			Group 2	Rows 27 to 47	1	2	3	4	X	n.a	n.a.	8	9	10	11	12
			Group 3	Rows 15 to 26	1	n.a	n.a	4	X	n.a	n.a.	8	9	n.a	n.a.	12
			Group 4	Rows 1 to 14	1	n.a	n.a	4	n.a	n.a	n.a.	n.a	9	n.a	n.a.	12
Case 29	3	AVB 6, 7, 8 Missing	Group 1	Rows 48 to 142	1	2	3	4	5	X	X	X	9	10	11	12
			Group 2	Rows 27 to 47	1	2	3	4	5	n.a	n.a.	X	9	10	11	12
			Group 3	Rows 15 to 26	1	n.a	n.a	4	5	n.a	n.a.	X	9	n.a	n.a.	12
			Group 4	Rows 1 to 14	1	n.a	n.a	4	n.a	n.a	n.a.	n.a	9	n.a	n.a.	12

**Table 2-8. Possible AVB Support Cases with Adjacent Ineffective AVBs (Page 6 of 15)**

Case 30	3	AVB 7, 8, 9 Missing	Group 1	Rows 48 to 142	1	2	3	4	5	6	X	X	X	10	11	12		
			Group 2	Rows 27 to 47	1	2	3	4	5	n.a	n.a.	X	X	X	10	11	12	
			Group 3	Rows 15 to 26	1	n.a	n.a	4	5	n.a	n.a.	X	X	n.a	n.a.	12		
			Group 4	Rows 1 to 14	1	n.a	n.a	4	n.a	n.a	n.a.	n.a	X	n.a	n.a.	12		
Case 31	3	AVB 8, 9, 10 Missing	Group 1	Rows 48 to 142	1	2	3	4	5	6	7	X	X	X	11	12		
			Group 2	Rows 27 to 47	1	2	3	4	5	n.a	n.a.	X	X	X	11	12		
			Group 3	Rows 15 to 26	1	n.a	n.a	4	5	n.a	n.a.	X	X	n.a	n.a.	12		
			Group 4	Rows 1 to 14	1	n.a	n.a	4	n.a	n.a	n.a.	n.a	X	n.a	n.a.	12		
Case 32	3	AVB 9, 10, 11 Missing	Group 1	Rows 48 to 142	1	2	3	4	5	6	7	8	X	X	X	12		
			Group 2	Rows 27 to 47	1	2	3	4	5	n.a	n.a.	8	X	X	X	12		
			Group 3	Rows 15 to 26	1	n.a	n.a	4	5	n.a	n.a.	8	X	n.a	n.a.	12		
			Group 4	Rows 1 to 14	1	n.a	n.a	4	n.a	n.a	n.a.	n.a	X	n.a	n.a.	12		
Case 33	3	AVB 10, 11, 12 Missing	Group 1	Rows 48 to 142	1	2	3	4	5	6	7	8	9	X	X	X		
			Group 2	Rows 27 to 47	1	2	3	4	5	n.a	n.a.	8	9	X	X	X		
			Group 3	Rows 15 to 26	1	n.a	n.a	4	5	n.a	n.a.	8	9	n.a	n.a.	X		
			Group 4	Rows 1 to 14	1	n.a	n.a	4	n.a	n.a	n.a.	n.a	9	n.a	n.a.	X		
Case 34	4	AVB 1, 2, 3, 4 Missing	Group 1	Rows 48 to 142	X	X	X	X	5	6	7	8	9	10	11	12		
			Group 2	Rows 27 to 47	X	X	X	X	5	n.a	n.a.	8	9	10	11	12		
			Group 3	Rows 15 to 26	X	n.a	n.a	X	5	n.a	n.a.	8	9	n.a	n.a.	12		
			Group 4	Rows 1 to 14	X	n.a	n.a	X	n.a	n.a	n.a.	n.a	9	n.a	n.a.	12		
Case 35	4	AVB 2, 3, 4, 5 Missing	Group 1	Rows 48 to 142	1	X	X	X	X	6	7	8	9	10	11	12		
			Group 2	Rows 27 to 47	1	X	X	X	X	n.a	n.a.	8	9	10	11	12		
			Group 3	Rows 15 to 26	1	n.a	n.a	X	X	n.a	n.a.	8	9	n.a	n.a.	12		
			Group 4	Rows 1 to 14	1	n.a	n.a	X	n.a	n.a	n.a.	n.a	9	n.a	n.a.	12		



**Table 2-8. Possible AVB Support Cases with Adjacent Ineffective AVBs (Page 7 of 15)**

Case 36	4	AVB 3, 4, 5, 6 Missing	Group 1	Rows 48 to 142	1	2	X	X	X	X	7	8	9	10	11	12
			Group 2	Rows 27 to 47	1	2	X	X	X	n.a	n.a.	8	9	10	11	12
			Group 3	Rows 15 to 26	1	n.a	n.a	X	X	n.a	n.a.	8	9	n.a	n.a.	12
			Group 4	Rows 1 to 14	1	n.a	n.a	X	n.a	n.a	n.a.	n.a	9	n.a	n.a.	12
Case 37	4	AVB 4, 5, 6, 7 Missing	Group 1	Rows 48 to 142	1	2	3	X	X	X	X	8	9	10	11	12
			Group 2	Rows 27 to 47	1	2	3	X	X	n.a	n.a.	8	9	10	11	12
			Group 3	Rows 15 to 26	1	n.a	n.a	X	X	n.a	n.a.	8	9	n.a	n.a.	12
			Group 4	Rows 1 to 14	1	n.a	n.a	X	n.a	n.a	n.a.	n.a	9	n.a	n.a.	12
Case 38	4	AVB 5, 6, 7, 8 Missing	Group 1	Rows 48 to 142	1	2	3	4	X	X	X	X	9	10	11	12
			Group 2	Rows 27 to 47	1	2	3	4	X	n.a	n.a.	X	9	10	11	12
			Group 3	Rows 15 to 26	1	n.a	n.a	4	X	n.a	n.a.	X	9	n.a	n.a.	12
			Group 4	Rows 1 to 14	1	n.a	n.a	4	n.a	n.a	n.a.	n.a	9	n.a	n.a.	12
Case 39	4	AVB 6, 7, 8, 9 Missing	Group 1	Rows 48 to 142	1	2	3	4	5	X	X	X	X	10	11	12
			Group 2	Rows 27 to 47	1	2	3	4	5	n.a	n.a.	X	X	10	11	12
			Group 3	Rows 15 to 26	1	n.a	n.a	4	5	n.a	n.a.	X	X	n.a	n.a.	12
			Group 4	Rows 1 to 14	1	n.a	n.a	4	n.a	n.a	n.a.	n.a	X	n.a	n.a.	12
Case 40	4	AVB 7, 8, 9, 10 Missing	Group 1	Rows 48 to 142	1	2	3	4	5	6	X	X	X	X	11	12
			Group 2	Rows 27 to 47	1	2	3	4	5	n.a	n.a.	X	X	X	11	12
			Group 3	Rows 15 to 26	1	n.a	n.a	4	5	n.a	n.a.	X	X	n.a	n.a.	12
			Group 4	Rows 1 to 14	1	n.a	n.a	4	n.a	n.a	n.a.	n.a	X	n.a	n.a.	12
Case 41	4	AVB 8, 9, 10, 11 Missing	Group 1	Rows 48 to 142	1	2	3	4	5	6	7	X	X	X	X	12
			Group 2	Rows 27 to 47	1	2	3	4	5	n.a	n.a.	X	X	X	X	12
			Group 3	Rows 15 to 26	1	n.a	n.a	4	5	n.a	n.a.	X	X	n.a	n.a.	12
			Group 4	Rows 1 to 14	1	n.a	n.a	4	n.a	n.a	n.a.	n.a	X	n.a	n.a.	12

**Table 2-8. Possible AVB Support Cases with Adjacent Ineffective AVBs (Page 8 of 15)**

Case 42	4	AVB 9, 10, 11, 12 Missing	Group 1	Rows 48 to 142	1	2	3	4	5	6	7	8	X	X	X	X
			Group 2	Rows 27 to 47	1	2	3	4	5	n.a	n.a.	8	X	X	X	X
			Group 3	Rows 15 to 26	1	n.a	n.a	4	5	n.a	n.a.	8	X	n.a	n.a.	X
			Group 4	Rows 1 to 14	1	n.a	n.a	4	n.a	n.a	n.a.	n.a	X	n.a	n.a.	X
Case 43	5	AVB 1, 2, 3, 4, 5 Missing	Group 1	Rows 48 to 142	X	X	X	X	X	6	7	8	9	10	11	12
			Group 2	Rows 27 to 47	X	X	X	X	X	n.a	n.a.	8	9	10	11	12
			Group 3	Rows 15 to 26	X	n.a	n.a	X	X	n.a	n.a.	8	9	n.a	n.a.	12
			Group 4	Rows 1 to 14	X	n.a	n.a	X	n.a	n.a	n.a.	n.a	9	n.a	n.a.	12
Case 44	5	AVB 2, 3, 4, 5, 6 Missing	Group 1	Rows 48 to 142	1	X	X	X	X	X	7	8	9	10	11	12
			Group 2	Rows 27 to 47	1	X	X	X	X	n.a	n.a.	8	9	10	11	12
			Group 3	Rows 15 to 26	1	n.a	n.a	X	X	n.a	n.a.	8	9	n.a	n.a.	12
			Group 4	Rows 1 to 14	1	n.a	n.a	X	n.a	n.a	n.a.	n.a	9	n.a	n.a.	12
Case 45	5	AVB 3, 4, 5, 6, 7 Missing	Group 1	Rows 48 to 142	1	2	X	X	X	X	X	8	9	10	11	12
			Group 2	Rows 27 to 47	1	2	X	X	X	n.a	n.a.	8	9	10	11	12
			Group 3	Rows 15 to 26	1	n.a	n.a	X	X	n.a	n.a.	8	9	n.a	n.a.	12
			Group 4	Rows 1 to 14	1	n.a	n.a	X	n.a	n.a	n.a.	n.a	9	n.a	n.a.	12
Case 46	5	AVB 4, 5, 6, 7, 8 Missing	Group 1	Rows 48 to 142	1	2	3	X	X	X	X	X	9	10	11	12
			Group 2	Rows 27 to 47	1	2	3	X	X	n.a	n.a.	X	9	10	11	12
			Group 3	Rows 15 to 26	1	n.a	n.a	X	X	n.a	n.a.	X	9	n.a	n.a.	12
			Group 4	Rows 1 to 14	1	n.a	n.a	X	n.a	n.a	n.a.	n.a	9	n.a	n.a.	12
Case 47	5	AVB 5, 6, 7, 8, 9 Missing	Group 1	Rows 48 to 142	1	2	3	4	X	X	X	X	X	10	11	12
			Group 2	Rows 27 to 47	1	2	3	4	X	n.a	n.a.	X	X	10	11	12
			Group 3	Rows 15 to 26	1	n.a	n.a	4	X	n.a	n.a.	X	X	n.a	n.a.	12
			Group 4	Rows 1 to 14	1	n.a	n.a	4	n.a	n.a	n.a.	n.a	X	n.a	n.a.	12



**Table 2-8. Possible AVB Support Cases with Adjacent Ineffective AVBs (Page 9 of 15)**

Case 48	5	AVB 6, 7, 8, 9, 10 Missing	Group 1	Rows 48 to 142	1	2	3	4	5	X	X	X	X	X	11	12
			Group 2	Rows 27 to 47	1	2	3	4	5	n.a	n.a	X	X	X	11	12
			Group 3	Rows 15 to 26	1	n.a	n.a	4	5	n.a	n.a	X	X	n.a	n.a	12
			Group 4	Rows 1 to 14	1	n.a	n.a	4	n.a	n.a	n.a	n.a	X	n.a	n.a	12
Case 49	5	AVB 7, 8, 9, 10, 11 Missing	Group 1	Rows 48 to 142	1	2	3	4	5	6	X	X	X	X	X	12
			Group 2	Rows 27 to 47	1	2	3	4	5	n.a	n.a	X	X	X	X	12
			Group 3	Rows 15 to 26	1	n.a	n.a	4	5	n.a	n.a	X	X	n.a	n.a	12
			Group 4	Rows 1 to 14	1	n.a	n.a	4	n.a	n.a	n.a	n.a	X	n.a	n.a	12
Case 50	5	AVB 8, 9, 10, 11, 12 Missing	Group 1	Rows 48 to 142	1	2	3	4	5	6	7	X	X	X	X	X
			Group 2	Rows 27 to 47	1	2	3	4	5	n.a	n.a	X	X	X	X	X
			Group 3	Rows 15 to 26	1	n.a	n.a	4	5	n.a	n.a	X	X	n.a	n.a	X
			Group 4	Rows 1 to 14	1	n.a	n.a	4	n.a	n.a	n.a	n.a	X	n.a	n.a	X
Case 51	6	AVB 1, 2, 3, 4, 5, 6 Missing	Group 1	Rows 48 to 142	X	X	X	X	X	X	7	8	9	10	11	12
			Group 2	Rows 27 to 47	X	X	X	X	X	n.a	n.a	8	9	10	11	12
			Group 3	Rows 15 to 26	X	n.a	n.a	X	X	n.a	n.a	8	9	n.a	n.a	12
			Group 4	Rows 1 to 14	X	n.a	n.a	X	n.a	n.a	n.a	n.a	9	n.a	n.a	12
Case 52	6	AVB 2, 3, 4, 5, 6, 7 Missing	Group 1	Rows 48 to 142	1	X	X	X	X	X	X	8	9	10	11	12
			Group 2	Rows 27 to 47	1	X	X	X	X	n.a	n.a	8	9	10	11	12
			Group 3	Rows 15 to 26	1	n.a	n.a	X	X	n.a	n.a	8	9	n.a	n.a	12
			Group 4	Rows 1 to 14	1	n.a	n.a	X	n.a	n.a	n.a	n.a	9	n.a	n.a	12

**Table 2-8. Possible AVB Support Cases with Adjacent Ineffective AVBs (Page 10 of 15)**

Case 53	6	AVB 3, 4, 5, 6, 7, 8 Missing	Group 1	Rows 48 to 142	1	2	X	X	X	X	X	X	9	10	11	12
			Group 2	Rows 27 to 47	1	2	X	X	X	n.a.	n.a.	X	9	10	11	12
			Group 3	Rows 15 to 26	1	n.a.	n.a.	X	X	n.a.	n.a.	X	9	n.a.	n.a.	12
			Group 4	Rows 1 to 14	1	n.a.	n.a.	X	n.a.	n.a.	n.a.	n.a.	9	n.a.	n.a.	12
Case 54	6	AVB 4, 5, 6, 7, 8, 9 Missing	Group 1	Rows 48 to 142	1	2	3	X	X	X	X	X	X	10	11	12
			Group 2	Rows 27 to 47	1	2	3	X	X	n.a.	n.a.	X	X	10	11	12
			Group 3	Rows 15 to 26	1	n.a.	n.a.	X	X	n.a.	n.a.	X	X	n.a.	n.a.	12
			Group 4	Rows 1 to 14	1	n.a.	n.a.	X	n.a.	n.a.	n.a.	n.a.	X	n.a.	n.a.	12
Case 55	6	AVB 5, 6, 7, 8, 9, 10 Missing	Group 1	Rows 48 to 142	1	2	3	4	X	X	X	X	X	X	11	12
			Group 2	Rows 27 to 47	1	2	3	4	X	n.a.	n.a.	X	X	X	11	12
			Group 3	Rows 15 to 26	1	n.a.	n.a.	4	X	n.a.	n.a.	X	X	n.a.	n.a.	12
			Group 4	Rows 1 to 14	1	n.a.	n.a.	4	n.a.	n.a.	n.a.	n.a.	X	n.a.	n.a.	12
Case 56	6	AVB 6, 7, 8, 9, 10, 11 Missing	Group 1	Rows 48 to 142	1	2	3	4	5	X	X	X	X	X	X	12
			Group 2	Rows 27 to 47	1	2	3	4	5	n.a.	n.a.	X	X	X	X	12
			Group 3	Rows 15 to 26	1	n.a.	n.a.	4	5	n.a.	n.a.	X	X	n.a.	n.a.	12
			Group 4	Rows 1 to 14	1	n.a.	n.a.	4	n.a.	n.a.	n.a.	n.a.	X	n.a.	n.a.	12
Case 57	6	AVB 7, 8, 9, 10, 11, 12 Missing	Group 1	Rows 48 to 142	1	2	3	4	5	6	X	X	X	X	X	X
			Group 2	Rows 27 to 47	1	2	3	4	5	n.a.	n.a.	X	X	X	X	X
			Group 3	Rows 15 to 26	1	n.a.	n.a.	4	5	n.a.	n.a.	X	X	n.a.	n.a.	X
			Group 4	Rows 1 to 14	1	n.a.	n.a.	4	n.a.	n.a.	n.a.	n.a.	X	n.a.	n.a.	X



**Table 2-8. Possible AVB Support Cases with Adjacent Ineffective AVBs (Page 11 of 15)**

Case 58	7	AVB 1, 2, 3, 4, 5, 6, 7 Missing	Group 1	Rows 48 to 142	X	X	X	X	X	X	X	8	9	10	11	12
			Group 2	Rows 27 to 47	X	X	X	X	X	n.a	n.a	8	9	10	11	12
			Group 3	Rows 15 to 26	X	n.a	n.a	X	X	n.a	n.a	8	9	n.a	n.a	12
			Group 4	Rows 1 to 14	X	n.a	n.a	X	n.a	n.a	n.a	n.a	9	n.a	n.a	12
Case 59	7	AVB 2, 3, 4, 5, 6, 7, 8 Missing	Group 1	Rows 48 to 142	1	X	X	X	X	X	X	X	9	10	11	12
			Group 2	Rows 27 to 47	1	X	X	X	X	n.a	n.a	X	9	10	11	12
			Group 3	Rows 15 to 26	1	n.a	n.a	X	X	n.a	n.a	X	9	n.a	n.a	12
			Group 4	Rows 1 to 14	1	n.a	n.a	X	n.a	n.a	n.a	n.a	9	n.a	n.a	12
Case 60	7	AVB 3, 4, 5, 6, 7, 8, 9 Missing	Group 1	Rows 48 to 142	1	2	X	X	X	X	X	X	X	10	11	12
			Group 2	Rows 27 to 47	1	2	X	X	X	n.a	n.a	X	X	10	11	12
			Group 3	Rows 15 to 26	1	n.a	n.a	X	X	n.a	n.a	X	X	n.a	n.a	12
			Group 4	Rows 1 to 14	1	n.a	n.a	X	n.a	n.a	n.a	n.a	X	n.a	n.a	12
Case 61	7	AVB 4, 5, 6, 7, 8, 9, 10 Missing	Group 1	Rows 48 to 142	1	2	3	X	X	X	X	X	X	X	11	12
			Group 2	Rows 27 to 47	1	2	3	X	X	n.a	n.a	X	X	X	11	12
			Group 3	Rows 15 to 26	1	n.a	n.a	X	X	n.a	n.a	X	X	n.a	n.a	12
			Group 4	Rows 1 to 14	1	n.a	n.a	X	n.a	n.a	n.a	n.a	X	n.a	n.a	12
Case 62	7	AVB 5, 6, 7, 8, 9, 10, 11 Missing	Group 1	Rows 48 to 142	1	2	3	4	X	X	X	X	X	X	X	12
			Group 2	Rows 27 to 47	1	2	3	4	X	n.a	n.a	X	X	X	X	12
			Group 3	Rows 15 to 26	1	n.a	n.a	4	X	n.a	n.a	X	X	n.a	n.a	12
			Group 4	Rows 1 to 14	1	n.a	n.a	4	n.a	n.a	n.a	n.a	X	n.a	n.a	12



**Table 2-8. Possible AVB Support Cases with Adjacent Ineffective AVBs (Page 12 of 15)**

Case 63	7	AVB 6, 7, 8, 9, 10, 11, 12 Missing	Group 1	Rows 48 to 142	1	2	3	4	5	X	X	X	X	X	X	X	
			Group 2	Rows 27 to 47	1	2	3	4	5	n.a	n.a.	X	X	X	X	X	X
			Group 3	Rows 15 to 26	1	n.a	n.a	4	5	n.a	n.a.	X	X	n.a	n.a.	X	X
			Group 4	Rows 1 to 14	1	n.a	n.a	4	n.a	n.a	n.a.	n.a	X	n.a	n.a.	X	X
Case 64	8	AVB 1, 2, 3, 4, 5, 6, 7, 8 Missing	Group 1	Rows 48 to 142	X	X	X	X	X	X	X	X	9	10	11	12	
			Group 2	Rows 27 to 47	X	X	X	X	X	n.a	n.a.	X	9	10	11	12	
			Group 3	Rows 15 to 26	X	n.a	n.a	X	X	n.a	n.a.	X	9	n.a	n.a.	12	
			Group 4	Rows 1 to 14	X	n.a	n.a	X	n.a	n.a	n.a.	n.a	9	n.a	n.a.	12	
Case 65	8	AVB 2, 3, 4, 5, 6, 7, 8, 9 Missing	Group 1	Rows 48 to 142	1	X	X	X	X	X	X	X	X	10	11	12	
			Group 2	Rows 27 to 47	1	X	X	X	X	n.a	n.a.	X	X	10	11	12	
			Group 3	Rows 15 to 26	1	n.a	n.a	X	X	n.a	n.a.	X	X	n.a	n.a.	12	
			Group 4	Rows 1 to 14	1	n.a	n.a	X	n.a	n.a	n.a.	n.a	X	n.a	n.a.	12	
Case 66	8	AVB 3, 4, 5, 6, 7, 8, 9, 10 Missing	Group 1	Rows 48 to 142	1	2	X	X	X	X	X	X	X	X	11	12	
			Group 2	Rows 27 to 47	1	2	X	X	X	n.a	n.a.	X	X	X	11	12	
			Group 3	Rows 15 to 26	1	n.a	n.a	X	X	n.a	n.a.	X	X	n.a	n.a.	12	
			Group 4	Rows 1 to 14	1	n.a	n.a	X	n.a	n.a	n.a.	n.a	X	n.a	n.a.	12	
Case 67	8	AVB 4, 5, 6, 7, 8, 9, 10, 11 Missing	Group 1	Rows 48 to 142	1	2	3	X	X	X	X	X	X	X	X	12	
			Group 2	Rows 27 to 47	1	2	3	X	X	n.a	n.a.	X	X	X	X	12	
			Group 3	Rows 15 to 26	1	n.a	n.a	X	X	n.a	n.a.	X	X	n.a	n.a.	12	
			Group 4	Rows 1 to 14	1	n.a	n.a	X	n.a	n.a	n.a.	n.a	X	n.a	n.a.	12	

**Table 2-8. Possible AVB Support Cases with Adjacent Ineffective AVBs (Page 13 of 15)**

Case 68	8	AVB 5, 6, 7, 8, 9, 10, 11, 12 Missing	Group 1	Rows 48 to 142	1	2	3	4	X	X	X	X	X	X	X	X
			Group 2	Rows 27 to 47	1	2	3	4	X	n.a	n.a	X	X	X	X	X
			Group 3	Rows 15 to 26	1	n.a	n.a	4	X	n.a	n.a	X	X	n.a	n.a	X
			Group 4	Rows 1 to 14	1	n.a	n.a	4	n.a	n.a	n.a	n.a	X	n.a	n.a	X
Case 69	9	AVB 1, 2, 3, 4, 5, 6, 7, 8, 9 Missing	Group 1	Rows 48 to 142	X	X	X	X	X	X	X	X	X	10	11	12
			Group 2	Rows 27 to 47	X	X	X	X	X	n.a	n.a	X	X	10	11	12
			Group 3	Rows 15 to 26	X	n.a	n.a	X	X	n.a	n.a	X	X	n.a	n.a	12
			Group 4	Rows 1 to 14	X	n.a	n.a	X	n.a	n.a	n.a	n.a	X	n.a	n.a	12
Case 70	9	AVB 2, 3, 4, 5, 6, 7, 8, 9, 10 Missing	Group 1	Rows 48 to 142	1	X	X	X	X	X	X	X	X	X	11	12
			Group 2	Rows 27 to 47	1	X	X	X	X	n.a	n.a	X	X	X	11	12
			Group 3	Rows 15 to 26	1	n.a	n.a	X	X	n.a	n.a	X	X	n.a	n.a	12
			Group 4	Rows 1 to 14	1	n.a	n.a	X	n.a	n.a	n.a	n.a	X	n.a	n.a	12
Case 71	9	AVB 3, 4, 5, 6, 7, 8, 9, 10, 11 Missing	Group 1	Rows 48 to 142	1	2	X	X	X	X	X	X	X	X	X	12
			Group 2	Rows 27 to 47	1	2	X	X	X	n.a	n.a	X	X	X	X	12
			Group 3	Rows 15 to 26	1	n.a	n.a	X	X	n.a	n.a	X	X	n.a	n.a	12
			Group 4	Rows 1 to 14	1	n.a	n.a	X	n.a	n.a	n.a	n.a	X	n.a	n.a	12
Case 72	9	AVB 4, 5, 6, 7, 8, 9, 10, 11, 12 Missing	Group 1	Rows 48 to 142	1	2	3	X	X	X	X	X	X	X	X	X
			Group 2	Rows 27 to 47	1	2	3	X	X	n.a	n.a	X	X	X	X	X
			Group 3	Rows 15 to 26	1	n.a	n.a	X	X	n.a	n.a	X	X	n.a	n.a	X
			Group 4	Rows 1 to 14	1	n.a	n.a	X	n.a	n.a	n.a	n.a	X	n.a	n.a	X



**Table 2-8. Possible AVB Support Cases with Adjacent Ineffective AVBs (Page 14 of 15)**

Case 73	10	AVB 1, 2, 3, 4, 5, 6, 7, 8, 9, 10 Missing	Group 1	Rows 48 to 142	X	X	X	X	X	X	X	X	X	X	11	12
			Group 2	Rows 27 to 47	X	X	X	X	X	n.a	n.a.	X	X	X	11	12
			Group 3	Rows 15 to 26	X	n.a	n.a	X	X	n.a	n.a.	X	X	n.a	n.a.	12
			Group 4	Rows 1 to 14	X	n.a	n.a	X	n.a	n.a	n.a.	n.a	X	n.a	n.a.	12
Case 74	10	AVB 2, 3, 4, 5, 6, 7, 8, 9, 10, 11 Missing	Group 1	Rows 48 to 142	1	X	X	X	X	X	X	X	X	X	X	12
			Group 2	Rows 27 to 47	1	X	X	X	X	n.a	n.a.	X	X	X	X	12
			Group 3	Rows 15 to 26	1	n.a	n.a	X	X	n.a	n.a.	X	X	n.a	n.a.	12
			Group 4	Rows 1 to 14	1	n.a	n.a	X	n.a	n.a	n.a.	n.a	X	n.a	n.a.	12
Case 75	10	AVB 3, 4, 5, 6, 7, 8, 9, 10, 11, 12 Missing	Group 1	Rows 48 to 142	1	2	X	X	X	X	X	X	X	X	X	X
			Group 2	Rows 27 to 47	1	2	X	X	X	n.a	n.a.	X	X	X	X	X
			Group 3	Rows 15 to 26	1	n.a	n.a	X	X	n.a	n.a.	X	X	n.a	n.a.	X
			Group 4	Rows 1 to 14	1	n.a	n.a	X	n.a	n.a	n.a.	n.a	X	n.a	n.a.	X
Case 76	11	AVB 1, 2, 3, 4, 5, 6, 7, 8, 9, 10, 11 Missing	Group 1	Rows 48 to 142	X	X	X	X	X	X	X	X	X	X	X	12
			Group 2	Rows 27 to 47	X	X	X	X	X	n.a	n.a.	X	X	X	X	12
			Group 3	Rows 15 to 26	X	n.a	n.a	X	X	n.a	n.a.	X	X	n.a	n.a.	12
			Group 4	Rows 1 to 14	X	n.a	n.a	X	n.a	n.a	n.a.	n.a	X	n.a	n.a.	12
Case 77	11	AVB 2, 3, 4, 5, 6, 7, 8, 9, 10, 11, 12 Missing	Group 1	Rows 48 to 142	1	X	X	X	X	X	X	X	X	X	X	X
			Group 2	Rows 27 to 47	1	X	X	X	X	n.a	n.a.	X	X	X	X	X
			Group 3	Rows 15 to 26	1	n.a	n.a	X	X	n.a	n.a.	X	X	n.a	n.a.	X
			Group 4	Rows 1 to 14	1	n.a	n.a	X	n.a	n.a	n.a.	n.a	X	n.a	n.a.	X

**Table 2-8. Possible AVB Support Cases with Adjacent Ineffective AVBs (Page 15 of 15)**

Case 78	12	AVB 1 ALL - Missing	Group 1	Rows 48 to 142	X	X	X	X	X	X	X	X	X	X	X	X
			Group 2	Rows 27 to 47	X	X	X	X	X	n.a	n.a.	X	X	X	X	X
			Group 3	Rows 15 to 26	X	n.a	n.a	X	X	n.a	n.a.	X	X	n.a	n.a.	X
			Group 4	Rows 1 to 14	X	n.a	n.a	X	n.a	n.a	n.a.	n.a	X	n.a	n.a.	X

Table 2-9. Wear Projection Results for Limiting Active Tubes and Plugged Tubes

Tube	SG No	Tube Status	Max Wear Depth, %		Baseline Calculations @ 6 Months in Cycle 17					Additional Missing AVB Check - @ 6 Months				
			ECT Reported	Expected Value	FASTVIB Case	No Seq AVBs	Wear Depth @ Power			FASTVIB Case	No Seq AVBs	Depth @ Power		
							Cycle 1	80%	70%			Cycle 1	80%	70%
R97C87	88	Active	25	27.4	38	4	29.9	27.4	27.4	46	5	29.6	27.8	27.4
R119C89	89	Active	28	30.3	46	5	32.8	31.3	31.2	54	6	32.9	31.8	31.7
R121C91	89	Active	28	30.3	37	4	33.3	31.2	31	45	5	32.6	31.0	30.9
			x	30.3	x	x	x	x	x	46	5	33.2	31.6	31.3
			x	30.3	x	x	x	x	x	53	6	33.1	31.5	31.4
R131C91	89	Active	21	23.5	17	2	25.4	23.5	23.5	38	4	25.9	24.2	23.8
R129C93	89	Active	22	24.5	29	3	-	-	-	47	5	26.8	25.9	25.8
R126C90	89	Active	21	23.5	45	5	24.7	24.1	24.0	60	7	25.6	24.7	24.6
R112C88	88	Plugged	35	37.2	47	5	38.7	38.1	37.9	x	x	x	x	x
R133C91	88	Plugged	35	37.2	38	4	40.7	38.4	38.1	45	5	41.8	39.7	39.4
R114C90	88	Plugged	22	24.5	48	5	26.7	25.7	25.4	60	7	26.6	25.7	25.6
R111C91	88	Plugged	26	28.4	38	4	29.9	28.4	28.4	x	x	x	x	x
R116C86	88	Plugged	29	31.3	46	5	34.4	32.7	32.4	61	7	34.0	33.1	32.9
R117C93	88	Plugged	27	29.4	47	5	31.9	30.7	30.4	x	x	x	x	x
R115C85	88	Plugged	27	29.4	48	5	32.0	30.8	30.6	61	5	31.9	31.2	31.0
R114C86	88	Plugged	21	23.5	53	6	25.7	24.6	24.5	66	8	25.5	24.7	24.6
R112C88	88	Plugged	35	37.2	55	6	39.7	38.7	38.5	x	x	x	x	x
R128C94	88	Plugged	32	34.3	60	7	37.3	36.1	35.7	x	x	x	x	x
R120C92	88	Plugged	32	34.3	66	8	37.4	36.4	36.2	x	x	x	x	x
R121C83	89	Plugged	24	26.4	16	2	29.0	26.4	26.4	46	4	29.3	27.6	27.4
R117C89	89	Plugged	26	28.4	46	5	30.6	29.4	29.2	x	x	30.6	x	x
R108C90	89	Plugged	27	29.4	53	6	32.2	30.9	30.7	x	x	32.1	x	x
R117C81	89	Plugged	29	31.3	55	6	33.4	32.8	32.7	x	x	33.4	x	x
R134C90	89	Plugged	26	28.4	56	6	31.6	30.8	30.6	67	8	31.6	30.7	30.6
R114C88	89	Plugged	24	26.4	56	6	30.4	29.3	28.9	67	8	29.2	28.5	28.3
R117C85	89	Plugged	24	26.4	62	7	28.9	28.2	28.1	74	10	29.4	28.3	28
R122C82	89	Plugged	27	29.4	66	8	32.3	31.2	31.0	x	x	32.3	x	x
R112C84	89	Plugged	27	29.4	67	8	32.1	31.4	31.2	x	x	32.1	x	x
R111C81	89	Plugged	18	20.5	38	4	22.0	20.6	20.6	55	6	22.5	21.9	21.7
			x	20.5	x	x	x	x	x	67 (1st)	8	22.4	21.8	21.7
			x	16.6	x	x	x	x	x	67 (2nd)	8	18.5	17.2	16.8



Table 2-10. In-Plane Stability Ratios for Limiting Tubes

Tube	SG	Case	No Missing AVBs	IP SR 100% power	IP SR 70% power	
R133C91	2e88	45	5	0.763	0.40	Note1
R112C88	2e88	55	6	0.590	0.36	
R120C92	2e88	66	8	<b>1.071</b>	<b>0.71</b>	
R97C85	2e88	66	8	0.827	0.56	
R99C93	2e88	67	8	0.718	0.48	
R117C81	2e89	55	6	0.583	0.38	
R122C82	2e89	66	8	<b>1.083</b>	<b>0.72</b>	
R106C84,	2e89	66	8	0.929	0.62	
R105C83	2e89	66	8	0.929	0.62	
R104C86	2e89	66	8	0.929	0.60	
R98C86	2e89	66	8	0.865	0.56	
R123C91	2e89	66	8	<b>1.096</b>	<b>0.72</b>	
R98C88	2e89	66	8	0.853	0.55	
R112C84	2e89	67	8	0.821	0.58	
R100C84	2e89	67	8	0.718	0.49	

Note 1: AVB5 assumed to be ineffective even though no wear was reported at this location



Table 2-11. Benchmarking Results for Boundary and Adjacent Tubes (Page 1 of 2)

SONGS-3 SG88																						Out of Plane					In Plane					All Wear Contained within AVB?		
Selected Tubes with < 8 AVB Indications (Bobbin) with Adjacent Neighbor																	Cases					SR for β=5.0					SR for β=7.8							
TubeID	SG	Row	Col	B01	B02	B03	FS <sub>H</sub>	B04	B05	B06	B07	B08	B09	FS <sub>C</sub>	B10	B11	B12	1	2	3	4	5	OP1	OP2	OP3	OP4	OP5	IP1	IP2	IP3	IP4		IP5	
114074	SG88	114	74		X	13	26	12										15	25				1.00	1.52				0.41	0.57				Yes	
112074	SG88	112	74	X		X	25	X	7			Xs→	X		X	X		26	27	43	76		1.45	1.15	2.60	6.68		0.55	0.37	0.80	1.55		No	
110074	SG88	110	74	X			19	11	11	X			X	X				27	36	67	71	76	1.12	1.68	2.56	3.59	6.63			0.76	1.08	1.51		Yes
103075	SG88	103	75		X	6d→	19	7d→	X	X	X	X	6d→	18	X	10	7	77					5.40					1.38					No	
101075	SG88	101	75			X	5	8	5				X	19				36	60	69			1.57	2.12	4.00			0.50	0.66	0.93			Yes	
115075	SG88	115	75	X	X	X	26	10	9	X	X	X			12	5		64	76	78		4.20	7.15	8.50			1.02	1.60	1.85				Yes	
113075	SG88	113	75		5	7	26	X	X	6?	X			23			X	52				2.60					0.75						Yes	
111075	SG88	111	75	X	5	7	22	7s→	X	Xd→	Xd→	Xd→	6s→	23	Xs→	X	6	78				7.92					1.75						No	
100076	SG88	100	76	X	X	6	32	5	X	X	6s→	X	5s→	15	6	9	X	78				6.88					1.54						No	
98076	SG88	98	76		X			6	X	6	9	5	15				X	47	55	61	68	0.96	1.30	1.70	2.40		0.34	0.43	0.60	0.56			Yes	
121077	SG88	121	77		X	12	24	24	20	8	Xd→	X	10					36	52	65		1.86	2.79	3.80			0.62	0.82	1.00				No	
119077	SG88	119	77		14	11	55	←19d→	←19d→	←14s→	←11d→	12	10	8	5	11	16	77	78			7.10	9.20				1.65	2.00					No	
98078	SG88	98	78		10	16		X		14	8s→	10s→	7	30	15	16	22	63	77	78		1.95	5.40	7.00			0.42	1.35	1.57				No	
96078	SG88	96	78		X	28		37	37	17	X	11	19	20	15			36	66	70	74	1.55	2.50	3.36	4.00		0.5	0.83	0.98	1.15			Yes	
122078	SG88	122	78			26	18	17	9	X	X						6	26	45			1.54	2.19				0.57	0.65					Yes	
120078	SG88	120	78	7	8	16	18	17	21	←6d→	9	14d→	23d→	44	14	6	11	78				9.34					2.02						No	
113083	SG88	113	83	X	X	14	41	17	24	X	9	12	6		X	X		76		78		7.25		8.60			1.60		1.85				Yes	
111083	SG88	111	83	14	17	15	40	10	←11d→	5d→	12s→	11d→	9		11	6	7	78				8.29					1.80						No	
92084	SG88	92	84	11	11			9	12	5	13	12	13	23	7		7	61	73	78		1.75	4.50	6.80			0.60	1.10	1.40				Yes	
90084	SG88	90	84		X			13	17	19	X		X	23	11			27	45	61	66	70	0.96	1.60	1.67	2.32	3.04	0.32	0.45	0.55	0.76	0.90		Yes
93085	SG88	93	85	X	5	X	46	8	←7d→	13	13s→	13d→	8s→	20	X	8	8	78				6.80					1.40						No	
91085	SG88	91	85		X			X		8	8	9	X	12				29	39	47	65	70	0.47	0.60	1.05	2.75	3.10	0.14	0.19	0.34	0.74	0.90		Yes
111085	SG88	111	85				19		8	7	8s→		8		X			55	66			1.65	3.13				0.54	0.98					No	
109085	SG88	109	85		7	X	19	14	20s→	X	14	14	X	19	X	X	X	16	46	70	77		0.99	1.52	4.10	6.3		0.25	0.45	1.15	1.50			No
107085	SG88	107	85	13	9	7	48	16	←11d→	←8d→	←8d→	10	9d→	20	8	12	21	78				8.00					1.74						No	



Table 2-11. Benchmarking Results for Boundary and Adjacent Tubes (Page 2 of 2)

96088	SG88	96	88	6 7 X 21 6 ←11d ←12d→ 8d→ 9d→ 11 23 Xs→ 7 11												78		6.90		1.50	No										
94088	SG88	94	88	19 X 6 12 7 X												28	37	45	54	60	0.70	1.08	1.70	1.39	2.06	0.21	0.30	0.48	0.45	0.63	Yes
105089	SG88	105	89	X 8 X 33 7 12 X X ←7s 8 6												76	78				6.41	7.62				1.46	1.66	No			
103089	SG88	103	89	X X 31 ←10s X Xs→ 6s→ 11 X X												47	61	66	74		1.13	1.95	2.70	4.50		0.39	0.67	0.92	1.27	No	
106090	SG88	106	90	6 8 7 X 6 X 24 X X												55	66	75			1.50	2.90	4.60		0.50	0.95	1.20	Yes			
104090	SG88	104	90	X X X X X 6s→ X 25 X												55	70				1.52	3.90				0.50	1.10	No			

Notes/Legend:

**##** Numbers in black font under AVB locations indicate bobbin %TW from original data file

**##** Numbers in red font under AVB locations indicate RPC %TW from original data file

**X** Indicates low level wear from WEC evaluation of RPC ECT file

Black box shows extent of consecutive AVBs in the OP mode that best fits the data and analyses

Dark red box shows extent of consecutive AVBs in IP mode that best fits the data and analyses

s→ d→ Arrows show direction of wear scar extent outside AVB, s or d for single- or double-sided wear on tube

**R C** Light red shading indicates AVB anomaly such as observable taper/twist in wear scar

Light green shading indicates one of a number of consecutive AVBs with wear

Yellow shading indicates a potential ineffective site when defining cases to evaluate

Orange shading corresponds to tubes with 4 or more TSP wear calls on both sides

AVB misalignment or off-nominal interaction (other than twist)

**ID SG Row Col** Tubes identified by blue font indicate tubes that could have TtT wear due to IP instability (either alone or due to adjacent tube in same column)



Table 2-12. Benchmarking Results for Interior Tubes (Page 1 of 2)

Selected Tubes with > 7 AVB Indications (Bobbin)														Cases					SR for $\beta=5.0$					SR for $\beta=7.8$									
TubeID	SG	Row	Col	B01	B02	B03	F5 <sub>H</sub>	B04	B05	B06	B07	B08	B09	F5 <sub>C</sub>	B10	B11	B12	1	2	3	4	5	OP1	OP2	OP3	OP4	OP5	IP1	IP2	IP3	IP4	IP5	
106076	SG88	106	76	13	14	11	40	21	5	15	13	11	16	46	17	10	15	78						7.56					1.68				
103077	SG88	103	77	13	18	23	37	14	6	9	8	12	7	19	8	7	22	78						7.30				1.60					
107077	SG88	107	77	15	21	28	80	20	X	8	9	14	16	48	16	13	17	78						7.80				1.70					
109077	SG88	109	77	21	19	25	39	14	X	6	7	11	13	48	11	8	17	78						8.10				1.74					
113077	SG88	113	77		9	14	11	21	6	9	6		5	31	15	12		52	78				2.60	8.50				0.75	1.85				
115077	SG88	115	77	25	22	9	10	11	14			5	12	20	16	13		43	76	78			2.70	7.25	8.70			0.78	1.62	1.90			
117077	SG88	117	77		17	7	58	12	8	22	27		12	7	12	13		52	74	78			2.70	5.70	8.90			0.80	1.41	1.93			
102078	SG88	102	78	10	21	18	99	13	15	16	17	7	14		24	14	14	78						7.30				1.60					
104078	SG88	104	78	25	13	24	99	23	14	10	14	13	23		18	25	20	78						7.60				1.65					
106078	SG88	106	78	19	13	15	99	X	6	9	12	16	16	46	18	23	24	78						7.80				1.69					
108078	SG88	108	78	22	14	17	66	10	6	17	9	11	13	49	15	27	25	78						8.00				1.71					
118078	SG88	118	78	8	24	17	18	12	11	10	10	15	12	22	5	6	X	78						9.00				1.97					
103079	SG88	103	79	19	17	18	39	20	11	9	6	13	23	45	14	11	23	78						7.50				1.60					
105079	SG88	105	79	13	9	15	50	20	10	9	13	11	17	38	13	23	26	78						7.72				1.67					
107079	SG88	107	79	11	11	13	57	14	7	13	8	13	20	43	17	19	24	78						8.00				1.71					
109079	SG88	109	79	10	18	18	39	16	17	10	12	16	10	41	13	13	25	78						8.10				1.75					
115079	SG88	115	79	10	18	15	24	10	8	9	11	7	14	35	21	14	18	78						8.80				1.90					
117079	SG88	117	79	17	11	18	50	10	16	8	11	11	10	38	13	10	20	78						9.00				1.98					
121079	SG88	121	79			21	22	17	27	13	13	13	13		12	7		71	77				4.40	7.30			1.22	1.68					
96080	SG88	96	80	7	16	10	15	15	31	9	9	10	13	32	13	13	8	78						6.75				1.50					
98080	SG88	98	80	11	16	18	72	26	16	X	8	7	8	31	12	17	10	78						7.00				1.54					
100080	SG88	100	80	19	22	18	81	11	18	7	10	12	9	19	15	16	19	78						7.24				1.56					
102080	SG88	102	80	20	16	14	57	19	7	X	6	9	10	14	11	16	17	78						7.40				1.60					
104080	SG88	104	80	13	22	17	59	23	7	12	5	9	14	30	17	18	26	78						7.50				1.64					
106080	SG88	106	80	31	24	11	11	12	7	5	8	9	19	57	15	23	26	78						7.75				1.68					
108080	SG88	108	80	17	22	18	22	22	13	14	6	9	16	51	17	14	26	78						8.00				1.72					
112080	SG88	112	80	10	18	20	33	21	9	X	X	8	9	53	9	12	16	78						8.50				1.82					
114080	SG88	114	80	6	15	17	35	22	5	13	11	7	8	47	6	9	19	78						8.60				1.88					
116080	SG88	116	80	22	24	12	31	17	7	9	8	7	12		6	7		76	78				7.58	8.98			1.66	1.93					
118080	SG88	118	80	7	25	28	19	19	18	20	10	13	10		10	11		76	78				7.70	9.15			1.69	1.98					



Table 2-12. Benchmarking Results for Interior Tubes (Page 2 of 2)

Selected Tubes with > 7 AVB Indications (Bobbin)														Cases					SR for $\beta=5.0$					SR for $\beta=7.8$										
TubeID	SG	Row	Col	B01	B02	B03	FS <sub>H</sub>	B04	B05	B06	B07	B08	B09	FS <sub>C</sub>	B10	B11	B12	1	2	3	4	5	OP1	OP2	OP3	OP4	OP5	IP1	IP2	IP3	IP4	IP5		
95081	SG88	95	81	22	9	18	68	16	12	8	11	11	10	41	12	5	19	78						6.63					1.49					
97081	SG88	97	81	18	16	18	67	16	16	7	12	9	5	45	6	8	21	78						6.75					1.51					
99081	SG88	99	81	17	12	15	72	20	13		6	5		44	12	10	18	43	63	78			2.25	1.95	7.10			0.69	0.42	1.55				
101081	SG88	101	81	20	15	18	78	25	15	7	6	5	8	27	6	10	18	78						7.30					1.59					
103081	SG88	103	81	13	15	20	50	16	6	12	6	7	11	41	9	10	17	78						7.50					1.63					
105081	SG88	105	81	22	19	23	60	13	X	9	7	11	10	38	X	13	17	78						7.69					1.66					
107081	SG88	107	81	10	19	22	59	15	6	8	5	8	9	35	11	9	14	78						8.00					1.70					
111081	SG88	111	81	7	12	17	56	14	5		6	8	6	13	10	10	23	57	43	78			1.86	2.56	8.32			0.39	0.75	1.78				
113081	SG88	113	81	9	10	18	58	23	10		9	9		9	9	11	5	43	57	78			2.65	1.90	8.50			0.77	0.42	1.85				
115081	SG88	115	81	X	26	21		14	15	22	18	X	8	6	25	10		76	78					7.40	8.80			1.60	1.90					
96082	SG88	96	82	9	8	13	43	22	22	7	6	9	8	30	9	11	18	78						6.75					1.41					
100082	SG88	100	82	13	7	14	42	14	10	6	10	8	10	39	11	7	21	78						7.20					1.57					
104082	SG88	104	82	15	10	11	59	18	15	6	12	8	13	48	16	11	20	78						7.50					1.64					
106082	SG88	106	82	20	8	15	52	13	17	14	16	10	8	51	9	15	19	78						7.75					1.70					
108082	SG88	108	82	13	12	13	46	12		7	8	15	14	22	16	20	19	63	78				2.20	8.00				0.47		1.75				
114082	SG88	114	82		12	12	18	15	7	19	27	8	6		9	X	X	77	78				6.60	8.50				1.60		1.85				
101083	SG88	101	83	9	8	15	31	15	13	10	6		9	54	9	17	23	78						7.30					1.60					
103083	SG88	103	83	12	12	16	42	16	9		X	X	10	X	46	8	21	25	78						7.50					1.64				
100084	SG88	100	84	17	17		38	7	25	X	8	11	8		7	6	13	72	78				3.31	7.17				0.80	1.56					
102084	SG88	102	84	15	23	11	41	X	18	12		10	11	36	12	10	17	51	50	78			2.70	1.25	7.40			0.79	0.29	1.60				
104084	SG88	104	84	11	21	17	32	17	11	11	5	11	12	66	19	8	18	78						7.70					1.65					
108084	SG88	108	84	10	20	22	37	9		X	16	13	7	9	10	11	17	78						8.10					1.74					
112084	SG88	112	84		11	8	14	6	5	6	9	6	23	14	10			70	73	76			4.30	6.00	7.20			1.20	1.40	1.84				
99085	SG88	99	85	13	21	12	37	14	8	6	9	12	10	44	11	6	15	78						7.10					1.53					
104086	SG88	104	86	14	20	9	50	6	9	12		11	9	44	8	9	15	51	50	78			2.80	1.30	7.70			0.80	0.29	1.63				



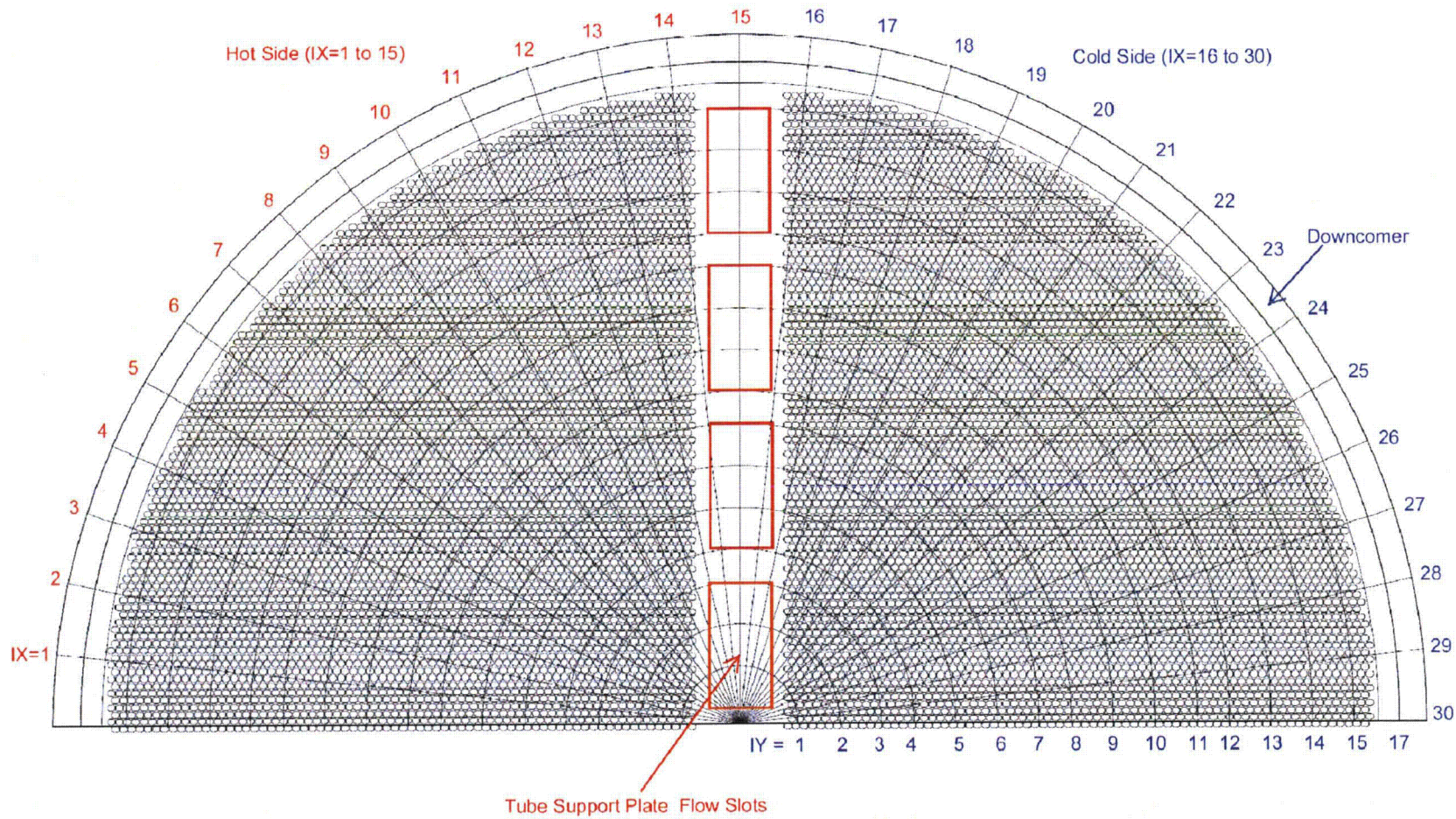
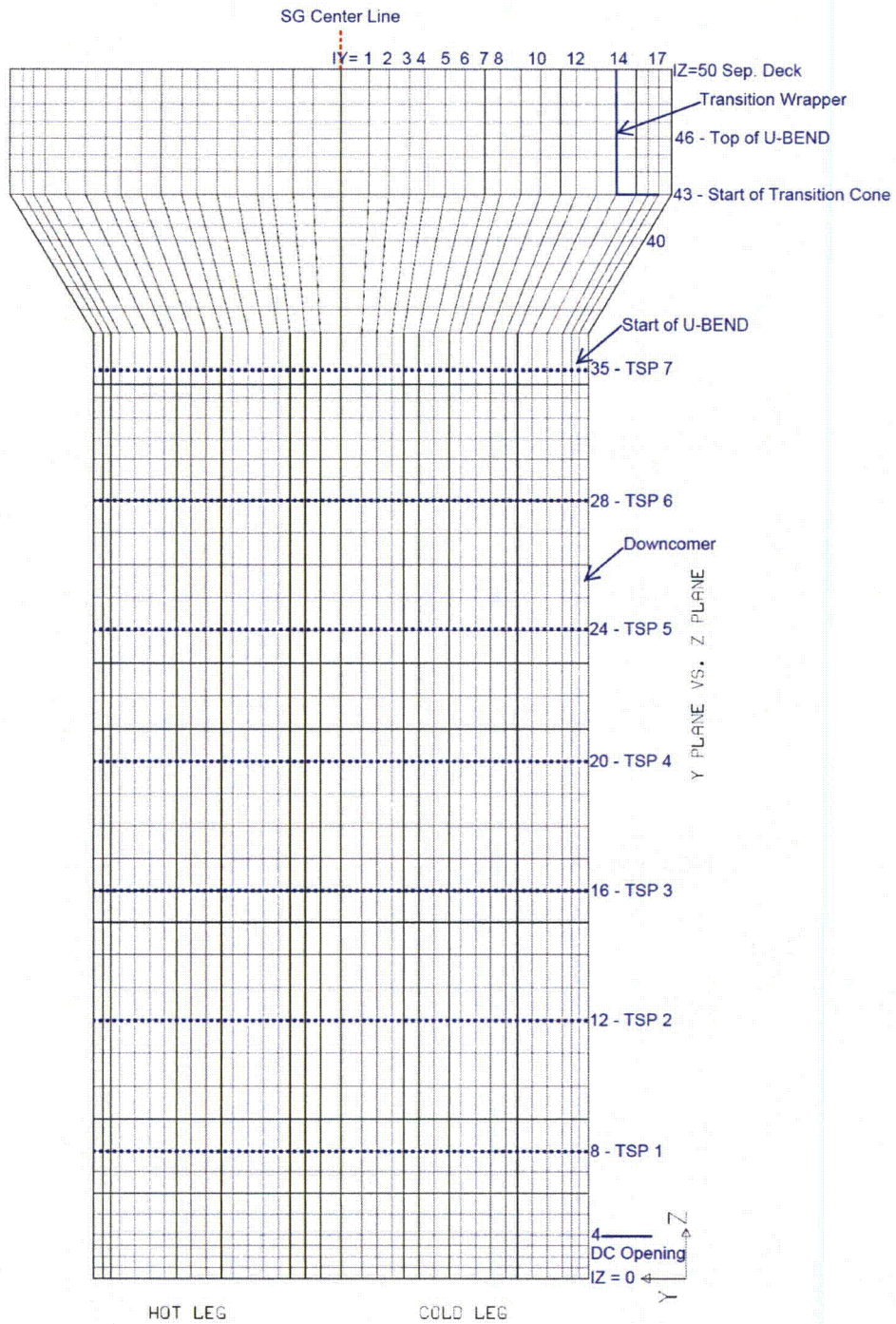


Figure 2-1. ATHOS Finite Difference Grid in the Horizontal (R-θ) Plane





**Figure 2-2. ATHOS Finite Difference Grid in the Vertical (R-θ) Plane**

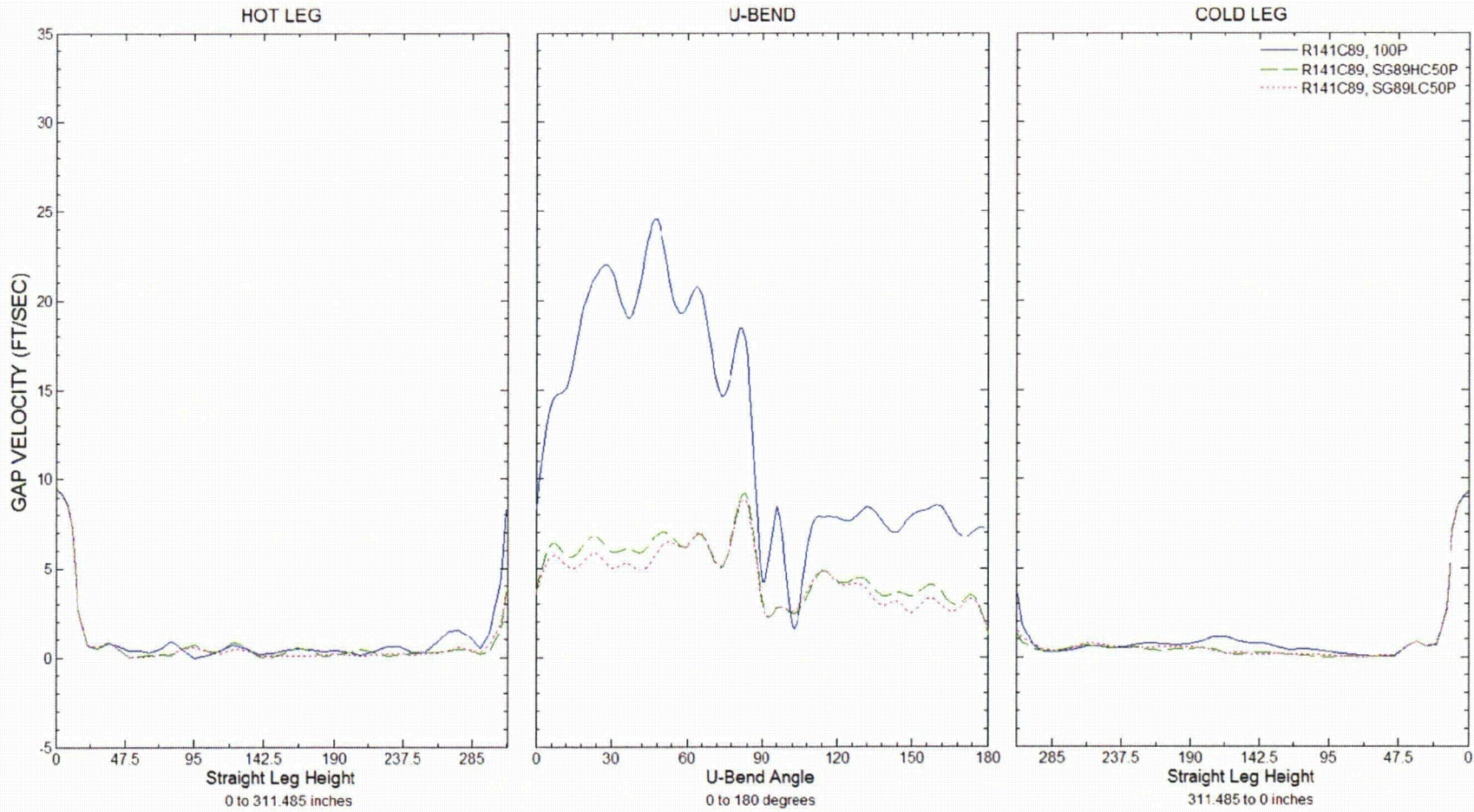


Figure 2-3. SG 2E089 Tube Row 141/Col. 89: Comparison of Gap Velocities at 50% Power

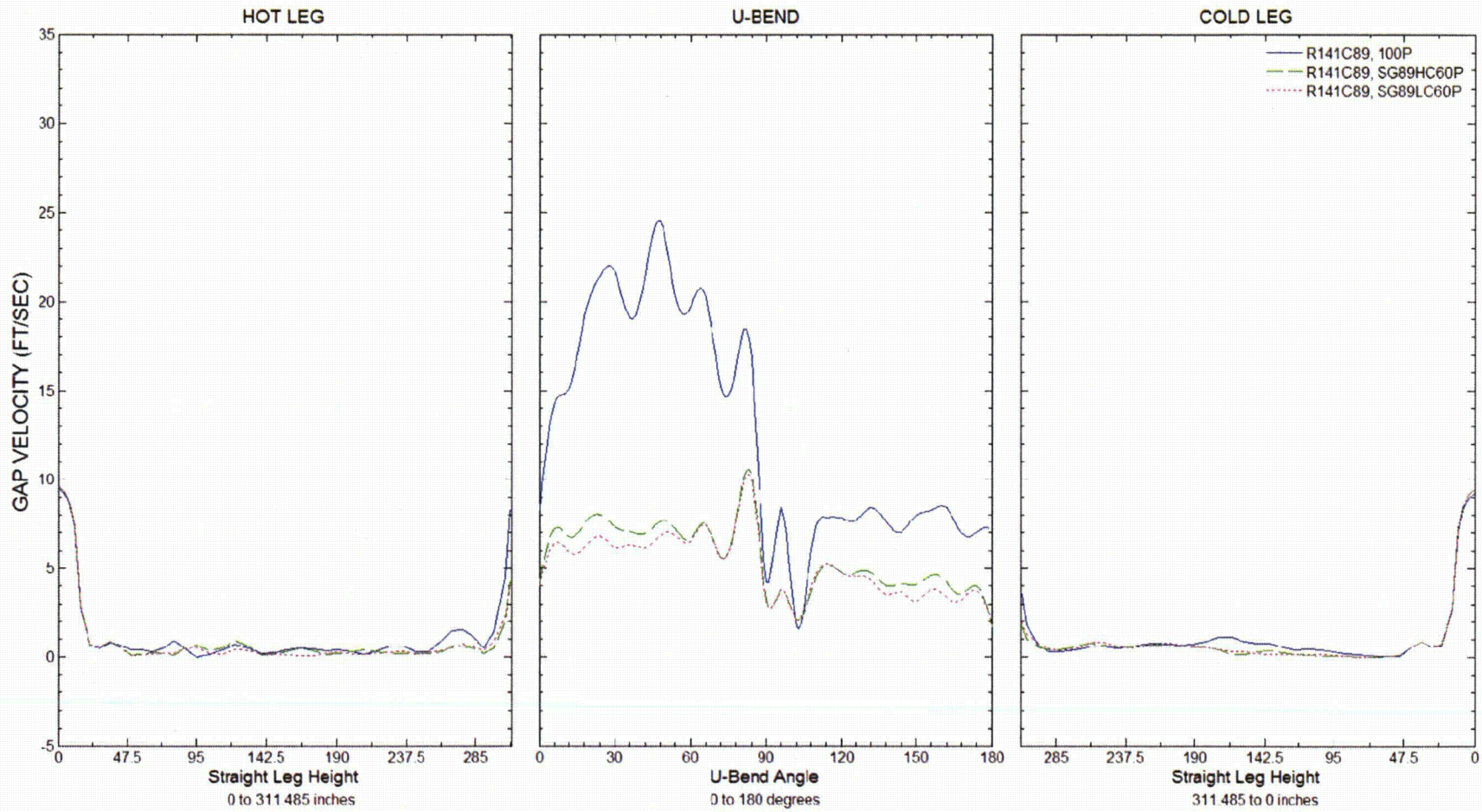


Figure 2-4. SG 2E089 Tube Row 141/Col. 89: Comparison of Gap Velocities at 60% Power



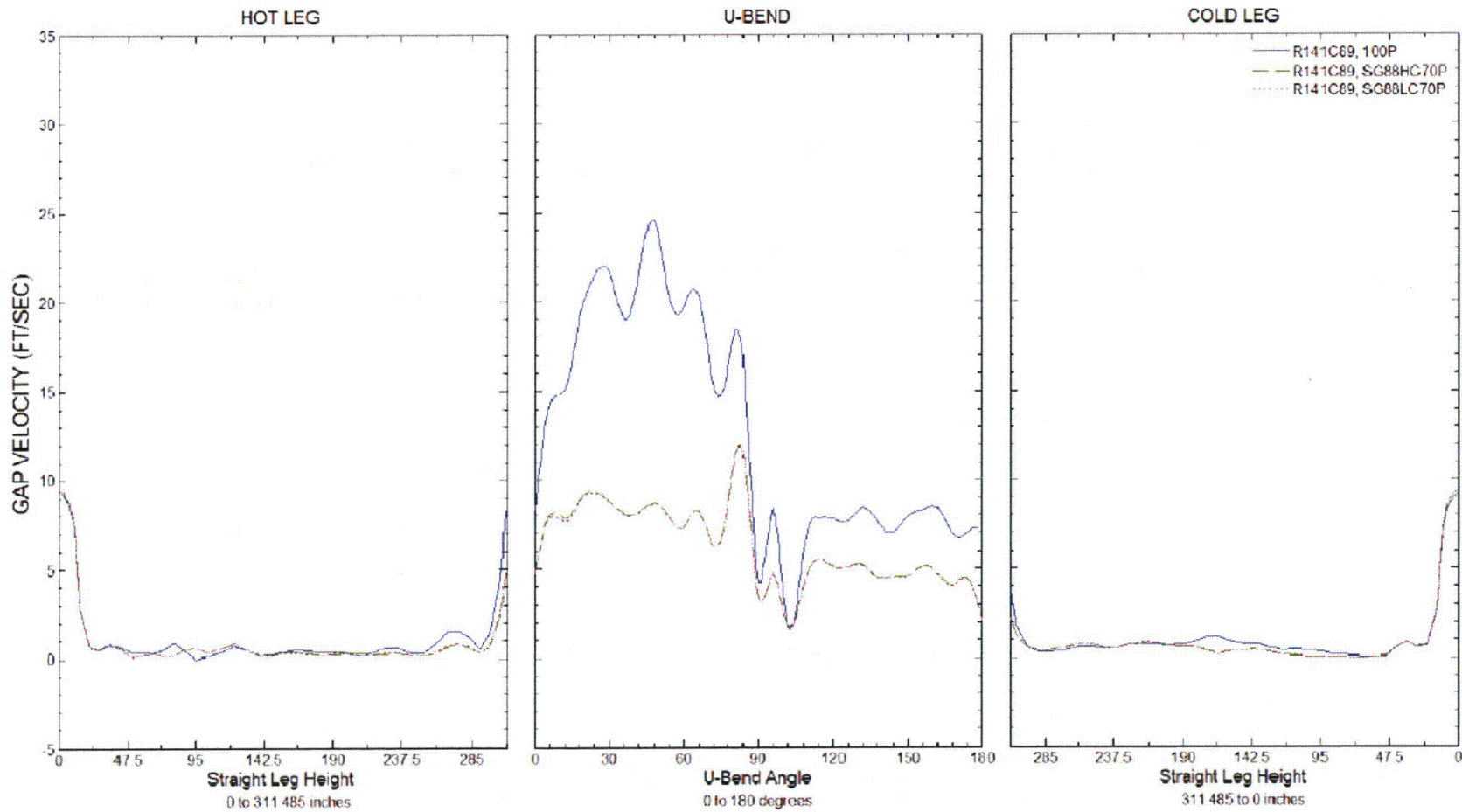


Figure 2-5. SG 2E088 Tube Row 141/Col. 89: Comparison of Gap Velocities at 70% Power



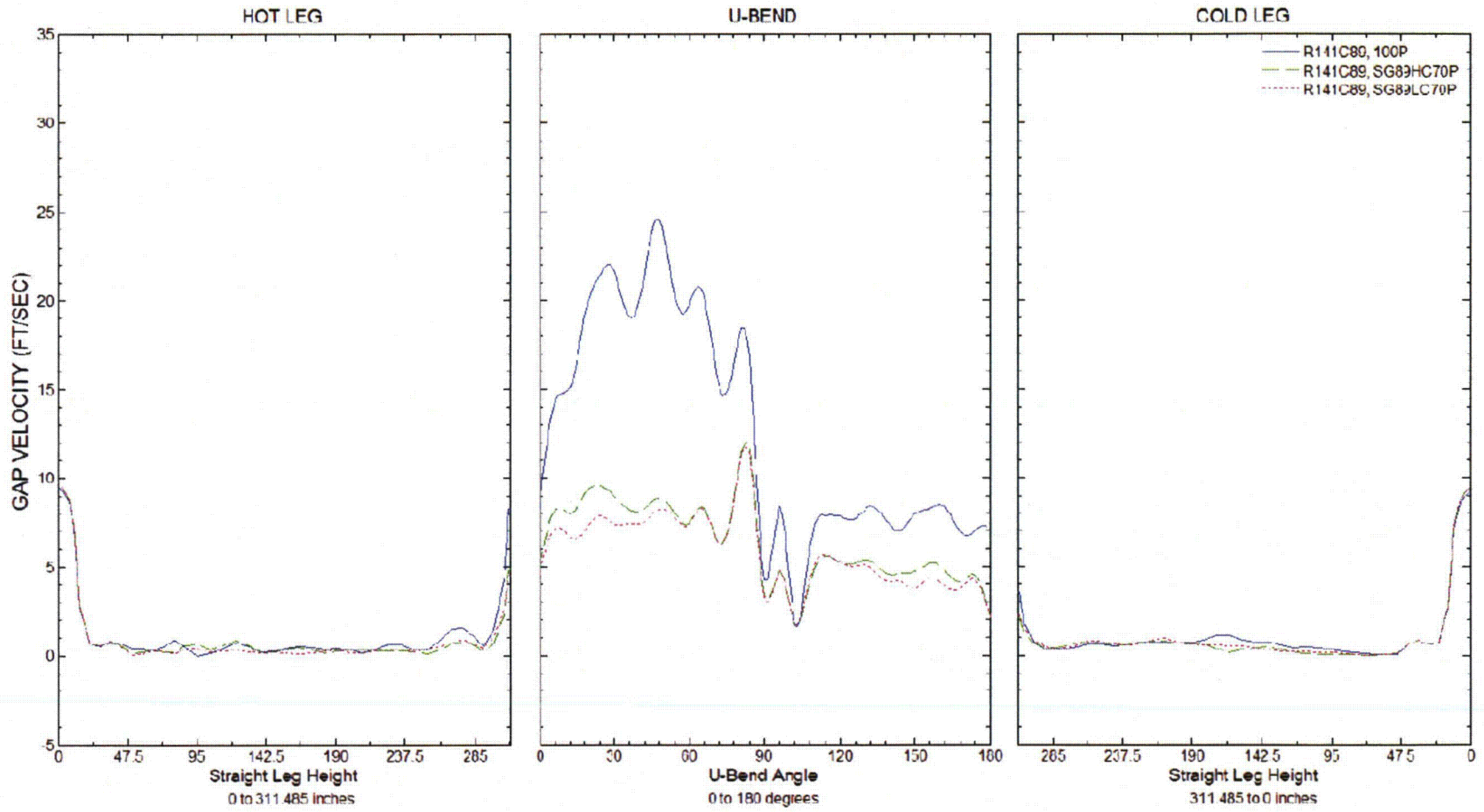


Figure 2-6. SG 2E089 Tube Row 141/Col. 89: Comparison of Gap Velocities at 70% Power

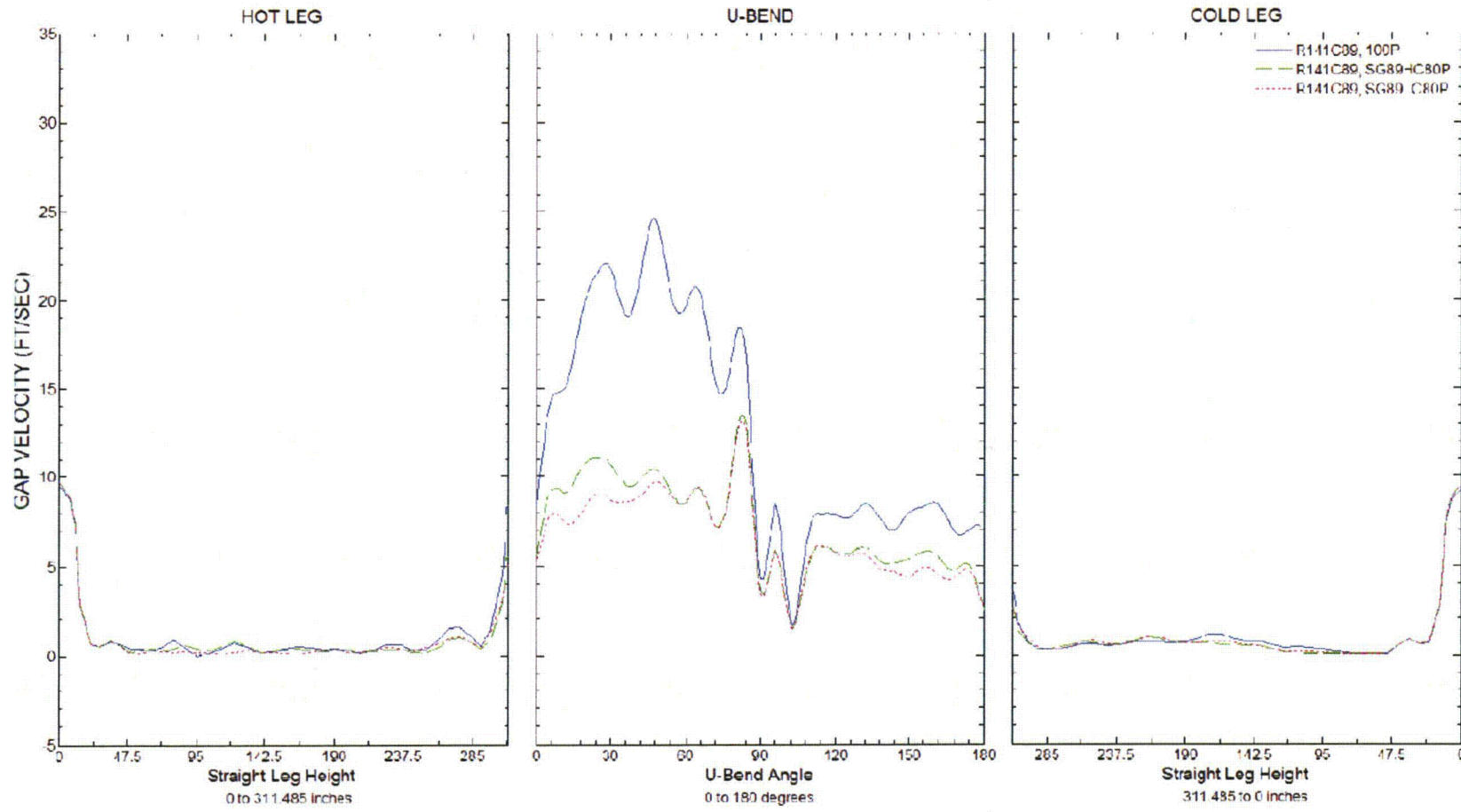
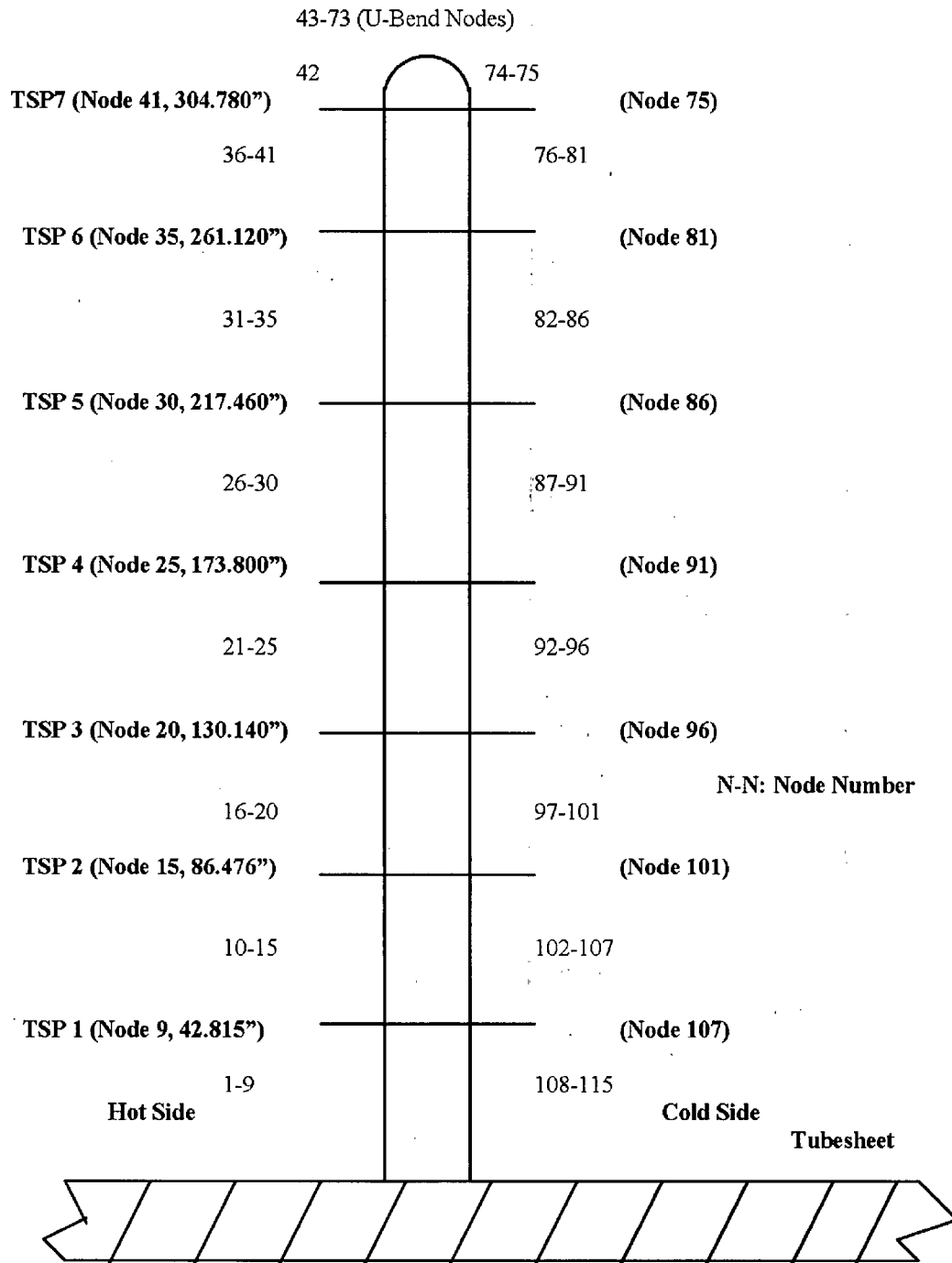


Figure 2-7. SG 2E089 Tube Row 141/Col. 89: Comparison of Gap Velocities at 80% Power



**Figure 2-8. Representative FASTVIB / FLOVIB Tube Model**

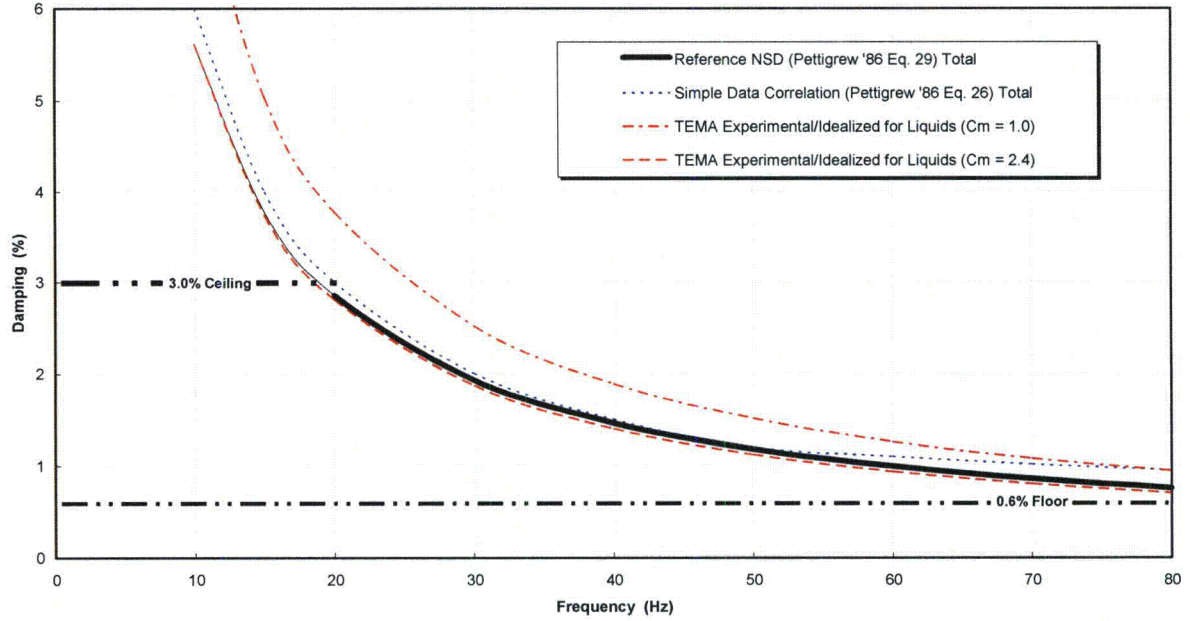


Figure 2-9. Straight Leg Tube Damping in Liquid



COL	49	60	74	80	85	90	94	95	100	105	110	111	120	122	124	125	127	130	135	137	138	139	140	141	142
9	0.82																								
11	0.77																								
12		1.00																							
13	0.76																								
14		0.98																							
15	0.76																								
16		0.99	1.13																						
17	0.77																								
18		1.00	1.31	1.28																					
19	0.77																								
20		0.98	1.31	1.43																					
21	0.78				1.68																				
22		0.98	1.27	1.43		1.35																			
23	0.77				1.59																				
24		0.98	1.29	1.43		1.75	1.44																		
25	0.78				1.55			1.68																	
26		0.98	1.28	1.41		1.65	1.84																		
27	0.79				1.53			1.86																	
28		0.97	1.30	1.42		1.60	1.76		1.77																
29	0.78				1.53			1.77																	
30		1.01	1.31	1.42		1.61	1.73		2.02																
31	0.79				1.53			1.75	1.92																
32		1.00	1.31	1.43		1.63	1.72		1.92																
33	0.79				1.54			1.74	2.22																
34		0.97	1.30	1.41		1.61	1.70		1.87	1.77															
35	0.77				1.53			1.74	2.05	2.04															
36		0.97	1.30	1.39		1.64	1.72		1.85	2.33															
37	0.74				1.53			1.75	2.02	2.35															
38		1.00	1.29	1.41		1.65	1.73		1.85	2.26															
39	0.75				1.54			1.75	1.99	2.30															
40		1.01	1.30	1.42		1.66	1.74		1.84	2.24															
41	0.79				1.55			1.73	1.95	2.25															
42		1.02	1.30	1.41		1.61	1.68		1.77	2.13	1.93														
43	0.80				1.55			1.70	1.92	2.11															
44		1.01	1.33	1.44		1.62	1.68		1.78	2.08	2.56	2.25													
45	0.80				1.55			1.71	1.90	2.07															
46		1.01	1.33	1.47		1.62	1.70		1.81	2.03	2.54	2.69	2.40												
47	0.81				1.55			1.73	1.92	2.06	1.82														
48		0.98	1.30	1.45		1.64	1.72		1.84	2.04	2.55	2.70	2.83												
49	0.79				1.55			1.74	1.95	2.12															
50		0.99	1.32	1.43		1.62	1.71		1.82	2.14	2.59	2.71	2.84												
51	0.79				1.55			1.72	1.97	2.19	2.88	2.50													
52		1.04	1.34	1.45		1.64	1.70		1.82	2.15	2.54	2.66	2.82												
53	0.79				1.57			1.74	1.99	2.17															
54		1.04	1.35	1.50		1.64	1.72		1.84	2.14	2.48	2.56	2.64												
55	0.77				1.56			1.76	2.00	2.17															
56		1.03	1.33	1.47		1.65	1.75		1.87	2.15	2.49	2.58	2.67												
57	0.78				1.57			1.78	2.02	2.17															
58		1.03	1.34	1.44		1.65	1.77		1.89	2.14	2.45	2.52	2.60												
59	0.79				1.54			1.81	2.02	2.19															
60		1.03	1.31	1.41		1.65	1.80		1.92	2.17	2.44	2.51	2.60												
61	0.78				1.55			1.82	2.07	2.19															
62		1.03	1.33	1.47		1.71	1.80		1.96	2.15	2.19	2.47	2.53	2.60											
63	0.77				1.61			1.84	2.09	2.21															
64		1.01	1.35	1.49		1.72	1.83		1.97	2.24	2.48	2.56	2.63												
65	0.77				1.62			1.86	2.11	2.30															
66		1.03	1.38	1.51		1.73	1.84		1.99	2.28	2.55	2.60	2.65												
67	0.84				1.64			1.88	2.13	2.33															
68		1.06	1.38	1.49		1.74	1.87		2.01	2.22	2.33	2.57	2.62	2.67											
69	0.83				1.64			1.94	2.22	2.38															
70		1.07	1.40	1.52		1.83	1.92		2.09	2.38	2.59	2.65	2.71												
71	0.84				1.72			2.00	2.26	2.41															
72		1.07	1.40	1.55		1.85	1.99		2.16	2.41	2.57	2.62	2.69												
73	0.85				1.72			2.04	2.26	2.39															
74		1.07	1.45	1.60		1.88	2.02		2.14	2.34	2.59	2.63	2.69												
75	0.89				1.78			2.02	2.24	2.35															
76		1.09	1.48	1.63		1.86	1.95		2.10	2.39	2.69	2.74	2.79												
77	0.86				1.76			2.01	2.30	2.45															
78		1.12	1.49	1.62		1.92	2.04		2.22	2.46	2.78	2.84	2.89												
79	0.81				1.75			2.12	2.38	2.54															
80		1.18	1.53	1.68		1.93	2.10		2.27	2.54	2.76	2.82	2.89												
81	0.86				1.80			2.09	2.39	2.54															
82		1.18	1.49	1.68		1.92	2.06		2.28	2.50	2.75	2.80	2.86												
83	0.95				1.87			2.12	2.38	2.54															
84		1.15	1.57	1.78		2.01	2.11		2.28	2.56	2.84	2.90	2.97												
85	0.91				1.93			2.20	2.47	2.58															
86		1.21	1.63	1.80		2.09	2.17		2.28	2.53	2.78	2.86	2.92												
87	0.96				1.92			2.15	2.44	2.55															
88		1.15	1.56	1.69		2.00	2.10		2.22	2.50	2.77	2.84	2.90												
89	0.84				1.80			2.07	2.37	2.48															
COL	49	60	74	80	85	90	94	95	100	105	110	111	120	122	124	125	127	130	135	137	138	139	140	141	142

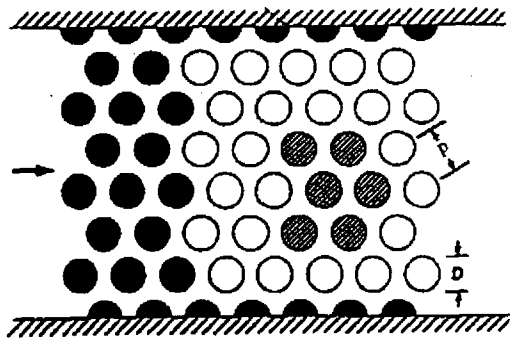
Figure 2-10. Out-of-Plane Excitation ratio Map – 100% Power – 7 AVBs Ineffective (Case 60)



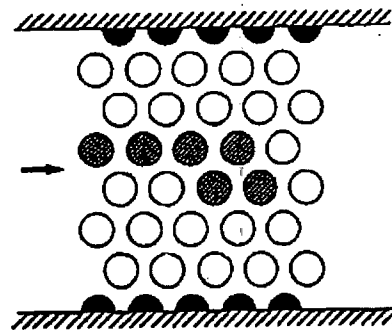
COL	49	60	74	80	85	90	94	95	100	105	110	111	120	122	124	125	127	130	135	137	138	139	140	141	142		
9	0.62																										
11	0.55																										
12		0.80																									
13	0.54																										
14		0.76																									
15	0.55																										
16		0.76	1.06																								
17	0.54																										
18		0.75	1.16	1.27																							
19	0.54																										
20		0.72	1.13	1.35																							
21	0.55				1.72																						
22		0.73	1.06	1.29		1.39																					
23	0.56				1.48																						
24		0.73	1.04	1.24		1.39	1.73	1.47																			
25	0.57				1.39			1.70																			
26		0.73	1.02	1.16		1.52	1.81																				
27	0.57				1.32			1.79																			
28		0.73	1.02	1.16		1.44	1.65		1.76																		
29	0.57				1.29			1.64																			
30		0.76	1.03	1.15		1.41	1.58		1.97																		
31	0.58				1.27			1.61	1.90																		
32		0.76	1.03	1.14		1.41	1.54		1.81																		
33	0.58				1.26			1.57	2.17																		
34		0.74	1.01	1.13		1.37	1.49		1.70	1.77																	
35	0.57				1.25			1.51	1.92	2.00																	
36		0.74	1.02	1.11		1.37	1.48		1.64	2.25																	
37	0.55				1.25			1.49	1.86	2.27																	
38		0.76	1.00	1.13		1.38	1.47		1.62	2.15																	
39	0.56				1.25			1.49	1.82	2.18																	
40		0.76	1.01	1.14		1.38	1.47		1.61	2.09																	
41	0.59				1.26			1.47	1.73	2.07																	
42		0.77	1.02	1.14		1.33	1.42		1.54	1.92	1.83																
43	0.59				1.26			1.44	1.68	1.89																	
44		0.77	1.04	1.14		1.34	1.41		1.54	1.84	2.39	2.11															
45	0.59				1.25			1.44	1.66	1.84																	
46		0.77	1.03	1.17		1.34	1.42		1.53	1.80	2.30	2.46	2.20														
47	0.60				1.26			1.44	1.66	1.82			1.68														
48		0.75	1.01	1.16		1.35	1.42		1.55	1.79	2.24	2.38	2.53														
49	0.59				1.26			1.44	1.66	1.84			2.15														
50		0.76	1.02	1.14		1.31	1.41		1.53	1.84	2.22	2.34	2.48														
51	0.59				1.24			1.43	1.67	1.85			2.49	2.20													
52		0.80	1.03	1.15		1.32	1.40		1.53	1.81	2.15	2.25	2.39														
53	0.59				1.25			1.44	1.66	1.82			2.38	2.56													
54		0.80	1.04	1.17		1.33	1.41		1.53	1.79	2.09	2.17	2.26														
55	0.58				1.24			1.44	1.66	1.81			2.31	2.43													
56		0.79	1.02	1.14		1.34	1.43		1.52	1.80	2.08	2.16	2.25														
57	0.59				1.24			1.43	1.66	1.80			2.28	2.40													
58		0.79	1.02	1.12		1.32	1.41		1.52	1.76	2.03	2.10	2.17														
59	0.60				1.22			1.44	1.65	1.78			2.17	2.27													
60		0.78	1.00	1.10		1.32	1.43		1.54	1.75	1.99	2.05	2.12														
61	0.59				1.22			1.45	1.66	1.76			2.15	2.23													
62		0.78	1.01	1.14		1.36	1.44		1.55	1.74	1.99	2.04	2.11														
63	0.57				1.27			1.45	1.66	1.77			2.14	2.22													
64		0.76	1.02	1.14		1.32	1.40		1.53	1.79	2.00	2.06	2.12														
65	0.58				1.23			1.43	1.65	1.82			2.15	2.22													
66		0.77	1.03	1.13		1.31	1.40		1.53	1.81	2.04	2.08	2.13														
67	0.62				1.23			1.42	1.66	1.84			2.15	2.19													
68		0.79	1.04	1.12		1.32	1.41		1.54	1.82	2.04	2.08	2.12														
69	0.60				1.24			1.47	1.71	1.85			2.16	2.21													
70		0.79	1.05	1.13		1.37	1.46		1.59	1.83	2.05	2.10	2.15														
71	0.61				1.28			1.52	1.71	1.85			2.16	2.18													
72		0.79	1.03	1.13		1.38	1.49		1.62	1.84	2.01	2.06	2.11														
73	0.62				1.26			1.52	1.69	1.80			2.14	2.19													
74		0.79	1.06	1.16		1.38	1.50		1.58	1.74	1.99	2.03	2.10														
75	0.65				1.28			1.47	1.64	1.75			2.14	2.19													
76		0.81	1.08	1.18		1.32	1.40		1.52	1.77	2.04	2.08	2.12														
77	0.62				1.25			1.43	1.69	1.83			2.16	2.21													
78		0.81	1.08	1.16		1.35	1.45		1.61	1.83	2.09	2.14	2.18														
79	0.58				1.24			1.52	1.74	1.88			2.22	2.25													
80		0.84	1.10	1.20		1.38	1.48		1.64	1.87	2.07	2.11	2.17														
81	0.62				1.26			1.46	1.73	1.86			2.17	2.19													
82		0.84	1.05	1.16		1.33	1.44		1.62	1.83	2.04	2.07	2.13														
83	0.68				1.30			1.50	1.72	1.86			2.20	2.26													
84		0.81	1.10	1.24		1.40	1.49		1.62	1.89	2.11	2.16	2.20														
85	0.65				1.34			1.57	1.80	1.90			2.18	2.24													
86		0.87	1.13	1.25		1.46	1.53		1.64	1.85	2.05	2.10	2.14														
87	0.68				1.33			1.53	1.76	1.88			2.18	2.25													
88		0.82	1.08	1.17		1.39	1.48		1.59	1.83	2.03	2.07	2.10														
89	0.59				1.24			1.46	1.69	1.80																	

COL	49	60	74	80	85	90	94	95	100	105	110	111	120	122	124	125	127	130	135	137	138	139	140	141	142			
9	0.17																											
11	0.15																											
12		0.22																										
13	0.15																											
14		0.20																										
15	0.15																											
16		0.20	0.26																									
17	0.14																											
18		0.20	0.30	0.30																								
19	0.14																											
20		0.20	0.29	0.34																								
21	0.14				0.40																							
22		0.20	0.28	0.33		0.33																						
23	0.15				0.38																							
24		0.20	0.28	0.33		0.42	0.36																					
25	0.15				0.36			0.40																				
26		0.20	0.27	0.31		0.38	0.43																					
27	0.15				0.34			0.43																				
28		0.20	0.28	0.31		0.37	0.41		0.41																			
29	0.15				0.34			0.42																				
30		0.20	0.28	0.31		0.37	0.41		0.47																			
31	0.15				0.34			0.41		0.44																		
32		0.20	0.28	0.31		0.37	0.40		0.45																			
33	0.15				0.34			0.40		0.51																		
34		0.20	0.27	0.30		0.36	0.39		0.42		0.42																	
35	0.15				0.33			0.40		0.47			0.46															
36		0.20	0.27	0.30		0.36	0.39		0.42		0.53																	
37	0.15				0.33			0.39		0.46			0.53															
38		0.20	0.27	0.31		0.37	0.39		0.42		0.51																	
39	0.15				0.34			0.39		0.45			0.52															
40		0.21	0.28	0.31		0.37	0.39		0.42		0.50																	
41	0.15				0.34			0.39		0.44		0.51																
42		0.21	0.27	0.31		0.36	0.38		0.41		0.49		0.43															
43	0.15				0.34			0.39		0.45		0.49		0.43														
44		0.20	0.28	0.31		0.36	0.38		0.41		0.48		0.48	0.57	0.49													
45	0.15				0.34			0.38		0.44		0.48		0.48														
46		0.20	0.28	0.32		0.36	0.38		0.41		0.47		0.47	0.55	0.58	0.51												
47	0.15				0.34			0.39		0.44		0.47		0.47		0.59												
48		0.20	0.27	0.31		0.37	0.39		0.42		0.47		0.47	0.54	0.57	0.59												
49	0.15				0.34			0.40		0.44		0.48		0.48		0.50												
50		0.20	0.28	0.30		0.36	0.39		0.41		0.48		0.48	0.55	0.57	0.59												
51	0.15				0.34			0.39		0.44		0.48		0.48		0.60	0.52											
52		0.21	0.28	0.31		0.36	0.38		0.41		0.48		0.48	0.54	0.56	0.58												
53	0.15				0.34			0.39		0.44		0.47		0.47		0.58	0.61											
54		0.20	0.28	0.32		0.36	0.38		0.41		0.47		0.47	0.52	0.54	0.55		0.52										
55	0.15				0.34			0.39		0.44		0.47		0.47		0.56	0.58											
56		0.20	0.27	0.31		0.36	0.39		0.41		0.46		0.47	0.52	0.54	0.55		0.56	0.58								0.61	
57	0.15				0.34			0.39		0.44		0.47		0.47		0.56	0.58											
58		0.20	0.27	0.30		0.36	0.39		0.41		0.47		0.47	0.52	0.53	0.54		0.54	0.56								0.60	
59	0.15				0.33			0.39		0.44		0.47		0.47		0.54	0.56											
60		0.20	0.27	0.30		0.35	0.38		0.41		0.47		0.47	0.52	0.53	0.54		0.54	0.56								0.55	
61	0.15				0.33			0.39		0.45		0.47		0.47		0.54	0.56		0.58									
62		0.21	0.27	0.31		0.36	0.38		0.41		0.47		0.47	0.52	0.53	0.54		0.55	0.56								0.63	
63	0.15				0.34			0.39		0.44		0.47		0.47		0.55	0.56		0.58									
64		0.20	0.28	0.31		0.36	0.38		0.41		0.48		0.48	0.52	0.53	0.54		0.55	0.56								0.62	
65	0.15				0.34			0.39		0.44		0.48		0.48		0.55	0.56		0.58	0.62	0.40							
66		0.20	0.27	0.31		0.36	0.38		0.41		0.48		0.48	0.53	0.54	0.55		0.55	0.56		0.58							
67	0.15				0.34			0.39		0.44		0.48		0.48		0.55	0.56		0.63	0.54							0.56	
68		0.20	0.27	0.31		0.36	0.39		0.41		0.47		0.48	0.53	0.54	0.55		0.55	0.56		0.57						0.42	
69	0.15				0.34			0.40		0.44		0.48		0.48		0.55	0.56		0.61	0.63		0.42						
70		0.20	0.28	0.30		0.37	0.39		0.42		0.48		0.48	0.53	0.54	0.55		0.58										
71	0.15				0.34			0.40		0.45		0.48		0.48		0.56	0.57		0.62	0.63		0.54						
72		0.21	0.27	0.30		0.37	0.40		0.43		0.48		0.48	0.52	0.54	0.55		0.59									0.41	
73	0.16				0.34			0.41		0.45		0.48		0.48		0.56	0.57		0.62	0.63		0.64					0.54	
74		0.20	0.28	0.31		0.37	0.40		0.43		0.48		0.48	0.53	0.54	0.55		0.59									0.64	
75	0.16				0.35			0.41		0.45		0.48		0.48		0.56	0.58		0.61	0.62		0.63					0.41	
76		0.20	0.28	0.31		0.37	0.39		0.42		0.48		0.48	0.53	0.54	0.55		0.59									0.64	
77	0.16				0.34			0.40		0.46		0.48		0.48		0.55	0.57		0.61	0.62		0.63					0.53	
78		0.20	0.28	0.31		0.37	0.40		0.43		0.48		0.48	0.53	0.54	0.55		0.59									0.40	
79	0.15				0.34			0.41		0.46		0.49		0.49		0.55	0.56		0.61	0.61		0.62					0.63	
80		0.21	0.29	0.32		0.37	0.40		0.43		0.49		0.49	0.53	0.53	0.55		0.58									0.40	
81	0.15				0.35			0.41		0.46		0.49		0.49		0.55	0.56		0.60	0.61		0.61					0.62	
82		0.22	0.29	0.33		0.38	0.40		0.43		0.49		0.49	0.53	0.53	0.54		0.57									0.39	
83	0.17				0.36			0.41		0.46		0.49		0.49		0.55	0.56		0.61	0.61		0.62					0.62	
84		0.22	0.29	0.34		0.39	0.41		0.43		0.49		0.49	0.53	0.54	0.55		0.58									0.39	
85	0.17				0.36			0.42		0.47		0.49		0.49		0.55	0.56		0.61	0.								

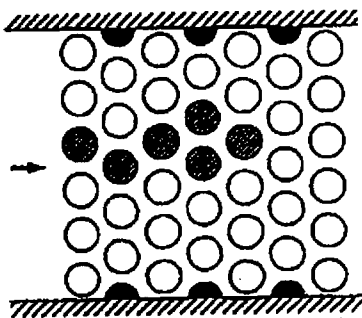




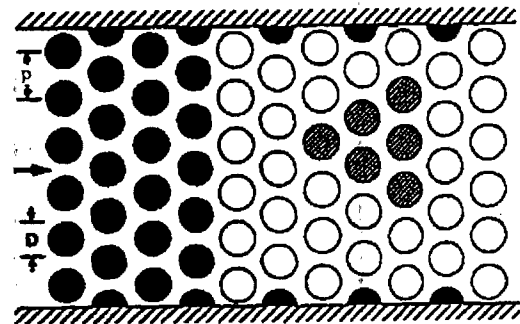
Test 1



Test 2



Test 3



Test 4

- Rigid Tube
- Flexible Tube
- ◐ Flexible Instrumented Tube

Figure 2-14. Schematic Illustrations of Triangular Pitch Tube Array Patterns Tested in the Water Tunnel with Pitch/Diameter Equal to 1.42

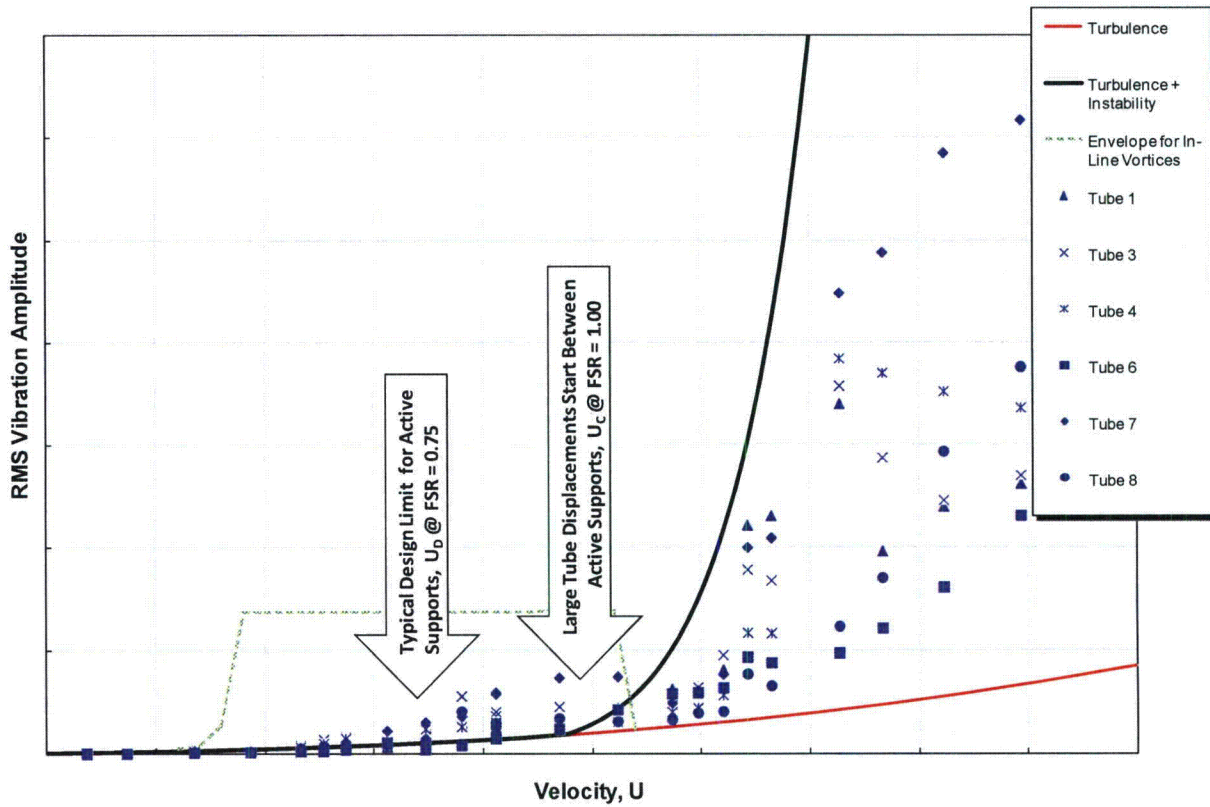


**Figure 2-15. Comparison of Analytical Models of FIV Mechanisms with RMS Tube Displacements for Sample Vibration Test Data**

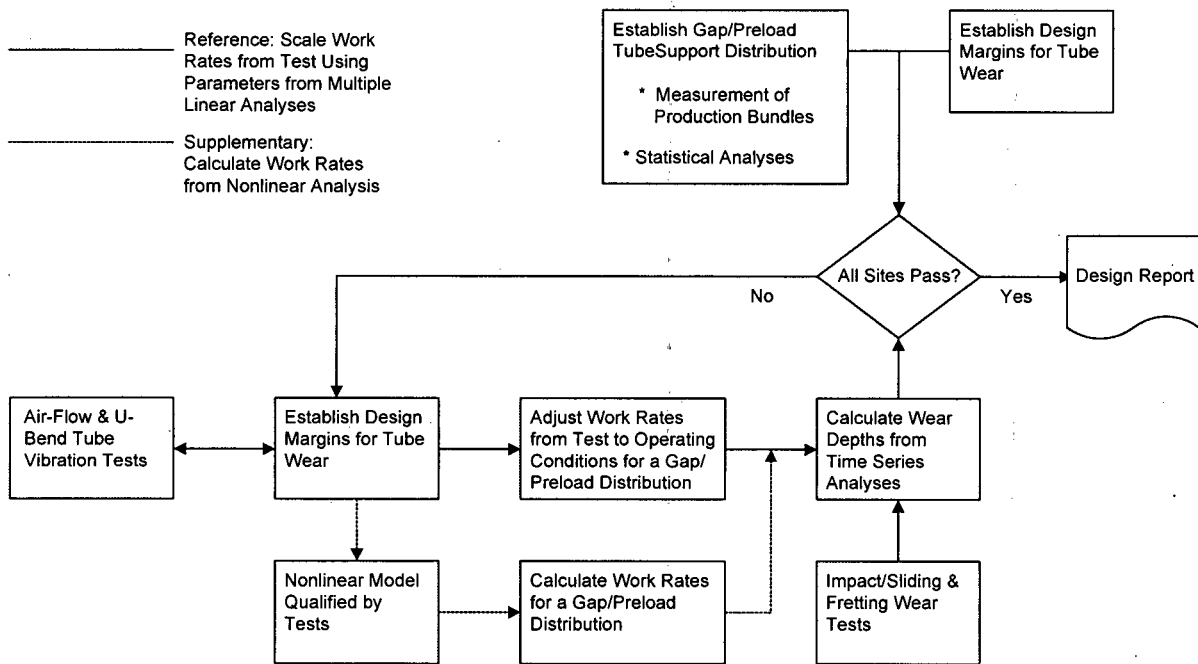


**Figure 2-16. Typical Application of Semi-Empirical Wear Calculation Methodology for Amplitude Limited Fluidelastic Excitation in Steam Generator Design**

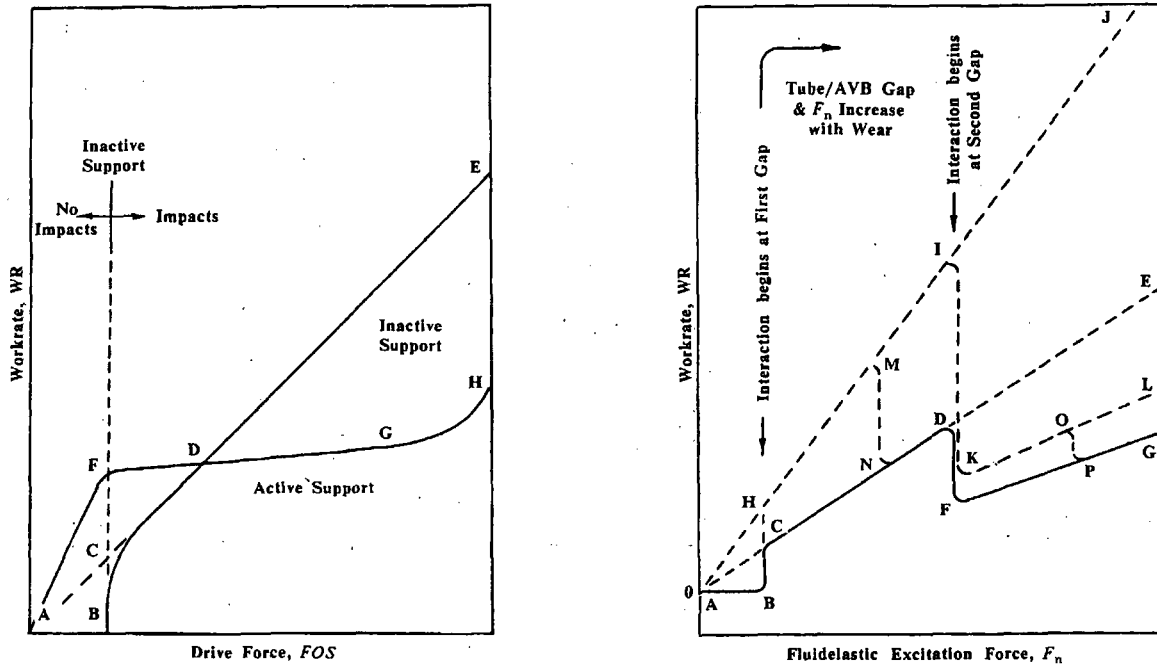


Figure 2-17. Fundamental Characteristic Trends Treated in Semi-Empirical Methodology

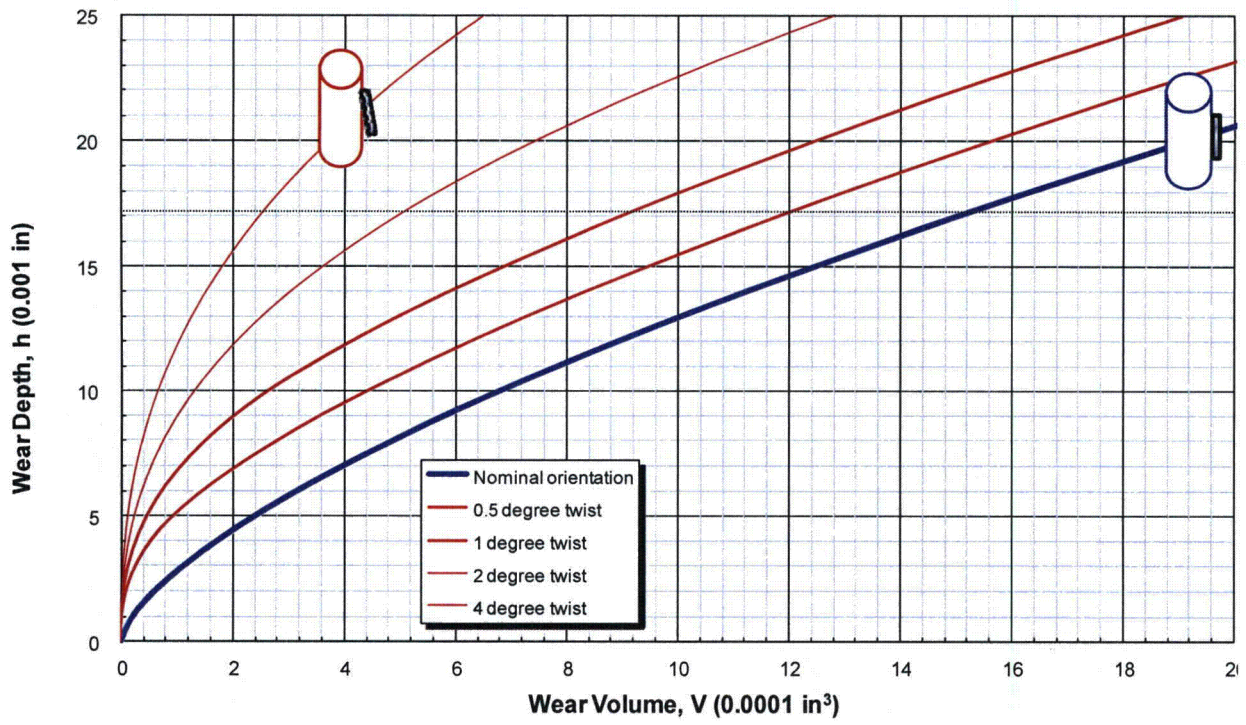
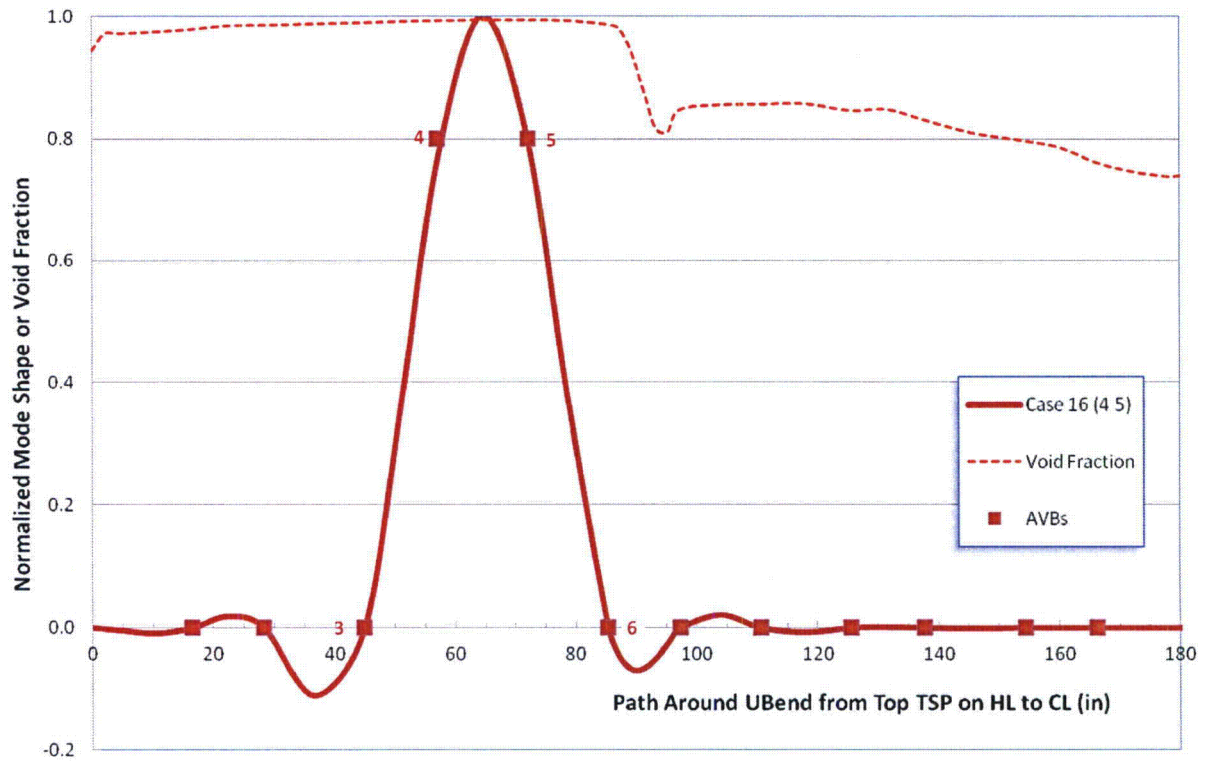
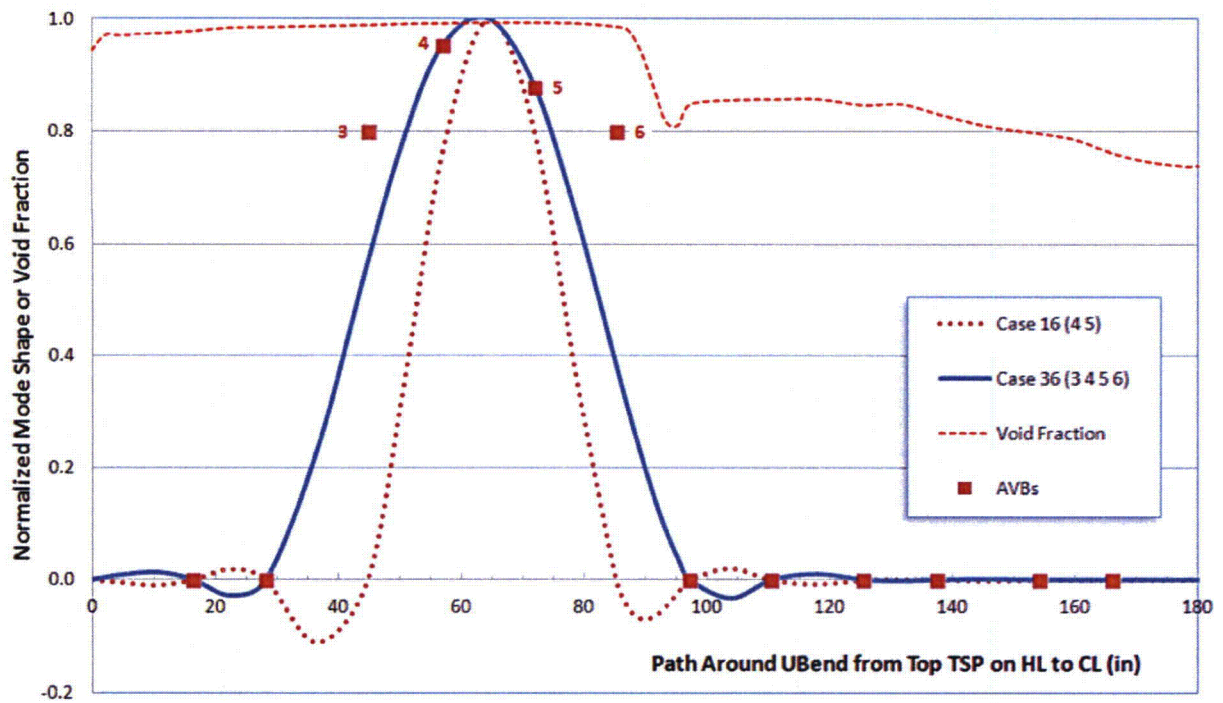


Figure 2-18. Wear Depth vs. Wear Volume (0.75 inch OD Tube, 0.59 inch AVB Width)





**Figure 2-19. U-bend OP Mode in Sample Evaluation Showing First Unstable FASTVIB Case and Postulated Initial Positions of AVBs 4 and 5 Relative to Mode Shape**



**Figure 2-20. Significant U-bend OP Modes in Sample Evaluation Showing Two FASTVIB Cases and Postulated Initial Positions of AVBs 3, 4, 5, and 6 Relative to Mode Shape**

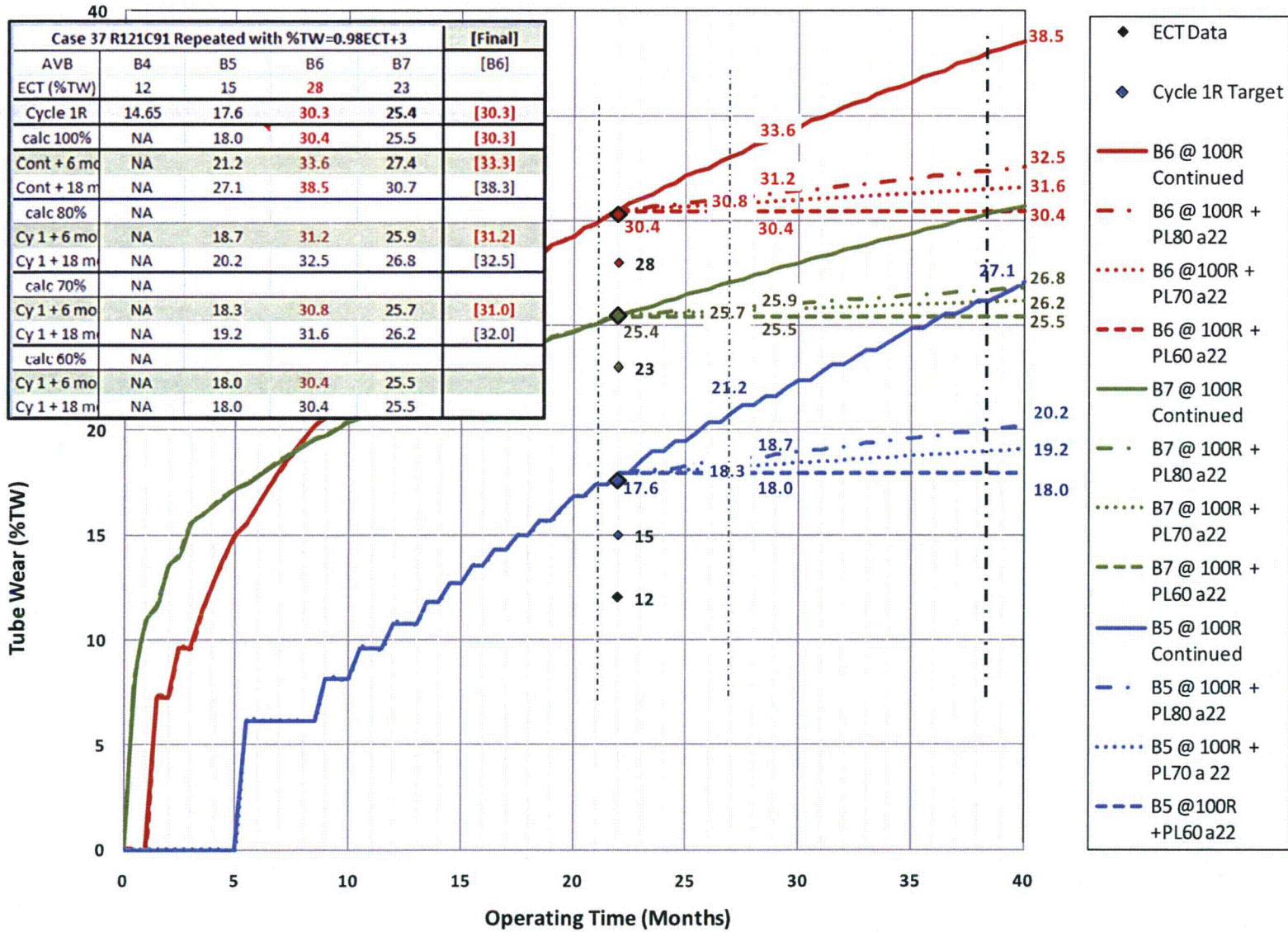
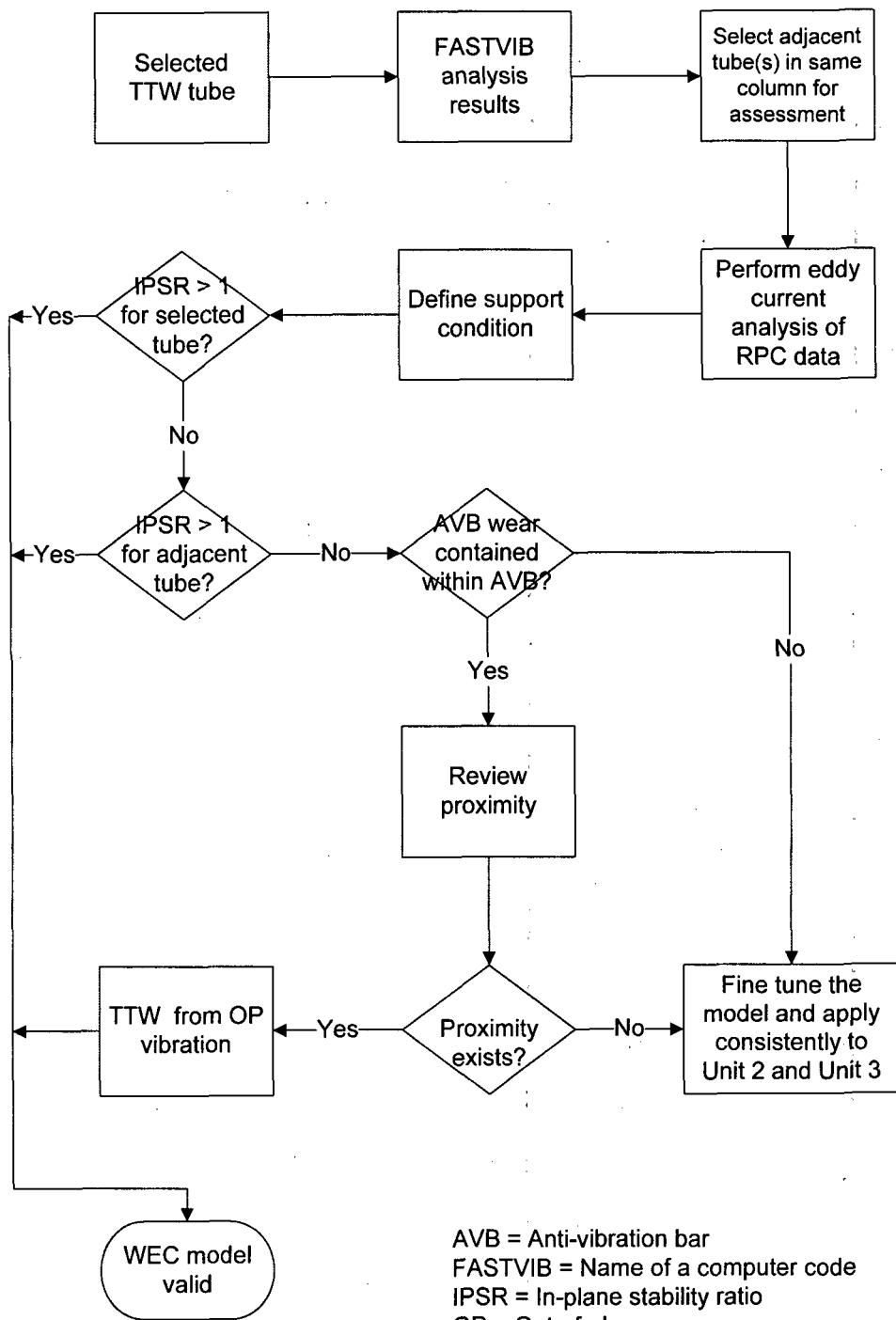


Figure 2-21. Example Illustration of AVB Wear Projection (Tube R121C91 in SG 2E089)



AVB = Anti-vibration bar  
 FASTVIB = Name of a computer code  
 IPSR = In-plane stability ratio  
 OP = Out-of-plane  
 RPC = Rotating pancake coil probe  
 TTW = Tube-to-tube wear (in U-bend free span)

**Figure 2-22. Logic Applied for Benchmarking the In-Plane Vibration Methodology Using Unit 3**



- 16 Boundary Tubes
  - Have FS wear but only a few bobbin ECT indications at AVBs
- ⊙ 15 Adjacent Tubes
  - Investigated as potential sources of TtT interaction
- 55 Interior Tubes
  - All have clear evidence of multiple ineffective AVB supports based on bobbin ECT indications

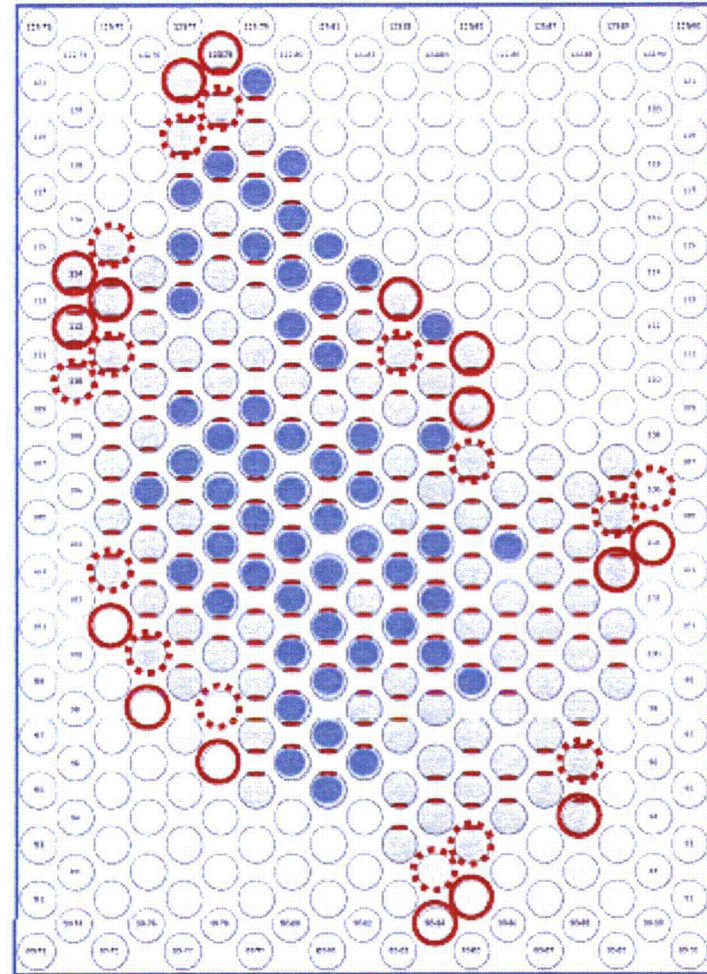


Figure 2-23. Location of SG 3E088 Tubes Evaluated for Benchmarking



### 3 Operational Assessment

The operational assessment is the forward-looking evaluation to assess if the steam generators will meet the structural, operating leakage, and accident condition leakage performance criteria until the next scheduled inspection.

This operational assessment covers three tube degradation mechanisms, namely, tube wear at AVBs, tube-to-tube wear in the U-bend free span, and the potential for in-plane vibration that can lead to tube-to-tube wear as has been observed in the Unit 3 SGs. These mechanisms are covered in the following subsections.

#### 3.1 Tube Wear at AVBs

##### 3.1.1 Structural Limits

This operational assessment deals with the tube wear indications reported in the U-bend region of the SONGS Unit 2 SGs. Tube degradation in the U-bend has resulted from wear at the AVB locations and wear from the interaction of two adjacent tubes in the same column. The structural limits for AVB wear are discussed in this sub-section.

Material properties of the tubes in the SONGS Unit 2 and Unit 3 SGs were provided by SCE (Reference 8). The parameters (mean and standard deviation) of the sum of yield and ultimate stress at temperature (650°F) were very close between the Unit 2 and Unit 3 tube populations. Hence, these parameters were determined for the combined population of both units and used in the current calculation. The mean value was found to be 116.22 ksi and the standard deviation was 2.42 ksi.

Operating conditions during the next cycle were provided by SCE for both full power and several part power conditions (Reference 9). Although SCE is planning to operate Unit 2 at part power until the next inspection, in the current calculation, the more conservative steam pressure at full power was used to determine the primary-to-secondary pressure differential. The full power steam pressure in the next cycle would be 926 psia. Since the primary side pressure is 2250 psia, the primary-to-secondary pressure differential for full power steam pressure in the next cycle would be 1324 psi.

The AVBs in the SONGS RSGs have a width of 0.59 inch and a thickness 0.114 inch. In the Unit 2 RSGs, the wear indications at the AVBs do not extend beyond the width of the AVBs. Hence, an axial length of 0.6 inch is used as the flaw length in this assessment.

Inspection results based on bobbin probe inspection are used in the current evaluation. For the detection and sizing of tube wear at an AVB location, SCE has applied the inspection technique described by Examination Technique Specification Sheet (ETSS) 96004.1 (Reference 25). It is anticipated that the same technique will be applied at the next inspection of the SGs. The actual-to-reported wear depth correlation, and its uncertainty associated with this ETSS, was used in the current calculation to determine the condition monitoring limits that would be applicable at the next inspection.

Tube wear at AVB locations can be either single-sided wear resulting from the interaction of the tube with an adjacent AVB or double-sided wear resulting from the interaction of the tube with both of the adjacent AVBs at the given location. A one-sided AVB flaw will become through-wall at a circumferential extent of 56 degrees. The total circumferential extent of a two-sided AVB flaw that becomes through-wall is 112 degrees or less. Since this is below the applicable threshold value of 135 degrees, the axial thinning correlation can be used to evaluate the burst pressure for

AVB wear indications. For flaws of circumferential extent greater than 135 degrees, the uniform thinning correlation would be applicable. Hence, the structural and condition monitoring limits for such flaws can be calculated based on the correlation for axial thinning provided in the Electric Power Research Institute (EPRI) Flaw Handbook (Reference 26).

The limiting performance criterion for burst is that the tube must meet three times the normal full power pressure differential ( $3\Delta P_{\text{NOP}}$ ) between the primary side and the secondary side. In the next fuel cycle, assuming full power steam pressure, the  $3\Delta P_{\text{NOP}}$  will be 3972 psi. The structural limit for axial thinning for a 0.6 inch long flaw is 66% through-wall (TW). Applying the uncertainties for burst relation, material properties, and inspection technique (including eddy current analysis), the condition monitoring (CM) limit at 95% probability at 50% confidence is calculated as 54% for the bobbin inspection results. The condition monitoring limits as a function of axial length of the flaw are shown in Table 3-1 and are plotted in Figure 3-1. The table and the figure show the CM limit based on bobbin inspection, which is the inspection of record for this degradation mechanism.

As noted above, the CM limit is 54% (maximum) depth from bobbin inspection. The actual maximum depth of such a flaw is expected to be below 60% (at 95% probability). Hence, a flaw of this size will not result in leakage either at normal operating conditions or at limiting accident conditions. Thus an indication satisfying the performance criterion for burst will also satisfy the performance criteria for leakage at normal operating and accident conditions.

### 3.1.2 Evaluation Method

As discussed in more detail in Section 2, the analytical methodology involves projection of the flaw size (depth) of indications reported at the current inspection to the next inspection. This evaluation is performed for the most limiting tubes on an individual basis. ATHOS results provide the thermal-hydraulic boundary conditions – flow velocity, density, and void fraction along the length of the tube. These are used in the FIV analysis to generate the excitation ratios for out-of-plane and in-plane vibration of the tube for various tube support conditions. The support conditions define whether or not a support location such as an AVB intersection is effective, meaning that the structure provides adequate support with respect to motion of the tube due to vibration. The actual tube support boundary conditions for a tube are deduced from U2C17 inspection results based on the presence or absence of a wear indication at the support location. Presence of a wear indication suggests the absence of adequate support; and hence, such locations are treated as ineffective support locations for that tube. The absence of a wear indication at a given structure is generally treated as a supported location. However, there are exceptions to this, such as an AVB location without wear indication nestled between wear indications in adjacent AVB locations in the same tube. In addition, evaluations have been performed to demonstrate that raising the number of unsupported locations does not significantly affect the projected wear depths at the next inspection (Reference 3).

The vibration analysis results and support conditions are used to make wear projection in the next operating cycle. This calculation is based on empirical test results and involves several input assumptions related to tube-to-AVB gap, wear coefficient for the tube and the AVB, the AVB twist, etc. The expected ranges of these parameters are known from test data and experience. Wear depth projection is made taking into consideration the inspection results at the current outage (U2C17). After setting the inputs to match the U2C17 inspection results for a given flaw, the wear calculations are extended to determine the projected wear depth at the next inspection.

Thus, the depth of an AVB wear indication is projected at the next inspection. In order to meet the performance criteria (operational assessment), the projected wear depth must remain below the condition monitoring limit.

### 3.1.3 Results for Active Tubes

The tubes left in service with the deepest wear indications in the U-bend are shown in Table 3-2. The fourth column in this table lists the bobbin reported wear depth and the fifth column shows the expected or "true" depth based on the correlation between metallurgical and NDE wear depth for the inspection technique (Reference 25). Both of these values are in %TW. The penultimate column of the table shows the projected wear depth at six months of operation in the next cycle, without accounting for method uncertainty. As shown in Section 2.5.4, the uncertainty associated with the wear projection method may be expressed using the normalized standard deviation of 0.20 in the estimated growth rate. This uncertainty was applied to the projected wear depth to calculate the wear depth with uncertainty as shown in the last column of Table 3-2.

The deepest AVB indication returned to service in the Unit 2 SGs has a reported wear depth of 28% TW by bobbin probe, in Tubes R119C89 and R121C91 in SG 2E089. Applying the methodology described in Section 2, these flaws are calculated to grow to a maximum wear depth of 32% at the next planned mid-cycle inspection based on the 70% power operating condition in Cycle 17. The projected flaw depth is well below the condition monitoring limit of 54% TW. There is considerable margin from the CM limit. Hence, these tubes are predicted to satisfy the SG performance criteria during the next operating period. The projected flaw depths of all of the remaining flaws in the active tubes are smaller than 30% TW; and hence, they also will satisfy the performance criteria. Operating experience with SGs indicate that wear at indications below the detection threshold or in tubes not exhibiting AVB wear will not develop large AVB wear scars that could threaten tube integrity within a five-month operating period. SCE is planning to perform a Unit 2 mid-cycle inspection after operating for 150 effective days of operation at 70% power.

### 3.1.4 Results for Plugged Tubes

Tube wear projection evaluation was carried out for flaws in the limiting plugged tubes. Stainless steel rope stabilizers were installed in many of the plugged tubes prior to plugging. Testing performed by Mitsubishi Heavy Industries (MHI) indicated that the stabilizers would not improve tube damping in the in-plane mode. Although stabilizers are expected to provide a benefit for the out-of-plane mode of vibration, since the quantification of the impact was not available, no beneficial impact from stabilizers was applied in the current evaluation.

The results of the evaluation for the limiting plugged tubes (tubes with the largest wear indications) are shown in Table 3-3. This table is quite similar to Table 3-2, including the calculation of projected wear depth with uncertainty. It may be noted that the increase in wear depth during the first 6 months of Cycle 17 is small. The projected maximum wear depth for the AVB wear indications is 39% TW. Unlike the active tubes, the acceptance criteria for plugged tubes are much broader. Plugged tubes do not need to meet the condition monitoring limits applicable to active tubes. A conservative criterion for plugged tubes may be that the projected wear depth should remain below 100% through-wall. As can be noted from Table 3-3, none of the indications in the plugged tubes approach the 100% TW depth, the maximum projected wear depth being 39%. Hence, the plugged tubes meet the acceptance criteria for the next operating cycle.

### 3.1.5 Evaluation for 18 Months of Operation

The results discussed in Sections 3.1.3 and 3.1.4 were for six months of operation in the next fuel cycle (17). Even though SCE is planning to perform a mid-cycle inspection of the Unit 2 RSGs after five months of operation in the next cycle, the wear projection was carried out for an operating duration of 18 months in the next cycle. The results for both active tubes and plugged tubes are shown in Table 3-4. It may be noted that the maximum projected wear depth with uncertainty for active tubes is 34% TW which is well below the CM limit of 54%. Similarly, the maximum projected wear depth for plugged tubes is 43% TW which is well below the criterion value of 100% TW. These wear depths satisfy the acceptance criteria established in Section 3.1.1. Therefore, it is acceptable to operate the SGs for 18 months in the next cycle with this degradation mechanism (tube wear at AVBs).

## 3.2 **Tube-to-Tube Wear in U-bend Free Span**

### 3.2.1 Eddy Current Inspection Results

Free span wear in the U-bend was reported (from +Point inspection) in two tubes during the U2C17 outage. They were in Tubes R111C81 and R113C81 in SG 2E089. These are adjacent tubes in the same column. In both tubes, the wear is located between AVB9 and AVB10 in the cold leg. The matching wear locations confirm that the wear resulted from contact between the two tubes. The wear depths in both tubes were shallow at 14% TW and the axial extents were six inches by eddy current inspection. An ultrasonic inspection (UT) was also performed on these tubes. The UT results indicated flaw depths of 7% TW.

Bobbin inspection identified AVB wear at five locations in Tube R111C81 (at AVBs 5, 6, 7, 8, and 10) and at three locations in Tube R113C81 (at AVBs 5, 6, and 7). Subsequent review of +Point data at all AVB intersections in these tubes confirmed the bobbin reported indications and in addition revealed low level wear indications from AVB4 through AVB10. There were no low level wear indications at the other AVBs. Therefore, both of these tubes had ineffective support at seven continuous AVB locations from AVB4 through AVB10.

None of the AVB wear scars extended beyond the width of the AVBs. In-plane motion of a tube against an AVB results in the wear scar extending beyond the width of the AVB (this was observed extensively in the Unit 3 RSGs). Since the AVB wear scars on two of the Unit 2 tubes with TTW were contained within the width of the AVBs, it indicates that the tube motion was not in-plane in either tube. This observation and conclusion were true for not only these two tubes but all tubes in the Unit 2 SGs. Thus the eddy current inspection data suggests that the AVB wear indications in Unit 2 did not result from in-plane vibration of the tubes.

A reanalysis of the pre-service inspection (PSI) data performed by Westinghouse in 2012 revealed proximity signals in these two tubes suggesting that the tubes were close to one another during the PSI. The PSI inspection was performed with the SGs in horizontal condition. No proximity signal was reported during the U2C17 inspection.

### 3.2.2 Flow-Induced Vibration Analysis Results

The flow-induced vibration analysis was performed considering many postulated boundary conditions regarding how AVBs can support the SG tubes in SONGS Unit 2. A detailed discussion of the FIV analysis is provided in Section 2.3. For the two tubes with free span wear, as discussed above, there are seven continuous ineffective AVB support locations (from 4

through 10). The support conditions for these two tubes, derived from the eddy current inspection results, are depicted in the following chart.

SG	Row	Col	07C	B12	B11	B10	FS <sub>c</sub>	B09	B08	B07	B06	B05	B04	FS <sub>s</sub>	B03	B02	B01	07H
SG89	113	81				X	14	X	X	5	5	16	X					
SG89	111	81				7	14	X	18	13	8	14	X					

X - Low level wear observed on +pt data from WEC review

This condition is covered by Case 61 (see Table 2-8). The out-of-plane excitation ratio (ER) for this case at 100% power is 2.12 showing that these tubes were unstable in the out-of-plane mode during Cycle 16. The ER for other FASTVIB cases with different numbers of ineffective AVB support locations is shown in the following table. As a point of clarification, no benefit from stabilization was included in the calculation of the results shown in the last two columns.

#### Out-of-Plane Excitation Ratio

Case Number	Number of Ineffective AVBs	100% Power Excitation Ratio	80% Power Excitation Ratio	70% Power Excitation Ratio
38	4	0.99	0.75	0.69
55	6	1.60	1.40	1.35
61	7	2.12	1.83	1.77
67	8	2.72	2.41	2.32
71	9	3.88	3.27	3.15

The in-plane stability ratio (IPSR) for Case 61 is 0.72 at 100% power in Cycle 16. The value of less than 1 indicates that the tubes were stable against in-plane vibration. The following table shows the IPSR for other support conditions and power levels. No benefit from stabilization was included in the calculation. It may be noted that these tubes will be stable in-plane at full power even with eight ineffective AVB supports. The IPSR calculation is based on a value of 7.8 for the instability constant ( $\beta$ ). This is considered to be conservative in that the value of  $\beta$  is expected to be higher such that the true IPSR values may indeed be lower since the higher the value of  $\beta$ , the smaller the stability ratio.

#### In-Plane Stability Ratio

Case Number	Number of Ineffective AVBs	100% Power Stability Ratio	80% Power Stability Ratio	70% Power Stability Ratio
38	4	0.33	0.16	0.20
55	6	0.53	0.39	0.35
61	7	0.72	0.52	0.47
67	8	0.81	0.60	0.54
71	9	1.15	0.83	< 0.83



Thus, the vibration analysis indicates that the two tubes with free span wear were stable against in-plane vibration during Cycle 16. This further corroborates the evidence from eddy current test data showing no evidence of in-plane vibration in these tubes.

This paragraph provides a plausible explanation about how the tube-to-tube contact and wear may have occurred in the two tubes. The PSI data showing proximity of these tubes offers an insight. When one considers the proximity of the tubes and the fact that the tubes were vibrating out-of-plane, one can draw the conclusion that it is this combination that led to tube-to-tube wear in these tubes. The explanation is that the tubes were in contact as a result of tube expansion from heat up and pressurization during plant operation and that as a result of the out-of-plane vibration of these tubes due to fluidelastic excitation and turbulence, the free span wear occurred with the tubes fretting against each other at the contact location. Appendix A provides additional information that supports this plausible explanation.

### 3.2.3. Assessment of Tube-to-Tube Wear Mechanism

As discussed in the previous paragraphs, all available data suggest that the tube-to-tube wear in the U-bend free span did not result from in-plane vibration of the tubes. There is strong indication that it resulted from out-of-plane vibration of the two tubes in close proximity to the level of actual contact during operation.

It is expected that if the two tubes continue to wear, they may lose close proximity (i.e., contact during plant operation). It is not clear whether the loss of contact has already occurred or how much longer they will maintain contact and wear against each other. When loss of contact occurs, the wear arrest will result. The two tubes have been stabilized and plugged. The stabilizer will reduce the potential for, and the severity of, out-of-plane vibration. Stabilization will also tend to reduce the wear rate, if they remain in contact. Since the tubes are plugged, they can neither burst nor lead to primary-to-secondary leakage and hence, cannot challenge SG performance criteria.

Tube-to-tube wear in the free span was reported only in the two tubes. It is understandable that this is the case since close proximity of the tubes to the level of contact during operation as well as out-of-plane vibration of the tubes is required for this wear mechanism to occur. If there are other tubes with similar conditions, they would have exhibited tube-to-tube wear. If indeed there are a few other tubes with similar conditions, the lack of reported wear suggests that the wear progression has remained below the detection threshold. Hence, wear rates in such potential cases were even smaller. SCE is planning to perform a Unit 2 mid-cycle inspection after operating for 150 effective days of operation at 70% power. Since the reported free span wear was 14% by eddy current inspection and 7% by UT inspection after one full cycle of operation, a lower wear rate for only five months of operation at reduced power will result in only very small wear depths until the next inspection. As discussed in the last paragraph, when the wear depth increases, the tubes will lose contact and the wear will arrest itself.

Thus, it is extremely unlikely that other tubes in these SGs will exhibit free span wear similar to those reported in two tubes during U2C17. If there are a few remaining tubes with similar conditions, the wear rates and wear depths in such tubes will be even smaller than in the reported cases. An evaluation was conducted as described below.

An evaluation was carried out for a hypothetical undetected flaw left in service. The evaluation projected its size at the next inspection and compared it to the condition monitoring (allowable) limit for burst. The size of the undetected flaw at the beginning of cycle (BOC) was assumed to be the same as the size of the detected TTW flaws in SG 2E089. These flaws had a depth of 14% TW and an axial length of 6 inches (Reference 27) from +Point inspection using

ETSS 27902.2. These dimensions were conservatively used as the BOC conditions for the undetected flaw. The growth rate of these TTW flaws were calculated based on the operating length of 22 calendar months for Cycle 16. Using a conservative 6-month operation until the next inspection, a depth growth of 14% times 6/22 or 4% TW was calculated. Similarly, a growth value of 6 inches times 6/22 or 2 inches was calculated for axial length. These values were rounded up, conservatively. Please note that the next cycle of operation will be at 70% power; however, no credit was taken for the potentially lower growth rate resulting from the reduction in power level. The size of the undetected flaw at the next inspection was determined by adding the growth values to the BOC conditions. This yielded the projected flaw size as 18% TW and 8 inches in axial length.

The allowable depth for an 8-inch long flaw was determined based on the  $3\Delta P_{NOP}$  value of 3972 psi (see Section 3.1.1). The EPRI Flaw Handbook (Reference 26) methodology for axial thinning was used in conjunction with the material properties of tubes in the SONGS RSGs and the NDE uncertainties for the ETSS 27902.2 (Reference 28). The calculation yielded an allowable limit of 48% TW. Since the projected wear depth of 18% TW is lower than the allowable limit, the burst performance criterion will be satisfied. The projected flaw depth is far below 100% TW and hence, no leakage will occur either during normal operation or during a postulated accident condition.

The evaluation was extended for an operating length of 18 months in Cycle 17. The projected dimensions of the undetected flaw for this operating length are 26% TW and 11 inch axial length. The condition monitoring limit for an 11 inch long flaw is 48% TW. Since the projected flaw depth is less than the allowable limit, and well below 100% TW, the burst and leakage criteria will be satisfied for an operating length of 18 months as well.

Therefore, the SG performance criteria will be satisfied for this degradation mechanism until the next inspection.

### 3.3 Potential for In-Plane Vibration

As discussed in Section 3.2, all available information indicates that in-plane vibration has not occurred in the Unit 2 SGs during their first cycle of operation. This section addresses the potential for in-plane vibration to occur during operation until the next inspection. Figure 3-2 shows a simplified diagram of the operational assessment methodology for this degradation mechanism.

Justification for the use of eddy current data to determine the support conditions in the U-bend is discussed in Section 2.4. It was also shown that an effective support at an AVB location will remain effective for several fuel cycles because the tube wear rate from out-of-plane vibration at such an AVB location will be negligible. Section 2.4.2 also shows that a contact force is not required to prevent in-plane vibration, but a small AVB gap is sufficient to provide effective support. Benchmarking of the methodology against Unit 3 findings is discussed in Section 2.6.1. By applying the methodology, it showed that the TTW indications in Unit 3 resulted from in-plane vibration of the given tube or from in-plane vibration of the neighboring tube. The same methodology was applied to the evaluation of Unit 2 RSGs.

All tubes in the Unit 2 SGs that will be returned to service were evaluated for the potential for in-plane vibration to occur in the next cycle. This flow-induced vibration evaluation was discussed in Section 2.6. It showed that there are no tubes in the Unit 2 SGs that are likely to become unstable in the in-plane vibration mode during the upcoming operating cycle. This is not surprising because the operation in the first cycle was at full power when no tubes were subjected to in-plane vibration. The next cycle of operation will be at 70% power. The vibration potential in the U-

bend decreases significantly as the power is reduced. Since the tubes were stable in-plane at 100% power, they will be stable in-plane at 70% power with additional margin. Evaluation of the most limiting tubes in the Unit 2 RSGs was discussed in Section 2.6. The results for the limiting tubes are shown in Table 2-10. Please note that all of these limiting tubes have already been stabilized and plugged, most of them preventively. The evaluation showed that the in-plane stability ratios of all tubes in Unit 2 are less than 1 at 70% power. Hence, in-plane vibration will not occur in the Unit 2 SGs during the upcoming operating cycle at power levels up to 70%.

Since all active tubes will be stable against in-plane vibration in the next cycle, tube-to-tube wear due to in-plane vibration in the U-bend free span, as has been observed in Unit 3, will not occur in Unit 2 during the next cycle of operation. SG performance criteria will be satisfied for this degradation mechanism until the next inspection.

### **3.4 Operational Assessment Conclusion**

Three degradation mechanisms were evaluated as described in the prior subsections. They are tube wear at AVBs, tube-to-tube wear in the U-bend free span observed in two tubes in the Unit 2 SGs during the current refueling outage, and the potential for in-plane vibration that can lead to tube-to-tube wear in the U-bend free span as has been reported in the Unit 3 SGs. SCE is planning to perform a Unit 2 mid-cycle inspection after operating for 150 effective days of operation at 70% power. The operational assessment was performed in conformance with the EPRI Guidelines. It clearly demonstrates that for a 5-month operating period at 70% power the SGs will meet the performance criteria established in the Steam Generator Program Guidelines, NEI 97-06 (Reference 1), for both burst strength and for primary-to-secondary leakage during normal operation and accident conditions.

The evaluations also show that, for these degradation mechanisms, the SG performance criteria will be satisfied for the duration of 18 months and hence, it is acceptable to operate the Unit 2 SGs for a period of 18 months in the next fuel cycle at 70% power.

**Table 3-1. Condition Monitoring Limit for Axial Thinning**

<b>Axial Thinning</b>	
<b>Length (inch)</b>	<b>CM Limit Depth (Bobbin ETSS 96004.1)</b>
0.3	62.6%
0.4	58.5%
0.5	56.1%
0.6	54.5%
0.7	53.5%
0.8	52.6%
0.9	51.9%
1	51.3%
1.125	50.8%
1.2	50.5%
1.5	49.7%
2	48.9%
2.5	48.5%
3	48.2%

**Table 3-2. Wear Projection Results for Active Tubes with Limiting AVB Wear Indications**

Tube	SG No	Tube Status	Max Wear Depth, %		Max Depth @ at 70% Power After 6 Months			
			ECT Reported	Expected Value	FASTVIB Case	No Seq AVBs	Without Uncertainty	With Uncertainty
R97C87	88	Active	25	27.4	38	4	27.4	27.4
R119C89	89	Active	28	30.3	46	5	31.2	31.5
R121C91	89	Active	28	30.3	37	4	31.0	31.2
R131C91	89	Active	21	23.5	17	2	23.5	23.5
R129C93	89	Active	22	24.5	47 *	5	25.8	26.2
R126C90	89	Active	21	23.5	45	5	24.0	24.2

\* Baseline Case 29 being stable, Case 47 was used for wear projection



**Table 3-3. Wear Projection Results for Plugged Tubes with Limiting AVB Wear Indications**

Tube	SG No	Tube Status	Max Wear Depth, %		Max Depth @ at 70% Power After 6 Months			
			ECT Reported	Expected Value	FASTVIB Case	No Seq AVBs	Without Uncertainty	With Uncertainty
R112C88	88	Plugged	35	37.2	47	5	37.9	38.1
R133C91	88	Plugged	35	37.2	38	4	38.1	38.4
R114C90	88	Plugged	22	24.5	48	5	25.4	25.7
R111C91	88	Plugged	26	28.4	38	4	28.4	28.4
R116C86	88	Plugged	29	31.3	46	5	32.4	32.8
R117C93	88	Plugged	27	29.4	47	5	30.4	30.7
R115C85	88	Plugged	27	29.4	48	5	30.6	31.0
R114C86	88	Plugged	21	23.5	53	6	24.5	24.8
R112C88	88	Plugged	35	37.2	55	6	38.5	38.9
R128C94	88	Plugged	32	34.3	60	7	35.7	36.2
R120C92	88	Plugged	32	34.3	66	8	36.2	36.8
R121C83	89	Plugged	24	26.4	16	2	26.4	26.4
R117C89	89	Plugged	26	28.4	46	5	29.2	29.5
R108C90	89	Plugged	27	29.4	53	6	30.7	31.1
R117C81	89	Plugged	29	31.3	55	6	32.7	33.2
R134C90	89	Plugged	26	28.4	56	6	30.6	31.3
R114C88	89	Plugged	24	26.4	56	6	28.9	29.7
R117C85	89	Plugged	24	26.4	62	7	28.1	28.7
R122C82	89	Plugged	27	29.4	66	8	31.0	31.5
R112C84	89	Plugged	27	29.4	67	8	31.2	31.8
R111C81	89	Plugged	18	20.5	38	4	20.6	20.6

Table 3-4. Wear Projection Results for Limiting AVB Wear Indications for 18 Months of Operation

Tube	SG No	Tube Status	Max Wear Depth, %		Max Depth @ at 70% Power After 18 Months			
			ECT Reported	Expected Value	FASTVIB Case	No Seq AVBs	Without Uncertainty	With Uncertainty
R97C87	88	Active	25	27.4	38	4	27.4	27.4
R119C89	89	Active	28	30.3	46	5	32.8	33.6
R121C91	89	Active	28	30.3	37	4	32.0	32.5
R131C91	89	Active	21	23.5	17	2	23.5	23.5
R129C93	89	Active	22	24.5	47 *	5	28.0	29.2
R126C90	89	Active	21	23.5	45	5	24.9	25.4
R112C88	88	Plugged	35	37.2	47	5	38.5	38.9
R133C91	88	Plugged	35	37.2	38	4	39.8	40.7
R114C90	88	Plugged	22	24.5	48	5	27.2	28.1
R111C91	88	Plugged	26	28.4	38	4	28.4	28.4
R116C86	88	Plugged	29	31.3	46	5	34.7	35.8
R117C93	88	Plugged	27	29.4	47	5	32.4	33.4
R115C85	88	Plugged	27	29.4	48	5	32.8	33.9
R114C86	88	Plugged	21	23.5	53	6	26.3	27.2
R112C88	88	Plugged	35	37.2	55	6	41.5	42.9
R128C94	88	Plugged	32	34.3	60	7	39.0	40.6
R120C92	88	Plugged	32	34.3	66	8	39.5	41.2
R121C83	89	Plugged	24	26.4	16	2	26.4	26.4
R117C89	89	Plugged	26	28.4	46	5	30.7	31.5
R108C90	89	Plugged	27	29.4	53	6	33.2	34.5
R117C81	89	Plugged	29	31.3	55	6	35.2	36.5
R134C90	89	Plugged	26	28.4	56	6	34.4	36.4
R114C88	89	Plugged	24	26.4	56	6	33.2	35.4
R117C85	89	Plugged	24	26.4	62	7	31.0	32.5
R122C82	89	Plugged	27	29.4	66	8	33.8	35.3
R112C84	89	Plugged	27	29.4	67	8	34.4	36.1
R111C81	89	Plugged	18	20.5	38	4	20.6	20.6

\* Baseline Case 29 being stable, Case 47 was used for wear projection



Condition Monitoring Limit for Volumetric Indications -- Axial Thinning

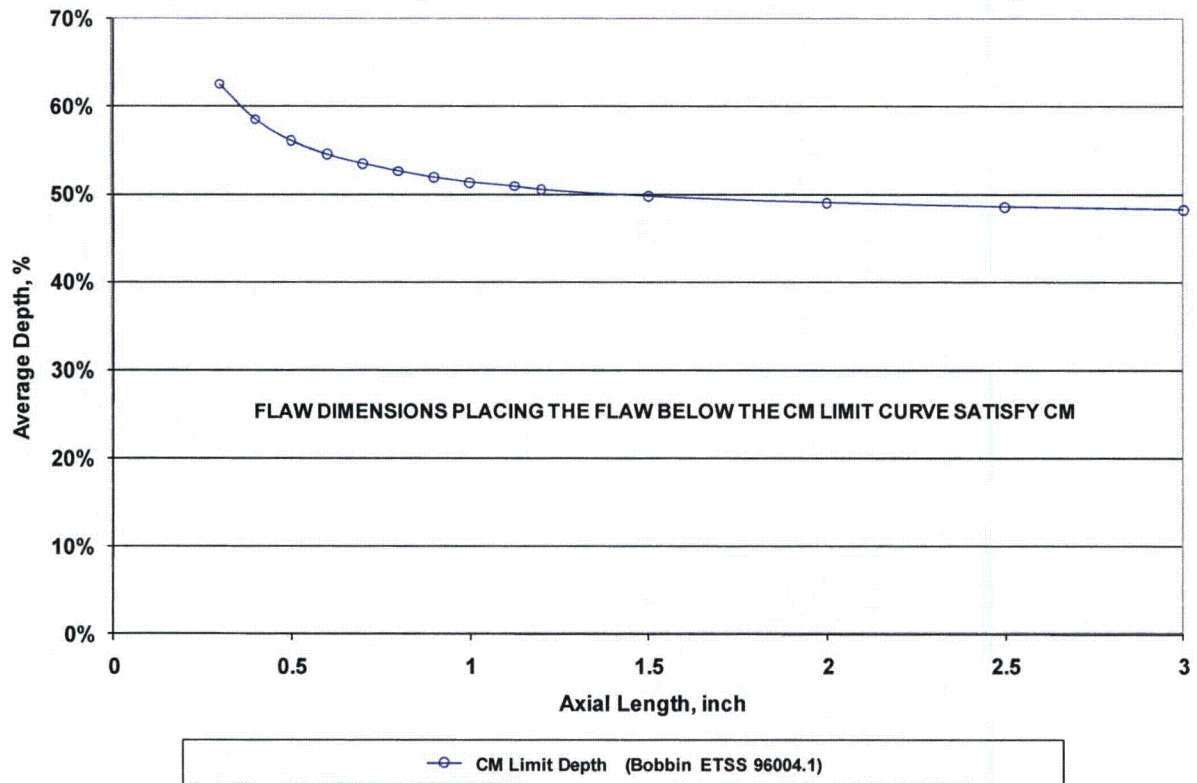
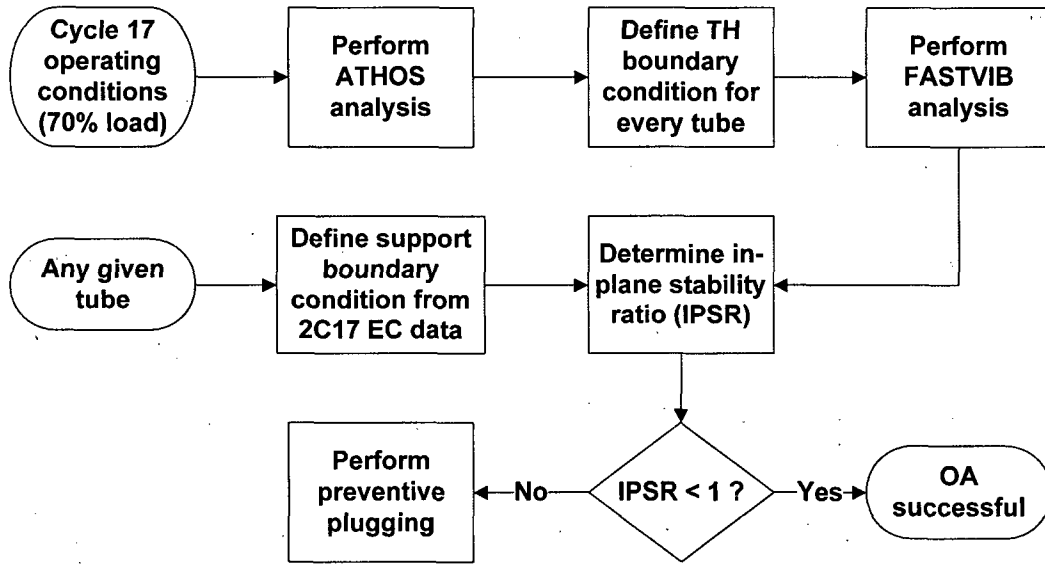


Figure 3-1. Condition Monitoring Limit for Axial Thinning



In concept, this analysis is repeated for every tube; in practice, for every limiting tube  
**Figure 3-2. Operational Assessment Methodology for the Potential for In-Plane Vibration**

## 4 References

1. "Steam Generator Program Guidelines," NEI 97-06 Revision 3, January 2011.
2. "Steam Generator Integrity Assessment Guidelines Revision 3", EPRI Report 1019038, October 2008.
3. "Operational Assessment for SONGS Unit 2 Steam Generators for Upper Bundle Tube-to-Tube Wear Degradation at End of Cycle 16," APTECH Report, AES 12068150-2Q-1, September 2012.
4. "SONGS 2C17 Steam Generator Operational Assessment for Tube-to-Tube Wear," AREVA Report, 51-9187230, September 2012.
5. "Flow-Induced Vibration and Tube Wear Analysis of the San Onofre Nuclear Generating Station Unit 2 Replacement Steam Generators Supporting Restart," Westinghouse Report LTR-SGDA-12-36, Revision 1, September 13, 2012.
6. "ATHOS3: A Computer Program for the Thermal-Hydraulic Analysis of Steam Generators," EPRI-NP-4604-CMM, July 1986.
7. "Software Release Letter for Modules of the ATHOS Family of Codes and Executable Scripts: GPP60 Version 4.0, RUN\_ATHOGPP Version 1.4, PLATES60 Version 3.0, and RUN\_PLATES Version 1.4," Westinghouse letter LTR-SGDA-08-148, June 13, 2008.
8. "SONGS Material Properties," E-mail transmittal with Excel files "SONGS2 CMTR.xlsx" and "SONGS3 CMTR.xlsx" from Mr. David Calhoun of SCE to Vince Merritt of Westinghouse, June 22, 2012.
9. "San Onofre Nuclear Generating Station Units 2 and 3 Replacement Steam Generators Evaluation of Stability Ratio for Return to Service," Mitsubishi Heavy Industries Ltd., L5-04GA567, Revision 4, July 21, 2012.
10. "User's Manual for the Version 4.0 of PLTATHOS and VGUB to Read SG Model Data at Execution Time," Westinghouse document LTR-NCE-04-105, February 11, 2005.
11. M. J. Pettigrew, C. E. Taylor, and B. S. Kim, "Vibration of Tube Bundles in Two-Phase Cross-Flow: Part I—Hydrodynamic Mass and Damping," Transactions of the ASME Vol. 111, Nov. 1989, pp. 466-477.
12. F. Axisa, M. Wullschlegel, B. Villard, and C. E. Taylor, "Two-Phase Cross-Flow Damping," ASME Publication PVP Vol. 133, Damping—1988, ASME PVP Conference, Pittsburgh, Pa., June 1988.
13. Standards of Tubular Exchanger Manufacturers Association, Tubular Exchanger Manufacturers Association, Inc., 7th Edition, New York, NY.
14. M. J. Pettigrew, R. J. Rogers, and F. Axisa, "Damping of Multispan Heat Exchanger Tubes: Part 2 In Liquids," ASME PVP Publication PVP Vol. 104, Chicago, IL, July 20-24, 1986, pp. 89-98.
15. M. J. Pettigrew and C. E. Taylor, "Damping of Heat Exchanger Tubes in Two-Phase Flow," ASME 4th International Symposium on Fluid-Structure Interactions, Aeroelasticity, Flow-Induced Vibration and Noise AD Vol. 53-2, Nov. 16-21, 1997, Dallas, TX pp. 407-418.
16. H. J. Connors, "Flow-Induced Vibration and Wear of Steam Generator Tubes," Nuclear Technology Vol. 55, Nov. 1981, pp.311-331.
17. H. J. Connors, "Fluidelastic Vibration of Tube Arrays Excited by Nonuniform Cross Flow,"



Flow-Induced Vibration of Power Plant Components –PVP-41 edited by M. K. Au-Yang, The American Society of Mechanical Engineers, New York, pp. 93-107, 1988.

18. "N-1331 Instability of Tube Arrays in Cross Flow," Nonmandatory Appendix N, ASME Boiler and Pressure Vessel Code Section III, "Rules for Construction of Nuclear Power Plant Components," 1998 Edition, The American Society of Mechanical Engineers, New York.
19. D. R. Polak and D. S. Weaver, "Vortex Shedding in Normal Triangular Tube Arrays," Flow-Induced Vibration 1994, The 1994 Pressure Vessels and Piping Conference, Minneapolis, Minnesota, ASME Pressure Vessels and Piping Division Report PVP-Vol. 273, pp. 145-156, June 19-23, 1994.
20. A. Zukauskas and V. Katinas, "Flow Induced Vibration in Heat Exchanger Tube Banks," Proceedings of the IUTAM-IAHR Symposium on Practical Experiences with Flow-Induced Vibrations, Karlsruhe, Editors E. Naudascher and D. Rockwell, Springer-Verlag, Berlin, pp.188-196, 1980.
21. D. S. Weaver, J. A. Fitzpatrick, and M. El-Kashlan, "Strouhal Numbers for Heat Exchanger Tube Arrays in Cross Flow," ASME Journal of Pressure Vessel Technology, Vol. 109, pp 219-223.
22. H. J. Connors, "Vortex Shedding Excitation and Vibration of Circular Cylinders," paper presented at the ASME Pressure Vessels and Piping Technology Conference, PVP-52, San Francisco, CA, Aug. 14, 1980, pp. 47-73.
23. P. J. Langford and H. J. Connors, "Calculation of Tube/AVB Wear from U-Bend Shaker Test Data," Fifth International Conference on Flow-Induced Vibrations, Paper C416/040, IMechE, Brighton, U. K., May, 1991, pp. 45-55.
24. D. S. Weaver and W. Schneider, "The Effect of Flat Bar Supports on the Crossflow Induced Response of Heat Exchanger U-tubes," Journal of Engineering for Power, October 1983, pp. 775-781.
25. "Examination Technique Specification Sheet 96004.1," Revision 13, EPRI, April 2010.
26. "Steam Generator Degradation Specific Management Flaw Handbook, Revision 1," EPRI Report 1019037, December 2009.
27. "SONGS Unit 2 Tube-to-tube Wear Indication Data" Westinghouse letter LTR-SGMP-12-80, October 2, 2012.
28. "Examination Technique Specification Sheet 27902.2," Revision 1, EPRI, May 2012.

## 5 Nomenclature

A	area
$A_i$	tube inside area
$A_s$	stabilizer area
A, B, C	empirical constants in damping correlations
ASME	American Society of Mechanical Engineers
ATHOS	Analysis of the Thermal-Hydraulics of Steam Generators
ATHOGPP	Westinghouse's version of the pre-processor program to ATHOS
ATHOSGPP	EPRI's version of the pre-processor program to ATHOS
AVB	anti-vibration bar
$C_1$	empirical turbulence constant (magnitude)
$C_L$	lift coefficient
$C_m$	added mass coefficient
$C_R$	random excitation coefficient
CCQR	pressure loss factors for AVBs in the U-bend region
CE	Combustion Engineering
CFD	computational fluid dynamics
CL	cold leg
CLCOLD	pressure loss factors for the downcomer on cold leg
CLEGGC	pressure loss factors for the tube support plates
CLHOT	pressure loss factors for the downcomer on hot leg
CLSEP	pressure loss factors for the primary separators
d, D	tube diameter
$D_e$	equivalent hydraulic diameter
Ditube	tube inner diameter
E	modulus of elasticity
ECT	eddy current test
EFPM	effective full power months
EPRI	Electric Power Research Institute
ER	Excitation Ratio, used in the context of OP vibration
$f_n$	vibration frequency in $n^{\text{th}}$ mode (Hz)
F	force
FASTVIB	computer code for FIV analysis
FLOVIB	computer code for FIV analysis
FIV	flow-induced vibration
FSR	fluidelastic instability ratio = $U_e/U_c$
FW	feedwater
HL	hot leg
HTRESF	fouling factor value input to ATHOS
ID	inside diameter
IP	in-plane
ISI	in-service inspection
IX, IY, IZ	index directions, x, y, and z in ATHOS model
K	appropriate tube wear coefficient

L	length
m	mass per unit length
MHI	Mitsubishi Heavy Industries
Ms, m <sub>s</sub>	stabilizer weight per length
N	number
NDD	no detectable degradation
NSSS	nuclear steam supply system
OD	outer diameter
OP	out-of-plane
p	tube pitch
PDRUM	pressure in the steam dome
Peff_Air	stabilizer effective density with air surrounding
Peff_Water	stabilizer effective density with water surrounding
PLATES	pre-processor program to ATHOS
Ps, p <sub>s</sub>	stainless steel density
Pw, p <sub>w</sub>	water density
R	radius, radial direction
RMS	root mean square
RPC	rotating pancake coil
RSG	replacement steam generator
RxCy	row x column y tube location
S	empirical turbulence constant (slope)
SCE	Southern California Edison
SG	steam generator
SONGS	San Onofre Nuclear Generating Station
SR	stability ratio (same as FSR), used in the context of IP vibration
SS	stainless steel
SVI	single volumetric indication
t	time
TAPE7, TAPE20	binary files to the PLATES program
Tod	tube outer diameter
TW	throughwall
TEMA	Tubular Exchanger Manufacturers Association
TH	thermal-hydraulic
TSP	tube support plate
TTW	tube-to-tube wear
U	velocity
U <sub>cr</sub> , U <sub>cn</sub>	critical velocity
U <sub>e</sub> , U <sub>en</sub>	effective velocity
V	calculated wear volume
VGUB	post-processor program from ATHOS
W <sub>r</sub>	workrate coefficient
WR	workrate
ZW	axial locations in ATHOS model

## Appendix A. Tube-to-Tube Wear in Unit 2 U-bend Free Span

This appendix provides a reasonable explanation of how the two tubes in SG 2E089 could have come in contact during plant operation so as to produce the free span wear found on R111C81 and R113C81. It is recognized that there may be other explanations regarding how this wear was produced; however, the following provides a basis for the observations found during both the PSI and the recent ISI inspections. Based on a reanalysis of the pre-service inspection data performed by Westinghouse, it was determined that a proximity condition existed for these two tubes (R111/113C81). These indications are likely to be associated with conditions that developed during SG manufacture. How proximity and increased AVB gap could result from fabrication is discussed in Section A.1. Evaluation of the eddy current inspection results and its conclusions are discussed in Section A.2. Evaluation of the impact of plant operation and shut down on the gap between the two tubes is discussed in Section A.3. The overall gap closure considerations are summarized in Section A.4.

### A.1 Manufacturing Considerations

There are several potential manufacturing considerations associated with review of the design drawings based on Westinghouse experience. The first two are related to increased proximity potential that is likely associated with the ECT evidence for proximity that is described in Section A-2. Two others are associated with the AVB configuration and the additional orthogonal support structure that can interact with the first two during manufacturing. Another relates to AVB fabrication tolerances. These potential issues include:

1. The smaller nominal in-plane spacing between large radius U-bend tubes than comparable Westinghouse experience.
2. The much larger relative shrinkage of two sides (cold leg and hot leg) of each tube that can occur within the tubesheet drilling tolerances. Differences in axial shrinkage of tube legs can change the shape of the U-bends and reduce in-plane clearances between tubes from what was installed prior to hydraulic expansion.
3. The potential for the ends of the lateral sets of AVBs (designated as side narrow and side wide on the Design Anti-Vibration Bar Assembly Drawing (LU-04FU116, Rev. 2) that are attached to the AVB support structure on the sides of the tube bundle to become displaced from their intended positions during lower shell assembly rotation.
4. The potential for the 13 orthogonal bridge structure segments that are welded to the ends of AVB end cap extensions to produce reactions inside the bundle due to weld shrinkage and added weight during bundle rotation.
5. Control of AVB fabrication tolerances sufficient to avoid undesirable interactions within the bundle. If AVBs are not flat with no twist in the unrestrained state they can tend to spread tube columns and introduce unexpected gaps greater than nominal inside the bundle away from the fixed weld spacing.

The weight of the additional support structure after installation could accentuate any of the above potential issues. There is insufficient evidence to conclude that any of the listed potential issues are directly responsible for the unexpected tube wear, but these issues could all lead to unexpected tube/AVB fit-up conditions that would support the amplitude limited fluidelastic

vibration mechanism described in Section 2.3. None were extensively treated in the SCE root cause evaluation.

#### A.1.1 Nominal In-Plane Tube Spacing

Table A-1 shows that the nominal tube spacing between the apex of successive tubes in the same column is 0.400 inch for the largest radius tubes and only 0.344 inch for the tubes in Rows 101 through 124 that have much of the observed tube wear. This nominal value at the apex is misleading in the sense that it is the maximum clearance if all tube fabrication tolerances are precisely maintained including the length of the straight legs which positions the U-bend relative to the primary face of the tubesheet. The distance between tubes on the sides at the intersection with the top TSP is 0.250 inch plus or minus the small broached hole tolerances. The actual shape of the U-bend has a profile tolerance that is not provided in the referenced drawings, but Westinghouse experience is that it may be between 0.040 and 0.120 inch (1-3 mm) for similar size tubing. The only check during tube bundle assembly is the ability to pass a 0.12 to 0.14 inch pin gauge between successive tubes<sup>4</sup>. Any tube that fits between the adjacent tubes in a given column during fabrication will satisfy this check. However, any variations in leg length or form tolerances will lead to tubes that are much closer than the nominal spacing, and most deviations will lead to tubes being closer on one side, for example near AVB3 and AVB4 and farther from AVB9 and AVB10, or vice versa. Westinghouse nominal spacing in this region is typically about 50 percent greater with a required simultaneous (rather than a sweep gauge) check of 0.18 inch clearance all around in the unrestrained as-installed condition, and it is not rare to require the use of spare tubes or trimming of tube ends to meet this requirement. Therefore, it is expected that it would have been difficult to maintain uniform spacing in the U-bend given the smaller incremental spacing on the SONGS manufacturing drawings. The root cause evaluation notes that between 132 and 390 tubes required adjustment of tube bending radius for each of the steam generators. This process is inherently difficult to control in a manufacturing environment.

#### A.1.2 Tube Leg Shrinkage During Hydraulic Expansion (HX)

The entire tube bundle is assembled before hydraulic expansion is performed with no ability to see the consequences of variations in leg shrinkage inside the bundle. Expansion is a process that involves plastic deformation of the portion of tubing that is inside the tubesheet, and plastic deformation is a constant volume process that necessitates shortening the length of the straight portions of tubing to account for the increase in diameter because wall thinning is small for the pressures involved. Figure A-1 shows expectations for the range of relative shrinkage for Plant B and for the SONGS steam generators using drawing tolerances shown on Table A-1. For most of the holes, both applications would have a maximum variation of about 0.10 inch between different sides of the same tube. However, the SONGS drawing allows up to one percent of the holes to be so large that a difference twice that large is possible for about 100 tubes in each RSG. When combined with the small clearances that are possible after installation, the superimposed HX shrinkage could lead to the level of proximity indications observed as discussed in Section A.2. When installed and then heated and pressurized, it is possible that tube-to-tube contact may occur, and in the extreme, there could be interference leading to tubes pushing against each other and then against adjacent AVBs tending to increase the column spacing. Any such conditions would tend to make the next two issues more problematic during fabrication.

---

<sup>4</sup> Westinghouse does not have access to the assembly procedures. The 0.12 to 0.14 dimensions are anecdotal without verification.



### A.1.3 Lateral AVB Nose Movement During Shop Rotation

The side-wide and side-narrow AVBs that are cantilevered from the sides of the bundle must be held in place by attachments to the retaining bars, and these bars must in turn be held in position by the orthogonal support bridge structure. For this design, gravity and friction tend to interact with the cantilevered AVBs whenever the horizontal SG is rotated during fabrication in an asymmetric way that could potentially move the noses of the AVBs and deform the straight portions leading to bending or twisting that could expand the column spacing in some regions and leave some regions of tubing with larger than nominal clearances. During shop rotation the overhanging portion of the tube bundle (about 83 inches or almost 7 feet for SONGS) bends downward several inches when the tube U-bends are horizontal, less when they become vertical, and then several inches in the opposite direction at 180 degrees from the starting position. This rotation occurs several hundred times during welding operations for not only the channel head but also the closing weld after AVB assembly. The ends of each leg of each AVB are deflected the same amount for AVBs that have their bends along the bundle centerline, but each rotation of the cantilevered AVBs deflects the leg that is nearest the center more than the one that is nearest the TSP. If the noses do not return to the original position they had when installed during the tube column and AVB layering process, the tube column spacing could be adversely impacted from consequential bending or twisting of the AVB legs. If there were any extreme proximity conditions from a combination of the first two potential issues that tended to push one tube locally against its neighbor, there could be a tendency to push the AVB legs apart locally and make it more difficult for all AVBs to maintain their original positions after rotation.

### A.1.4 Orthogonal Bridge Structure Impact on Bundle During Fabrication

The segments of the orthogonal bridges are welded to the ends of longer than normal AVB end caps at 13 columns spaced evenly around each retaining ring. Weld shrinkage at these attachments could possibly impose forces on the ends of those AVBs that must be reacted inside the bundle. The added weight of the structure would also tend to amplify gravitational effects during shop rotations.

### A.1.5 Control of AVB Fabrication Tolerances

Large radius U-bend tubing has very little flexural rigidity out-of-plane of the U-bend even when pressurized during SG operation. The tops of the straight leg portions are held in place by the TSP broached hole spacing, and the AVB end cap-to-retaining bar welds maintain spacing around the periphery, more at the bundle center, but less so around the bundle because the bars are also flexible. However, there is no structural component to keep the interior of the bundle at the intended nominal spacing in the region of most wear in the SONGS steam generators, especially along a line between the bottoms of the locations where the weight of the structure is reacted by retainer bars that can tend to push the columns apart near the Row 111 tube radius. Therefore, it is even more critical for the SONGS steam generators to maintain flatness and twist tolerances on AVBs so they will not have any tendency to separate the tube columns anywhere between the end caps and the bends deep inside the bundle. If acceptance criteria for AVB tolerances did not include inspections for flatness and twist in the unrestrained condition<sup>5</sup>, the AVBs could contribute to the apparent off-nominal spacing in the SONGS steam generators.

---

<sup>5</sup> Westinghouse does not have access to final manufacturing or inspection details, but anecdotal input indicates that six-pound weights were allowed and used during AVB inspection for consistency with AVB drawing tolerances.

### A.1.6 Additional Considerations from Unit 3

Except as noted, the discussion included in Section A.1.6 is related to the Unit 3 RSGs. It is included to here to point out the manufacturing considerations. Extensive review of ECT data available for the Unit 3 RSGs was conducted to benchmark the Westinghouse methodology against Unit 3 findings of tube-to-tube wear. Figures A-2 through A-6 identify various findings of tube proximity, AVB symmetry variance on opposite sides of the same intersection, and tapered wear scars associated with twisted AVB legs that are inconsistent with assuming tube/AVB interactions based on Gaussian distributions about nominal design conditions. Figure A-2 is an overview of all the noted variables. There is a line of proximity indications in Rows 121 and 122 that is not random, but there is insufficient information to know if it is associated with the weight of the AVB structure imparted here through the retainer bar supports or if it could be that the next incremental tube index does not occur until Row 124. The distribution of significant symmetry variances and tapered wear scar locations also does not appear random. The boundary between tubes with mostly double-sided wear scars inside the affected region (the region of the bundle with tube-to-tube wear indications) and single-sided wear scars above and below is not shown here, but the boundary is consistent and markedly not random.

Figure A-3 shows both the spatial and quantitative distribution of AVB symmetry variance in this region. The maximum symmetry variance of 0.78 inches occurs at AVB 6 on Row 87 in Column 85, and it decreases both going outward at larger radii going towards the tube/AVB weld and inward going towards the bend region. It is not likely that the middle of an AVB can be displaced this much in-plane without introducing significant bending and twist beyond design expectations. The ECT review noted that more tubes in Unit 2 had symmetry variances than in Unit 3, but they were more scattered with a smaller maximum (about 0.5 inch). Figure A-4 shows that locations with twist are present in the vicinity with the largest taper distribution from about 5 to 35%TW shown on Figure A-5.

## A.2 **Eddy Current Review**

The FIV analysis performed by Westinghouse concludes that tube locations R111 C81 and R113 C81 in SG 2E089 remain stable in the in-plane direction at both 100% and 70% power levels. The review of AVB wear scar characteristics indicates that there was no extension of the wear scars beyond the width of the AVBs, thus supporting the analysis results that these tubes, as well as all other tubes in SGs 2E088 and 2E089 which had a review of their ECT data performed, remained stable in the in-plane direction.

Westinghouse was requested to provide an explanation as to how freespan wear could be observed on R111C81 and R113C81 without in-plane vibration of the tubes. The following discussion presents an explanation of how this could occur.

### A.2.1 Industry Freespan Wear Experience Without In-Plane Instability

In recirculating SGs, there are numerous examples of tube-to-tube wear without in-plane instability; these examples are exclusive to the original Combustion-Engineering (C-E) SGs, in the upper bundle square bend region. The tube OD and triangular pitch array in the original C-E style is identical to the SONGS RSGs. In the original C-E SG design, variances in the tube horizontal run dimension, square bend control, and eggcrate tube support positioning can create a reduced tube-to-tube gap condition. Tube wear patterns at the vertical strap assembly often showed tapered wear scars on both of the vertical strips, and sometimes at both edges of the

vertical strips. This would indicate that the tube was experiencing out-of-plane displacement, with an oscillatory pattern. It is then entirely plausible that tube-to-tube wear could be experienced at reduced tube-to-tube gap conditions just below the square bend region.

At one plant, tube-to-tube wear was experienced in the horizontal run region, just outside of the square bend. In this instance, variance in the tube vertical straight leg dimension created a reduced tube-to-tube gap at this location.

At another plant in 2004, tube-to-tube wear was reported on a tube in the vertical straight leg region, just below the square bend. The elevation of the indication was actually within the bounds of the diagonal bar, but clearly rotated 90 degrees from the diagonal bar on the +Point terrain plot. One of the adjacent tubes in the same column was degradation free; the other tube was plugged several outages prior and no RPC data was available for this tube at the time of plugging. It should be noted that this indication would have remained in service if the RPC testing had not been performed. This SG has mill annealed tubing and one of the special interest RPC programs implemented was a sampling of historic bobbin signals at tube support structures to confirm the degradation morphology. Due to the tubing material, axial ODS/SCC was a potential degradation mechanism thus the RPC sampling program intended to confirm the morphology of the historic bobbin signals. Scrutiny of the bobbin data could not identify presence of tube-to-tube proximity below the indication. In the square bend region, it was judged that the inherent interference associated with the square bend geometry limited the detection of proximity using the bobbin coil. Figure A-7 presents the 0.115 pancake coil terrain plot showing the proximity signal and the tube-to-tube wear signal. The cursor (small white arrow) is located at the upper edge of the wear signal.

#### A.2.2 Causative Mechanism for Freespan Wear Without Wear Extension from AVBs

A reanalysis of the pre-service inspection (PSI) data performed by Westinghouse in 2012 for SG 2E089 indicates that numerous proximity signals were present on the Row 95 to 123 tubes in Column 81. Based on the bobbin coil proximity amplitude on R111C81, the estimated gap with R113C81 is 0.11 to 0.12 inch. The signal amplitude on R113C81 could estimate the gap at 0.02 to 0.03 inch, however, a proximity signal with R115C81 is also present. Since RPC data was not collected at the PSI, the true contribution to the signal observed on R113C81 cannot be determined. Therefore, the gap condition has to apply the most conservative value of 0.11 to 0.12 inch.

The proximity review shows that between the PSI and ISI inspections, proximity signals can remain unaffected, could no longer be observable, could be created, or could shift from one leg to the other on the same tube. With that said, the proximal condition at any point in time during the first operating cycle could be indeterminate.

The PSI proximity condition suggests that the U-bend shape could be non-uniform. This non-uniform condition will create residual stresses within the U-bend. Contact forces between tubes and AVBs could be such that tubes could be held in position for some operating period until such time that these forces are reduced or relaxed, thereby allowing the tube to return to its equilibrium condition.

An evaluation of tube motions due to thermal, pressure, and turbulence effects indicate that relative displacements of these tubes to each other can close a proximal gap of 0.03 inch but not quite sufficient to close a gap of 0.11 to 0.12 inch.

The ISI bobbin data could not identify a proximity condition on these (R111/R113 C81) tubes. Similarly, a proximity condition was not observed on R115C81 in the ISI data. UT examination

performed by AREVA suggests a tube-to-tube proximity condition between R111C81 and R113C81 of approximately 0.19 inch in the area of the tube-to-tube wear, while at the same elevation, the tube-to-tube gap between R113C81 and R115C81 was approximately 0.31 inch, or near the design nominal condition. Thus, the UT data suggests that the proximity condition between R111, R113, and R115 could imply that if these tubes returned to an equilibrium condition during the first operating cycle, the gap between R113 and R115 is near nominal, whereas the gap between R111 and R113 could suggest that the R111 U-bend length is longer than design nominal. Alternatively, this condition could be attributed to a longer than by design vertical straight leg dimension for R111, which would only increase the potential for tube-to-tube wear due to out-of-plane vibration. The UT data for R111C81 also indicates that the dimensions to R112C80 and R112C82 are much smaller than nominal, while the dimensions to R110C80 and R110C82 are larger than nominal. These observations also support the judgment that either the R111C81 U-bend is not near normal, or the vertical straight leg length of R111C81 is longer than nominal.

Still the question which must be answered is how the current gaps could be justified. An extensive review of the wear scars on the Column 81 tubes was performed. A pattern quickly emerged, which was that oddly shaped wear scars were observed at AVB 5. The profile of these wear scars has a differing depth profile that is not uniformly deep (flat wear) and not a single tapered indication. Instead, these wear scars exhibited a "saw-tooth" profile, clearly formed by two distinct wear scars. This pattern can be explained by a sudden shift in the tube position relative to the AVB, in other words, the tube "skipped" relative to the AVB. The proximity review concludes that changing proximity condition is common within these SGs. To rule out displacement of the AVB, the bobbin data of the PSI and ISI examinations was reviewed. Since no RPC data is available for the PSI, bobbin data must be used. The bobbin low frequency differential channel was used to establish that the overall length of the bobbin signal response (from a null-to-null condition) was essentially identical between the PSI and ISI exams. If one of the AVBs on either side of the tubes in Column 81 had moved, then the relative position of the two AVBs with respect to each other would change. This would also change the combined AVB width as observed by the bobbin probe along the axial length of the tubes in Column 81. Since the lengths of the AVB signals (combined AVB width) in the PSI and ISI were identical, it is concluded that the AVBs did not change position.

These characteristic wear scars were observed on R113C81, R115C81, R117C81, R119C81, R121C81 and R123C81, all at the AVB 5 location. An example of such wear scars is shown on Figure A-8, Figure A-9, and Figure A-10. Figure A-10 presents the +Point terrain plot of R113C81 at the AVB 5 location. Each figure includes the +Point 300/100 mix channel (for flaw detection) and the 35 kHz channel response, for identification of the edges of the AVBs. If the wear bounded by the AVB edges represents the most recent wear (prior to shutdown), and the wear is tapered, the distance from the edge of the original wear to the edge of the AVB can be used to estimate the amount of tube displacement. This dimension has been estimated to range from 0.12 to 0.40 inches, for those tubes which show this characteristic. Note also that this same characteristic was observed on R129C91, at AVB 5. This tube was reported with a proximity call on the cold leg in the PSI data and on the hot leg in the ISI data.

Another characteristic of the wear at AVB 5 on these tubes was that shallow depth, short length wear scars were sometimes observed on the opposite AVB. These wear scars were clearly of much shallower depth than the wear scars which exhibited the odd shape. The only way that a wear scar could be observed in the middle of the AVB (not extending to any AVB edge) is if the tube shifted relative to the AVB at some point in time during operation.

These atypical indications are associated with significant observations of AVB symmetry variance. The term symmetry variance is used to describe the relative position (axial distance) of

the two AVBs on either side of a tube along the tube axis. In SG 2E089, the largest AVB symmetry variance is observed at AVB 6, and for Column 81; AVB 7 also has significant AVB symmetry variance. If the AVB symmetry variance is associated with AVB twist, and the amount of twist is correlated with symmetry variance, then the largest contact forces would be observed for AVB 6 and AVB 7. As the larger contact forces would reduce the potential for wear, once sufficient wear has occurred at other AVBs to reduce the overall contact force thus permitting the tube to return to its equilibrium condition, the tube would then skip to its current condition. For AVBs 5, 6, 7, and 8, the 95<sup>th</sup> percentile AVB wear depths are essentially equal, but the wear indications at AVB 5 are deeper for Column 81. For R113C81, the deepest AVB wear is observed at AVB 5 (based on +Point results).

The deepest AVB wear indication (from +Point analysis) in SG 2E089 was reported on R121C83 at AVB 5. The indication appears to be uniformly deep and does not show signs of tube displacement relative to the AVB. The wear is single sided; the opposite AVB has not caused degradation of the tube. The +Point 35 kHz residual data suggest no AVB twist on either AVB, however the residual responses for the AVB without wear are modestly less than for the AVB with wear. The deepest indication in SG 2E089 reported by bobbin coil analysis was reported on R117C81 at AVB 9; this indication also appears to have a uniformly deep profile. The deepest wear from bobbin coil analysis in SG 2E088 was reported on R133C91 at AVB 6. The +Point terrain plot for this location showed that the indication is stepped. The opposite AVB does not contain wear. The +Point 35 kHz residual voltages are essentially equal for this AVB, indicating no twist. The 35 kHz +Point residual voltages on the AVB with wear show a large variance, suggesting significant AVB twist (estimated to be about 2 degrees).

#### A.2.3 Detection Condition Associated with Wear Extension from AVBs

The detection condition associated with wear extension from AVBs was investigated. To perform this assessment, the +Point 300/100 mix channel noise was compared for the middle of the AVB region and the freespan region just outside of the AVB. The vertical maximum noise condition outside of the AVB was exceptionally small; on the order of 0.02 to 0.04 volt. The noise condition within the AVB was typically 50% larger than just outside of the AVB. Therefore, if tapered wear is experienced, and the shallower edge of the wear has a distinct character (i.e., the tapered wear extends for the full length of the AVB width) and no wear is observed outside of the AVB, it can be concluded that no wear is present outside of the AVB as the length along the tube axis from the edge of the wear to just outside of the AVB is short, and not of sufficient length to allow the wear to runout to the tube OD. Since the noise condition within the AVB is greater than just outside of the AVB, the detection of wear within the AVB would then imply a detectable condition and the wear extension outside the AVB would be detected if present.

### **A.3 Temperature, Pressure and FIV Effects**

A tube-to-tube gap of approximately 0.19 inch between the R111C81 and R113C81 tubes near the tube-to-tube wear region was measured by ultrasonic testing (UT) after the first cycle of operation. The gaps between AVBs 3 and 4 were also measured for these tubes. The gap between R111C81 and R113C81 was not measurable at this location, but a gap of 0.18 inch was measured between R109C81 and R111C81. The gaps between AVBs 3 and 4 and AVBs 9 and 10 between R113C81 and R115C81 were measured around 0.30 to 0.31 inch which is close to the nominal gap of 0.31 inch for this location in the U-bend. The maximum design spacing is 0.344 inch at the top of the U-bend for these tubes. The design spacing of the tubes is shown in Figure A-11. In the UT data there is no reference point to determine if any of the tubes are in the



design shape so an assumption needs to be made for the geometry of these tubes. It appears that the R111C81 tube is deformed relative to the other tubes so it will be assumed that the R113C81 tube is nominal in shape and the R111C81 tube is deformed in a way that follows the gap measurements (see discussion in Section A-2). A sketch of this geometry is shown in Figure A-12.

### A.3.1 Tube Thermal Expansion

One way to postulate a closure in the tube spacing to occur is for the two tubes with tube-to-tube wear to move within the tube support plate holes as they expand due to operating temperature and pressure.

Using the tube support plate drawing (Reference A-1), the maximum geometrical tolerances for the tube support plate holes were considered. Using the maximum tube support plate dimensions and the minimum tube size, it was determined that the tube can move 0.033 inch within the tube support plate before it comes to rest on the opposite side of the broached hole. The maximum dimensions of the tube support plate broaching are shown in Figure A-13. The maximum tube movement within the tube hole is also shown in Figure A-13. The scenario that would cause the maximum movement between the tube support plate is when R111C81 is resting on the left side of the broach at the hot leg and cold leg side. When the tube is brought up to the normal operating temperature and pressure, the tube will expand outward which will cause the tube to move to the outside positions in the tube support plate holes. The R113C81 tube is assumed to be in the exact opposite configuration where the tube is pushed to the right side of the tube support plate holes. A schematic of this effect is shown in Figure A-14.

This tube model was simulated using the ANSYS finite element program using Solid186 three-dimensional structural solid elements and Solid90 thermal elements. These elements are a 20 node brick element. A plot of the meshed model in the U-bend region is shown in Figure A-15. The temperature solution was obtained from the FASTVIB output for the 100% power case for the R111C81 tube. The temperature profile for the R113C81 tube was almost identical to the R111C81 tube so the same temperature profile was applied to both tubes. The temperature distribution was applied to the tube by fixing the temperature at the tube support plate locations and then solving for the steady state temperature solution. The temperature change around the tube is fairly gradual such that the steady state solution from ANSYS matches the ATHOS data fairly closely.

The tubes were fixed at the tubesheet end of the model and nodes were pinned in the X and Z directions at the tube support plate locations. The AVB supports were neglected in the model. The AVB supports are assumed to be sufficiently loose such that they do not provide support in the in-plane direction.

### A.3.2 Tube Movement at AVB 5

It has been found from the shape of the wear scar in the eddy current data that at AVB 5 for Tube R113C81 there appears to be a shift in the tube position. There are two sawtooth shapes on the wear scar on one side of the tube which indicates that the AVB is twisted and wore a mark that twice moved slightly and resumed wear in a different spot. In the opposite side of the tube, the AVB also appears to be twisted but the wear scar is near the center of the AVB position at the cold leg. This is an indication that the tube has shifted in position relative to AVB 5. The postulation that R111C81 and R113C81 were initially much closer than suggested by the current gap measurement states that they moved farther apart when this shift in tube position occurred. The finite element model works backwards from this scenario by assuming the inspection

geometry of the tubes and then applying a displacement to determine how close the tubes were prior to the displacement. The eddy current wear scars indicate that the tube moved approximately 0.12 inch to 0.18 inch.

The deformed shape model from Section A.2 was used and the tube was displaced towards the cold leg side in the X direction 0.12 inch then 0.18 inch. The displacement was applied to the model at the centerline where AVB 5 would cross Tube R113C81. A local coordinate system was then used to determine the amount of displacement of Tube R111C81 relative to Tube R113C81.

The results of the displacement models are shown in Figure A-16 and Figure A-17 for the 0.12 inch and 0.18 inch displacement, respectively. It is shown that for a displacement of 0.12 inch or 0.18 inch, the close up in the gap is approximately one for one. The difference in displacement versus gap closure is only 1 mil.

### A.3.3 Impact of In-Plane Turbulence

In addition to the finite element models used to show that the tube gap closes, there can also be in-plane motion due to flow turbulence. This in-plane turbulence motion is displacement limited and should not be considered a similar effect as in-plane stability. The purpose of this section is to evaluate the magnitude of turbulent displacement to be used to support the explanation that the tubes with tube-to-tube contact are not unstable in-plane. It is known that these tubes have closer than nominal proximity at the cold condition so the tube-to-tube contact is being explained as extreme tube-to-tube proximity with a combination of in-plane turbulent motion and out-of-plane fluidelastic motion.

A FASTVIB evaluation was performed for the tubes that had tube-to-tube contact in Steam Generator 2E089. These tubes are R111C81 and R113C81. The turbulent constants C1 and S applicable to the SONGS steam generators are shown in Table A-2. There are two sets of constants based on the flow characteristics around the tube. Two FASTVIB runs for each case are evaluated based on each set of constants. The FASTVIB evaluation was condensed to only include the tubes in Row 111 and Row 113. The two tubes, R111C81 and R113C81, have a defined missing AVB Case 61.

The results of the FASTVIB runs show that the root mean square (RMS) turbulent displacement is approximately 0.003 inch for each tube using either set of turbulence constants. Using Reference A-2, the RMS turbulent displacement can be converted to a peak displacement using a factor of 3.5. Assuming both tubes are vibrating, the maximum distance the tubes can be apart and still come into contact due to turbulent displacement is  $2 \times 3.5 \times 0.003 = 0.021$  inch.

## A.4 Summary

From the review of the eddy current data and the analysis of the tubes response due to pressure temperature and FIV effects, it appears that the two tubes were very close or were in contact at the start of operation following replacement. The tubes would not have necessarily been in contact before operation, but could have contacted due to peak displacements as a result of in-plane turbulence. Note that displacements associated with the fluidelastic mechanism are not similar to turbulence induced displacements, as the turbulence mechanism is self limiting.

UT measurements performed during the recent outage indicates that the tubes could be as close as 0.19 inch. As with all measurements of this type, there are measurement uncertainties that are present in the signals. The uncertainty associated with the UT measurements could range from an estimated low of 4 mils to ~20 mils. This means that the actual low end of the gap could range from 170 mils to 186 mils. This is the range of gap sizes that could have developed after

the tubes have shifted to the current location. Figure A-18 describes how the tubes could have initially worn due to proximity, and then moved or shifted during operation coupled with temperature and pressure effects to result in the currently observed condition.

In summary, it appears as if the tubes were initially very close, or actually contacting prior to operation, where FIV induced turbulence vibration could have produced the observed wear. Then after operation for a period of time, the tubes moved, or skipped to a new location, similar to the skip found in other tubes in the region (up to 0.4 inches). Figures A-19 and A-20 provide a visual indication of how these tubes could have moved. Additional movement of the tubes is possible due to pressure and temperature effects that would then result in the currently observed condition.

## A.5 References

- A-1. San Onofre Nuclear Generating Station Units 2 and 3 Replacement Steam Generators MHI Design Drawings:
- A. L5-04FU001, Rev. 6, "Component and Outline Drawing 1/3".
  - B. L5-04FU051, Rev. 1, "Tube Bundle 1/3".
  - C. L5-04FU052, Rev. 1, "Tube Bundle 2/3".
  - D. L5-04FU053, Rev. 3, "Tube Bundle 3/3".
  - E. L5-04FU101, Rev. 5, "Wrapper Assembly 1/5"
  - F. L5-04FU107, Rev. 3, "Tube Support Plate Assembly 2/3".
  - G. L5-04FU108, Rev. 3, "Tube Support Plate Assembly 3/3".
  - H. L5-04FU112, Rev. 1, "Anti-Vibration Bar Assembly 2/9".
  - I. L5-04FU118, Rev. 3, "Anti-Vibration Bar Assembly 8/9".
  - J. L5-04FU134, Rev. 6, "Moisture Separator Assembly 4/6".
  - K. L5-04FU135, Rev. 5, "Moisture Separator Assembly 5/6".
- A-2. B. Brenneman and J. Q. Talley, "RMS Fatigue Curves for Random Vibrations," Transactions of the ASME, Volume 108, November 1986.

**Table A-1. Feature Comparison of SONGS and Plant B Steam Generators**

<b>Feature</b>	<b>SONGS</b>	<b>Plant B</b>
Number of Tubes	9727	10637
Tube Material	Alloy 690 TT	Alloy 690 TT
Tube Dimensions (in)	0.750 OD x 0.043 t	0.688 OD x 0.040 t
Triangular Pitch (in)	1.00	0.95
Pitch/Diameter	1.33	1.38
Largest Radius, $R_{max}$ (in)	76.27	74.025
Number of TSPs	7	8
TSP Material	405 SS	405 SS
Trifoil Broach Radius (in)	0.381-0.384	0.349-0.353
Radial Tube Clearance (in)	0.006-0.009	0.005-0.009
TSP Thickness (in)	1.38 (0.2-1.07 land height)	1.125 (0.94-1.08 land height)
TSP CL Spacing (in)	42.82 first, 43.66 typical	34.67 first, 35.23 typical
Number of AVB Sets	6 (2 Each Side, 2 Centered)	5 Centered + Staggered
AVB Material	405 SS	405 SS
AVB Dimensions (in)	0.590 W x 0.114 t	0.480 W x 0.133 t
Nominal* Diametrical Gaps (in)	0.0020	0.0017
Average U-bend Span @ $R_{max}$	13 @ ~ 19.4 in	11 @ ~ 23.9 in
U-bend Overhang (in)	83	89
IP Tube Spacing** at Apex (in)	0.298, 0.344, 0.400	0.442, 0.502, 0.562
Alloy 690 Retainer Bars (in)	24 Round (12 ea @ 0.19, 0.41)	20 @ 0.63 W x 0.125 t
Alloy 690 Retaining Rings (in)	0.38 Round	0.38 Square
Alloy 690 End Caps (in)	0.38 t x 1.00 W x 1.97 L	0.451 t x 0.860 W x 2.00 L
End Cap to Ring Welds (in)	0.12 leg	0.19 leg x 0.38-0.63 long
Orthogonal Structure	13 Segmented Bridges	None
SG Power Level (MWt)	1729	1522
Maximum Steam Quality	0.89	0.75
Maximum Void Fraction	0.9955	0.9851
Operating Time @ Last ISI	Cycle 16 (1.7 EFPY)	Cycle 6 (8.1 EFPY)
Tubesheet Thickness (in)	27.95	31.56
Hole Tolerances (in)	0.756-0.762 (0.769 for 1%)	0.696-0.701
Diametrical Expansion (in)	0.006-0.012 (0.019 for 1%)	0.008-0.013

\*Assuming AVBs are welding at the nominal TSP hole pitch spacing.

\*\*For larger tubes in radial zones ~41-55, 56-67, and 68-maximum.

**Table A-2. Turbulence Constants**

Parameter	Straight Leg Region	U-bend Region
Turbulence ( $fD/U > 0.13$ )		
$C_1$	$1 \times 10^{-3}$	$1 \times 10^{-3}$
S	2.34	2.34
Turbulence ( $fD/U < 0.13$ )		
$C_1$	$7.8 \times 10^{-3}$	$7.8 \times 10^{-3}$
S	0.304	0.304



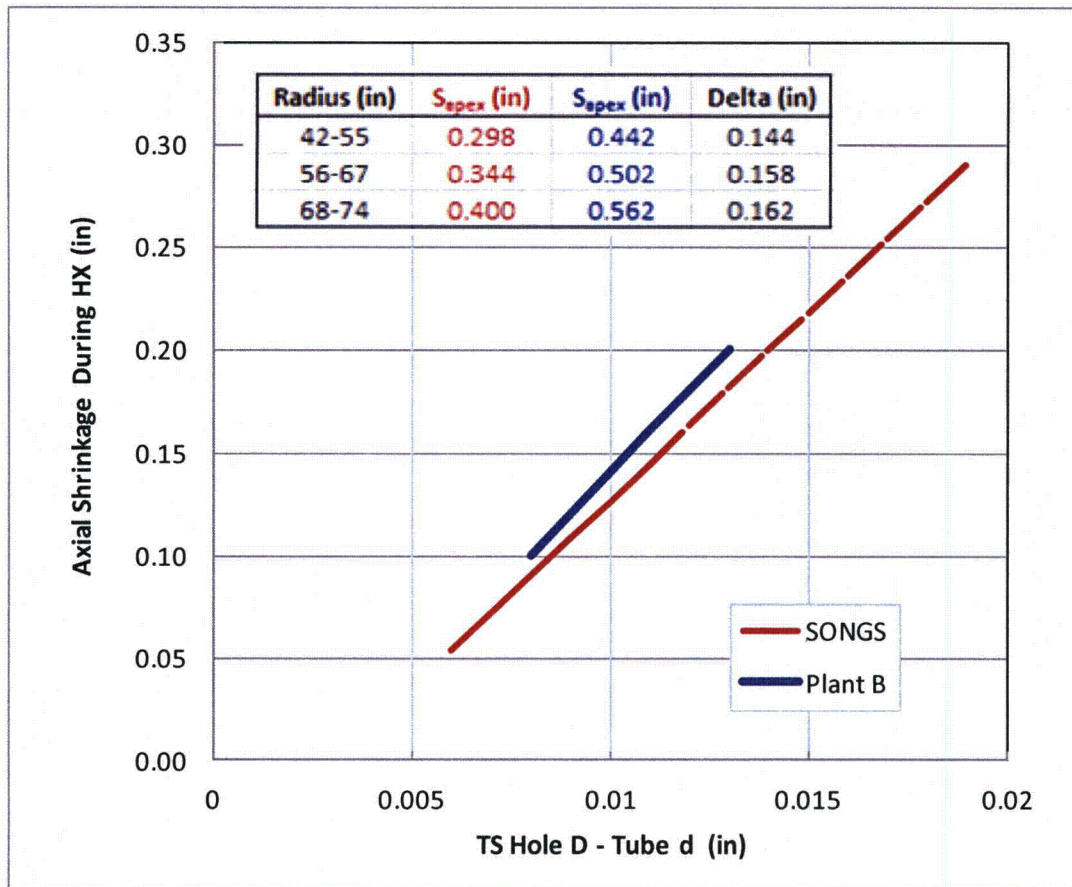


**Figure A-1. Potential Range of Axial Shrinkage for Plant B and SONGS Steam Generators Using Drawing Tolerances for TS Drilled Hole Diameter**

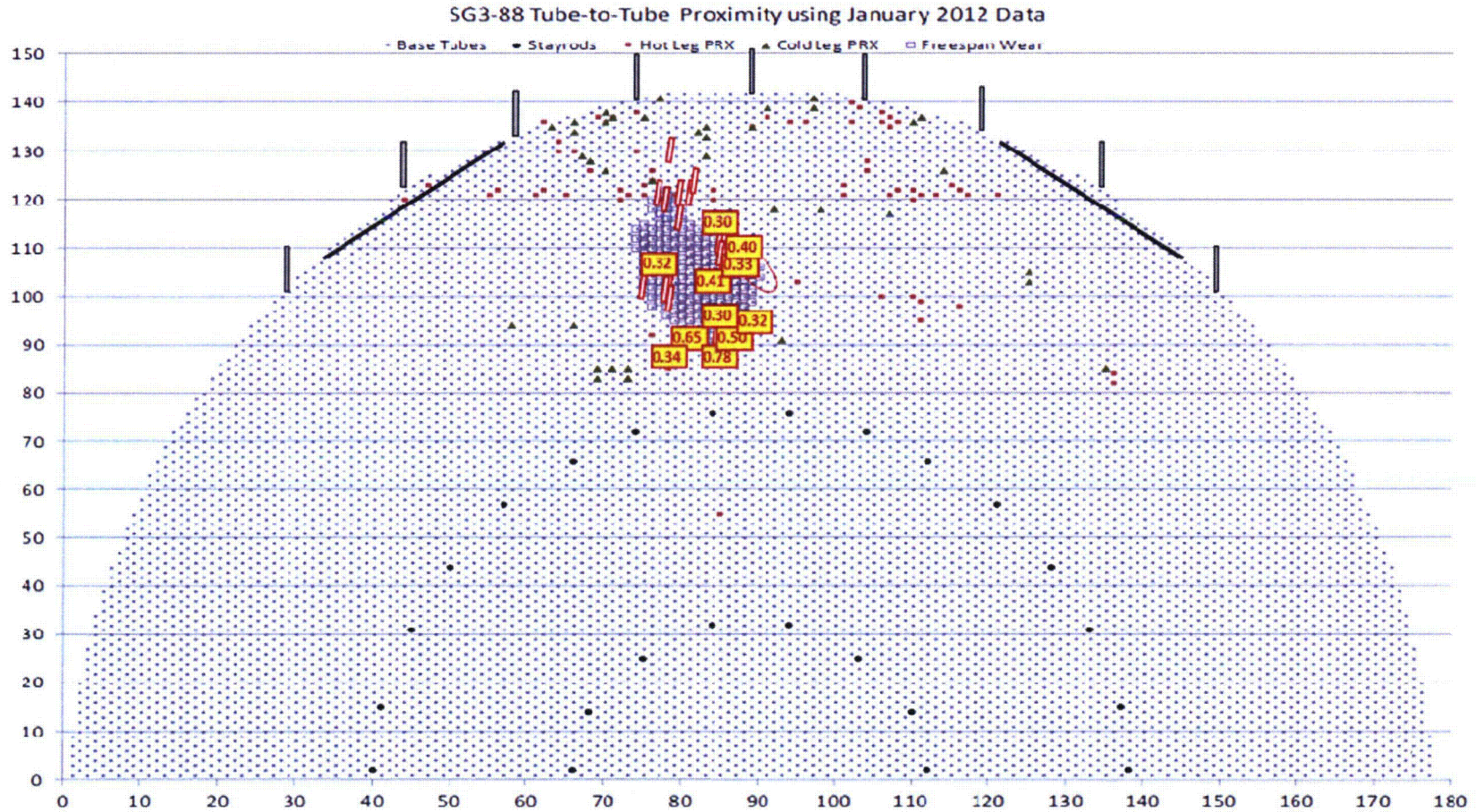


**Figure A-2. Overview of ECT Results from SG 3E088 Using ISI Proximity Results Map with AVB Support Structure (Boxes with numbers are locations of AVB symmetry variance; smaller rectangles are locations with twist)**



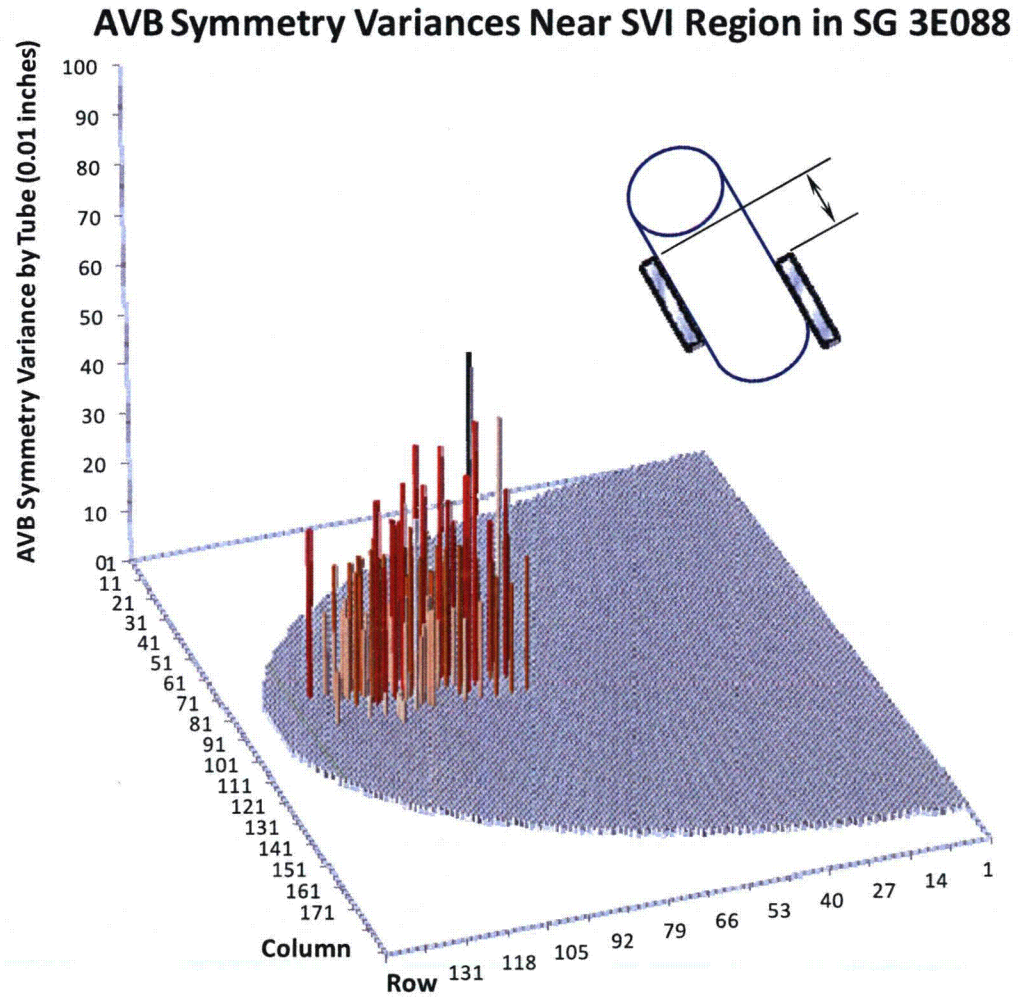


**Figure A-3. Locations and Magnitudes of AVB Symmetry Variances Near TTW Region of SG 3E088 (SVI Region  $\equiv$  TTW Region)**

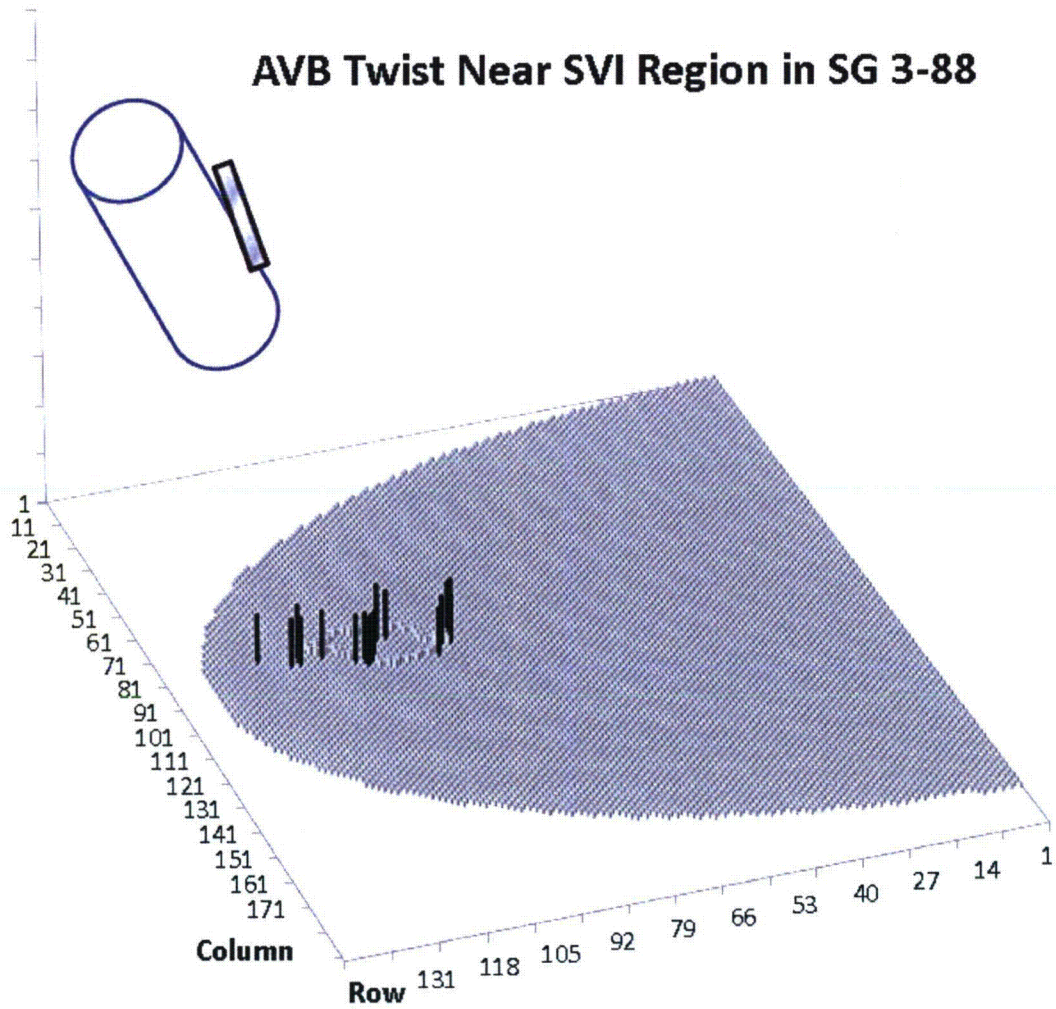


**Figure A-4. Distribution of AVB Locations with Tapered Wear Scars Indicating AVB Twist (SVI Region  $\equiv$  TTW Region)**

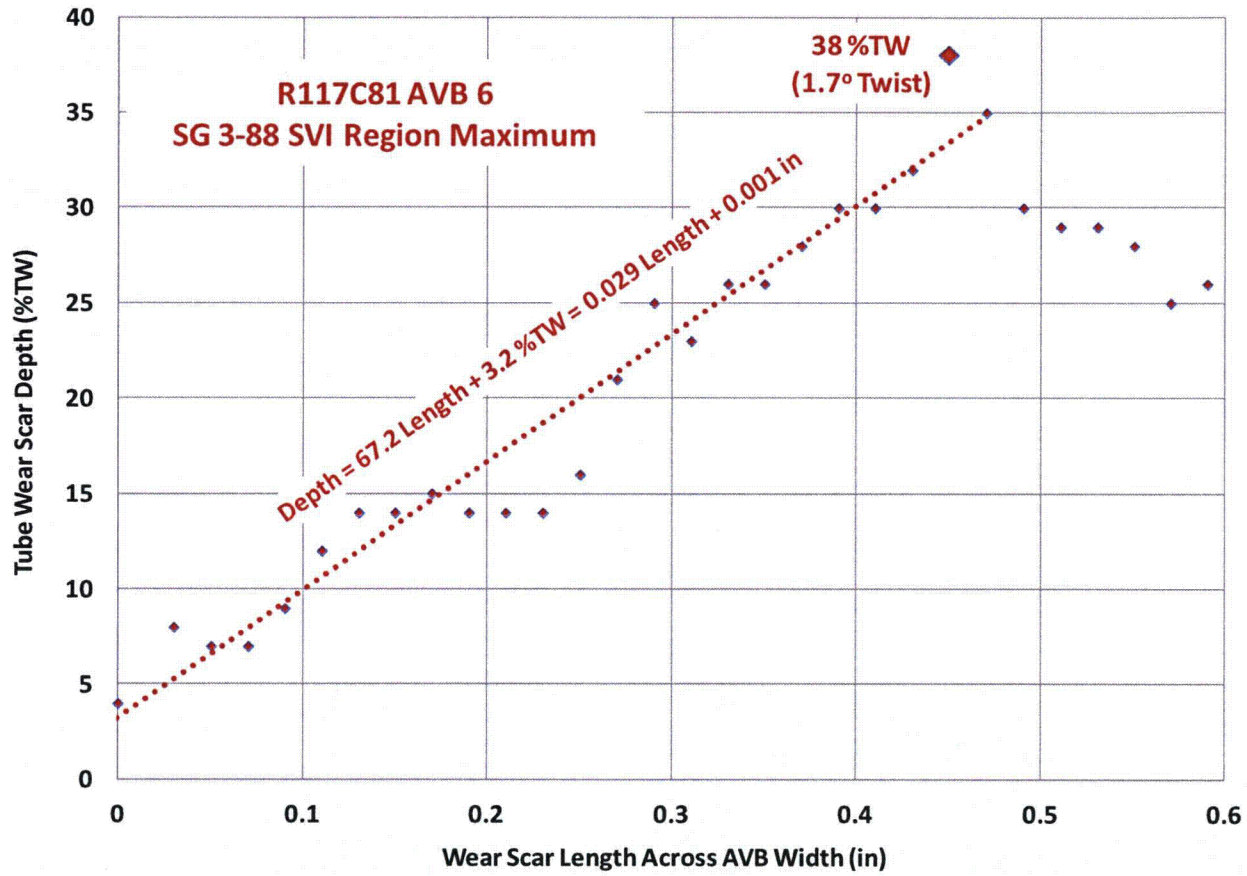


**Figure A-5. Largest Implied Twist from Preliminary Tapered Wear Scar Review Near TTW Region of SG 3E088 (SVI Region ≡ TTW Region)**



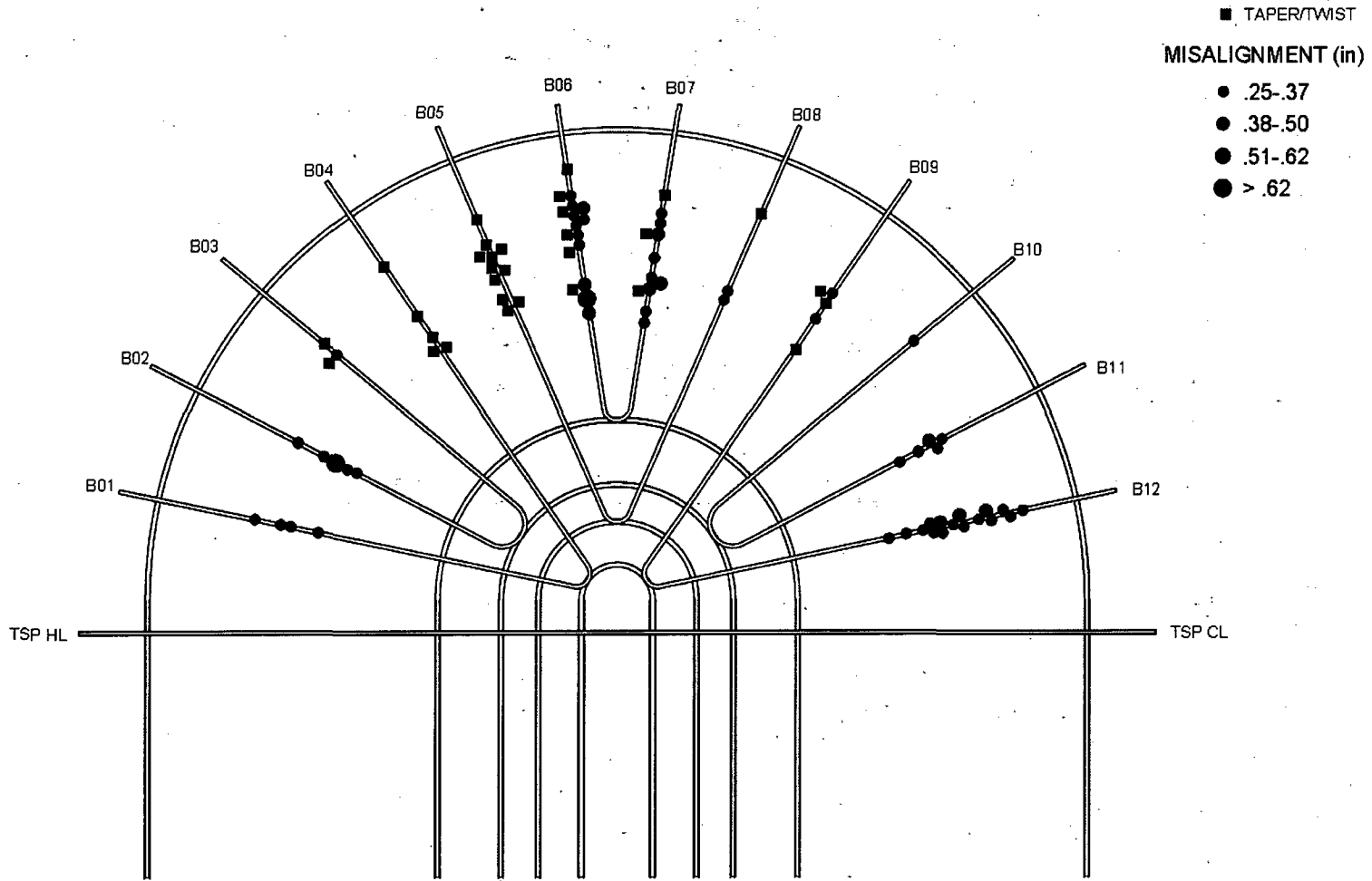


Figure A-6. Elevation View of Locations of AVB Misalignment and Tapered Wear Scars Obtained During ECT Review of the SG 3E088 TTW Region

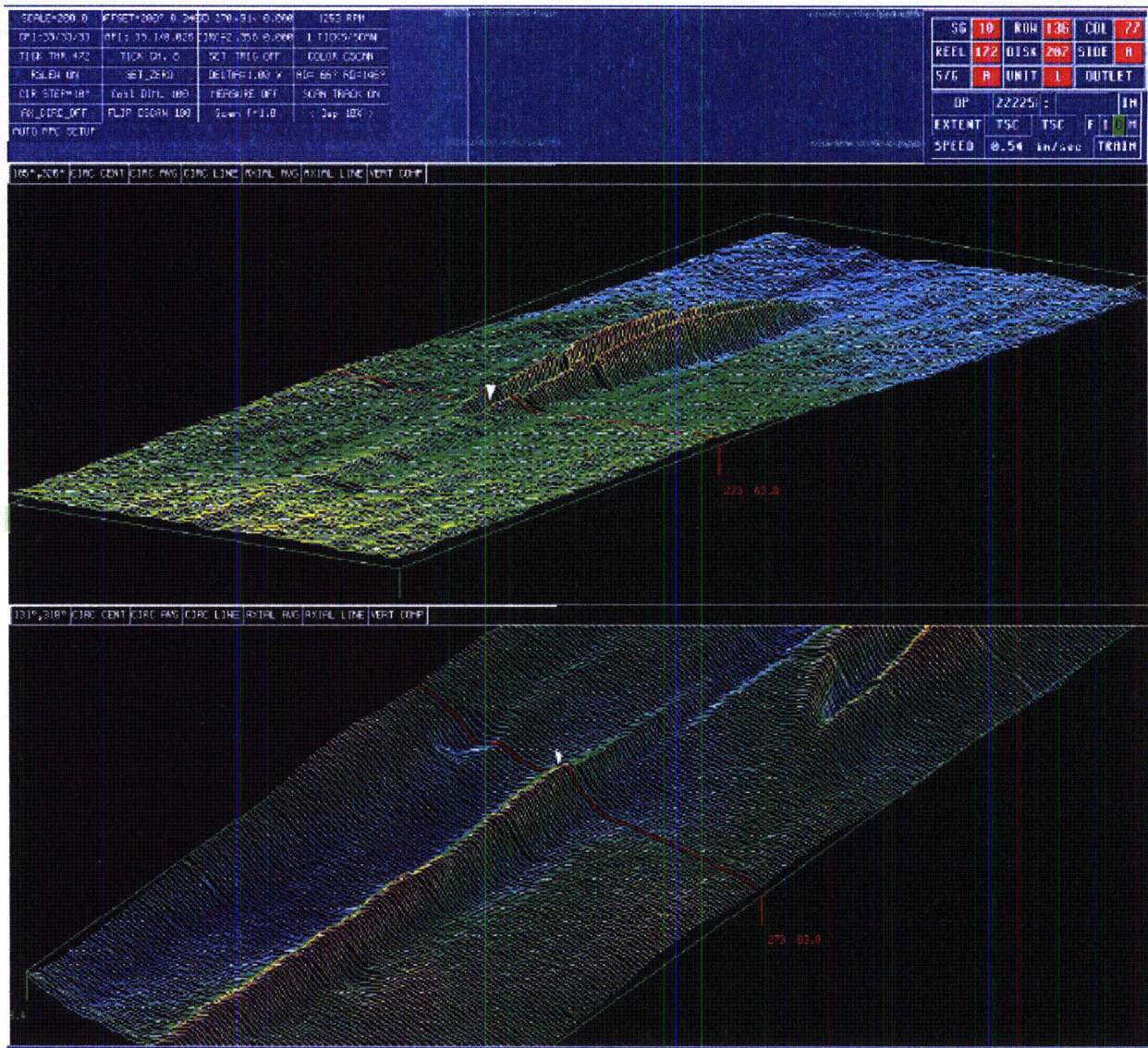


Figure A-7. Other Plant Experience Showing Relation of Tube-to-Tube Wear and Proximity at Shutdown Condition



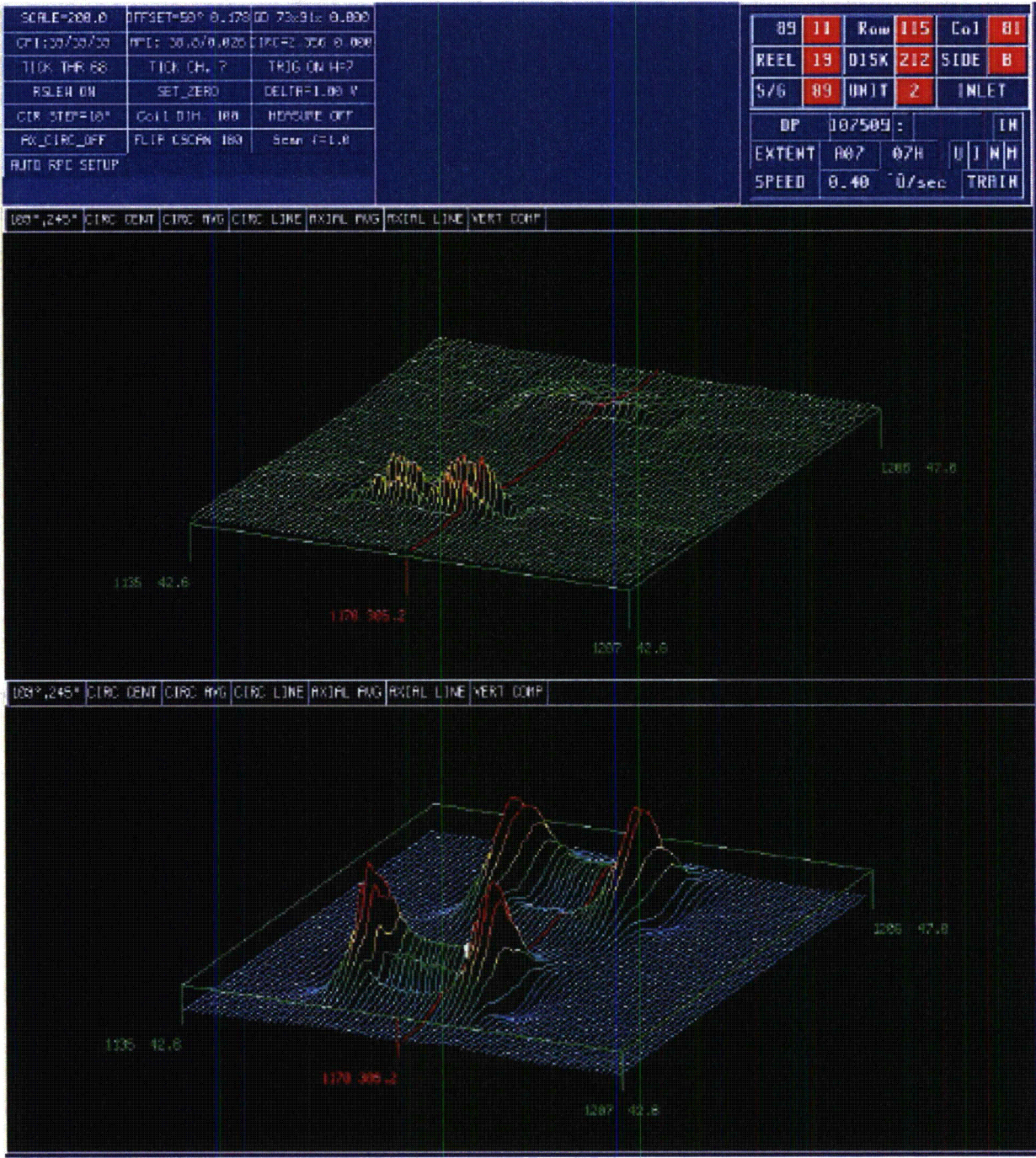


Figure A-8. SONGS SG 2E089 Stepped Indication at AVB 5 on R115C81



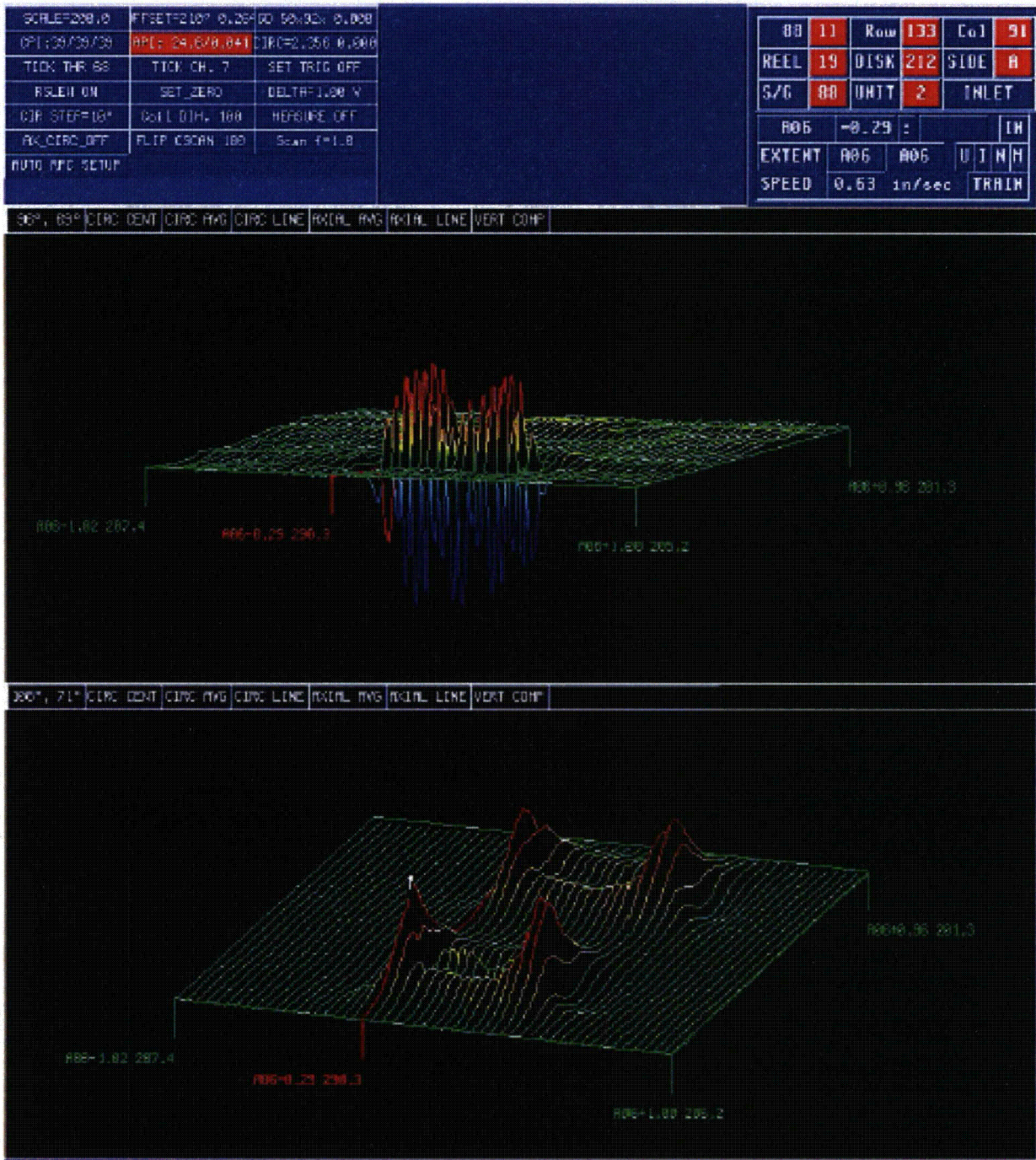


Figure A-9. SONG SG 2E088 Stepped Indication at AVB 6 on R133C91



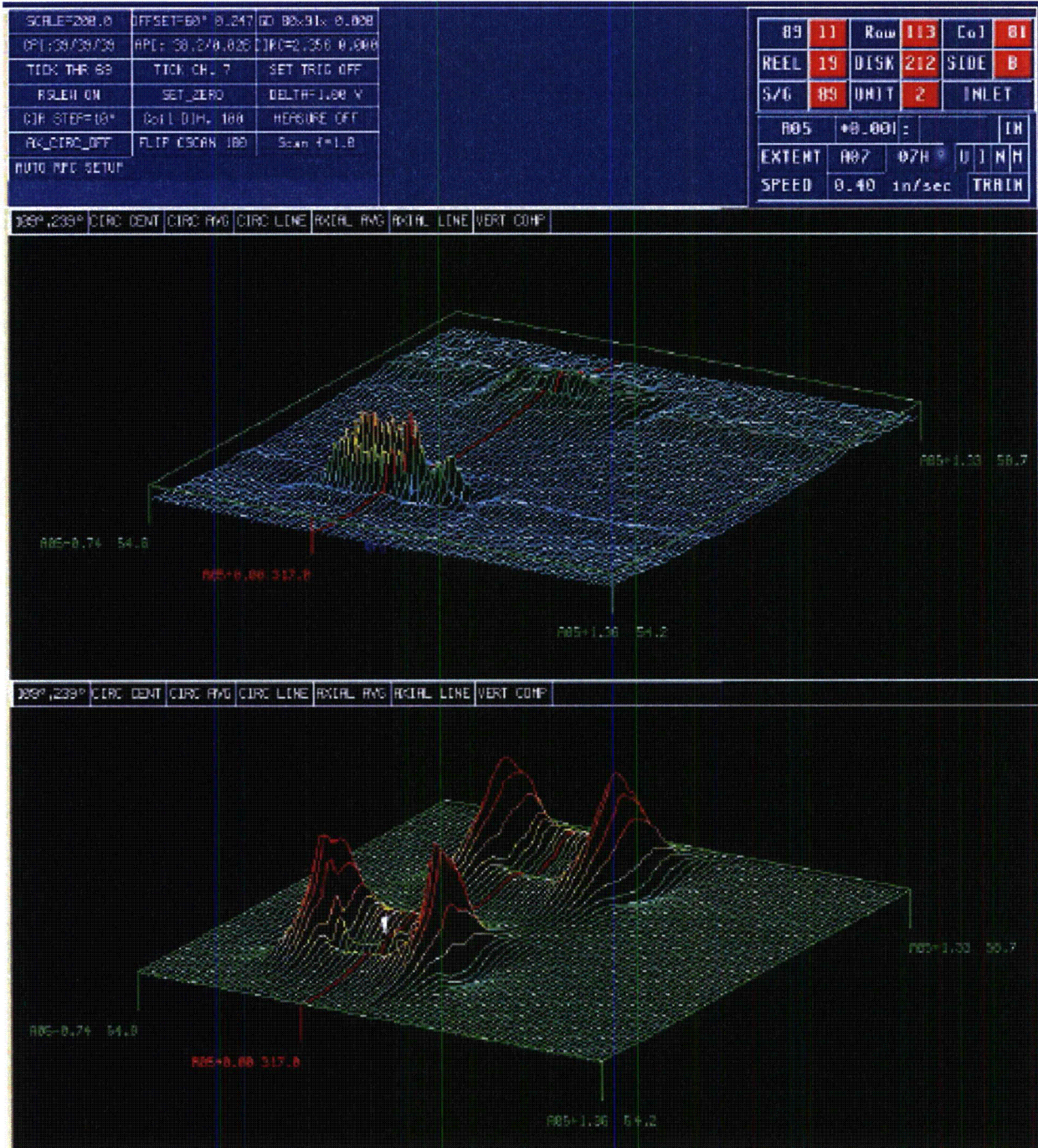
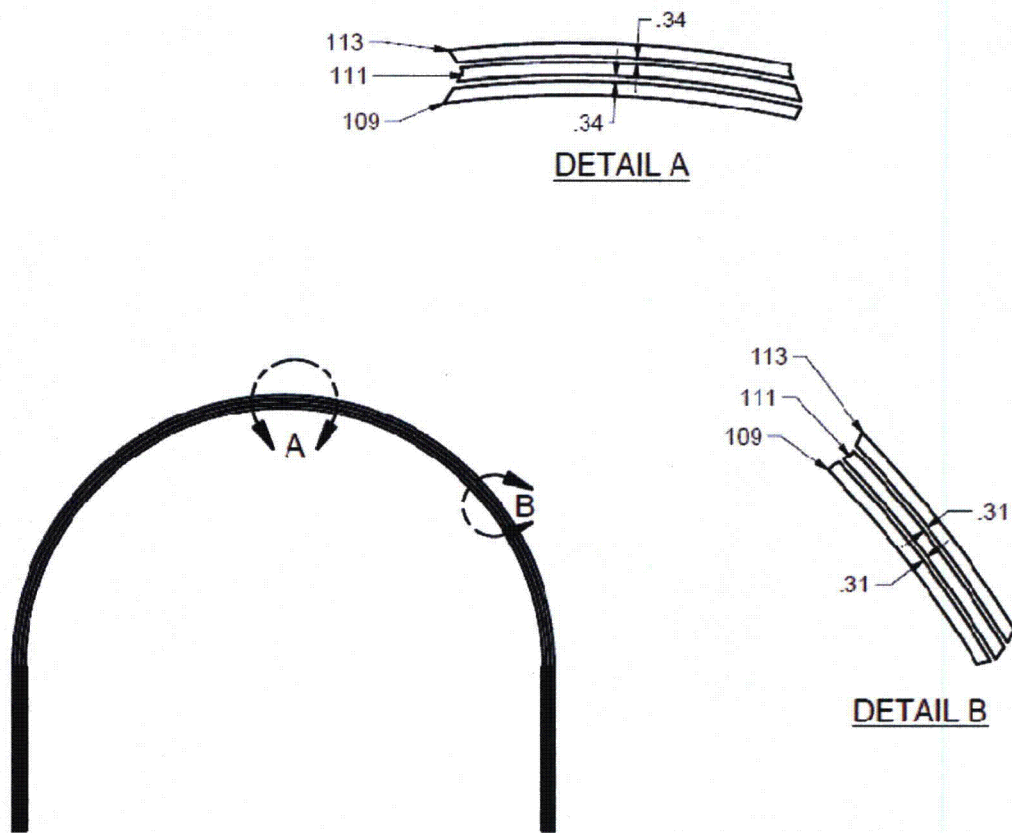
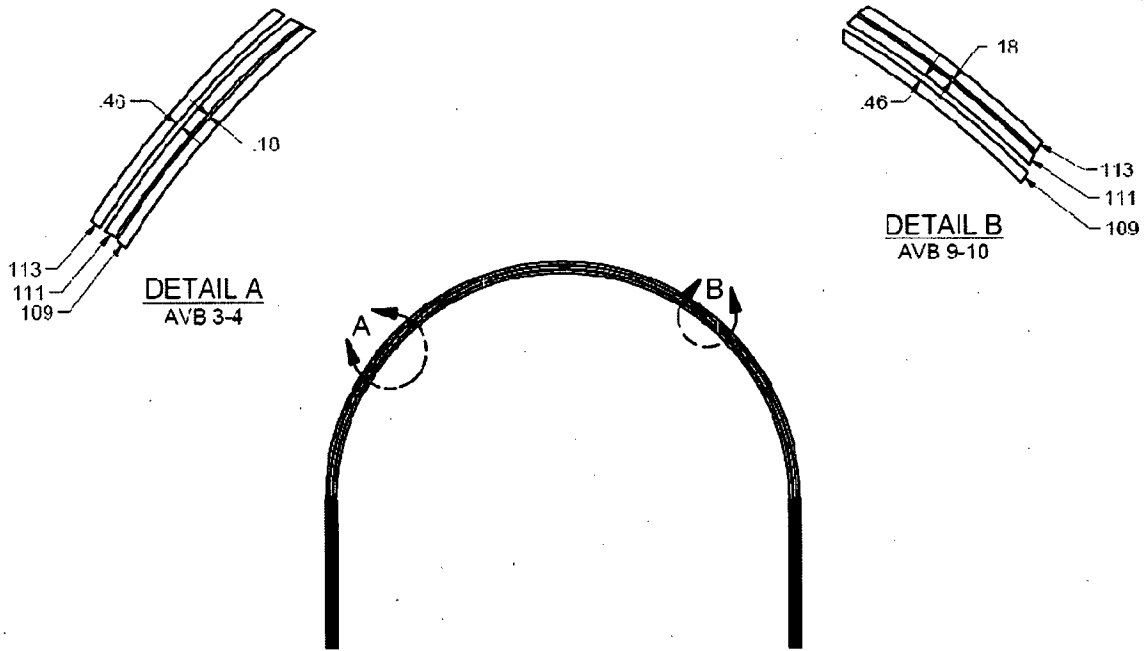


Figure A-10. SONGS SG 2E089 Stepped Indication at AVB 5 on R113C81

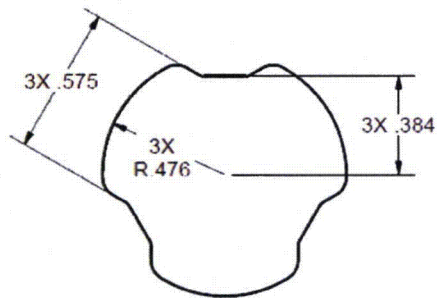




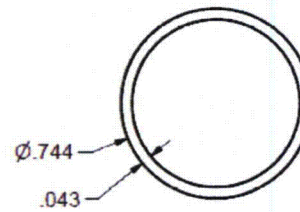
**Figure A-11. Shape of R111C81 and R113C81 Tubes Based on Nominal Dimensions**



**Figure A-12. Shape of R111C81 and R113C81 Tubes Based on Measured Gaps**



**MAX BROACH SIZE**  
REF DWG: L5-04FU108



**MIN TUBE DIA**  
REF DWG: L5-04FU051

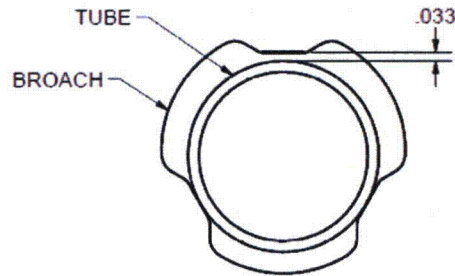
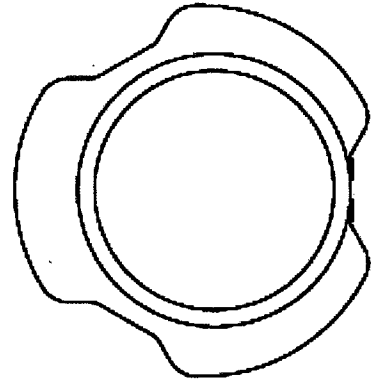
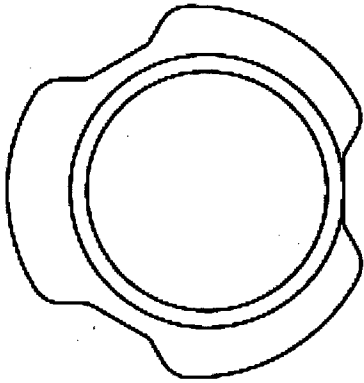
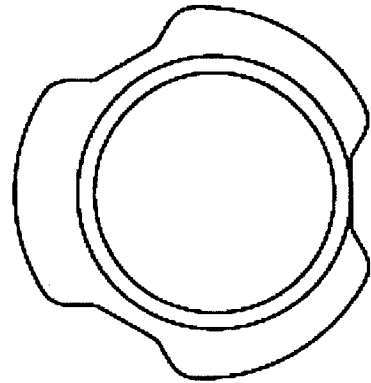
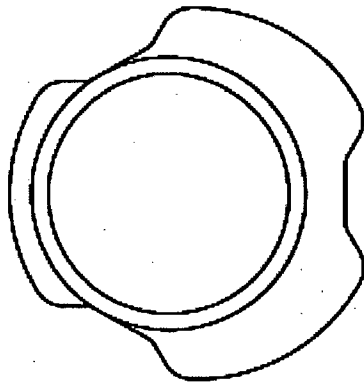


**Figure A-13. Tube Support Plate Maximum Dimensions**



COLD



HOT

\*TUBE NOT TO SCALE TO SHOW EXAGGERATED MOVEMENT.\*

**Figure A-14. Tube Support Plate Hole – Tube Movement**

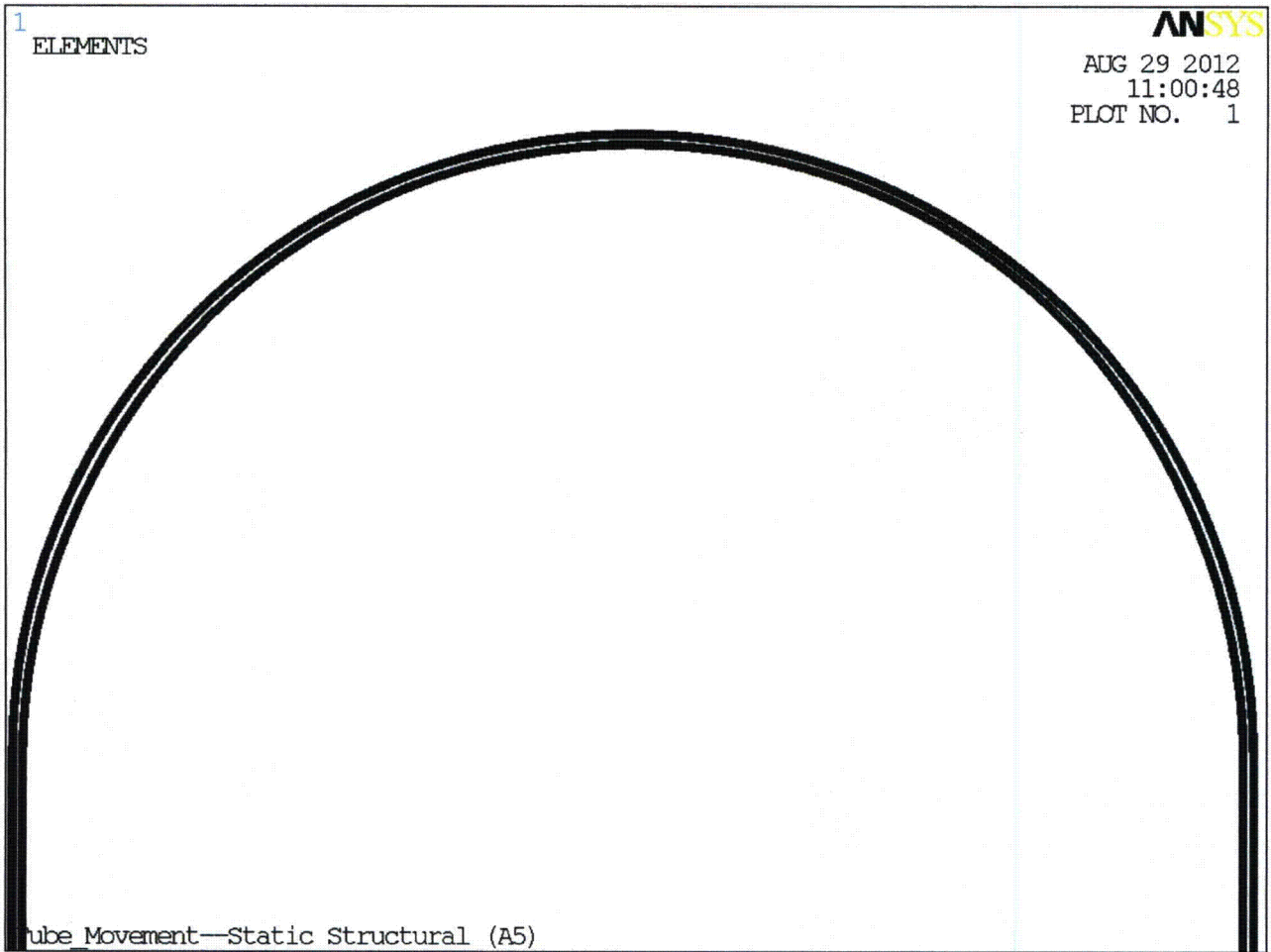


**Figure A-15. Meshed Tube Model**



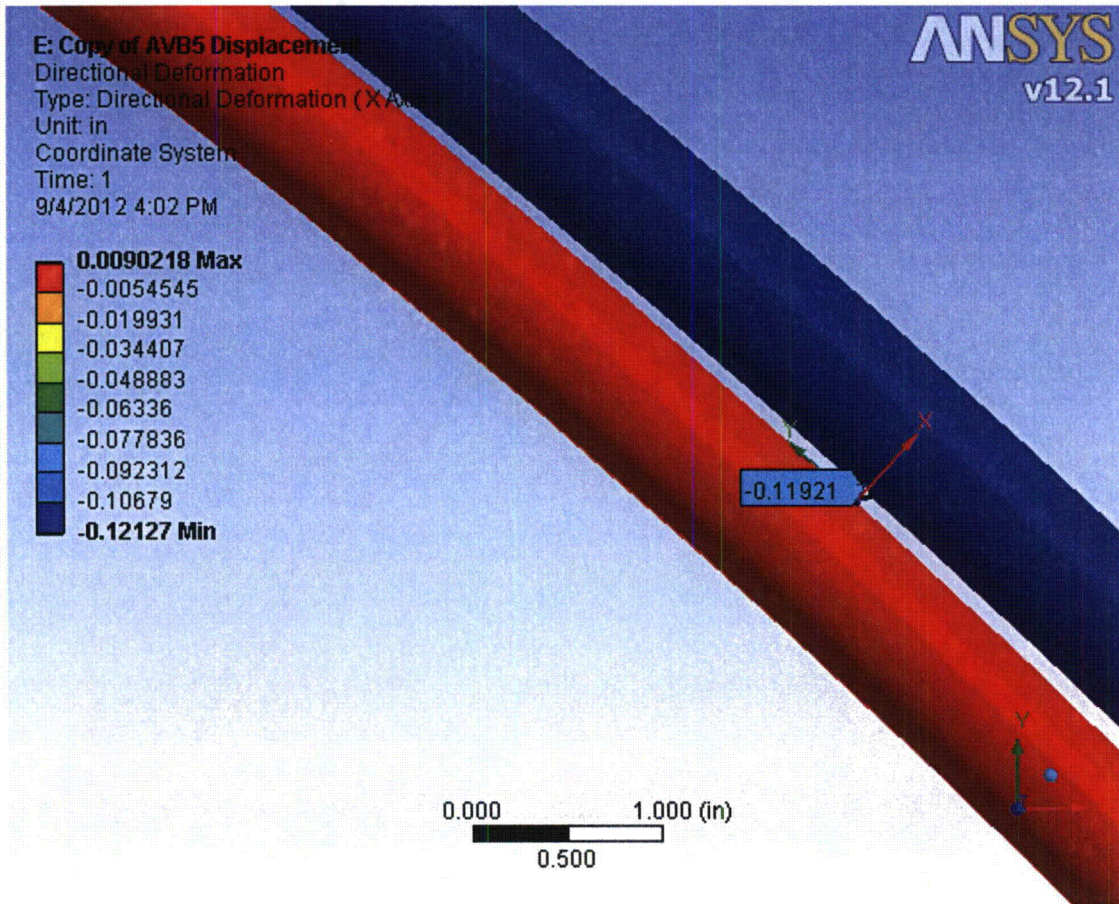


**Figure A-16. 0.12 Inch Displacement at AVB 5 Results (inches)**

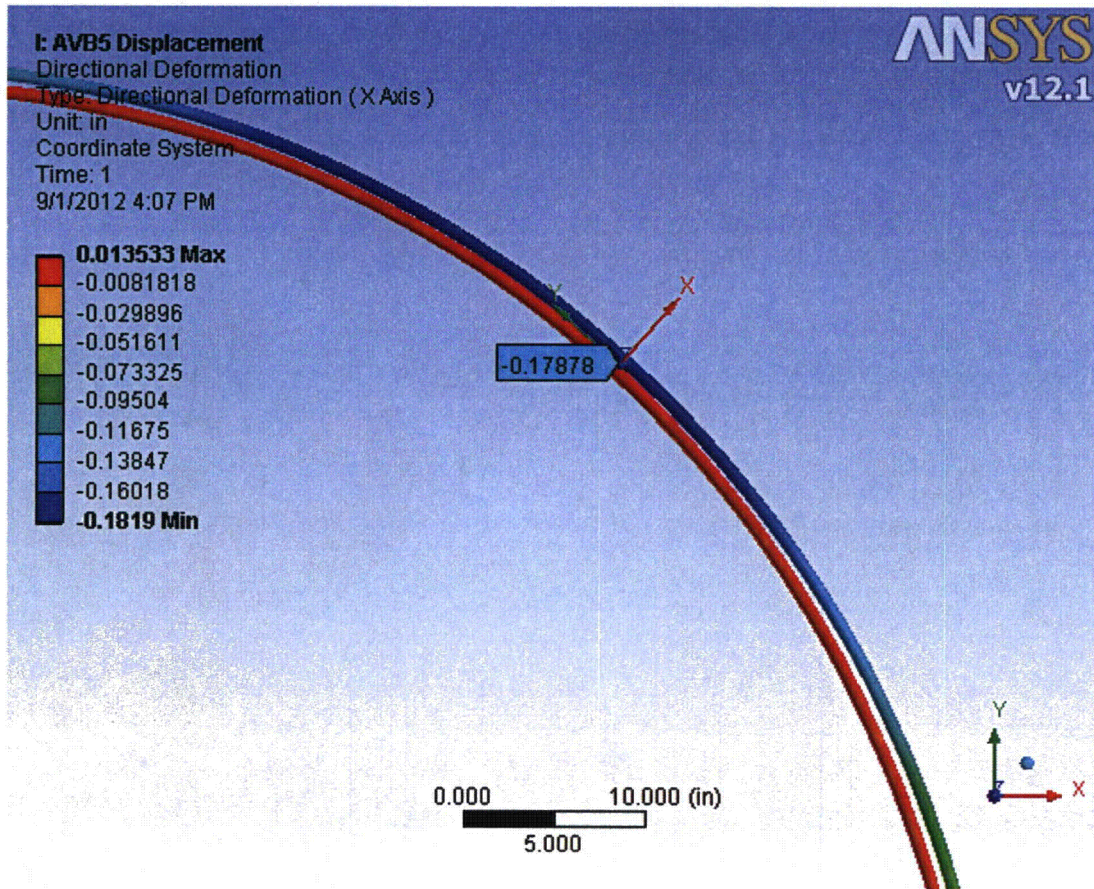


**Figure A-17. 0.18 Inch Displacement at AVB 5 Results (inches)**

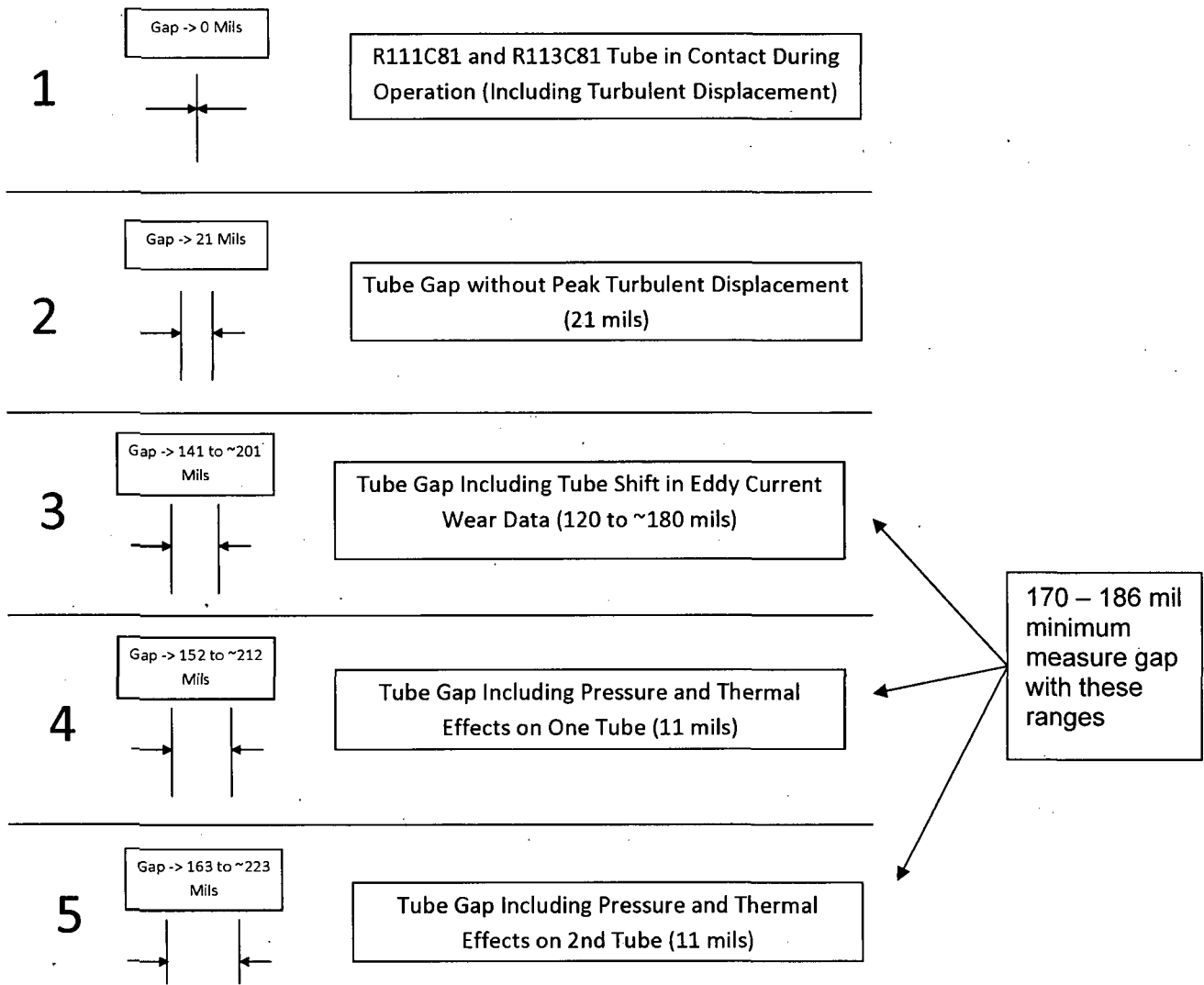


**Figure A-18. Tube Gap Development**



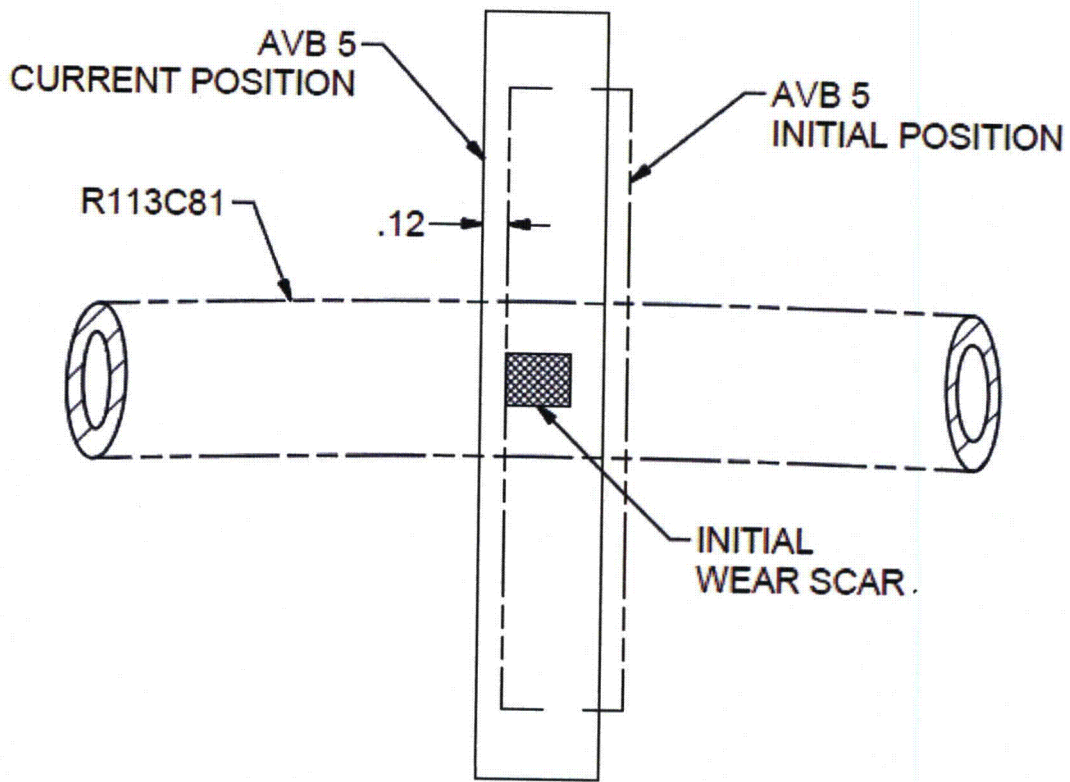


Figure A-19. R113C81 AVB "A" Eddy Current Wear Profile

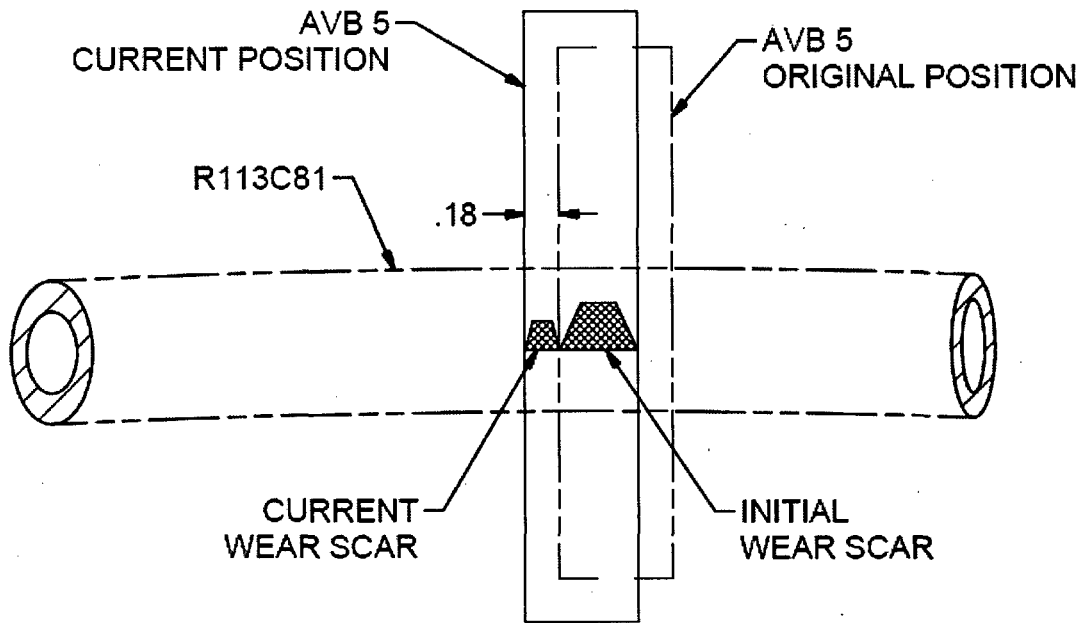


Figure A-20. R113C81 AVB "B" Eddy Current Wear Profile